The evolutionary relationship between epoxide hydrolases and dehalogenases

Inauguraldissertation

zur

Erlangung des akademischen Grades eines

Doktors der Naturwissenschaften (Dr. rer. nat.)

der

Mathematisch-Naturwissenschaftlichen Fakultät

der

Universität Greifswald

vorgelegt von

Eva Daniëlle Schuiten

Greifswald, August 2022

Dekan: Prof. Dr. Gerald Kerth

1. Gutachter: Prof. Dr. Uwe T. Bornscheuer
2. Gutachter: Prof. Dr. Romas Kazlauskas

Tag der Promotion: 20 Oktober 2022

Contents

Chapter 1

Enzymes and promiscuity

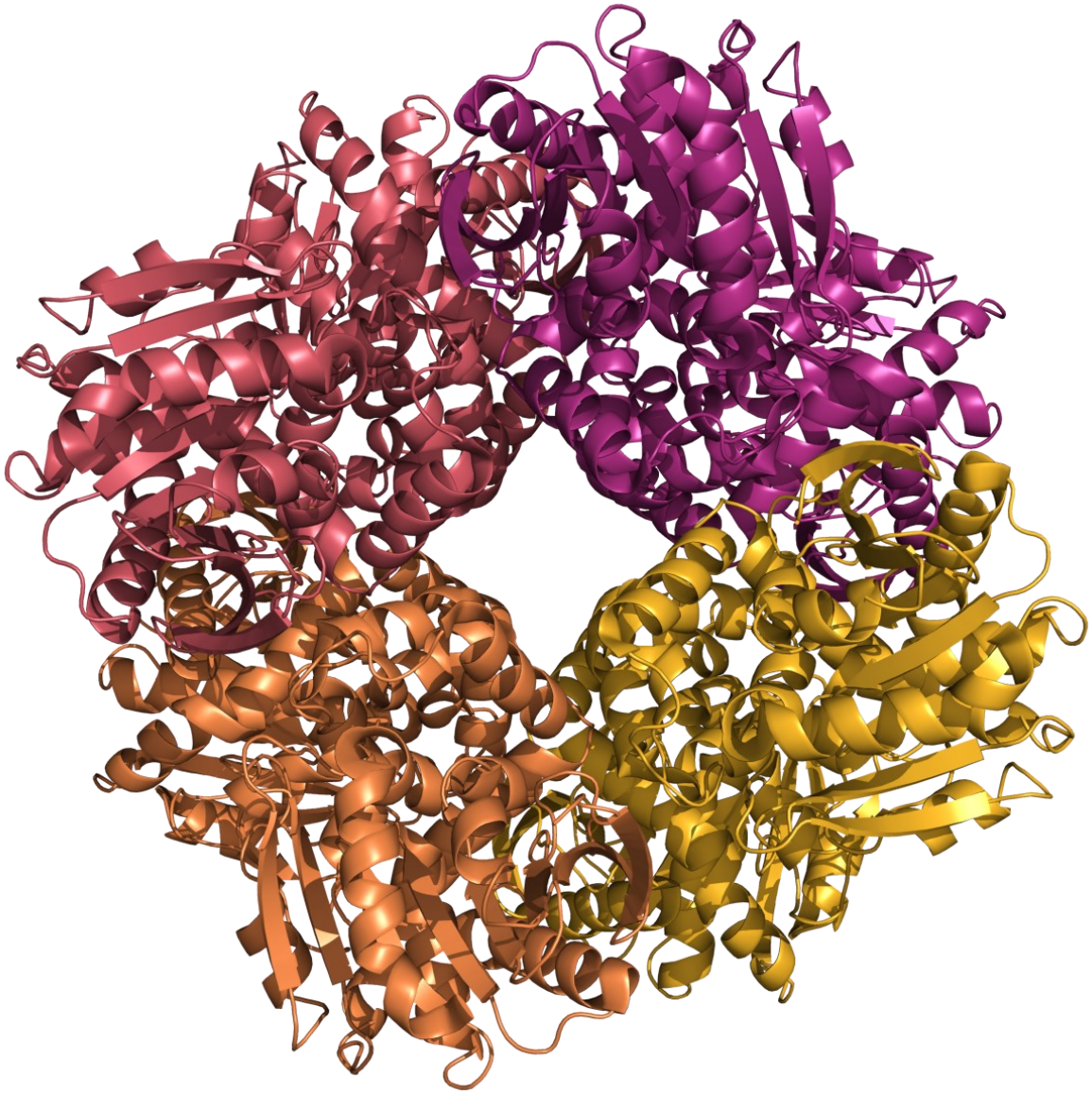

1.1 Catalysis for life

Under biologically relevant conditions chemical reactions tend to be slow because there is an energy barrier that needs to be overcome. Catalysts lower this energy barrier and thus increase the rate of the reaction without being consumed themselves. In biology, most catalysts are highly specialized protein-based biomolecules called enzymes[1]. Compared to other catalysts, these biocatalysts can accelerate chemical reactions under very mild conditions. Nature hosts an incredible variety of enzymes that are classified by the type of reaction catalysed. Enzymes play a central role in every biochemical process and catalyse an incredible variety of reactions from nutrient degradation to the production of biological macromolecules. They are involved in many diseases, where deficiency, total absence or overactivity of an enzyme causes problems and sometimes their activity or presence can be used to diagnose certain illnesses. Aside from medical uses, enzymes can also be employed to perform useful chemical reactions in chemical engineering, food technology, and agriculture. In addition, enzymes are wonderfully complex machines and understanding them and their evolution may help us understand the natural world better.

The catalytic activity of enzymes depends on the integrity of their protein conformation, if the three-dimensional folded structure is lost, the catalytic activity is usually also lost[2]. An enzyme is made up of amino acid building blocks that form the primary structure: a polypeptide chain (Figure 1A). Amino acids are organic compounds that contain an amino ($-NH_3^+$) and a carboxylate ($-CO_2^-$) functional group that together with an additional carbon form the backbone of the polypeptide chain. In addition, each amino acid has a side chain (R) that is specific to that amino acid and gives each amino acid different chemical properties[2]. The polypeptide chain is folded into secondary structural elements called α-helices and β-sheets (Figure 1B). In an α-helix the carbonyl (C=O) of one amino acid forms a hydrogen bond with the amino hydrogen (N-H) of an amino acid four positions down in the polypeptide chain. These bonds pull the chain into a helical structure called the α-helix. A β-sheet is formed when two or more segments of a polypeptide chain line up next to each other, forming a sheet-like structure held together by hydrogen bonds.

The strands of a β-sheet can be parallel, pointing in the same direction, or antiparallel, pointing in opposite directions. In both α-helices and β-sheets the R-groups of the amino acids stick outwards and are free to interact. The tertiary structure is the overall three-dimensional structure of the polypeptide chain and is mostly formed through the interactions between the R-groups of the amino acids (Figure 1C). Examples of these interactions include hydrogen bonding, ionic bonding, and hydrophobic interactions. Many enzymes consist of multiple polypeptide chains, or subunits. When multiple of these subunits come together, they give the enzyme its quaternary structure (Figure 1D). The subunits can be identical, similar, or completely different polypeptide chains. They are held together mostly by weak interactions such as hydrogen bonding[2].

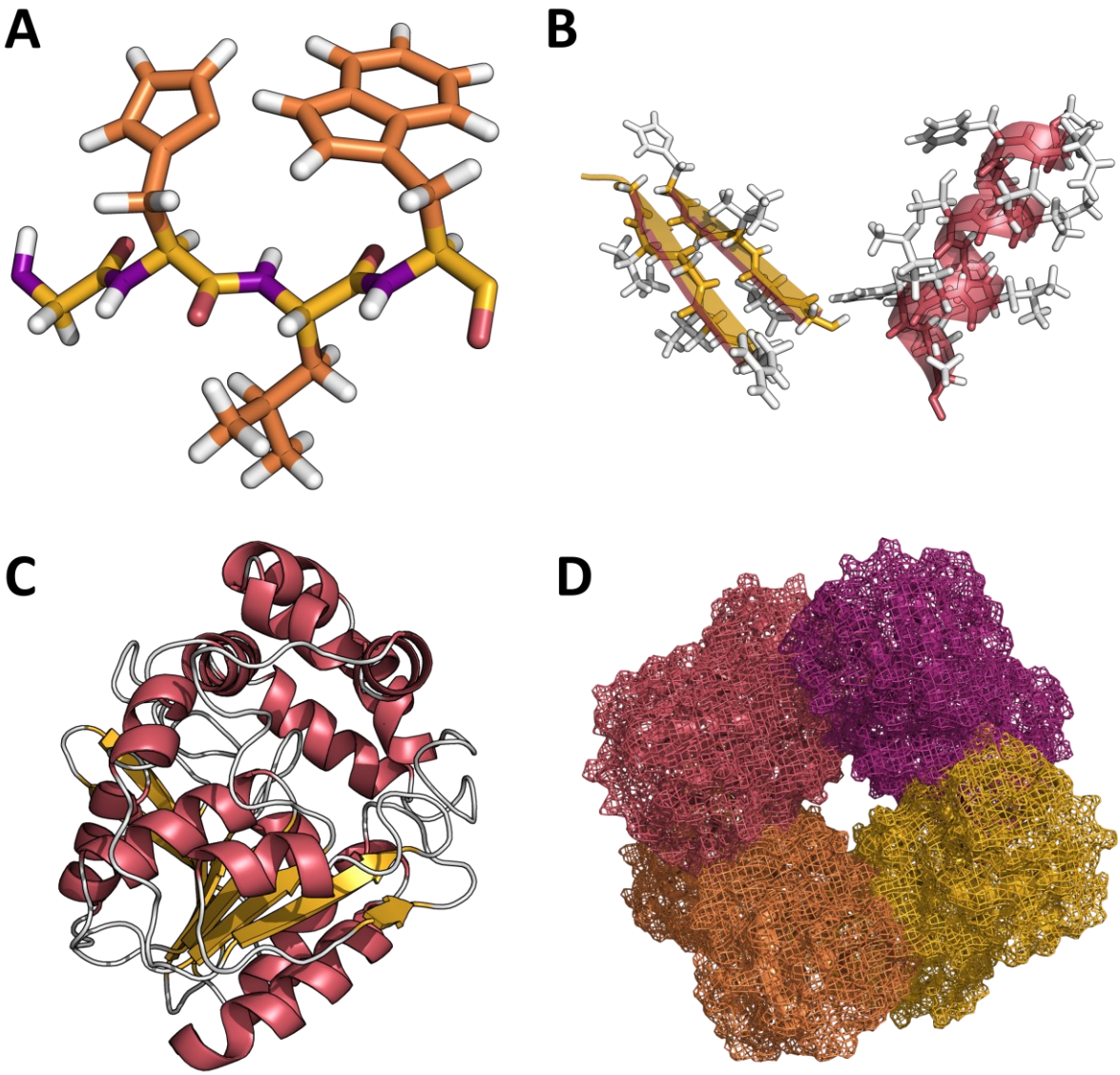

Figure 1. Different levels of enzyme structure. A) Primary structure of the enzyme showing the backbone of the polypeptide (carbon atoms in yellow, nitrogen atoms in purple and oxygen atoms in pink). Each amino acid has a different sidechain residue (orange with hydrogen atoms in white). These sidechain residues all have different characteristics and are important for the overall protein structure and catalytic activity. B) Secondary structural elements called β-sheets (yellow) and α-helices (pink). C) Tertiary structure of an enzyme with the secondary structural elements in pink (α-helices) and yellow (β-sheets), sometimes referred to as a subunit. D) Quaternary structure with four separate subunits. Many enzymes are large complexes of multiple polypeptides, these polypeptides can be identical, similar, or completely different.

In chemical reactions one or more substances are converted to one or more different substances. The conversion can only take place when the energy barrier is overcome (Figure 2A). For an uncatalysed reaction the energy barrier is very high (ΔG_{uncat}), but catalysts can lower the energy barrier (ΔG_{cat}) and thus increase the reaction rate[1]. One way in which enzymes catalyse reactions is by providing a specific environment in which a given reaction can occur more rapidly because the activation energy for the reaction is lower. The active site of an enzyme consists of amino acid residues that form temporary bonds with the substrate molecule and the catalytic residues that catalyse the conversion of the substrate to the product (Figure 2B). Enzymatic reactions with one substrate are commonly simplified as:

$$E + S \rightleftharpoons ES \rightleftharpoons EP \rightleftharpoons E + P$$

The enzyme (E) and substrate molecule (S) form an enzyme-substrate complex (ES) and once the substrate is bound and oriented correctly in the active site the reaction with the catalytic residues can take place. The substrate binding site is usually very close to the catalytic site and often binding residues are also involved in the catalysis. Many enzymes use a catalytic triad, a set of three coordinated amino acids, to catalyse a reaction[2]. A common motif is the acid-base-nucleophile catalytic triad such as in the example in Figure 2B. The acid and base amino acids form a charge-relay network to activate a nucleophile, which attacks the substrate to form a covalent intermediate, which is then hydrolysed to release the product (E+P).

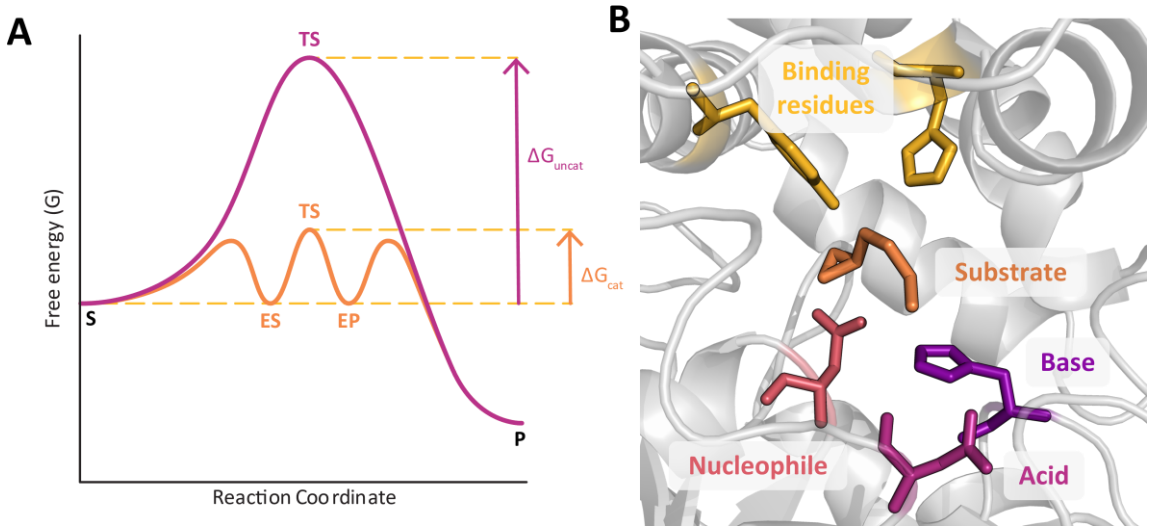

Figure 2. Reaction coordinate diagram and an enzyme active site. A) Reaction coordinate diagram comparing enzyme-catalysed (orange) and uncatalysed (purple) reactions. In the reaction from substrate (S) to product (P), the enzyme-substrate (ES) and enzyme-product (EP) intermediates occupy minima in the energy progress curve of the enzyme-catalysed reaction. The difference in energy between the ground state of the substrate and the transitions state (TS), represented by ΔG, is the activation energy required for the reaction to proceed from S to P. The enzyme lowers the activation energy so the reaction can occur more rapidly. B) Example of an enzyme active site. Most enzymes have some binding residues (yellow) that bind the substrate to stabilise intermediates or the product of the reaction by weak interactions like hydrogen bonds or hydrophobic interactions. Catalytic residues (pink & purple) are more actively involved in the reaction. Many enzymes make use of a catalytic triad consisting of three residues, the acid, base, and nucleophile. The acid and base amino acids form a charge-relay network to activate the nucleophile, which attacks the substrate to form a covalent intermediate.

1.2 Protein engineering

Enzymes can catalyse a great variety of useful chemical reactions, but sometimes they do not accept the desired substrate or make the desired product. In addition, natural enzymes are rarely suited for the reaction conditions in industrial processes. Protein engineering can be used to tailor the properties of enzymes to catalyse the desired chemical transformations under the desired conditions.[3] The pioneering gene cloning experiments of Stanley Cohen, Annie Chang, Herbert Boyer, and Robert Helling in the early 1970s[4] were the start of a new era in which proteins could be made and modified at will. Since then, the ability to modify protein properties has been refined to a point where is possible to engineer almost any property. Enzymes can be engineered to be more stable, more active, or even perform new functions. There are two general strategies for protein engineering that are often both applied; rational design and directed evolution[5].

Rational design makes use of protein structural information to design mutations to obtain new or improved function. Site-directed mutagenesis is used to introduce the designed mutations into the protein, producing very small variant libraries. To be successful, rational design requires detailed structural knowledge of the protein, but this is often unavailable. Even when the protein structure is available, it can be very difficult to predict the effects of various mutations on the protein structure and function. In contrast, directed evolution makes use of the advances in recombinant DNA technology to create thousands of possible variants, which are screened using high-throughput screening methods to find the most promising variants. This approach has been proven to be a powerful alternative to rational design, especially when the relationship between structure and function is not well understood. In fact, the directed evolution approach has made such an impact in the field of biocatalysis that in 2018 Frances H. Arnold was awarded the Nobel Prize in Chemistry for her pioneering work on directed evolution. However, directed evolution is highly dependent on the correct selection pressure provided by the screening method and can only be used if a suitable screening method is available[5,6]. In addition, generating and screening large variant libraries is expensive and incredibly time-consuming.

Therefore, both methods are often combined into a semi-rational approach by using rational design to identify potential positions (or regions) of interest and generating variants using saturation mutagenesis to generate more focused, smart libraries[7].

1.3 Proteins and phylogenetics

Enzymes are grouped together with other similar proteins into structural families and superfamilies. Members of a structural family share significant structural elements and mechanistic similarity is also quite common. These structural similarities suggest a common evolutionary origin, even though members of the family can sometimes catalyse very different chemical reactions or accept a variety of different substrates. Molecular phylogenetics explores the evolutionary relationships between closely related biomolecules. This branch of phylogeny, the study of evolutionary history of a group of organisms, focuses on the analysis of genetic, hereditary molecular differences found in the amino acid or DNA sequences of biomolecules such as proteins. In the 1960s the work of molecular biologists like Emile Zuckerkandl and Linus Pauling[8,9] revolutionized the field of evolutionary biology by advancing

the use of nucleotide and protein sequences to explore evolution. Their idea was deceptively simple; if two organisms are closely related, the sequences of their genes and proteins should be similar. As the evolutionary distance between the organisms grows, the sequences become more and more distinct. However, biological systems are complicated, and evolution has rarely taken a simple linear path.

A phylogenetic tree is a branching diagram that visualizes the relationships between the different species in a dataset (Figure 3). The free end points in the phylogenetic tree are called the external nodes or leaves, each representing an existing species. The points where two lines come together are called internal nodes, and they represent a theoretical common ancestor. Often, the length of the branches of the tree is proportional to the evolutionary distance between nodes. The line at the start of the tree is called the root, which is usually determined using an outgroup. The outgroup is quite different from the other extant species, so that the common ancestor for the other group can be determined with a certain accuracy. The root of a phylogenetic tree is therefore always an approximation of reality. In the example in Figure 3, frogs were used as an outgroup to root the tree and find the common ancestor of the other species in the tree.

The phylogenetic analysis of enzymes starts with building a solid dataset of related extant amino acid sequences (Figure 3). The dataset should include homologous sequences and adequately cover sequence space, meaning that the diversity of amino acid sequences within the family is well-represented. Homologous proteins are usually found through protein databases such as NCBI[10] or UniProt[11] using search algorithms like BLAST[12]. Homology is similarity due to a shared ancestry, not to be confused with homoplasy, where the similarity is coincidental, and the trait has developed at least twice in separate unrelated species. In evolutionary biology, the sequence space represents all possible sequences for a protein, gene, or genome. Although enzymes can be extremely diverse, functional protein sequences are a rare occurrence among the vast number of sequences in sequence space. Most random amino acid sequences will have no fold or function and thus, even large enzyme superfamilies like the α/β-hydrolases exists as a tiny cluster of active proteins in sequence space. Therefore, in practice adequately covering sequence space in a dataset means covering the variety of sequences in a cluster of active proteins.

Next, a multiple sequence alignment (MSA) is made using alignment software such as Clustalω[13], MAFFT[14], MUSCLE[15] or T-Coffee[16]. In a sequence alignment, multiple sequences are compared and arranged so that identical or similar residues are aligned. In regions where residues are very different or non-existent, gaps (-) are inserted to ensure the more similar regions can still be aligned. Sequence alignment is one of the methods to identify and visualize regions of similarity between sequences. The quality of the MSA is extremely important, as it determines the overall accuracy of the phylogenetic analysis. The MSA is generally also used to assess the quality of the dataset. When necessary, sequences can be added or removed, and often the alignment itself must be adjusted manually, especially at gap-positions, to improve the overall alignment. Once the alignment is satisfactory, a phylogenetic tree can be constructed using computational methods such as maximum parsimony[17] or maximum likelihood [18,19] phylogeny.

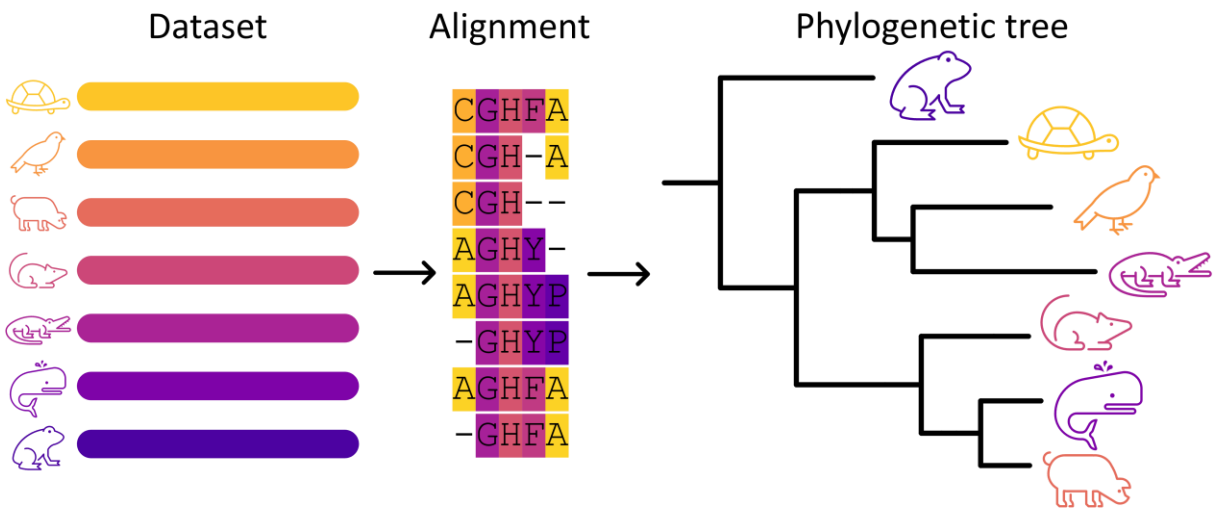

Figure 3. Schematic overview of phylogenetic analyses. First, sequences are collected from an interesting and representative set of organisms. Next, the sequences are aligned using appropriate alignment software. Finally, a phylogenetic tree is constructed using computational methods.

The maximum parsimony method assumes that a tree with the minimum number of substitutions is most likely. This means that the branches of the most likely tree are organised in such a way that going from one branch to another requires the minimal number of steps. However, this method does not consider the biased substitution of amino acids. Although in theory every amino acid in the sequence can be exchanged for any other, in reality not all substitutions are equally likely. First, which amino acid is inserted in the polypeptide chain is determined by three-letter codes, or codons, in the DNA. Point mutations change one of letters in the codon, resulting in a different codon and a different amino acid in the polypeptide. Some three-letter codes are more similar than others and require fewer mutations to be interconverted. Second, each amino acid has different chemical properties and substitution to an amino acid with similar properties is more likely to have no negative consequences. Finally, some positions are essential for the function of the protein. The residues at these positions will often be conserved because loss of function results in negative selection pressure[1]. Different proteins will have different numbers of variable amino acid residues, which is one of the reasons why different proteins evolve at different rates. In addition to not considering substitution bias, maximum parsimony does not consider long branch attraction. Long branch attraction is the grouping of two or more long branches as closely related groups, even though they are not at all closely related. These two major flaws lead to bad representation of datasets, especially those including fast-evolving genes, and wrongful assumption of homoplasy for homology.

In more recent studies, these problems have been addressed by the maximum likelihood method by using evolution models in the calculations. The evolution models are so-called substitution models, which represent how likely it is that one amino acid replaces another for different genes and organisms. Which evolutionary model gives the most accurate representation of reality is dependent on the dataset. Programs that can determine which substitution model is the best fit for the dataset are available as separate programs (e.g., ProtTest[20]) or sometimes included in tree-building software (e.g., IQ-TREE[21]).

1.3.1 Reconstructing ancestral sequences

Already early in the 1960s, an idea to use molecular phylogeny and protein sequences to resurrect extinct ancient proteins was proposed[22]. Ancestral sequence reconstruction (ASR) tries to reconstruct ancestral sequences based on their extant descendants and characterise them in the laboratory. By combining the multiple sequence alignment, the evolutionary relationships from the phylogenetic tree, and evolutionary models, a hypothetical sequence of the theoretical ancestor can be determined. ASR has been performed mostly on proteins but can also be used on other biomolecules such as regulatory sequences, RNA, viruses, and even entire genomes[23–26]. ASR is often used to study functional divergence within protein families but can also be used to obtain similar enzymes with different properties like higher thermostability[27–32].

1.4 Highly selective and promiscuous catalysts

Enzymes are well-known for being remarkably selective catalysts. They are often able to catalyse reactions for certain substrate molecules while leaving other similar molecules completely unchanged. Enzymes can be chemo-, regio-, and stereoselective. Chemo selectivity is the selective reaction with one group or atom in a molecule in preference to another group or atom in the same molecule but with different properties. Regioselectivity, sometimes referred to as site-selectivity, means that a reaction is performed selectively at one out of several possible positions in the substrate molecule. Stereoselective enzymes can discriminate between enantiomeric substrates or products. Enantiomers are molecules that have the same chemical bonds but are mirror images of each other. These mirror images often have different chemical reactions with other enantiomeric substances, especially with macromolecules like enzymes or receptors. Many biological molecules are enantiomers as well and the different enantiomers can have significantly different effects on biological systems. For living organisms, the selectivity of enzymes is vital. For us, it is very useful to produce chemically pure products.

Despite their selectivity, many enzymes are capable of catalysing other reactions and/or transforming other substrates in addition to their evolved and physiologically relevant activities[33–35]. This phenomenon is referred to as enzyme promiscuity and is more specifically divided into substrate promiscuity and catalytic promiscuity. Substrate promiscuity is the catalysis of reactions with substrates other than the physiologically relevant, or native, activity. For example, a large screening study of 217 enzymes from the haloacid dehalogenase family against 169 phosphorylated compounds revealed that 204 of these enzymes were able to dephosphorylate on average 15.5 different substrates. Many catalysed significantly more, with 101 enzymes hydrolysing between 6 and 40 substrates and 50 between 41 and 143 different substrates.[33] The study aimed to identify physiologically relevant activities, but it is likely that many of the identified activities are actually cases of substrate promiscuity instead of the real physiological function. Some enzymes have evolved to transform a whole range of substrates, such as cytochrome P450 monooxygenases or lipases. These enzymes are sometimes referred to as substrate-promiscuous enzymes. However, in these enzymes their broad substrate specificity is integral to their evolved native activities, and they are more accurately described as multi-specific or broad-specificity enzymes[36].

Catalytic promiscuity is defined as the ability of an enzyme active site to catalyse distinctly different chemical transformations. For example, a superfamily-wide analysis of the evolutionary and functional connectivity in the metallo-β-lactamase superfamily found that enzymes of this family are generally promiscuous, each catalysing on average 1.5 reactions in addition to their native reaction[35]. Promiscuous activities often differ to such an extent that the reactions belong to different classes of substrates and in the case of catalytic promiscuity even different reaction classes. Enzyme Commission (EC) numbers are used to classify enzymes. If different enzymes catalyse the same reaction, they have the same EC number, while the same reaction in reverse has a different EC number. It is possible for structurally completely different enzymes to have the same EC number. The major EC classes are oxidoreductases (EC 1), transferases (EC 2), hydrolases (EC 3), lyases (EC 4), isomerases (EC 5) and ligases (EC 6). EC numbers consist of four digits in total, which represent a progressively more specific classification of the enzyme reaction. Thus, the degree of promiscuity can often be identified by comparing differences in the EC numbers of the reactions.[36]

1.4.1 Promiscuity and the evolution of novel enzyme functions

The selectivity of enzymes is context dependent and shaped by natural selection[36]. Promiscuous activities that are harmful will be selected against, but neutral or positive activities can persist or be promoted respectively. Even highly selective and conserved enzymes such as those involved in DNA or protein synthesis, often have surprisingly high substrate infidelity. Many enzymes perform secondary tasks that likely originated in promiscuity[37]. Some of these enzymes are under intense selection pressure for high selectivity, but nevertheless developed a secondary function well after the emergence of the primary function[36].

Only few of the promiscuous activities found *in vitro* have any physiological or evolutionary meaning *in vivo*[36]. The selectivity of enzymes *in vivo* is partly achieved through regulation, not by restriction of enzyme selectivity itself. Regulation can occur at a cellular level, for example by preventing the expression of unnecessary protein or at a protein level where post-translational modifications like phosphorylation can activate or deactivate the enzyme. Sometimes, like with post-translational modifications, an effector molecule binds to the enzyme somewhere outside of the active site and either promotes or inhibits its catalytic activity. Many enzymes are regulated through inhibition by the reaction product, but in some cases, enzymes are subject to substrate inhibition instead.[1]

Although enzyme selectivity is increased by natural selection through shaping of the active site and regulation, cross-reactivity is a common occurrence in living cells[38]. Cross-reactivity is often found by the analysis of knockout strains that lack a certain enzyme. The lack of one enzyme in crucial pathways is often compensated for by the promiscuous activity of other enzymes or sometimes entire pathways[39]. It is important for enzymes to be selective to avoid harmful side-products and increase reaction efficiency, but often catalysts are not optimised beyond what is necessary[38]. Life profits from the cross-reactivity and enzyme promiscuity through accidental discovery of new helpful molecules and pathways, while using regulation to quickly adapt to changing circumstances.

Within protein superfamilies the primary function of one family member is often found as promiscuous activity in other family members and the same promiscuous activity is usually shared by more than one family member[36,40]. Together with the structural similarities, this prevalent cross-reactivity suggests a common evolutionary origin. It is commonly thought that catalytic promiscuity plays an important role in the emergence of novel functions by providing a starting point for divergent evolution towards different enzymatic activities[41–46].

1.4.2 Evolutionary mechanisms behind new functions

Gene duplication is assumed to be the core evolutionary mechanism behind the emergence and divergence of protein functions. In 1970 Susumu Ohno proposed a model describing evolution by gene duplication[47] (Figure 4). Following Ohno's model, gene duplication is a mostly neutral and frequent event, free from selection pressure. After duplication, the copied gene is redundant and can accumulate mutations freely. When the mutations result in an advantageous new function, it will be positively selected for, leading to further divergence of the new gene, protein, and function. Ohno's model is based on the negative trade-off assumption, which assumes that positive selection for the existing native function will impede mutations with adaptive potential and thus mutations can only accumulate in a redundant copy.

In contrast to the negative trade-off assumption, many promiscuous functions have evolved with little effect on the original native function of the enzyme[36]. Ohno's model assumes that gene duplication is a neutral event, but this is rarely the case. It seems that duplicated genes are often under selection against deleterious mutations, indicating that the duplicated gene is not truly free from selection[48]. In addition, the replication and expression of redundant genes costs energy and resources, applying negative selection pressure on gene duplication[49–51]. Random mutations are also often deleterious (1 in 3), while beneficial mutations are rare (1 in 10^3) [52,53]. It is therefore much more likely that a duplicated gene in the absence of any selection loses function because of mutations that cause misfolding and instability than that it gains new functions[54].

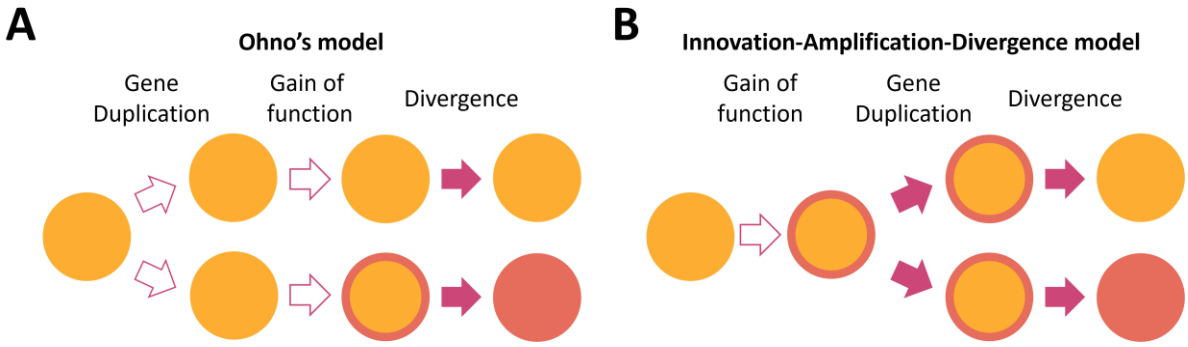

Figure 4. Evolutionary models for enzyme evolution through gene duplication. A) In Ohno's model gene duplication occurs as a neutral and frequent event, resulting in a redundant copy free from selection pressure towards the original function. The duplicate gene can then acquire mutations that can result in gain of function and thus diverge from the original gene. B) In the innovation-amplification-divergence model a promiscuous function is gained first. The promiscuous activity is high enough to be physiologically relevant and after gene duplication the genes can re-specialise towards each function separately.

Other evolutionary models, like the innovation-amplification-divergence model[55] or the escape from adaptive conflict model[56], assume that the new function is gained before duplication (Figure 4). The promiscuous activity becomes high enough to be physiologically relevant while also keeping the primary function. After gene duplication the genes can re-specialise separately towards either the original or the new function. Within these models it is possible that gene duplication is positively selected for. When a higher promiscuous activity is in demand, protein doses can be increased through duplicate genes[57]. It is also possible that a gene with a certain function can be recruited for a different, moonlighting function without any changes in the coding region. Following the gene sharing model, the gene does not duplicate but can be positively selected for towards an increase in the original and moonlighting function simultaneously.

In summary, although enzymes are known to be very selective catalysts, promiscuous activities are not at all rare and promiscuity is often found in protein superfamilies. Selectivity and promiscuity can occur within the same active site, the mechanism for the promiscuous activity can overlap, partly overlap or be completely different from the mechanism for the native function. Even weak promiscuous activity can provide a starting point for the evolution of new functions and eventually can evolve into a new primary, native function.

1.5 Promiscuity in α/β-hydrolases

One of the largest structural superfamilies is the α/β-hydrolase-fold family. Despite sharing a highly conserved core structure, this superfamily is catalytically diverse and spans several distinct enzyme classes including hydrolases, acyltransferases, oxidoreductases, lyases, and isomerases[58,59]. The versatility of their core catalytic machinery makes the α/β-hydrolases excellent case studies to understand the mechanisms underlying catalytic promiscuity and the evolution of novel enzyme functions.

1.5.1 Structure and catalytic motifs

Members of the α/β-hydrolase-fold superfamily share a common fold where the core is formed by a mostly parallel 6-8 stranded β-sheet packed between two layers of α-helices (Figure 5). These secondary structural elements are connected through flexible chains of amino acid residues, called loops. Aside from the highly conserved core domain, several different additional structural domains can be inserted in the fold. This includes helical caps, lids, and additional domains at the N- or C-termini, resulting in 12 different possible conformations. The core domain of α/β-hydrolases has two highly conserved motifs; the GxS_mxS/T and the HGxP motif, where x is any residue and S_m is a small amino acid residue. The GxS_mxS/T motif is found in the loop between the strand β4 and helix α2, removed from the active site, and thus does not play a direct role in catalysis. The HGxP motif in the loop after strand β3 always includes a histidine, glycine, and proline, but the x can be any amino acid residue. The main chain amide of the variable x-residue is part of the oxyanion hole. The oxyanion hole is a pocket in the active site that stabilises a negative charge on a deprotonated oxygen or alkoxide in the transition state of the reaction. The side chain of the x-residue is part of the active site and can interact with the substrate.

The catalytic versatility of α/β-hydrolase-fold enzymes is based in the versatility of their catalytic triads. α/β-hydrolases use an acid-base-nucleophile catalytic triad located at conserved positions across the core domain[60] (Figure 5). The catalytic nucleophile is located in the loop at the C-terminus of strand β5, in a conserved structural motif called the "nucleophile elbow". The catalytic base, always a histidine in α/β-hydrolases, is located in the flexible loop after strand β8. The catalytic acid, often referred to as the charge relay acid, can be located at C-terminus of strand β6 or on the turn after strand β7.

Adjacent to the catalytic nucleophile is the oxyanion hole, shaped mainly by the main-chain nitrogen atoms of the residues right next to the nucleophile and the x-residue in the HGxP motif. Sometimes the second oxyanion residue is located at a different position and the oxyanion hole is formed by a side chain instead. For example, this residue can also be a tyrosine or aspartic acid at the start of the loop between strand β3 and helix α1. For some α/β-hydrolases, the oxyanion hole is formed by three residues instead of two[61].

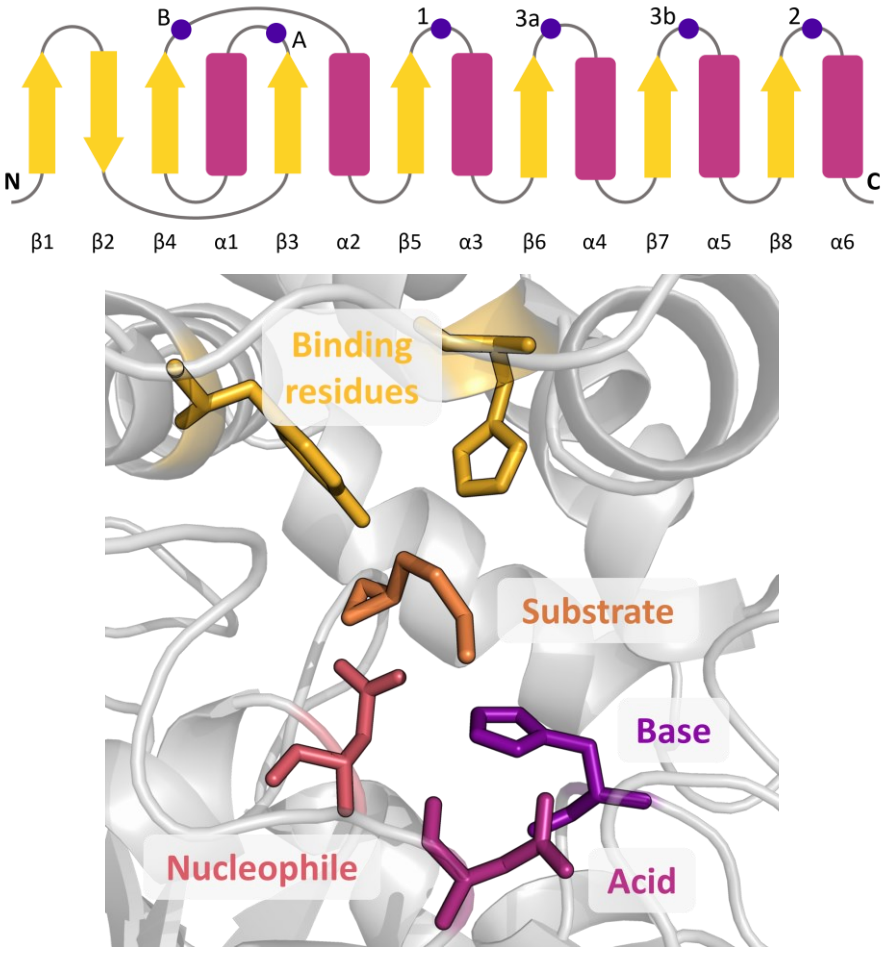

Figure 5. General topology of the core domain and overview of the active site in α/β-hydrolases. The main domain contains the characteristic α/β-hydrolase-fold consisting of a mostly parallel 6-8 stranded β-sheet connected through 4-6 α-helices. There are two highly conserved motifs; the HGxP motif (A) and the GxSmxS/T motif (B). The locations of the acid-base-nucleophile catalytic triad are marked with dark purple dots (1-3 respectively). The charge relay acid (3) can be located at two different positions in the sequence, either close to the catalytic nucleophile (3a) or closer to the histidine base (3b). Helical caps, lids and other domains can be inserted in the fold between β6 and α4, but the core structure is preserved.

1.5.2 Common catalytic triads

The most common catalytic triad in α/β-hydrolases is the Ser-His-Asp catalytic triad. This catalytic triad catalyses at least seventeen different reactions, including the hydrolysis of C-O, C-N, and C-C bonds (EC 3), oxidoreductases (EC 1), acyl transferases (EC 2), lyases (EC 4) and isomerases (EC 5)[58]. The hydrolysis reactions usually follow a canonical esterase mechanism, in which the triad facilitates the formation of an acyl-enzyme intermediate: an ester derivative of the catalytic serine (Ser). This intermediate can be hydrolysed by a water molecule activated by the His-Asp pair[58]. However, several reactions are variations where the formation or cleavage of the acyl-enzyme intermediate is different. In addition, the lyase-type reactions do not use an acyl-enzyme intermediate and sometimes do not even need the catalytic serine[58]. While the esterase mechanism with acyl-enzyme intermediate works very well for the hydrolysis of esters and amides, it is not suitable for the hydrolysis of epoxides and halocarbons, which would result in the formation of non-hydrolysable ether intermediates. Instead of the Ser-His-Asp triad, epoxide hydrolases (EH, E.C. 3.3.2.10), haloacetate dehalogenases (HacD, E.C. 3.8.1.3), and haloalkane dehalogenases (HLD, E.C. 3.8.1.5) use the Asp-His-Asp/Glu catalytic triad. This triad produces an alkyl-enzyme intermediate, an ester derivative of the catalytic aspartate, through a nucleophilic attack. Similar to the other triad, the alkyl-enzyme intermediate is then hydrolysed by an activated water molecule [62,63].

Due to the versatility of the catalytic triads employed by α/β-hydrolases, catalytic promiscuity is often observed among members of the α/β-hydrolase-fold family[58]. For example, some esterases can hydrolyse amides (and vice versa) via the same acyl-enzyme intermediate used in the esterase reaction[64]. However, while some promiscuous activities are frequently observed, at the start of this thesis no α/β-hydrolase-fold enzyme had been reported to have both epoxide hydrolase and dehalogenase activity.

1.5.3 Epoxides and hydrolysis

Epoxide hydrolases are enzymes that catalyse the hydration of epoxides to form diol products. Epoxides, also known as oxiranes, are molecules characterized by an epoxy group (Figure 6). The epoxy group is a highly reactive moiety, making epoxides an important group of industrial organic intermediates. Epoxides are produced on a large scale for many applications, including making antifreeze, adhesives, and surface coatings. Because many epoxides are highly reactive, they readily bind to nucleic acids and proteins, causing cellular toxicity, DNA mutations and carcinogenesis. Epoxide hydrolases convert the highly reactive epoxides to less reactive diols and are very important in toxication-detoxication processes. Epoxide hydrolases can be found in many different organisms and several organisms express several with different substrate preferences and functions in different subcellular locations. Most epoxide hydrolases are members of the α/β-hydrolase-fold family, but some, like the limonene-1,2-epoxide hydrolase, have an entirely different structure and mechanism[65].

1.5.4 Halocarbons and dehalogenation

Dehalogenases are enzymes that catalyse the removal of a halogen atom from a halogenated molecule. In modern life we use many halogenated molecules as pharmaceuticals, agrochemicals, detergents, pigments, and polymers[66] (Figure 6). Additionally, halogenated compounds are used as solvents, degreasing agents, and intermediates in industrial chemical syntheses[67,68]. The carbon-halogen bonds (C-F, C-Cl, C-Br, and C-I) in these molecules are important for their potency and function. In the last few decades, the production of these halogenated molecules, haloalkanes in particular, has increased drastically, and millions of tons of short-chain haloalkanes are produced annually. Although most halogenated compounds that we encounter in everyday life are man-made, each year several million tons of methyl halides, predominantly chloromethane, are released into the atmosphere by terrestrial and marine biomass[69,70]. Haloalkanes are toxic and improper disposal, evaporation, spillage, and deliberate release contribute to contamination of the atmosphere, soil, and water with these persistent pollutants[69–71]. The most promising strategy for environmental remediation is the biocatalytic degradation by dehalogenases[68,71,72]. Since the discovery of the first haloalkane dehalogenase DhlA from *Xanthobacter autotrophicus* GJ10 in 1984[71], over 40 haloalkane dehalogenases (HLD) have been described in scientific literature[73–82]. These enzymes hydrolyse a broad range of haloalkanes to the corresponding alcohols, accompanied by the release of a proton and halide ion. Known haloalkane dehalogenases originate from a diverse range of species, including bacteria, archaea, and eukaryotes[73–82]. The HLD family can be divided into three subfamilies, named HLD-I, HLD-II, and HLD-III[83], which mainly differ in the variable cap domain. How these enzymes evolved to degrade xenobiotic haloalkanes has sparked intense research for over three decades[28,30,84].

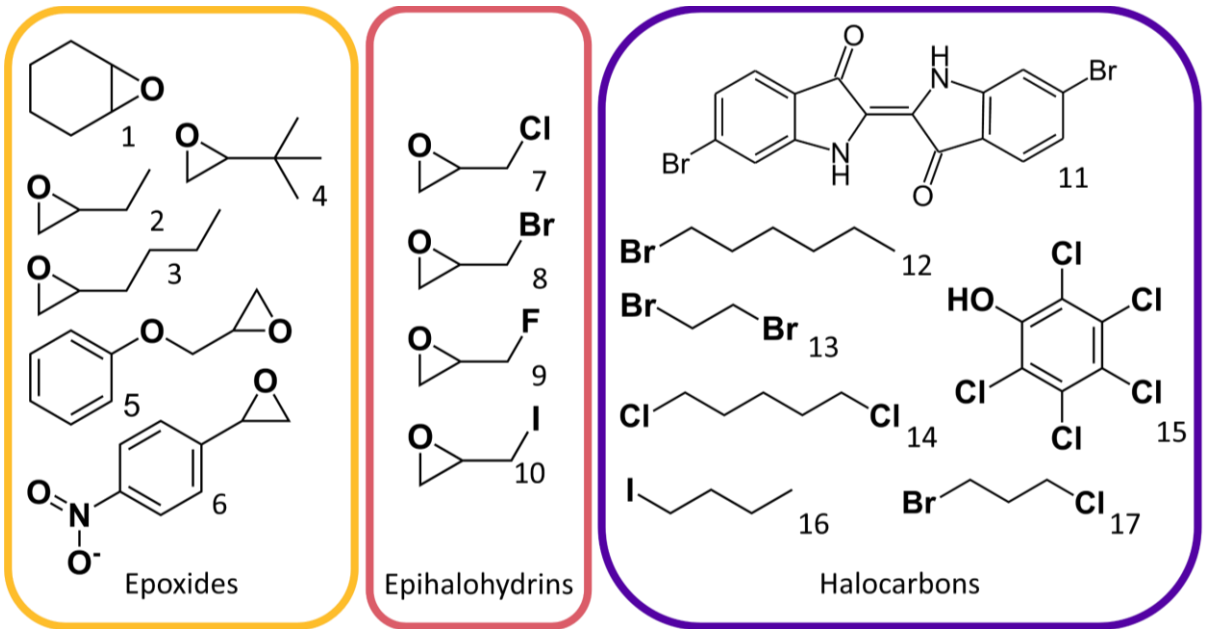

Figure 6. Examples of several epoxides, epihalohydrins, and halocarbons. **1**: cyclohexene oxide; **2**: 1,2-epoxybutane; **3**: 1,2-epoxyhexane; **4**: tert-butyloxirane; **5**: 1,2-epoxy-3-phenoxypropane; **6**: *para*-nitrostyrene oxide; **7**: epichlorohydrin; **8**: epibromohydrin; **9**: epifluorohydrin; **10**: epiiodohydrin; **11**: 6,6'-dibromoindigo (Tyrian Purple); **12**: 1-bromohexane; **13**: 1,2-dibromoethane; **14**: 1,5-dichlopentane; **15**: pentachlorophenol; **16**: 1-iodobutane; **17**: 1-bromo-3-chloropropane.

1.5.5 Catalytic triad or pentad?

Both epoxide hydrolases and haloalkane dehalogenases employ the Asp-His-Asp/Glu catalytic triad. The nucleophilic aspartate performs a nucleophilic attack on the primary carbon of the epoxide or organohalogen and forms an alkyl-enzyme intermediate (Figure 7). This alkyl-enzyme intermediate is hydrolysed by a water molecule that is activated by the His-Asp/Glu pair.

Epoxide hydrolases and haloalkane dehalogenases have very similar catalytic mechanisms, and they both accept epihalohydrins as substrates[63,76,85–87]. Epihalohydrins are small molecules that have both an epoxide ring and a halide (Figure 6). While epoxide hydrolases attack the C-O bond of the epoxide ring, haloalkane dehalogenases will instead attack the C-X bond. How do these enzymes control which functional group is attacked? Despite using the same nucleophilic aspartate for the S_N2 attack on the substrate, the epoxide hydrolase and dehalogenase reactions go through distinctly different transition states that need to be stabilised in the active site. Epoxide hydrolases and haloalkane dehalogenases have different supporting residues that help stabilise the transition states of the nucleophilic attack half reactions (Figure 7). These supporting residues are part of the oxyanion hole and are highly conserved within their respective groups. Combined with the catalytic triad they form what is sometimes referred to as a catalytic pentad.

In epoxide hydrolases the epoxide ring-opening is assisted by a His/Tyr-Tyr pair coordinating the epoxide oxygen. Most epoxide hydrolases utilise two tyrosine residues[88], but a few distinct epoxide hydrolases use a histidine-tyrosine pair[89]. Haloalkane dehalogenases make use of halide-stabilising residues, usually two, to stabilise the charge of the halide ion during the reaction. The primary halide-stabilising-residue is always a tryptophan, but the secondary residue differs. In the HLD-I subfamily the secondary residue is another tryptophan[90], but in subfamilies HLD-II and HLD-III the residue is an asparagine[62,91]. One haloalkane dehalogenase, DatA from *Agrobacterium tumefaciens*, has been reported to have a special halide-stabilising pair, consisting of an asparagine and a tyrosine[92,93]. Some dehalogenases, such as DmxA[94], DsaA[82], DmrB[78] and DsvA[95], have been reported to have only one halide-stabilising residue.

Enzymes that catalyse both dehalogenation and opening of the epoxide ring do exist outside of the α/β-hydrolase-fold superfamily in the form of halohydrin dehalogenases[96,97]. Halohydrin dehalogenases belong to the enzyme class of lyases and structurally belong to the short-chain dehydrogenase/reductase superfamily[98]. These enzymes catalyse the reversible dehalogenation of halohydrins to an epoxide, releasing a halide ion. The reverse reaction is highly substrate promiscuous, so the halide is often substituted by other nucleophiles, such as azide or water. Using water, they hydrolyse epoxides to vicinal diols. Despite the apparent similarity, halohydrin dehalogenases are unrelated to epoxide hydrolases and haloalkane dehalogenases and use entirely different catalytic machinery (Ser-Tyr-Arg-Asp).

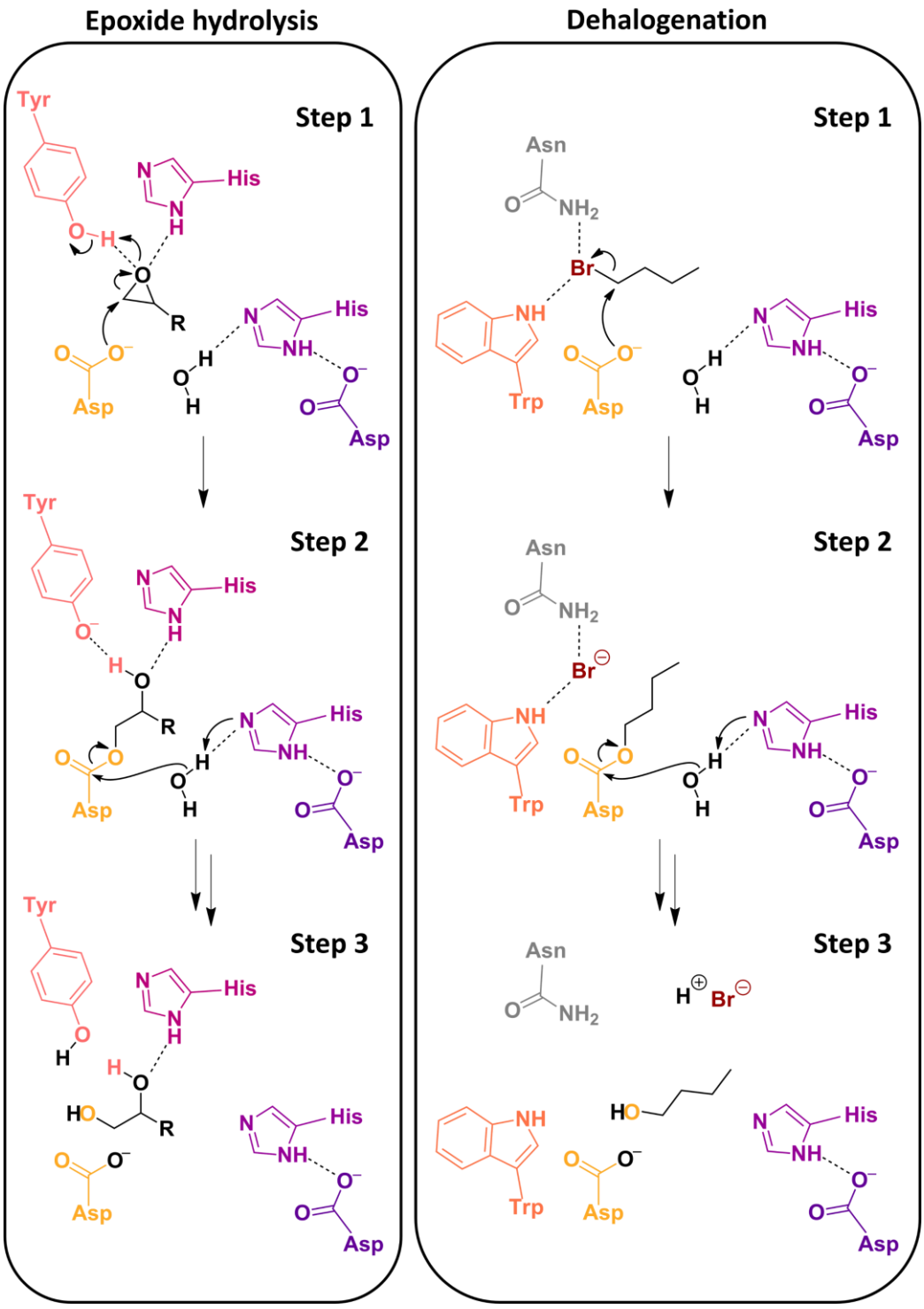

Figure 7. Simplified catalytic mechanisms for epoxide hydrolases[99,100] and haloalkane dehalogenases[90,91]. Both reactions start with a nucleophilic attack on the epoxide or halocarbon by the nucleophilic aspartate (yellow), which results in the formation of an alkyl-enzyme intermediate. The alkyl-enzyme intermediate is hydrolysed by a water molecule activated by the histidine-aspartate pair (purple). Some enzymes utilize a histidine-glutamate pair instead. This leads to the release of a vicinal diol after epoxide hydrolysis or the release of an alcohol in the case of dehalogenation. Possible further intermediates and transition states between step 2 and step 3 were omitted for clarity. Epoxide ring-opening is assisted by a tyrosine-tyrosine or histidine-tyrosine pair (pink), while the halide is stabilised by at least one tryptophan (orange) and usually one other halide-stabilising residue like asparagine or another tryptophan (grey).

1.5.6 Interconverting activities of α/β-hydrolases

Due to their catalytic versatility, α/β-hydrolases are often used as scaffolds for protein engineering in search of improved biocatalysts[101]. The structural and mechanistic similarities within the α/β-hydrolase-fold superfamily make these enzymes attractive targets for attempts at converting enzymes with one catalytic activity into enzymes that catalyse another reaction[28,29,102,103].

It was possible to convert an esterase from *Pseudomonas fluorescens* (PFE) into an epoxide hydrolase[103]. To achieve this, the catalytic serine of the esterase was replaced by an aspartate and two tyrosine residues were introduced at four different positions. However, these changes alone were not enough to convert the esterase into an epoxide hydrolase, and neither was the introduction of three additional conserved epoxide hydrolase residues. Finally, completely exchanging an active site loop from the esterase with one from the epoxide hydrolase EchA from *Agrobacterium radiobacter*[104] resulted in a variant with epoxide hydrolase activity. This demonstrated that it was possible to interconvert completely different α/β-hydrolase activities, but the new enzyme was only about 0.1% as active as a real epoxide hydrolase and suffered from strong substrate inhibition. In addition, due to the many changes needed to achieve the interconversion, it was not possible to explain exactly how the chimeric enzyme worked.[103]

Another successful example of interconversion within the α/β-hydrolase family is the conversion of a plant esterase into a hydroxynitrile lyase using only two amino acid substitutions[102]. The esterase reaction involves an acyl enzyme intermediate, while the hydroxynitrile lyase reaction has a single transition state. The active sites of esterases and hydroxynitrile lyases share a Ser-His-Asp catalytic triad and an oxyanion hole. Although they share the same catalytic triad, the catalytic serine acts as a nucleophile in esterases and a hydrogen bond donor in hydroxynitrile lyases. In hydroxynitrile lyases, a threonine residue partially blocks the oxyanion hole, forcing the aldehyde carbonyl in a different orientation in the active site so the serine interacts with the carbonyl oxygen instead of the carbonyl carbon. Hydroxynitrile lyases also have a lysine residue which hydrogen bonds to cyanide that the esterase did not.[102]

Initially, due to the successful conversion towards epoxide hydrolase activity, PFE was also selected as a starting scaffold for engineering dehalogenase activity. However, it was not possible to introduce the dehalogenase mechanism into the mechanistically simpler esterase. The esterase mechanism uses a Ser-His-Asp triad, and the same carbonyl carbon is attacked twice, once by the catalytic serine and once again by the activated water molecule. In dehalogenases two different carbon atoms are targeted by the nucleophilic attack (Figure 7). First, the catalytic aspartate attacks the carbon atom of the C-X bond of the halogenated substrate and forms the alkyl-enzyme intermediate. Then, the hydrolytic water attacks the Cγ of the catalytic aspartate residue to hydrolyse the alkyl-enzyme intermediate. In practice, the dehalogenase mechanism involves two transition states which are individually stabilised[90]. The difference in the core mechanism makes it challenging to introduce dehalogenase activity into an esterase [103].

Instead of using another esterase, an epoxide hydrolase was selected as the next starting scaffold since the epoxide hydrolases are closely related to haloalkane dehalogenases. The selected epoxide hydrolase, EchA, was the first epoxide hydrolase to be structurally characterised and like in haloalkane dehalogenases its catalytic mechanism had been confirmed to involve a hydroxyalkyl-enzyme intermediate[104–106]. Various mutants of EchA were created based on analysis of its crystal structure and comparison to the haloalkane dehalogenase DhlA, but none of the designed variants showed any detectable dehalogenase activity by the Iwasaki assay[107], phenol red assay[108], gas chromatography-mass spectrometry (GC-MS), or isothermal titration calorimetry (ITC). Introducing more random mutations through error-prone PCR (polymerase chain reaction) and focused directed evolution based on structural analysis did not yield any EchA variants with detectable dehalogenase activity either. A possible explanation for the failed rational design was that the crystal structure for EchA is unreliable due to a glutamine residue that, distorted by crystal packing forces, blocks the active site.

Thus, we searched for a new starting scaffold by modelling the active site of several epoxide hydrolases after the transition states of the dehalogenase DhaA for multiple model substrates. DhaA has a more accessible active site than DhlA, partly because one of its halide-stabilising residues is a smaller asparagine instead of a bulky tryptophan[109]. Of the fourteen modelled epoxide hydrolases, PaeCIF from *Pseudomonas aeruginosa* was most tolerant to the introduction of the mutations required to introduce the dehalogenase stabilising residues. PaeCIF was a promising scaffold, as its active site motifs share more features with haloacetate dehalogenases than with typical epoxide hydrolases. Due to its similarity and close relation to haloacetate dehalogenases PaeCIF was previously tested for both haloacetate and haloalkane dehalogenase activity, but none was reported for the wild-type enzyme[110]. A low level of dehalogenation activity with epibromohydrin was observed for a charge relay acid mutant of PaeCIF (E153Q)[85]. However, due to the mutation of the charge relay acid this variant cannot release the covalently attached hydroxyalkyl intermediate and is unable to complete the reaction.

PaeCIF does not have any of the dehalogenase active site motifs, neither the arginine-rich nucleophilic aspartate motif of haloacetate dehalogenases[111,112] nor the halide-stabilising residues of haloalkane dehalogenases[63,83,110]. After several rounds of designing and screening PaeCIF variants, minor dehalogenase activity was detected using the Iwasaki assay for some variants. Although the first results were promising, reliably reproducing the results proved difficult, primarily due to expression problems and the sensitivity of the available halide detection assays (data unpublished).

1.6 Scope of this thesis

The work in this thesis was performed as part the European Union's Marie Curie Innovative Training Network ES-Cat. The ES-Cat network consisted of ten academic and industrial groups combining rational and combinatorial protein engineering approaches to explore protein sequence space more efficiently. Greifswald University employed two ES-Cat researchers to work on epoxide hydrolases and dehalogenases. Besides further engineering and characterisation of the promising PaeCIF variants, we decided it was also necessary to identify other potential protein scaffolds for the introduction of dehalogenase activity. While my colleague, Aşkin Aslan-Üzel, worked on solving the problems with PaeCIF[113], I set out to identify interesting protein scaffolds through a phylogenetic analysis of the epoxide hydrolases and dehalogenases of the α/β-hydrolase fold family.

Although several established assays were available for the determination of dehalogenase activity, these assays suffer a few major drawbacks. For example, one of the most popular assays, the Iwasaki assay, is not very sensitive and uses extremely toxic chemicals, while pH assays like the phenol red assay are inherently unreliable and insensitive due to the required low buffer concentrations[107,114]. Thus, a new assay for the screening of dehalogenase activity through the selective detection of halides was developed[115]. The halide oxidation assay provides a safer, more reliable, and most importantly more sensitive method to detect dehalogenase activity. Chapter 2 thoroughly describes the methods of the halide oxidation assay, including selective variations of the assay reported by Tang *et al.*[116]

Since converting the epoxide hydrolase PaeCIF to a dehalogenase has proven to be more difficult than expected, especially due to expression problems, we decided to look for other potential scaffolds for protein engineering. Chapter 3 describes the phylogenetic analysis of epoxide hydrolases and haloalkane dehalogenases of the α/β-hydrolase-fold family and the identification of promising screening candidates.

Considering the prevalence of catalytic promiscuity among members of the α/β-hydrolase-fold family[58] and the close relationship and catalytic similarities between epoxide hydrolases and dehalogenases, it seemed odd that no enzyme is known to have both epoxide hydrolase and dehalogenase activity. We argued that it is highly probable that an epoxide hydrolase-dehalogenase enzyme exists, but that it simply had not been found yet due to the absence of sensitive high-throughput assays. Chapter 4 describes the screening of several promising epoxide hydrolases for dehalogenase activity using the newly developed halide oxidation assay.

After promising initial screenings for promiscuous dehalogenase activity, the epoxide hydrolase CorEH from *Corynebacterium* sp. C12 was selected for further screening. Chapter 4 describes the characterisation of CorEH and discusses a hypothetical mechanism to explain the promiscuous activity of CorEH based on its structure and docking experiments.

Chapter 2

Photometric assays for the selective detection of halides

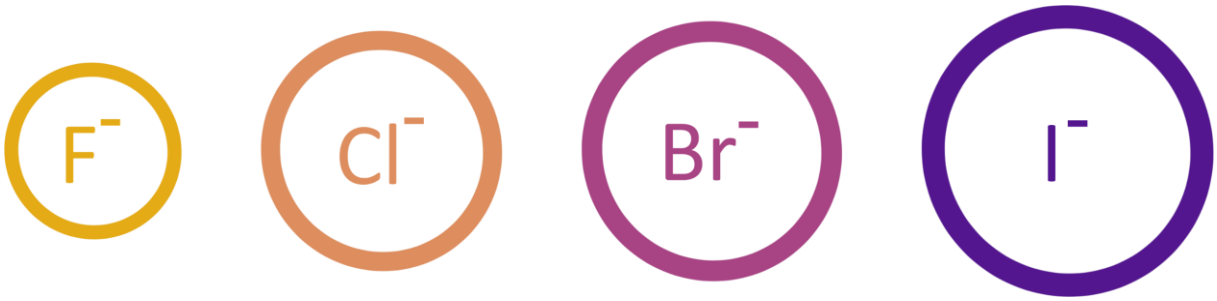

Adapted from:

'Enzymatic Photometric Assays for the Selective Detection of Halides'
Q. Tang, A.S. Aslan-Üzel, **E.D. Schuiten**, C.P.S. Badenhorst, I.V. Pavlidis, U.T. Bornscheuer, *Multienzymatic Assemblies: Methods and Protocols* 2022, 361-375

'An Ultrasensitive Fluorescence Assay for the Detection of Halides and Enzymatic Dehalogenation'
A.S. Aslan-Üzel, A. Beier, D. Kovář, C. Cziegler, S.K. Padhi, **E.D. Schuiten**, M. Dörr, D. Böttcher, F. Hollmann, F. Rudroff, M.D. Mihovilovic, T. Buryška, J. Damborský, Z. Prokop, C.P.S. Badenhorst, U.T. Bornscheuer, *ChemCatChem* 2020, *12* (7), 2032-2039

2.1 Halocarbons, halogenation, and dehalogenation

In modern life halogenated molecules are used as pharmaceuticals, agrochemicals, detergents, pigments, polymers, solvents, degreasing agents, and intermediates in industrial chemical syntheses[68,117]. The carbon-halogen bonds (C-F, C-Cl, C-Br, and C-I) give these molecules their potency and function. In the last few decades, the production of halogenated molecules has increased drastically, and millions of tons of short chain haloalkanes are produced annually and each year several million tons of methyl halides, predominantly chloromethane, are released into the atmosphere by terrestrial and marine biomass[69,70]. Improper disposal, evaporation, spillage, and deliberate release contribute to contamination of the atmosphere, soil, and water with these persistent pollutants[69–71]. Thus, both the incorporation and removal of halide ions are important reactions in organic chemistry and biocatalysis.

Halogenated molecules are widely used, still the chemical process for site specific halogenation remains challenging. Chemical synthesis of halocarbons employs toxic, environmentally hazardous methods, with harsh reaction conditions that rely on toxic reagents and solvents. Poor regioselectivity and unwanted side products are frequent problems that require additional chemical separation methods to obtain chemically pure products. Biocatalytic halogenation by enzymes known as halogenases[118] provides a more effective and ecological pathway. Halogenases, including *S*-adenosyl-L-methionine (SAM)-dependent fluorinases[119] and chlorinases[120], flavin-dependent brominases[121] and iodinases[122], non-haem iron halogenases[123], and Fe/α-ketoglutarate-dependent halogenases[124], introduce carbon-halogen bonds into molecules. These natural catalysts work under mild reaction conditions and are often highly regio- and stereoselective, reducing the number of steps required to obtain a pure product and making the entire process less harmful for the environment. Therefore, current developments in halogenation chemistry and process design are largely inspired by nature and there is a growing interest in identifying and using new halogenases to create new biosynthetic pathways towards new helpful halogenated molecules.

While haloalkanes are very useful molecules with many important applications, their toxicity towards humans and wildlife is problematic. The most promising strategy for environmental remediation is biocatalytic degradation by enzymes known as haloalkane dehalogenases[68,72]. Since their discovery in 1984[71], over 40 haloalkane dehalogenases have been described in scientific literature[78,80–82]. These enzymes hydrolyse a broad range of haloalkanes to the corresponding alcohols, releasing protons and halide ions. Known haloalkane dehalogenases originate from a diverse range of species, including bacteria, archaea, and eukaryotes. How these enzymes evolved to degrade xenobiotic haloalkanes has sparked intense research for over three decades[28,30,84]. Of particular interest is the characterisation of the thousands of putative dehalogenase sequences available in public databases[80]. The rapid accumulation of sequence data in the last few years has created an unmet demand for sensitive and high-throughput assays to screen for dehalogenase activity.

2.1.1 Common methods

Gas chromatography and mass spectrometry (GC-MS) remain the analytical gold standard for identifying the alcohol products of dehalogenation reactions. However, these methods lack the throughput required for screening large libraries, especially when several substrates are tested[62]. Preliminary characterisation of haloalkane dehalogenases therefore often relies on the detection of either the protons or halide ions released during the reaction.

The most popular phenol red[114] and Iwasaki[107] assays are based on the detection of pH changes and halide release, respectively. In 96-well microtiter plate format the phenol red assay has a detection limit of about 500 µM protons[108,114,125]. Recently, more sensitive assays have been developed that utilise fluorescent pH indicators, enabling the detection of 40 to 400 µM protons[108,114,125]. To measure the change in pH caused by dehalogenation, these assays use very low buffer concentrations (<2 mM). Unfortunately, this means that the pH is also easily changed by factors other than enzymatic dehalogenation, reducing the reliability of pH assays. For this reason, the Iwasaki assay has remained popular for the characterisation of dehalogenases. The Iwasaki assay can detect low halide concentrations if large samples are available. In the commonly employed microtiter plate format, variations of the Iwasaki assay were reported to have the detection limits for halide ions between 20 µM and 270 µM[126,127]. However, the assay employs mercuric thiocyanate, which is extremely toxic and fatal when accidentally inhaled or ingested. In addition, the highly toxic waste must be disposed of carefully since it is very harmful to aquatic ecosystems and can contribute to the bioaccumulation of mercury.

With specific activities commonly expressed in nmol/s/(mg protein), most of the currently characterised dehalogenases are not very fast enzymes[80]. Therefore, a significantly more sensitive assay for the detection of halide ions would likely facilitate the discovery of novel dehalogenases that would not be identified using existing methods.

2.1.2 Halide oxidation assay

For these reasons, we developed the halide oxidation (HOX) assay for the detection of halides under mild and environmentally friendly conditions[115]. This novel halide assay is based on the haloperoxidase-catalysed oxidation of chloride, bromide, and iodide. The detection limits of the HOX assay range from 1 µM for chloride and iodide to 20 nM for bromide, making the assay up to three orders of magnitude more sensitive than other halide detection assays currently available. Using the HOX assay, reaction volumes can be as small as 20 µL and less than a picomole of bromide can already be detected, requiring very little sample to give reliable results. This assay is much less toxic than the Iwasaki assay, because the most hazardous chemicals employed by the HOX assay are orthovanadate, used as a cofactor by vanadium-dependent haloperoxidases, and hydrogen peroxide, a common household bleach.

In the HOX assay, halides are first oxidized by the *Curvularia inaequalis* vanadium-dependent chloroperoxidase (*Ci*VCPO) to form hypohalous acids (Figure 8A). *Ci*VCPO was selected due to its high stability in the presence of hydrogen peroxide, compared to haem-dependent haloperoxidases. The resulting hypohalous acids HOCl, HOBr, and HOI, are bleaches that react with probes that generate absorbance, fluorescence, or even luminescence[128].

Aminophenyl fluorescein (APF) was chosen as a probe for the HOX assay, since it is stable in the presence of hydrogen peroxide and produces fluorescein, a bright fluorescent dye (excitation at 488 nm, emission at 525 nm) (Figure 8B)[129]. The hypohalous acids oxidise the aminophenyl group of APF, which then releases 1,4-benzoquinone imine to form fluorescein.

2.1.3 Selective variations

We found that contamination of reagents and buffers with chloride is a common source of background signal, complicating the accurate quantification of halides and requiring enzymes to be dialysed extensively. Therefore, some variations of the HOX assay were developed that could selectively detect bromide or iodide in the presence of chloride. This allows the enzymatic production of bromide and iodide to be detected even in the presence of high chloride concentrations, facilitating applications like screening recombinant enzyme variants in crude bacterial lysates without the need for desalting or dialysis.

The bromide-specific variation of the HOX assay makes use of the vanadium-dependent bromoperoxidase from *Corallina officinalis* (*Co*VBPO). Haloperoxidases are named after the most electronegative halide they can oxidise: chloroperoxidases catalyse the oxidation of chloride, bromide, and iodide, bromoperoxidases mostly use bromide and iodide, and iodoperoxidases only catalyse the oxidation of iodide[130,131]. The selectivity of the *Corallina officinalis* bromoperoxidase for bromide compared to chloride enables selective bromide detection. Amines interfere with the original HOX assay since HOCl and HOBr react with amines to form haloamines. However, bromamines are more reactive than chloramines toward HOX-sensors and thus, amines like taurine can be used to suppress the signal from chloride, further enhancing the selectivity for bromide[129,132–134].

The iodide-selective variation uses a different dye than the HOX assay for the specific detection of iodide in the presence of chloride (Figure 8C). The hypohalous acid oxidizes the chromogen 3,3',5,5'-tetramethylbenzidine (TMB) and generates visible colours, depending on the amount of bleach produced[135]. TMB is converted to the one-electron oxidized cation radical which is in equilibrium with the TMB-diimine complex. The TMB-diimine complex is detectable at 570 nm and colours the reaction blue. Eventually, the orange two-electron diamine product is formed, which is detectable at 460 nm[135]. This means that for lower concentrations of iodide, the assay turns blue and for higher concentrations the mixture turns purple, orange, then bronze, and finally black and the maximum absorption shifts from 570 nm to 460 nm[136]. In the process, the bleach HOI is reduced to iodide. Therefore, iodide is essentially used as a catalyst in the whole process, making the assay very sensitive. We measure production of the TMB-diimine complex at 570 nm and the rate of change ($v = A_{570nm} \cdot s^{-1}$) shows a linear relationship to iodide concentration from 5 µM to 400 µM (although nanomolar concentrations can be detected under optimised conditions). The linearity at 570 nm is lost once the diamine product of TMB is produced. Although TMB also reacts with HOCl, the assay detects micromolar quantities of iodide but is relatively insensitive to even millimolar concentrations of chloride[136,137]. Therefore, this assay can be used for detecting iodide in the presence of chloride-containing crude cell lysates, *in vitro* translation reactions, and whole-cell assays, and even for high-throughput screening. Apart from iodide, TMB can also be applied for the selective detection of bromide[137,138].

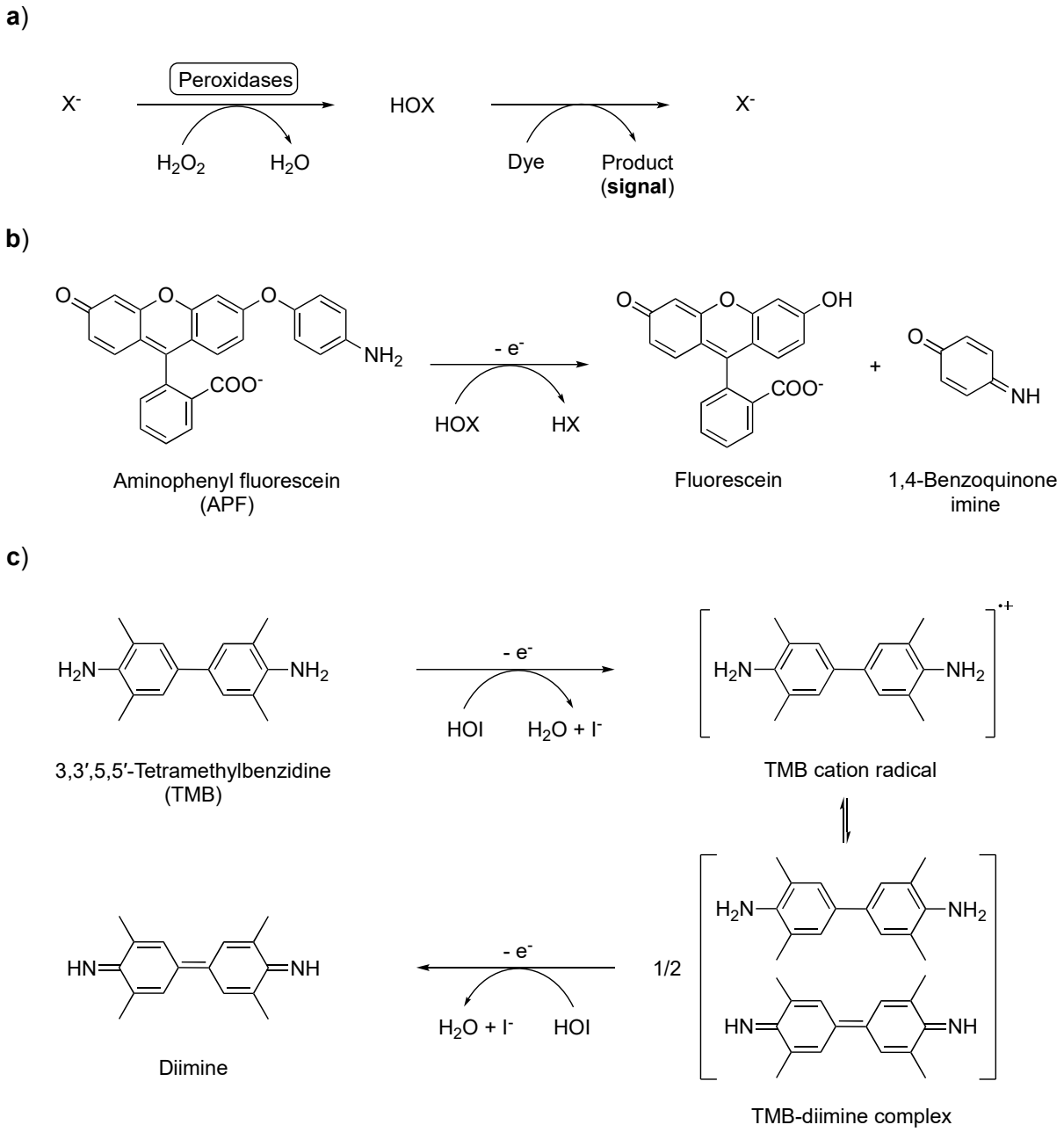

Figure 8. Principles of the halide detection assays. a) Halide ions are oxidized to hypohalous acids (HOX) using hydrogen peroxide (H_2O_2), catalysed by a haloperoxidase. The hypohalous acids react with a probe to form compounds detectable by their colorimetric or fluorescent properties. b) The principle behind the detection of halides by the original HOX assay. Oxidation of aminophenyl fluorescein (APF) by hypohalous acids results in the formation of fluorescein, a bright fluorescent dye that can be detected at nanomolar concentrations. APF can be used to detect chloride, bromide, and iodide ions. c) The principle behind the selective detection of iodide using 3,3′,5,5′-tetramethylbenzidine (TMB). TMB is first converted by hypoiodous acid (HOI) to the one-electron oxidized cation radical which is in equilibrium with the TMB-diimine complex. The TMB-diimine complex is detectable at 570 nm and colours the reaction blue. The TMB-diimine is then converted by another molecule of hypoiodous acid (HOI) to the orange two-electron oxidised diamine product, which is detectable at 460 nm. Figure from Tang 2022[139].

2.2 Results and discussion

2.2.1 Assay sensitivity and detection limits

To test the detection limits of the HOX assay, low concentrations of chloride, bromide, or iodide were added to 40 µL reaction mixtures containing *Ci*VCPO, hydrogen peroxide, and aminophenyl fluorescein. The fluorescence values for the controls were low and increased with the addition of halides (Figure 9). For chloride (Figure 9A) and iodide (Figure 9C) the detection limit was 1 µM. Linear relationships between the halide concentration and detected fluorescence values were observed for all three halides. Although iodide fluorescence values were lower compared to chloride, low-micromolar concentrations can be quantified using this method. In contrast, the fluorescence values for bromide were much higher than both chloride and iodide, making the assay significantly more sensitive. With a detection limit of 20 nM (Figure 9B), nanomolar concentrations of bromide could be quantified. These differences in sensitivity of the HOX assay regarding chloride, bromide, and iodide can be explained by the different reactivities of the hypohalous acids towards aminophenyl fluorescein and HOX-scavenging species (like protein tyrosine residues)[140–143].

With a detection limit of 1 µM for chloride, the HOX assay is 50 to 150-fold more sensitive than alternative existing halide assays like the most popular Iwasaki assay. The HOX assay is three orders of magnitude more sensitive for the detection of bromide and can detect less than a picomole of bromide in a 40 µL assay. Lastly, with a detection limit of 1 µM, the HOX assay is approximately 30-fold more sensitive for iodide than existing halide assays.[115]

2.2.2 Quantifying dehalogenase activity

Two model haloalkane dehalogenases were used to demonstrate that the HOX assay is suitable for the detection and quantification of dehalogenase activity. The recombinant His-tagged dehalogenases DhlA from *Xanthobacter autotrophicus* GJ10[71] and DhaA from *Rhodococcus rhodochrous*[144] were expressed in *Escherichia coli* (*E. coli*) and purified by immobilised metal-affinity chromatography (IMAC). The purified protein samples were dialysed to remove chloride and imidazole. DhaA was used to completely hydrolyse a series of 1-bromobutane solutions (0 to 2.5 mM). As these concentrations are well above the detection range of the HOX assay, the samples were diluted 1000-fold, resulting in a linear relationship between the 1-bromobutane concentration and fluorescence (Figure 10A).

Next, the HOX assay was used to calculate the specific activity of DhlA and DhaA with typical haloalkane dehalogenase substrates: 1,2-dibromoethane, 1,2-dichloroethane, 1,3-dichloropropane, 1-bromo-3-chloropropane and 1-bromohexane (Figure 10D). For the quantification of the chloride and bromide release, standard curves were determined using a series of chloride and bromide concentrations in buffer (Figure 10B and C). The calculated specific activities were comparable to the values determined via a standard GC-MS assay, confirming that the HOX assay can be used to accurately quantify dehalogenase activity. Thus, the HOX assay can be used to identify and characterise novel dehalogenases and may be of interest for those studying other halide-producing enzymes.

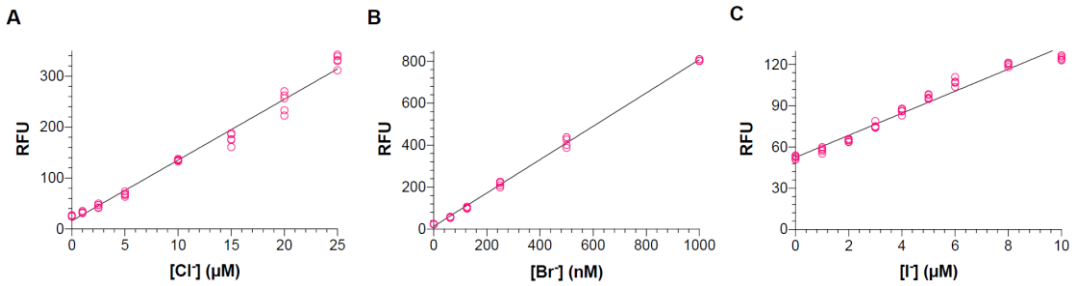

Figure 9. Calibration curves for A) chloride, B) bromide, and C) iodide. The HOX assay can quantify low micromolar concentrations of chloride and iodide and nanomolar concentrations of bromide. Each replicate is plotted as a separate data point (n=5) and the limits of detection are defined as the blank values plus three times the standard deviation of the blank. The detection limits are 1 µM for chloride, 20 nM for bromide, and 1 µM for iodide. GraphPad Prism was used for plotting data and linear regression. Figure from Aslan-Üzel 2021[113].

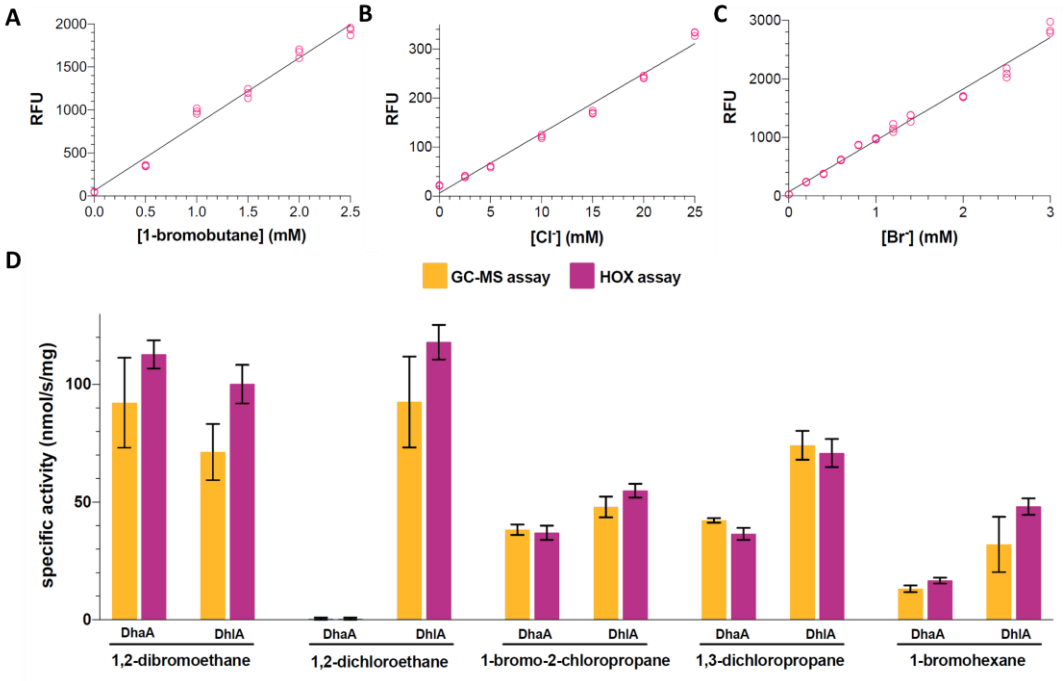

Figure 10. A) The fluorescence signal from the HOX assay is directly proportional to the amount of dehalogenase product formed. The dehalogenase DhaA was used to completely hydrolyse different concentrations of 1-bromobutane. The HOX assay was then used to quantify the amount of bromide produced and a linear increase in fluorescence with increasing 1-bromobutane concentration was observed. This demonstrated that the HOX assay is suitable for quantifying the amount of product produced by dehalogenase reactions. B/C) Standard curves for chloride (B) and bromide (C) allowed the dehalogenation of the five other substrates to be quantified as well. Each replicate is plotted as an individual data point (n=3). D) Comparison of the HOX assay to a standard GC-MS method. The specific activities for the dehalogenases DhaA and DhlA for several substrates were determined using the HOX assay and a standard GC-MS methods in nmol/s/mg. The results of both the HOX and GC-MS assays agree, confirming that the HOX assay is a reliable method for the quantification of dehalogenase activity. For the HOX assay, nine replicates are plotted with standard deviation from three reactions each assayed in triplicate. The small standard deviations demonstrate the excellent reproducibility of the method. For the GC-MS assay, three replicates are plotted with standard deviation. GraphPad Prism was used for plotting the data. Figures from Aslan-Üzel 2021[113].

2.2.3 Selective detection of bromide in the presence of chloride

Since the standard HOX assay is highly sensitive for chloride, significant background signal can be generated from chloride contaminations. To reduce the background signal the selective detection of bromide using a bromoperoxidase instead of *Ci*VCPO was investigated. Bromoperoxidases are more selective for bromide than chloroperoxidases[140]. The *Corallina officinalis* bromoperoxidase gives a significantly higher signal for bromide than for chloride (Figure 11A), with the best results at the optimal pH of 6.5 for the bromoperoxidase.

To reduce the chloride signal further, taurine was added to react with HOCl to form taurine chloramines (Figure 11B). The HOX assay is inhibited by amines and because chloramines are less reactive than bromamines[134] the formation of chloramines supresses the chloride signal. Combining both the bromide selective bromoperoxidase and the addition of taurine allows for the detection of lower concentrations of bromide in the presence of higher concentrations of chloride.

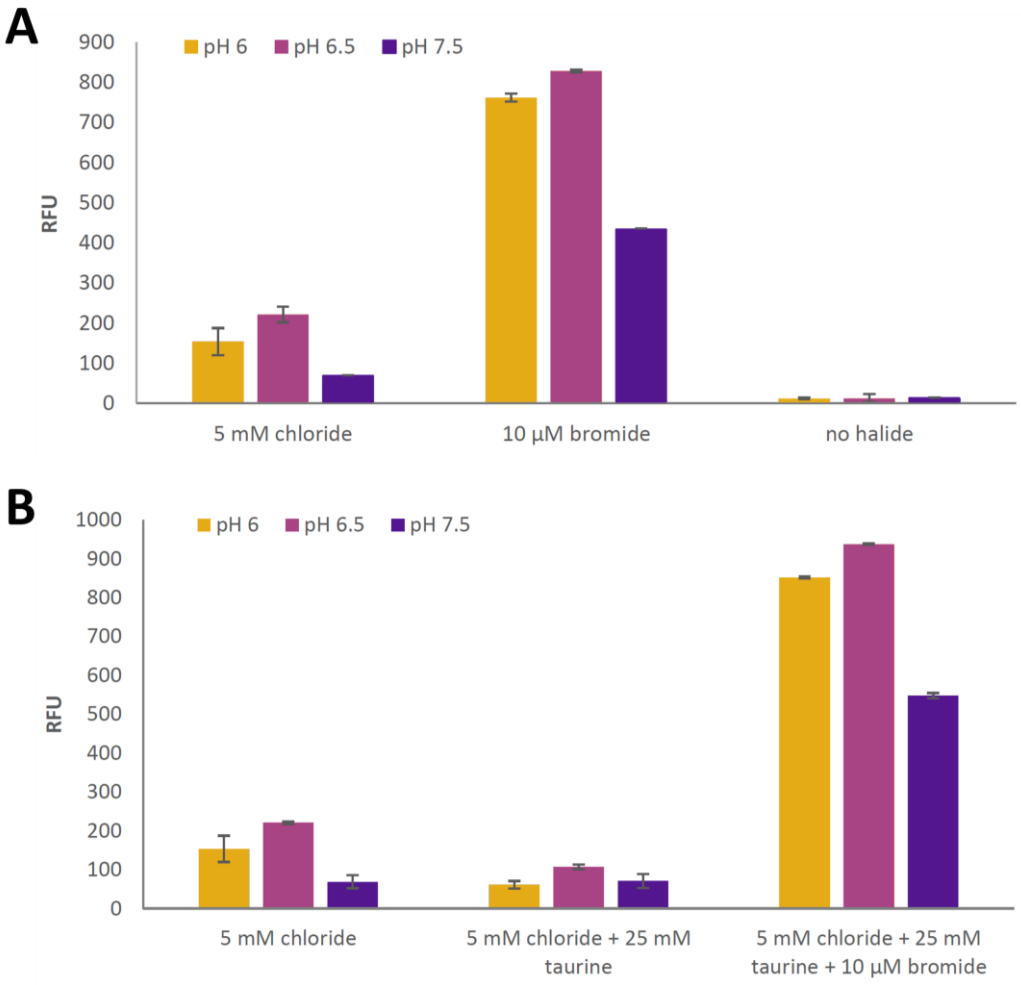

Figure 11. Fluorescence signal with the *Corallina officinalis* bromoperoxidase at different pH values. Standard 40 µL assays were incubated for 2 h before measuring the fluorescence. Reactions were performed in triplicate. A) With *C. officinalis* bromoperoxidase B) With 25 mM taurine added. Figure from Aslan-Üzel 2021[113].

2.3 Preparation and execution of the HOX assay

The following Materials and Methods were adapted from the book chapter 'Enzymatic Photometric Assays for the Selective Detection of Halides'[145]. The material section explains how to prepare all the necessary reagents and the methods section describes how to properly perform both the standard HOX assay and the selective variants.

2.3.1 Materials

Prepare all solutions using analytical grade reagents, analytical grade solvents, and Milli-Q water with a resistance of 18.2 MΩ·cm at 25 °C (or equivalent). Due to the high sensitivity of the general HOX assay towards chloride and the abundance of chloride in a biochemistry lab, extra care should be taken when preparing purified *Ci*VCPO, buffers, and stock solutions for the HOX assay. Prepare and store all reagents at room temperature (unless indicated otherwise). Diligently follow all waste disposal regulations when disposing waste materials, especially when using hazardous substrates such as haloalkanes. All solutions with halogenated compounds must be discarded with halogenated organic waste according to local regulations. All buffers and solutions with orthovanadate should be disposed in the heavy metal waste. For any experiments involving bleach standards, extra care should be taken not to bleach surfaces and clothing and it is important to use appropriate personal protective equipment (lab coats, gloves, and safety glasses).

2.3.1.1 Peroxidases

The wild-type *Ci*VCPO (GenBank: CAA59686.1) is used for the general halide assay. A commercial *Co*VBPO from Sigma-Aldrich (Catalogue No.: B2170) is used for the selective bromide assay. According to the supplier, the chloroperoxidase activity of this bromoperoxidase is <1%, which enables selective detection of bromide in the presence of chloride. The *Ci*VCPO mutant P395D/L241V/T343A (referred to as the *Ci*VCPO triple mutant) was used for iodide assays[146]. However, the wild-type *Ci*VCPO or *Co*VBPO could also be used. *E. coli* TOP10 with pBAD vectors encoding *Ci*VCPO or the *Ci*VCPO P395D/L241V/T343A triple mutant were used for the expression of the two chloroperoxidase variants[146].

2.3.1.2 Cultivation and purification of *Ci*VCPO and the triple mutant

1. Lysogeny broth (LB medium): Dissolve 10 g tryptone, 5 g yeast extract, and 10 g sodium chloride (NaCl) in about 900 mL of distilled or deionized water and adjust the volume to 1 L. Sterilize by autoclaving for 20 minutes at 15 psi (1.05 kg/cm^2) on liquid cycle.
2. Ampicillin stock solution (1000x, 100 mg·mL^{-1}): Dissolve 1 g ampicillin in about 9 mL Milli-Q water and adjust volume to 10 mL. Filter the solution through a 0.22 µm sterile filter into sterile tubes and store at -20°C.
3. L-Arabinose stock solution (500x, 10% w/w): Dissolve 10 g L-arabinose in about 90 mL Milli-Q water and adjust the volume to 100 mL. Filter the solution through a 0.22 µm sterile filter into sterile tubes and store at -20°C.
4. Loading buffer for ion exchange chromatography (50 mM Tris sulfate, pH 8.1): Dissolve 6.06 g tris(hydroxymethyl)aminomethane (Tris) in about 900 mL Milli-Q water. Adjust the pH with concentrated sulfuric acid (H_2SO_4) to pH 8.1 and adjust the volume to 1 L. Filter buffer through a 0.45 µm Corning filter and degas using vacuum or a sonicator.

5. Lysis buffer: Pour 50 mL loading buffer (see step 4) into a 50 mL tube and add 100 mg lysozyme, 50 mg DNaseI and one EDTA-free protease inhibitor cocktail tablet (cOmplete™, Roche, Mannheim, Germany) to prepare a lysis buffer containing 2 mg/mL lysozyme, 1 mg/mL DNaseI and protease inhibitor cocktail. Precool lysis buffer at 4 °C or on ice before purification.
6. Elution buffer for ion exchange chromatography (50 mM Tris sulfate, 1 M NaCl, pH 8.1): Dissolve 6.06 g Tris and 58.44 g NaCl in about 900 mL Milli-Q water. Adjust the pH with concentrated sulfuric acid (H_2SO_4) to pH 8.1 and adjust the volume to 1 L. Filter the buffer through a 0.45 µm Corning filter and degas using vacuum or a sonicator.
7. Washing buffer for ion exchange chromatography (50 mM Tris sulfate, 100 mM NaCl, pH 8.1): For purification using a peristaltic pump, add 45 mL loading buffer (see step 4) and 5 mL elution buffer (see step 6) to a 50 mL tube and mix thoroughly. For purification on a fast protein liquid chromatography (FPLC) system, add 450 mL loading buffer and 50 mL elution buffer to a glass bottle and mix thoroughly. Filter buffer through a 0.45 µm Corning filter and degas using vacuum or a sonicator.
8. Dialysis buffer (50 mM sodium phosphate, 100 µM Na_3VO_4, pH 8.0; chloride-free) (*see* **Note 1**): Weigh 1.65 g $NaH_2PO_4 \cdot H_2O$ (11.925 mmol), 76.31 g $Na_2HPO_4 \cdot 12\ H_2O$ (213.075 mmol), and 82.76 mg Na_3VO_4 (0.45 mmol) and put into a clean 5 L graduated beaker. Add 4.5 L Milli-Q water directly into the beaker according to the graduation scale or use a clean measuring cylinder. Put a clean magnetic stirring bar in the buffer and mix all components on a magnetic stirrer. Leave the magnet in the beaker for the dialysis step. Pour out a small amount of buffer (about 20 mL) into a 50 mL tube to confirm buffer pH using a pH meter (*see* **Note 2**). Precool the dialysis buffer at 4 °C.

2.3.1.3 Halide assay reagents

1. 40 mM hydrogen peroxide solution: Add 4.0 µL 30% (w/w) hydrogen peroxide solution (1.110 g/mL, 9.79 M) to 996 µL Milli-Q water and mix thoroughly (*see* **Note 3**).
2. 5 mM Aminophenyl fluorescein (APF) solution (for the general HOX assay) (*see* **Note 4**): APF solutions are commercially available. The 5 mM solution supplied in dimethylformamide (DMF) (Sigma, Catalogue No.: A4108) is ready to use. For solution supplied in methyl acetate (Cayman Chemicals, Item No.: 10157), the solvent needs to be removed before use. Completely evaporate methyl acetate from the bottle under a gentle stream of nitrogen. Before any APF is taken from the original bottle, add 472.4 µL DMF directly to the 1 mg APF and mix thoroughly to form a 5 mM APF stock solution. Store the APF solution at 4 °C. Alternatively, APF can also be synthesized from fluorescein and 4-fluoronitrobenzene as described in literature[115]. Dissolve 4.23 mg APF in 2 mL DMF and mix thoroughly to form a 5 mM APF stock solution.
3. 500 mM Taurine solution (for the selective bromide assay): Dissolve 62.6 mg taurine in 1 mL Milli-Q water.

4. 3,3',5,5'-tetramethylbenzidine (TMB) stock solution (for the selective iodide assay): A premixed solution of TMB and hydrogen peroxide in a mildly acidic buffer is commercially available (Liquid Substrate System for Membranes; Sigma Aldrich; Catalogue No.: T0565). Although concentrations of components are not known, the solution can be used directly for the assay. Alternatively, prepare a 25 mM TMB stock solution by dissolving 6 mg TMB in 1 mL DMSO.
5. 25 mM Monochlorodimedone (MCD) solution (for determination of the activity of *Ci*VCPO and the triple mutant): Dissolve 44 mg MCD in 10 mL ethanol.
6. Reaction buffers (20 mM sodium phosphate, 1 mM Na_3VO_4; chloride-free) (*see* **Notes 1** and **4**): Weigh 183.9 mg Na_3VO_4 (1 mmol) into a 1 L graduated glass bottle. Add 1 L of 20 mM sodium phosphate buffer (pH 6.0). Seal the glass bottle with the lid and shake until all components are completely dissolved and mixed properly. Pour out a small amount of buffer (about 20 mL) into a 50 mL tube to confirm buffer pH using a pH meter (*see* **Note 2**). For the selective bromide assay, use 20 mM sodium phosphate, pH 6.5, for preparation of this solution.

2.3.1.4 Halide standard solutions.

Halide standard solutions (10 mM): Weigh 29.2 mg NaCl or 37.3 mg KCl, 51.4 mg NaBr or 59.5 mg KBr, or 74.9 mg NaI or 83.0 mg KI directly in clean 50 mL tubes. Fill to 50 mL with Milli-Q water (*see* **Note 5**). Dilute stock solutions to give 10 mL standard solutions of 0 µM to 500 µM in 15 mL tubes and mix thoroughly (Table 1). For the bromide assay, dilute the 10 mM bromide stock solution to standard solutions of 0 µM to 20 µM in 50 mL tubes and mix thoroughly (Table 2).

Table 1. Preparation of 10 mL halide standard solutions from 10 mM stock solutions.

Final concentration (µM)	0	20	50	100	200	300	400	500
10 mM standard (µL)	0	20	50	100	200	300	400	500
Milli-Q water (mL)	10.00	9.98	9.95	9.90	9.80	9.70	9.60	9.50

Table 2. Preparation of 50 mL bromide standard solutions from a 10 mM bromide stock solution.

Final concentration (µM)	0	2	5	10	15	20
10 mM standard (µL)	0.00	10	25	50	75	100
Milli-Q water (mL)	50	49.99	49.98	49.95	49.93	49.90

2.3.1.5 Reaction mixtures for the assays

1. Reaction mixture for haloperoxidase activity: In 451 µL of the pH 6.0 reaction buffer (*see* Halide Assay Reagents step 6), add 1 µL of 25 mM MCD solution, 132 µL of 40 mM hydrogen peroxide solution, 6 µL of 10 mM bromide standard solution, and mix thoroughly.
2. Reaction mixture for general halide assay: Add 50 µL 40 mM hydrogen peroxide solution, 5 µL of 5 mM APF, and 50 µL of 50 U/mL *Ci*VCPO to 895 µL of reaction buffer (pH 6.0) in a centrifuge tube and mix thoroughly (*see* **Notes 6** and **7**).
3. Bromide assay solution: Add 50 µL 40 mM hydrogen peroxide solution, 5 µL 5 mM APF, and 50 µL 6 U/mL *Co*VBPO to 845 µL of reaction buffer (pH 6.5) in a centrifuge tube (*see* **Note 7**). Add 50 µL of 500 mM taurine to the assay solution to suppress the chloride signal and mix all components thoroughly (*see* **Note 8**).

4. Iodide assay solution: Mix 10 µL *Ci*VCPO triple mutant (137 U/mL) with 990 µL commercial TMB/hydrogen peroxide mixture solution (*see* **Notes 7** and **9**). If the commercial TMB solution is not available, add 50 µL 40 mM hydrogen peroxide solution, 10 µL 25 mM TMB solution, and 10 µL *Ci*VCPO triple mutant (137 U/mL) to 930 µL of reaction buffer (pH 6.0).

2.3.1.6 Consumables and measuring devices

Black 384-well microtiter plates are used to perform the fluorescence-based halide assays and transparent 384-well polystyrene microtiter plates are used for the iodide assays. Standard reaction volumes are 40 µL and 50 µL, respectively, but may be increased or decreased as desired. 96-well microtiter plates can be used for higher reaction volumes, for example 100 or 200 µL. The volume of each component should be adjusted accordingly. Fluorescence measurements are performed with plate readers that excite at 488 nm and measure emission at 525 nm. Plate readers that can measure absorbance at 570 nm are used for the iodide assay. Spectrophotometers that accept a 1 cm-pathlength quartz cuvette and measure at 290 nm are used for the MCD assay for determination of the activities of *Ci*VCPO and the triple mutant.

2.3.2 Methods

2.3.2.1 Cultivation and purification of *Ci*VCPO and the triple mutant

1. Add 10 µL ampicillin stock solution (100 mg/mL) to 10 mL LB medium, for a final concentration of 100 µg/mL ampicillin, in a sterile 50 mL tube. Inoculate with a single colony of *E. coli* TOP10 transformed with the pBAD-*Ci*VCPO or the pBAD-*Ci*VCPO triple mutant plasmid. Incubate the 50 mL tube overnight at 37 °C, shaking at 180 rpm.
2. Add 1 mL ampicillin stock solution (100 mg/mL) to 1 L LB medium, for a final concentration of 100 µg/mL ampicillin. Inoculate the LB medium with overnight culture. Incubate at 37 °C, shaking at 180 rpm. Monitor the OD_{600} of the culture until it reaches about 0.5. Then add 2 mL 10% (w/w) L-arabinose stock solution for a final concentration of 0.02% to induce expression of *Ci*VCPO. Incubate the culture at 25 °C, shaking at 180 rpm, for 24 h.
3. Harvest cells by centrifugation at 4,500 x *g* for 30 minutes in a precooled (4 °C) centrifuge. Resuspend cells in precooled lysis buffer (1 mL per gram of cells). Lyse cells on ice by sonication (three cycles of 5 min, 50% pulse, and 50% power) using a SONOPULS HD 2070 (BANDELIN electronic GmbH & Co. KG, Berlin, Germany) or an equivalent device. Centrifuge the crude cell lysate at 10,000 x *g* at 4 °C for 1 h for clarification. Transfer the clarified lysate to a 200 mL beaker.
4. Measure the volume of the clarified lysate. Add an equal volume of isopropanol, mix thoroughly, and incubate on ice for 20 min. Centrifuge the lysate-isopropanol mixture at 10,000 x *g* at 4 °C for 30 minutes to remove precipitated proteins. Transfer the supernatant to clean tubes.
5. Equilibrate the 5 mL DEAE Sephacel column with 25 mL loading buffer (5 column volumes). Load the cell lysate on the DEAE Sephacel column. Wash the column with 25 mL loading buffer and then with 25 mL washing buffer to remove weakly bound proteins. Elute *Ci*VCPO from the column using 30 mL elution buffer and collect the eluate in fractions of 1 to 1.5 mL. Confirm presence and purity of the haloperoxidase by SDS-PAGE (*see* **Note 10**) and combine the fractions containing the haloperoxidase.

6. To obtain the chloride-free, active vanadium-bound *Ci*VCPO, dialyse the *Ci*VCPO eluate three times against chloride-free, orthovanadate-containing dialysis buffer. After moistening the dialysis membrane (10 kDa MWCO) with some dialysis buffer, fold one end of the membrane twice and clamp it with clips. Transfer all *Ci*VCPO eluate carefully into the dialysis membrane, fold the open end twice and clamp (*see* **Note 11**). Dialyse the *Ci*VCPO eluate against 4.5 L precooled dialysis buffer on a magnetic stirrer in a cold room for 4 h. Replace the dialysis buffer and dialyse the eluate for another 4 h. Afterwards, replace the dialysis buffer and dialyse the eluate overnight (*see* **Note 12**). Aliquot the chloride-free, active vanadium-bound *Ci*VCPO into centrifuge tubes and store at 4 °C (*see* **Notes 13** and **14**). Measure the absorbance of *Ci*VCPO at 280 nm using a NanoDrop™ (Thermo Fisher, Hennigsdorf, Germany) or an equivalent device. Calculate the protein concentration of *Ci*VCPO (*see* **Note 15**).

2.3.2.2 Preparation of *Co*VBPO

The commercial *Co*VBPO described under *Peroxidases* was used for selective bromide detection in the presence of chloride. Dissolve the entire vial of *Co*VBPO by adding 400 µL dialysis buffer. Transfer the solution to a dialysis device fit for small volumes like the Thermo Scientific Slide-A-Lyzer MINI Dialysis Devices (10 kDa MWCO, Catalogue No.: 69570). Dialyse it three times against 800 mL dialysis buffer for 1 h to remove MES buffer and other salts and obtain the active vanadium-bound *Co*VBPO. Transfer the *Co*VBPO to a 2 mL tube and adjust the volume to 1.67 mL with the dialysis buffer to obtain a 6 U/mL *Co*VBPO stock solution. Store at 4 °C.

2.3.2.3 Determination of haloperoxidase activities

Specific activities of *Ci*VCPO and the triple mutant are determined using the MCD assay. Bromination of MCD results in a decrease in absorbance at 290 nm ($\Delta\varepsilon$ = 19,900 $M^{-1}\cdot cm^{-1}$). Add the haloperoxidase activity reaction mixture directly into a 1 cm-pathlength quartz cuvette and mix all components by pipetting. Final concentrations of MCD, hydrogen peroxide, and bromide in the reaction mixture are 42 µM, 8.8 mM, and 100 µM, respectively. Measurement of the brominating activity of *Ci*VCPO is initiated by adding 10 µL purified *Ci*VCPO or the triple mutant. The decrease in absorbance at 290 nm ($\Delta A_{290\ nm}$) is monitored in a spectrophotometer. One unit of *Ci*VCPO or the triple mutant produces 1 µmol of brominated MCD per minute (*see* **Note 16**).

2.3.2.4 General Halide Assay (HOX assay)

1. Add 38 µL assay solution per well of a black 384-well microtiter plate, then add 2 µL sample or the halide standard solutions (*see* **Notes 17** and **18**). Final concentrations of hydrogen peroxide, APF and *Ci*VCPO in the reaction mixture are 2 mM, 25 µM, and 2.5 U/mL, respectively. Mix reactions thoroughly by pipetting or shaking on a microplate shaker (2.2 mm amplitude) at 600-800 rpm for 10 s. Cover the plate with a microtiter plate sealing film to avoid contamination and evaporation. Incubate the microtiter plate at room temperature for 60 minutes in the dark.
2. After incubation, measure the fluorescence of the reactions at 525 nm with excitation at 488 nm (*see* **Note 19**). For determination of the halide concentrations in samples, first obtain the standard curve of the corresponding halide by plotting the fluorescence signal against the concentrations of halide standards (*see* **Note 20**). Then calculate the halide concentrations in samples by comparing to the corresponding halide standard curve (*see* **Note 21**).

2.3.2.5 Selective bromide detection in the presence of chloride

This assay is performed at pH 6.5 due to the different pH optimum of the *Co*VCPO[147]. Add 38 µL bromide assay solution per well of a black 384-well microtiter plate, then add 2 µL sample or the bromide standard solutions. Final concentrations of hydrogen peroxide, APF, and *Co*VBPO in the reaction mixture are 2 mM, 25 µM, and 0.3 U/mL, respectively. Then follow the mixing, incubation and measurements in **steps 1-2** described in for the general HOX assay (*see* **Note 21**).

2.3.2.6 Iodide detection

1. Add 50 µL iodide assay solution to the wells of a transparent 384-well polystyrene microtiter plate. Final concentrations of hydrogen peroxide, TMB, and *Ci*VCPO in the reaction mixture are 2 mM, 250 µM, and 1.37 U/mL, respectively. Then add 1 µL sample or the iodide standards to the assay solution. Mix reactions thoroughly by pipetting or shaking on a micro-plate shaker (2.2 mm amplitude) at 800 rpm for 10 s.
2. Immediately measure sample absorbance at 570 nm every 10 s for 2 minutes. Calculate the initial rate of increase in absorbance at 570 nm ($v = A_{570nm}/s$) (*see* **Note 23**). For determination of the iodide concentrations in samples, first obtain the standard curve of iodide by plotting the A_{570nm}/s against the concentrations of iodide standards (*see* **Note 24**). Then calculate the iodide concentrations in samples by comparison to the iodide standard curve (*see* **Note 19**).
3. For high-throughput screening, repeat **step 1** and incubate the reactions at room temperature for 30 minutes. By comparing the colours of sample reactions to the iodide standard reactions, iodide concentrations of samples can be estimated (*see* **Note 25**).

2.3.3 Notes

1. Try to use fresh buffer components and keep them only for the halide assays to avoid contamination with chloride. Rinse all glassware (glass bottles, measuring cylinders) and reusable utensils (spatulas and magnetic stirring bars) at least three times with Milli-Q water in addition to normal cleaning before use.
2. Avoid putting pH probes directly into the chloride-free buffers. Since pH probes are stored in 3 M KCl, chloride contamination from the electrode is highly likely. Thus, check the pH of chloride-free buffers using an aliquot that will be discarded after verification of the pH.
3. Prepare fresh 40 mM hydrogen peroxide solution prior to the assay.
4. Aliquot assay components after preparation. This prevents contamination of the reagent stocks.
5. Iodide standard solutions can be kept at room temperature for a few months. Discard when they turn yellow.
6. To avoid accidental contamination by chloride, use pre-packed (preferably filter) pipette tips for preparing assay solutions and during the assay.
7. Prepare fresh assay master mix prior to the assay. We recommend using 250 µM of TMB rather than 25 mM as described by Tang et al[116].
8. Taurine is added as a scavenger of HOCl. It forms taurine chloramine when reacting with HOCl. Chloramines are less reactive than bromamines, allowing HOBr to be detected selectively.
9. Prepare assay solutions in brown tubes and keep out of direct sunlight.
10. Expected size of *Ci*VCPO and the triple mutant is 67.5 kDa.
11. Wear clean gloves when handling the dialysis membrane to avoid introduction of chloride from sweat on the hands.
12. It is advisable to dialyse the enzyme after purification instead of using PD10 desalting columns. At 98% desalting capacity, PD10 columns do not remove enough of the salts used in purification. In contrast, three rounds of dialysis (100x sample volume, >4 h per round) will be sufficient.
13. Make sure to dialyse the purified *Ci*VCPO and the *Ci*VCPO triple mutant eluate three times to completely remove chloride and Tris since the HOX assay is highly sensitive to residues of chloride, and amines can inhibit the HOX assay.
14. *Ci*VCPO and the triple mutant are highly stable and can be stored in the fridge for extended periods.
15. Concentration of *Ci*VCPO or mutant in mg/mL

$$\text{Concentration } \left(\frac{mg}{mL}\right) = \frac{\text{Absorbance at 280nm}}{\text{Extinction coefficient } \times \text{ Pathlength}} \times \text{Molecular weight}$$

$$\text{Concentration } \left(\frac{\text{mg}}{\text{mL}}\right) = \frac{\text{Absorbance at 280nm}}{91915\ \text{M}^{-1}\text{cm}^{-1} \times\ 1\ \text{cm}} \times 67546\ \text{g/mol}$$

16. Specific activity of *Ci*VCPO or mutant in µmol·min^{-1}·mg^{-1} or U

$$\text{Specific activity } \left(\frac{\mu\text{mol}}{\text{min} \cdot \text{mg}}\right) = \frac{\Delta A_{290\text{nm}} \times \text{Reaction volume}}{\text{Extinction coefficient of MCD} \times \text{Pathlength} \times \text{EV x EC}}$$

With EV = enzyme volume in mL and EC = enzyme concentration in mg/mL

$$\text{Specific activtity } \left(\frac{\mu\text{mol}}{\text{min} \cdot \text{mg}}\right) = \frac{\Delta A_{290\text{nm}}\,(\text{min}^{-1}) \times 600\ \mu\text{L}}{19{,}900\ \text{M}^{-1}\text{cm}^{-1} \times 1\ \text{cm} \times 0.01\ \text{mL} \times \text{EC}\ \left(\frac{\text{mg}}{\text{mL}}\right)}$$

17. After preparation of the assay master mix, first use Milli-Q water as a sample and measure the background signal as a negative control. If the background signal is too high, check all components for chloride contamination and discard any contaminated aliquots.
18. Space out samples on the assay plate to avoid cross-contamination by, for example, accidentally pipetting into the wrong well (especially with 384-well plates).
19. Perform each assay in triplicate to increase accuracy of the assay. The amount of *Ci*VCPO and triple mutant used in the assays can be adjusted according to different requirements. However, make sure to use the same master mix for the standard curves and samples.
20. Fluorescence signal of the HOX assay is linear to halide ions in the following ranges: 0–25 µM for chloride, 0–1000 nM for bromide, and 0–10 µM for iodide[115].
21. Avoid using buffer reagents with amino groups in the samples. Amines can inhibit the HOX assay.
22. Buffer reagents with amino groups can be used in the samples in this assay.
23. Calculate the initial rate of change in absorbance at 570 nm (v = $A_{570\ nm}$/s) using the first few measured absorbance values that are linearly proportional to the measurement time. The linearity will be lost when the diimine product of TMB starts forming.
24. Initial rate of change in absorbance at 570 nm (v = $A_{570\ nm}$/s) of the selective iodide assay is linear to iodide standards ranging from 0 µM to 400 µM[116]. When using self-prepared TMB and hydrogen peroxide mixture in reaction buffer, the range of iodide detection can be different.
25. Reaction mixtures will turn blue, purple, bronze, orange, and eventually black with increasing iodide concentration and incubation time[116].

Chapter 3

Phylogenetic analysis of epoxide hydrolases and dehalogenases

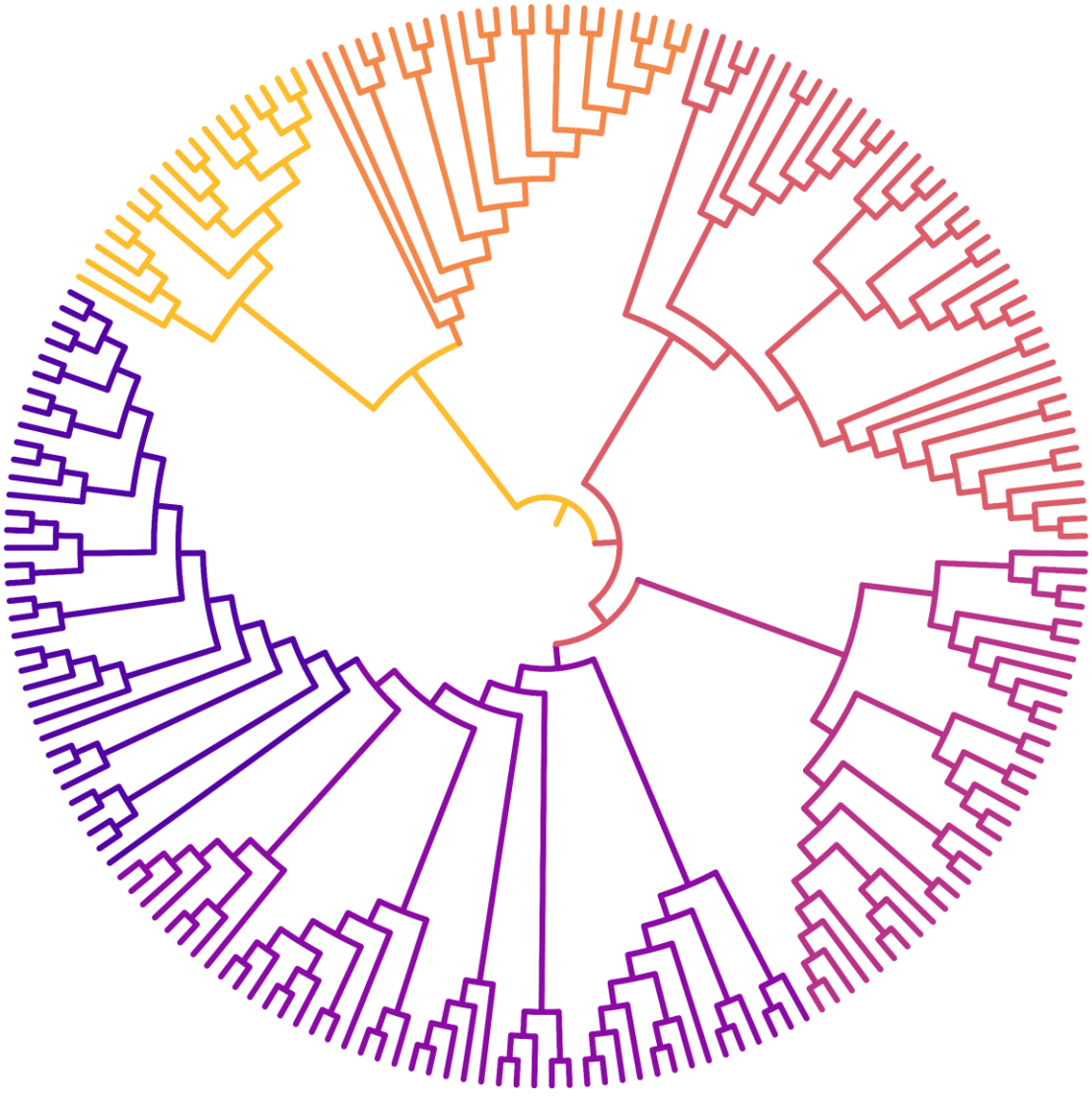

3.1 Evolutionary relationships between α/β-hydrolases

Enzymes are grouped together with other similar proteins into structural families and superfamilies. Members of a structural family share significant structural elements and mechanistic similarity is also quite common. One of the largest structural superfamilies is the α/β-hydrolase-fold family, which includes many enzymes such as acyltransferases, oxidoreductases, lyases, epoxide hydrolases and dehalogenases[58,59]. The adaptable scaffold and versatile catalytic residues of the α/β-hydrolase fold family enabled the divergent evolution of a large variety of enzymes with different catalytic activities. Within structural superfamilies like the α/β-hydrolase fold family the primary function of one family member is often found as promiscuous activity in other family members[36,40,64]. The structural similarities and prevalent cross-reactivity among α/β-hydrolases suggest a common evolutionary origin for the catalytically diverse enzymes in the family. Catalytic promiscuity is thought to play an important role in the emergence of novel functions by providing a starting point for divergent evolution towards different enzymatic activities[41–46]. However, while some promiscuous activities are frequently observed among α/β-hydrolases and no enzyme has been reported with both epoxide hydrolase and dehalogenase activity, despite their significant structural and mechanistic similarities. Here, phylogenetic analyses are used to explore the evolutionary relationships between epoxide hydrolases, haloacetate dehalogenases and haloalkane dehalogenases with the aim to identify promising candidates for protein engineering and screening towards dehalogenase activity.

3.1.1 Molecular phylogenetics

Evolutionary relationships between closely related biomolecules like epoxide hydrolases and dehalogenases can be explored through molecular phylogenetics. This branch of phylogeny focuses on the analysis of genetic molecular differences found in amino acid or DNA sequences. The idea is simple; if two organisms are closely related, the sequences of their genes and proteins should be similar. As the evolutionary distance between the organisms becomes larger, the sequences become more and more distinct[8,9]. Using this theory, a phylogenetic tree can be derived from looking at the similarities and differences in the amino acid or DNA sequences.

A phylogenetic tree is a branching diagram that visualizes the relationships between the different species in a dataset. The external nodes, or leaves, represent existing species and are connected through branches. Each branch combines with another to form an internal node, representing a theoretical common ancestor. A phylogenetic analysis starts with building a solid dataset of homologous extant sequences. These sequences are aligned, and a multiple sequence alignment (MSA) is used to construct a phylogenetic tree[17–19]. The most commonly used maximum likelihood computational method assumes that a tree with the minimum number of amino acid substitutions is most likely and uses evolution models to approximate realistic amino acid substitution. Which evolutionary model is the most accurate representation of reality is dependent on the dataset and can be determined using programs like ProtTest[20,21].

The resulting phylogenetic tree can be used to identify interesting extant enzymes. We are interested in finding suitable epoxide hydrolase protein scaffolds to engineer promiscuous dehalogenase activity. We also assume that it is highly probable that an epoxide hydrolase-dehalogenase enzyme exists but has not been identified yet. Therefore, we searched for promising epoxide hydrolases with close relations to the dehalogenase branches for screening for dehalogenation. In addition, we attempted to engineer a promiscuous enzyme through ancestral sequence reconstruction.

3.1.2 Reconstructing ancestral sequences

Molecular phylogeny and extant sequences can be used to resurrect extinct ancient proteins and other biomolecules[9,23–26]. Ancestral sequence reconstruction (ASR) attempts to reconstruct ancestral sequences based on their existing descendants and characterise them in the laboratory. By combining the multiple sequence alignment, the evolutionary relationships from the phylogenetic tree, and evolutionary models, a hypothetical sequence of the theoretical ancestor can be determined. ASR is often used to study functional divergence within protein families but can also be used to obtain similar enzymes with different properties such as higher thermostability[27–32].

3.2 Phylogenetics

3.2.1 Collecting sequences

To start the phylogenetic analysis, a dataset of epoxide hydrolases and dehalogenases was needed. Homologous proteins are usually found through protein databases such as NCBI[10] or UniProt[11] using search algorithms like BLAST[12]. Because we are interested in α/β-hydrolases, the 3DM α/β-hydrolase fold enzyme family database from Bio-Prodict[148] was used. The 3DM information systems collect, combine, and integrate many different types of protein-related data for protein super-families. The system allows for quick comparison between sequences through the high-quality structure-based multiple sequence alignment. 3DM determines a core of structurally conserved residues and aligns these residues. Any residues in equivalent 3D positions in the structure will be assigned the same core number, so that residues at interesting positions can easily be compared between many different protein sequences. The core numbering system is unique to 3DM, and core numbers will be annotated as c# (e.g. c1, c2 etc.). The α/β-hydrolase fold enzyme family database contains almost all available α/β-hydrolase-fold enzymes. To select only potential epoxide hydrolases and dehalogenases from the database we needed to identify the correct markers, or catalytic motifs, for their respective activities.

3.2.2 Identifying markers

Epoxide hydrolases (EH), haloacetate dehalogenases (HacD), and haloalkane dehalogenases (HLD) all use the same Asp-His-Asp/Glu catalytic triad. This triad produces an alkyl-enzyme intermediate, an ester derivative of the catalytic aspartate, through a nucleophilic attack, after which the alkyl-enzyme intermediate is hydrolysed by an activated water molecule [62,63]. To properly make use of the 3DM database, the 3DM core numbers of the important catalytic residues are determined. All three residues of the catalytic triad can be assigned a core number; the catalytic nucleophile is c96, the histidine base is c188 and the charge relay acid is either c121 or c159 depending on its position in the sequence (Figure 12).

In addition to the catalytic triad, all three enzyme classes have different additional supporting residues. Epoxide hydrolases have two epoxide ring-opening residues, of which only the second residue, the tyrosine in the helix α8, is represented in the core alignment at c132. Most epoxide hydrolases utilise two tyrosine residues[88], but a few distinct epoxide hydrolases use a histidine-tyrosine pair instead[89]. Haloacetate dehalogenases have two carboxylate-binding arginine residues close to the catalytic nucleophile at core positions c97 and c100 (Figure 12). In addition, many haloacetate dehalogenases have a halide pocket with three halide stabilising residues[112]. Two of these residues, a histidine and a tryptophan, are highly conserved among haloacetate dehalogenases but are in a highly variable part of the cap domain and thus are not present in the core alignment. The third residue of the halide pocket is a tyrosine residue at c132 in the core alignment. This tyrosine residue overlaps with the epoxide ring-opening tyrosine of epoxide hydrolases. In addition, the histidine residue of the halide pocket outside of the core alignment also overlaps with the histidine residue of the histidine-tyrosine epoxide ring-opening pair in epoxide hydrolases. Most haloalkane dehalogenases have two halide-stabilising residues. The primary halide-stabilising residue can be found in all haloalkane dehalogenases and corresponds to core number c97. The secondary halide-stabilising residue of DhlA (Figure 12) and other haloalkane dehalogenases of the HLD-I subfamily is not present in the core alignment. In haloalkane dehalogenases from the subfamilies HLD-II and HLD-III, the secondary halide-stabilising residue is found in the HGxP motif. This motif is represented in the core alignment and the secondary halide-stabilising residue can be assigned c30 (Figure 12).

The core numbers of the known important catalytic residues are used to filter the α/β-hydrolase fold enzyme family database and enable quick comparison of the catalytic residues of the sequences in the alignment. The catalytic nucleophilic aspartate at c96 and the histidine base at c188 were used to obtain a large dataset (D96H188) of 19,600 sequences. According to the annotations in 3DM, D96H188 contains 8,230 potential epoxide hydrolases and 2,920 potential dehalogenases. The charge relay acid was not used as a filter because it can be found at two different core positions (c121 and c159) and can also be either an aspartate or a glutamate. In addition, D96H188 already seemed to include mostly sequences that have a potential charge relay acid at either position making it unnecessary to apply this as an additional filter.

The sequences collected in D96H188 differ greatly in sequence length. While characterised α/β-hydrolases are usually approximately 300 residues long, D96H188 included several sequences over 1000 residues long. To improve the quality of the overall alignment, the length of the sequences was limited to a maximum deviation of 10% from the average sequence length of 294. The number of 294 residues was chosen as it is the most common length for the sequences included in the dataset and coincides with the average length for a representative set of epoxide hydrolases and dehalogenases (PaeCIF from *Pseudomonas aeruginosa,* EchA from *Agrobacterium radiobacter*, DhaA from *Rhodococcus rhodochrous* and DhlA from *Xanthobacter autotrophicus* GJ10). With the selection cut-off at 10%, only sequences with a length between 264 and 324 residues were included in the next iteration of D96H188.

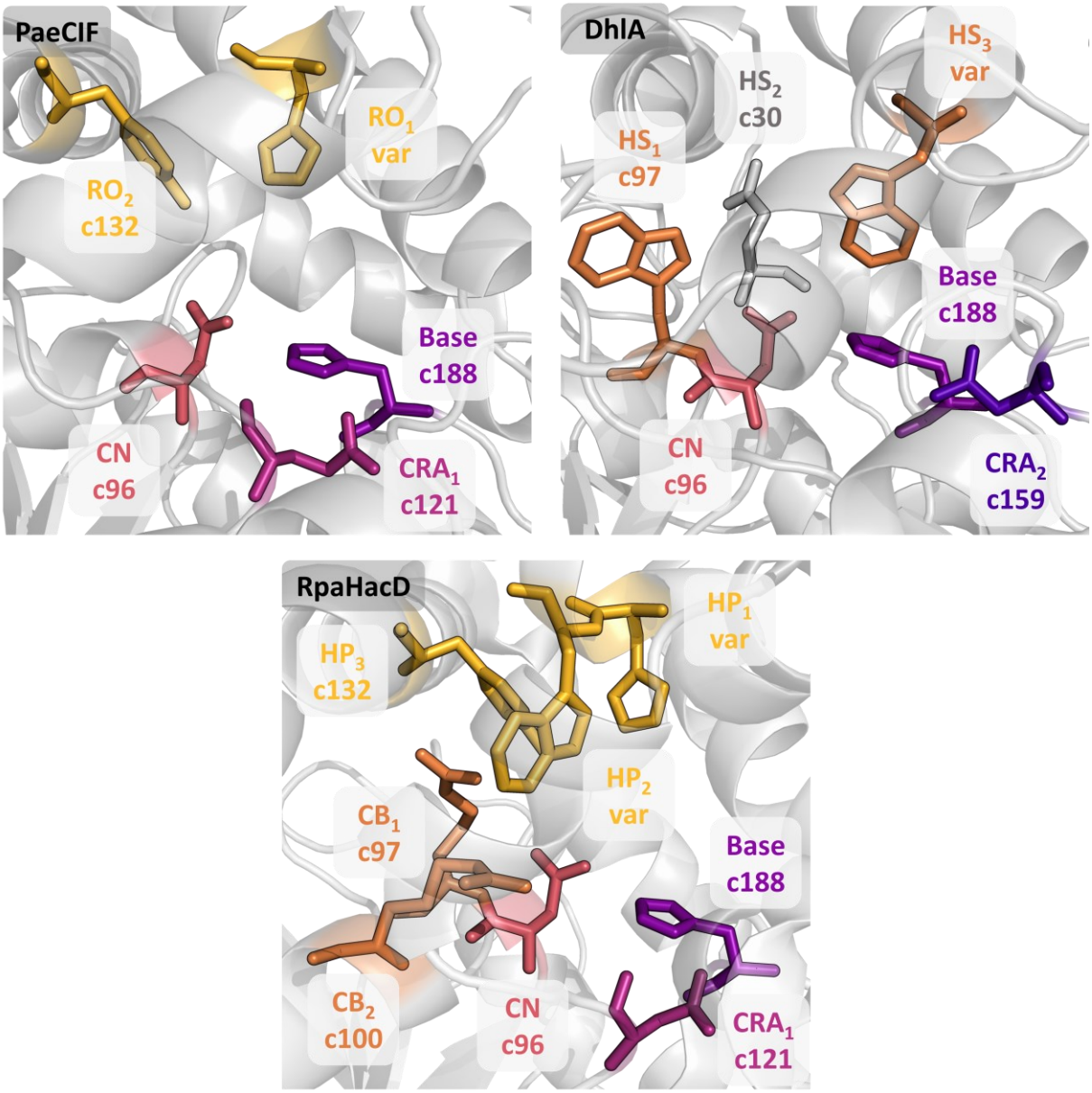

Figure 12. Overview of the active sites of epoxide hydrolases (PaeCIF from *Pseudomonas aeruginosa*[85,89], PDB ID: 3KD2), haloalkane dehalogenases (DhlA from *Xanthobacter autotrophicus* GJ10[90], PDB ID: 2HAD), and haloacetate dehalogenases (RpaHacD from *Rhodopseudomonas palustris*[149], PDB ID: 3R3U) with 3DM core numbers of the α/β-hydrolase fold enzyme family database[148]. The catalytic triad with the catalytic nucleophile (CN, pink), the charge-relay acid (CRA) at position 1 (CRA_1, dark pink) or 2 (CRA_2, dark purple), and the histidine base (B, purple) are shown. For the epoxide hydrolase CorEH, the epoxide ring-opening pair (RO_1 & RO_2, yellow) consists of one histidine and one tyrosine residue respectively. The primary halide-stabilising residue (HS_1, orange) and secondary halide-stabilising residue (HS_3, orange) in DhlA are both tryptophan residues. In many haloalkane dehalogenases the secondary halide-stabilising residue is in the HGxP motif. DhlA has a glutamate residue at this position instead and the residue is only shown for spatial orientation (HS_2, grey). Haloacetate dehalogenases have two carboxylate-binding arginine residues (CB_1 & CB_2, orange) and a halide pocket (yellow) consisting of a histidine (HP_1), tryptophan (HP_2), and tyrosine (HP_3).

The number of sequences in D96H188 was reduced significantly and the alignment was greatly improved by the removal of the extremely short and long sequences. However, D96H188 still contained many sequences that have extremely high sequence similarity. High sequence similarity is not necessarily a problem in phylogenetics, but in large datasets most of these sequences will be redundant and add to the computational load. Removing the redundant sequences by clustering highly similar sequences reduces the computational load during calculation and the clutter in the phylogenetic tree. To remove redundant sequences, sequences can be clustered with programs like CD-HIT[1502]. For D96H188 we decided to cluster all sequences above 95% similarity. By selecting on length and clustering redundant sequences the size of the dataset was reduced from 19,600 to 3,487 sequences. This dataset was used to start the construction of a phylogenetic tree.

3.2.3 Aligning sequences

Once the dataset was determined, a final multiple sequence alignment (MSA) is made. A combination of the structural alignment from the 3DM database and the alignment software MAFFT[14] was used to obtain a full MSA. 3DM divides their structural alignment in core and variable regions and while the core regions are all aligned in the system, the variable regions are not aligned. To obtain a full multiple sequence alignment, the 3DM partial alignment was split into core and variable regions. The core regions were left unaltered, while the variable regions were aligned using MAFFT. The full alignment is reconstructed by reuniting the aligned variable and core regions.

3.2.4 Big data and bad annotations

Finally a phylogenetic tree was constructed by maximum likelihood using IQ-TREE[21] (Figure 13). The built-in ModelFinder[151] was used to determine the most accurate evolutionary model for this dataset. Looking at the tree in Figure 13, several problems immediately became apparent. Due to the sheer number of sequences in the dataset the tree has become practically unreadable, and it is difficult to extract any useful information. In addition, based on our literature study, only the dark coloured labels in Figure 13 correspond to characterised enzymes. All other sequences are automatically annotated by the various databases that they originate from. These annotations are mostly based on the sequence similarity and are not verified experimentally. In the original D96H188 dataset of 19,600 sequences, 8,230 sequences were annotated as “epoxide hydrolase”, but only 45 epoxide hydrolases of the α/β-hydrolase-fold family had been experimentally characterised and described in literature. 2,075 sequences were annotated as “haloalkane dehalogenase” and 943 as “haloacetate dehalogenase”, while only around 30 haloalkane dehalogenases and 7 haloacetate dehalogenases were reported at the time. Although automated annotations can be used as predictions of catalytic activity, they are often wrong and should be interpreted carefully. Haloacetate dehalogenases, for example, have often been mistakenly annotated as epoxide hydrolases due to the significant overlap in possible supporting catalytic residues[152].

We were interested in sequences at the interface of both epoxide hydrolase and dehalogenase branches, but the unreliable annotations and clutter in the phylogenetic tree make it difficult to identify individual interesting extant sequences. In addition, due to computational limitations of the reconstruction method, ancestral sequence reconstruction would also be significantly more difficult with a tree of this size. Without suitable high-throughput screening methods, we had neither the proper methods nor the time required to screen a large number of sequences. Therefore, a change in strategy was necessary and we decided to rethink our approach.

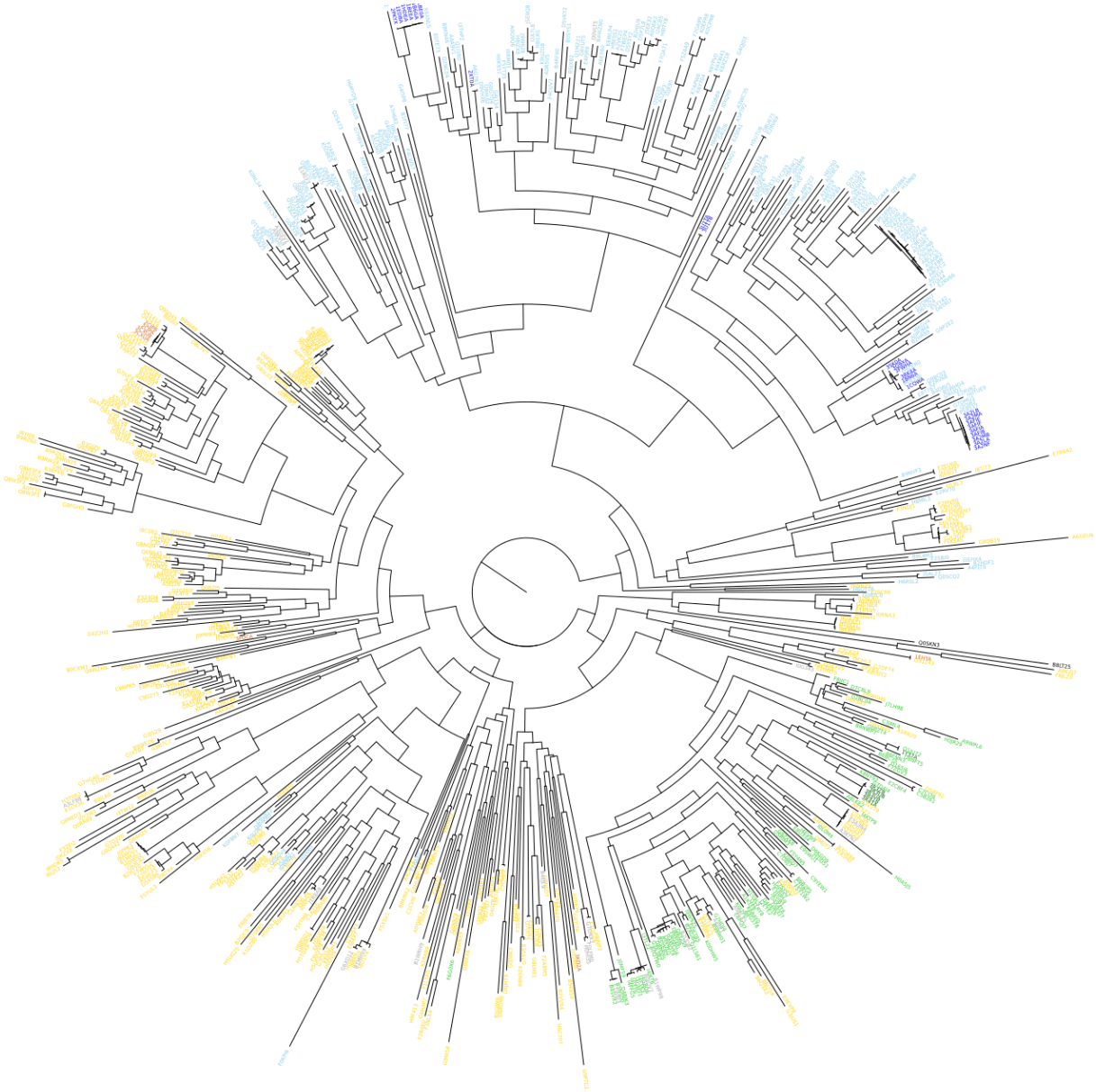

Figure 13. Resulting phylogenetic tree using the large dataset D98H188. Annotated epoxide hydrolases are shown in yellow, annotated haloalkane dehalogenases are shown in blue and annotated haloacetate dehalogenases are shown in green. Dark coloured labels correspond to sequences that were characterised through activity assays and/or crystallography.

3.2.5 Compiling a smaller dataset based on literature research

To avoid the problems encountered with the large D96H188 dataset, instead of trying to filter the α/β-hydrolase fold enzyme family database, sequences were collected through a literature search for characterised epoxide hydrolases and dehalogenases. The literature search yielded 45 characterised epoxide hydrolases, 30 characterised haloalkane dehalogenases, and 7 characterised haloacetate dehalogenases. A phylogenetic tree was created using the same methods as described for the large dataset (Figure 14).

Both the haloalkane dehalogenases and the haloacetate dehalogenases form distinct branches in the phylogenetic tree (Figure 14). Most epoxide hydrolases are grouped in one branch that separates early in the phylogenetic tree from the branches containing dehalogenase activity. Notably, the epoxide hydrolase EchA from *Agrobacterium radiobacter*[104], that was initially selected as a scaffold for protein engineering towards dehalogenase activity, is part of a group of epoxide hydrolases that splits off into their own separate branch almost at the root of the phylogenetic tree. This group is far removed from the dehalogenases in the phylogenetic tree, meaning that they have relatively low sequence similarity with both haloalkane and haloacetate dehalogenases. The distance in the phylogenetic tree shows that the epoxide hydrolase EchA is quite different from dehalogenases, which negatively affected its suitability as an epoxide hydrolase scaffold for dehalogenase activity.

Looking at the phylogenetic tree, the epoxide hydrolase PaeCIF from *Pseudomonas aeruginosa* seems to be a much more suitable choice to engineer towards dehalogenase activity. Together with three other epoxide hydrolases, PaeCIF forms a distinct group of α/β-hydrolase epoxide hydrolases with high similarity towards haloacetate dehalogenases that utilise a histidine-tyrosine ring-opening pair[89] instead of the canonical tyrosine-tyrosine pair. Interestingly, two of these epoxide hydrolases are even closer to haloacetate dehalogenases in the phylogenetic tree; ScoEH from *Streptomyces coelicolor*[63] and CorEH from *Corynebacterium* sp. C12[153,154]. Four other epoxide hydrolases are relatively close to haloalkane dehalogenases but are separated into two distinct branches. EliEH2 from *Erythrobacter litoralis*[155] and PpuEH from *Pseudomonas putida*[63] split off first, directly followed by SceEH from *Saccharomyces cerevisiae*[156] and NpuEH2 from *Nostoc punctiforme*[63]. These eight extant epoxide hydrolases were selected for further characterisation and screening for promiscuous dehalogenase activity (see Chapter 4).

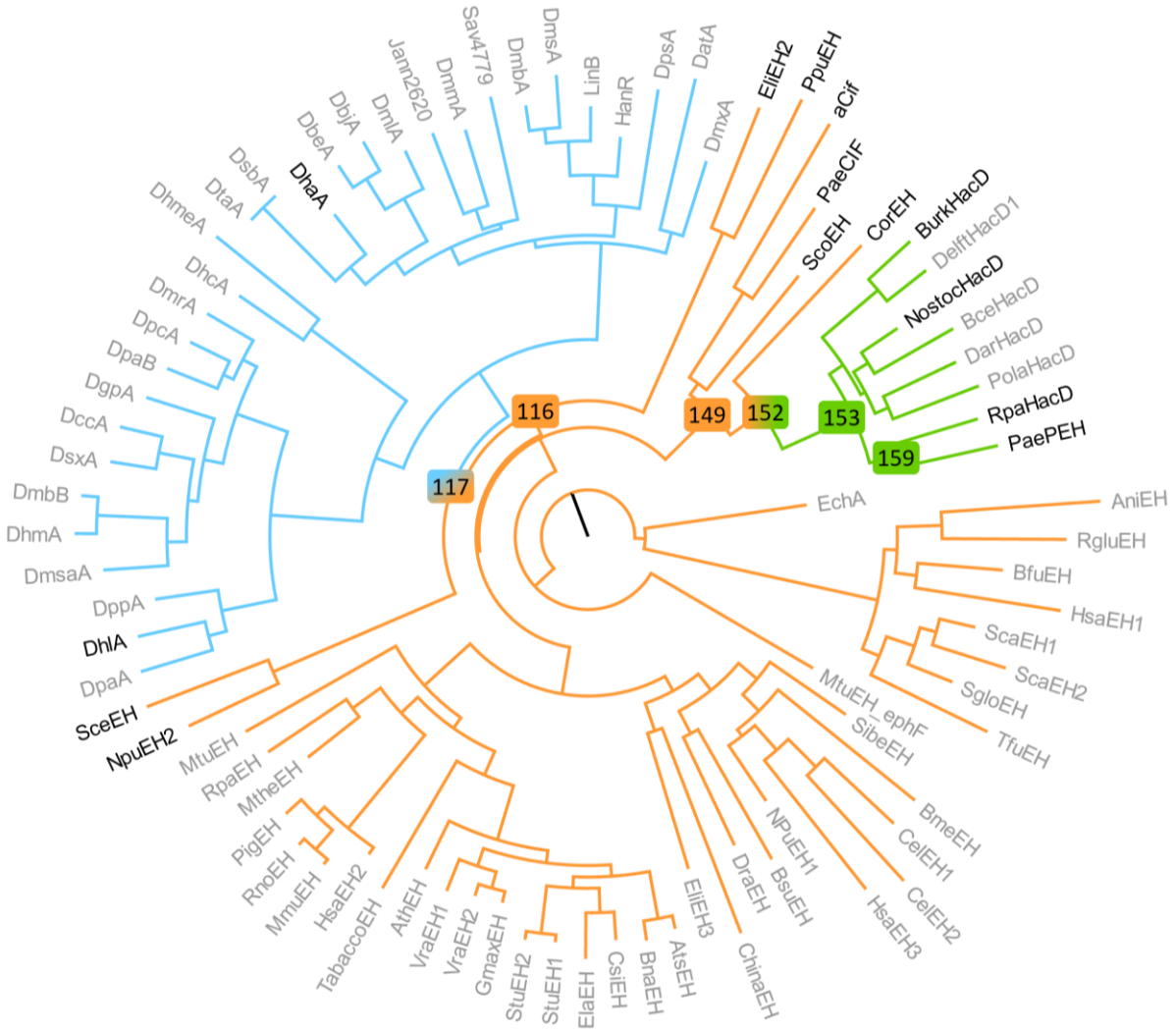

Figure 14. Phylogenetic tree based on characterized epoxide hydrolases, haloalkane dehalogenase and haloacetate dehalogenases. Haloacetate dehalogenases branches are shown in green, haloalkane dehalogenases in blue, and epoxide hydrolase branches are shown in yellow. Interesting ancestral nodes numbers are marked.

3.3 Ancestral sequence reconstruction

In addition, several interesting ancestral nodes were selected for ancestral sequence reconstruction. Using the program RAxML[157], ancestral sequences were derived from the phylogenetic tree and the sequence alignment. RAxML does not handle inserts or deletions (indels) well. Indels are a certain type of mutation where one or more residues are inserted or deleted[158]. The program will always insert a residue if one of the two descendant sequences has amino acid residues at that position in the alignment. Due to this oversight, the theoretical ancestral sequences become longer with each ancestral node moving closer towards the root of the tree . This results in extremely long sequences that are not realistic or viable. Therefore, the ancestral sequences need to be adjusted manually using a sequence editing software, like BioEdit[159]. In our manual adjustments, inserts were only kept if other nearby extant sequences show an insert at that position. Only one insert was kept if two of the same insert were included at nearby positions in the alignment. In the curated conserved core regions, indels were not a problem and thus these regions were not adjusted manually.

3.3.1 Structural modelling of ancestral sequences

Three-dimensional protein structures of the ancestral sequences were obtained through homology modelling using the SWISS-MODEL[160] server (Figure 16). Together with the alignment (Figure 15), these models make it easier to compare the active sites of the ancestral sequences with those of extant epoxide hydrolases and dehalogenases.

As expected from their position in the phylogenetic tree in Figure 14, both ancestral sequences Anc153 and Anc159 primarily have haloacetate dehalogenase motifs, including the carboxylate-binding arginine residues and a halide pocket. The histidine (H146 and H143) and tyrosine (Y208 and Y206) residues of the halide pocket can potentially also serve as epoxide ring-opening residues, but no haloacetate dehalogenase has been reported to hydrolyse epoxides.

Enzyme	HS_2	$CN/HS_1/CB_{1/2}$	CRA_1	$RO_1/HP_{1/2}$	HS_3	RO_2/HP_3	CRA_2	B
PaeCIF	HGFG	AHDIGIWNT	YMEAP	VWHFSF	-----	-YYRA	GGH--	CGHWL
DhlA	HGEP	VQDWGGFLG	IMNA-	------	TAW--	-FPKM	MKDKL	AGHFV
RpaHacD	HGFP	GHDRGARVS	VLDIL	IYHWSF	-----	-DYRA	ASG--	SGHFL
Anc116	HGYP	CHDYGGPIG	IMNTM	------	QAF--	FFYRQ	EKDPI	AGHFV
Anc117	HGNP	CQDWGSPIG	VMNTM	------	QAF--	FFPRQ	EKDAI	GGHFI
Anc149	HGFP	GHDWGATVA	FMDAV	IWHFFF	-----	-YYRA	SKGVV	CGHWL
Anc152	HGYP	GHDWGARVA	VLDIV	IYHWFF	-----	-DYRA	EWGVV	CGHFL
Anc153	HGYP	GHDRGARVA	VLDIV	YYHWFF	-----	-DYRA	EKGIV	CGHFL
Anc159	HGYP	GHDRGARVS	VLDIL	IYHWFF	-----	-DYRA	ERG--	SGHML

Figure 15. Alignment of the ancestral sequences with an epoxide hydrolase (PaeCIF[89]), a haloalkane dehalogenase (DhlA[90]) and a haloacetate dehalogenase (RpaHacD[149]). Epoxide ring-opening residues can be a histidine-tyrosine or tyrosine-tyrosine pair. Haloacetate dehalogenases typically have two carboxylate binding residues ($CB_{1/2}$) and a halide pocket (HP). The halide pocket consists of a histidine-tryptophan pair ($HP_{1/2}$) and tyrosine (HP_3) and overlaps with the epoxide ring-opening residues. The primary halide-stabilising residue (HS_1) is a tryptophan and the secondary halide-stabilising residue (HS_2 or HS_3) can be an asparagine or a tryptophan respectively. Full sequences can be found in Appendix A3.4.

The nodes of ancestral sequences Anc152 and Anc153 connect the haloacetate dehalogenase branch to several extant epoxide hydrolases. Remarkably, neither sequence has the carboxylate-binding arginine residues of haloacetate dehalogenases, but instead they both have the primary halide-stabilising tryptophan (W102 and W104) typical for haloalkane dehalogenases. Both Anc152 and Anc153 have the histidine-tyrosine pair from haloacetate dehalogenases and PaeCIF-like epoxide hydrolases. Anc153 completes the halide pocket with a tryptophan (W143), that could also act as a halide-stabilising residue together with another tryptophan next to the catalytic nucleophile (W102), as in haloalkane dehalogenases.

In contrast to the other 4 ancestral sequences, Anc116 and Anc117 are derived from both epoxide hydrolases and haloalkane dehalogenases. Their respective ancestral nodes are much closer to the base of the tree. Anc116 and Anc177 both have the charge relay acid in the second position, which is common for HLD-subfamilies I and III and for most epoxide hydrolases except the group of epoxide hydrolases with the histidine-tyrosine epoxide ring-opening pair, like PaeCIF. Anc117 has a potential asparagine-tryptophan halide-stabilising pair (N36/W104) as is typically found in haloalkane dehalogenase subfamilies II and III, but no ring-opening residues. Anc116 is very close to the root of the tree and due to the distance from the extant sequences and poor handling of inserts and deletions by the software, the predicted sequences are much less reliable. Anc116 does not have any of the canonical supporting residues, but instead has an unusual mix of tyrosine and tryptophan residues. It is difficult to say whether any activity can be expected from this ancestral sequence.

3.3.2 Cloning and expression of ancestral sequences

The adjusted ancestral sequences were ordered cloned in a pET-28a(+) vector, codon optimised for expression in *Escherichia coli*. The plasmids were transformed into *E. coli* BL21(DE3) and protein expression was tested under several different conditions, including induction of protein expression through the addition of isopropyl β-D-1-thiogalactopyranoside (IPTG) in lysogeny broth (LB) media and expression in autoinduction media, like ZYM-5052[161], at various temperatures. However, we were unable to achieve sufficient soluble protein expression for proper characterisation under any of the conditions tested (Figure 19). These expression problems temporarily put our ancestral sequence reconstruction efforts on hold, until we got the opportunity to test an automated ancestral sequence reconstruction pipeline, FireProt^{ASR}, that was under development by Bednar *et al*.[162]

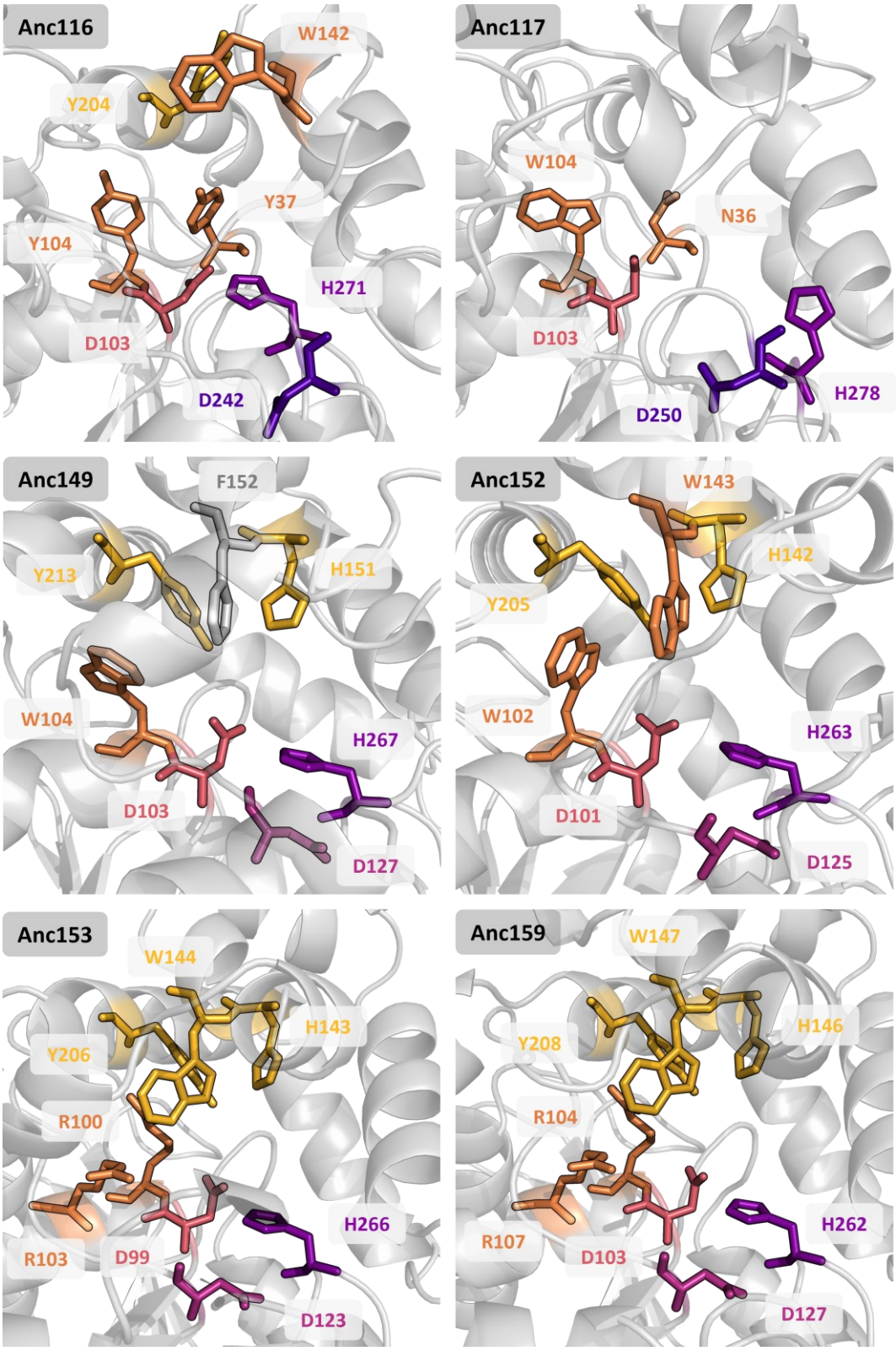

Figure 16. SWISS-MODEL[160] homology models for the ancestral nodes from the phylogenetic tree in Figure 14. The catalytic nucleophile (CN, pink), the charge-relay acid at position 1 (CRA_1, dark pink) or 2 (CRA_2, dark purple), and the histidine base (B, purple) are shown. Potential epoxide ring-opening residues and residues of a halide pocket are shown in yellow, while potential halide-stabilising residues and the carboxylate-binding arginine residues are shown in orange. Details of the homology models are listed in Appendix A1.4 Table S2.

3.3.3 Automated Ancestral Sequence reconstruction

FireProt^{ASR} combines several computational tools into a fully automated workflow, allowing unexperienced users to obtain ancestral sequences based on a sequence query as the only input[162]. As a secondment, as part of the Marie Curie Innovative Training Network ES-Cat, I was invited to test a prototype workflow of FireProt^{ASR} and help find potential bottlenecks. As we already had constructed a well-suited dataset for the first phylogenetic tree, we tested the FireProt^{ASR} workflow starting with the curated dataset of characterised epoxide hydrolases, haloacetate dehalogenases and haloalkane dehalogenases collected from literature. The sequences were realigned and pushed through the various programs embedded in the workflow[162], including some programs that were also used in the construction of the first tree, such as IQ-TREE and RAxML.

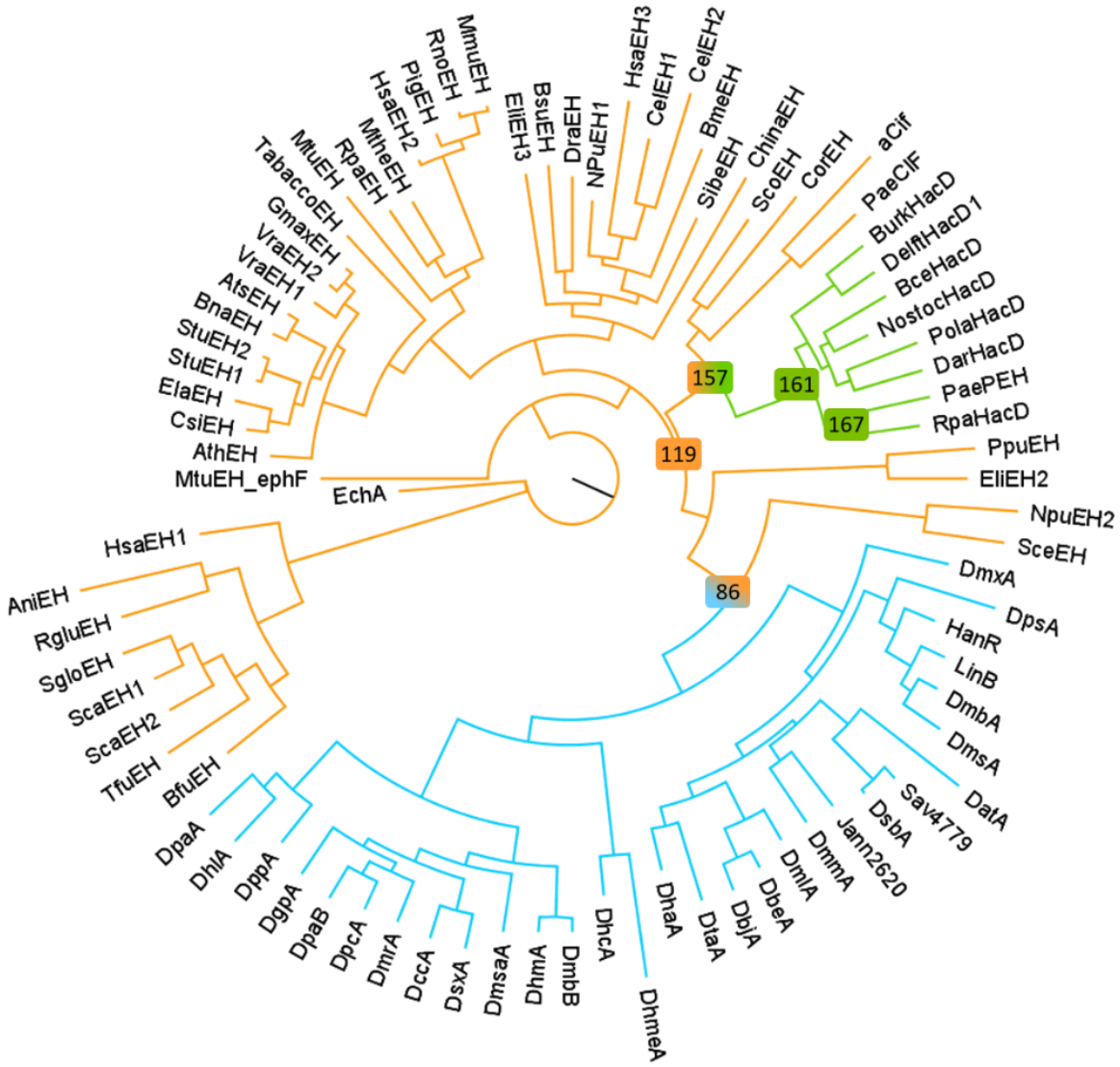

Figure 17. Phylogenetic tree based on characterized epoxide hydrolases and dehalogenases using a prototype of the fully automated ancestral sequence reconstruction tool (FireProt^{ASR})[162]. Haloacetate dehalogenase branches are shown in green, haloalkane dehalogenase branches in blue, and epoxide hydrolase branches are shown in yellow. Interesting ancestral nodes are marked with numbers corresponding to their node number in the phylogenetic tree.

As expected, when starting from the same dataset, the phylogenetic tree resulting from the automated workflow in Figure 17 is very similar to the first tree in Figure 14. Although the haloalkane dehalogenase branch is now shown on the opposite side of the tree, most internal relationships are the same between both trees. The group of distinct epoxide hydrolases including PaeCIF is again the closest branch to the haloacetate dehalogenases and are clearly separated from the other epoxide hydrolases. However, instead of having its own branch, CorEH is now grouped together with ScoEH. This means that there is no equivalent ancestral node for Anc152 in the new tree, and the equivalent of Anc149 in Figure 17, Brno157, is now the first node to connect the group of epoxide hydrolases with the haloacetate dehalogenases. The split between the haloalkane dehalogenases and the group of SceEH and NpuEH2 is the same between the two trees. The ancestral node of Brno86 in Figure 17 is therefore equivalent to the ancestral node of Anc117 in Figure 14. In addition to Brno157 and Brno86, we thought it would be interesting to look at the ancestral sequence for the first ancestral node, Brno119, connecting all three activities (Figure 17). The predicted ancestral sequences for these three ancestral nodes were scrutinised and carefully adjusted where necessary to increase our chances of finding a promiscuous epoxide hydrolase-dehalogenase protein.

3.3.4 Corrections of the ancestral sequences to promote promiscuity

Even though most of the workflow was already automated at the time, the correction of indels in the reconstructed ancestral sequences still had to be performed manually. Overall, the predicted ancestral sequences were reasonably well aligned with their respective extant sequences. The start of the ancestral sequences is usually uncertain due to the uncertainty in the alignment in that region and therefore the beginning of each ancestral sequence is replaced by the start of a suitable extant sequence. Unexpectedly, the tyrosine in the halide pocket of haloacetate dehalogenases and the overlapping epoxide ring-opening residue was often missing in the overall alignment. All extant sequences do have a tyrosine at this position and the misalignment was corrected manually for all sequences. In addition, the alignment is relatively bad around the halide pocket and around the second possible position for the charge relay acid. These regions were checked extensively by hand and corrected where necessary. Structural homology-models were obtained for all the three selected ancestral sequences using SWISS-MODEL[160] (Figure 18A) to visualize the active sites, complementary to the alignment (Figure 18B). To increase the chances of an enzyme with both epoxide hydrolase and dehalogenase activity, the supporting residues for both activities were introduced if not yet present.

Originally, the predicted sequence Brno86 did not have a complete pair of epoxide hydrolase or dehalogenase supporting residues. Adjustments were made to introduce a halide-stabilising pair (N43/W111) by changing the phenylalanine (F43) in the HGxP-motif to an asparagine (N43) and to introduce an epoxide ring-opening pair (Y151/Y207) by changing the phenylalanine (F151) to a tyrosine (Y151) (see Figure 18).

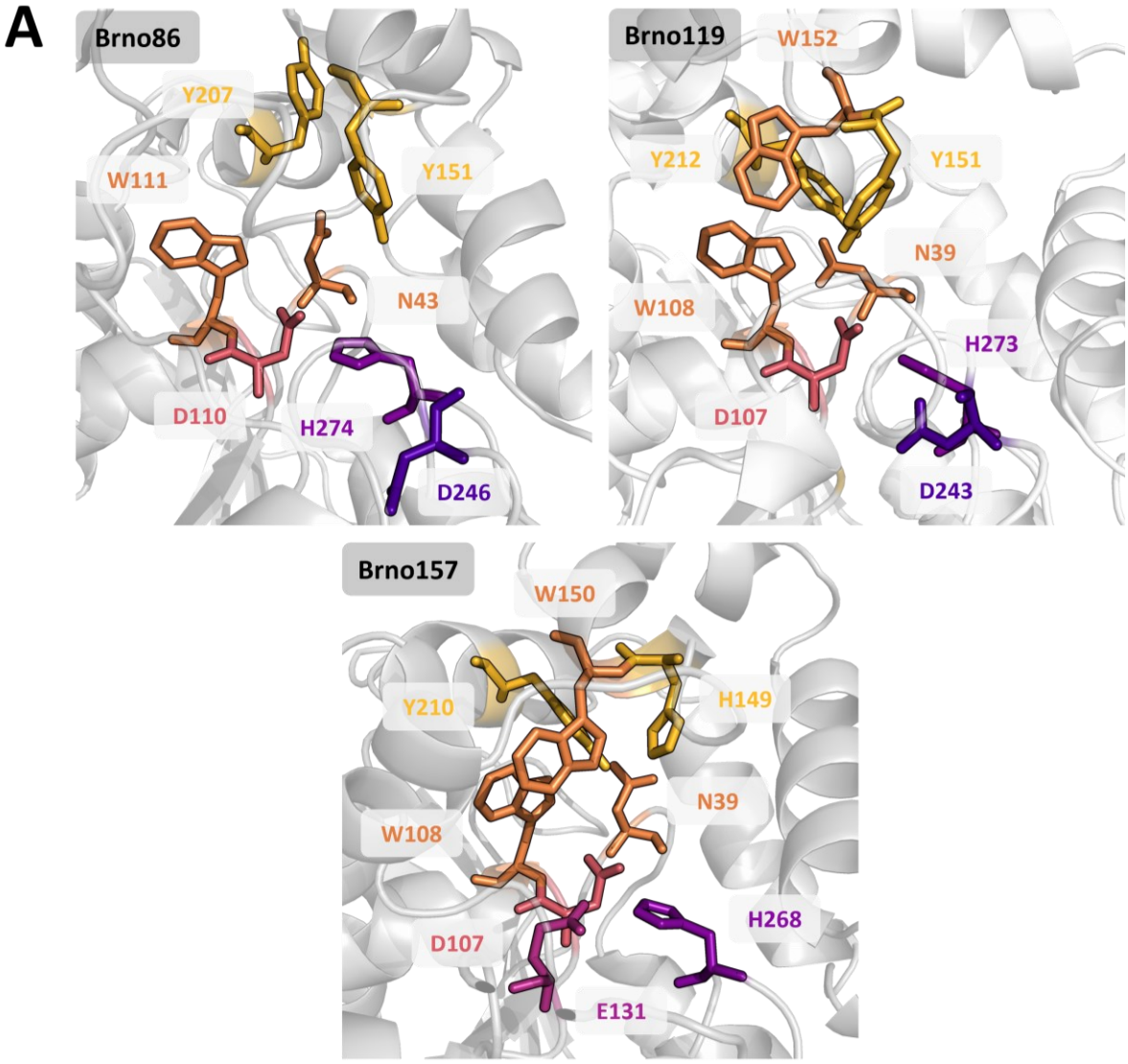

B

Enzyme	HS_2	$CN/HS_1/CB_{1/2}$	CRA_1	$RO_1/HP_{1/2}$	HS_3	RO_2/HP_3	CRA_2	B
PaeCIF	HGFG	AHDIGIWNT	YMEAP	VWHFSF	-----	-YYRA	GGH--	CGHWL
DhlA	HGEP	VQDWGGFLG	IMNA-	------	TAW--	-FPKM	MKDKL	AGHFV
RpaHacD	HGFP	GHDRGARVS	VLDIL	IYHWSF	-----	-DYRA	ASG--	SGHFL
Brno86	HGNP	CHDWGGAIG	IMNA-	--YQFF	-----	-FYRA	EKDPV	AGHFV
Brno119	HGNP	GHDWGGVVA	IMNA-	RAYWFF	-----	-FYRA	EGDPV	CGHFV
Brno157	HGNP	GHDWGAVVA	IMEA-	-FHWFF	-----	-DYRA	ERG--	CGHFL

Figure 18. SWISS-MODEL[160] homology models and active site alignment for the three most interesting nodes of the phylogenetic tree in Figure 17. Showing the catalytic nucleophile (CN, pink), the charge-relay acid (CRA_1, dark pink or CRA_2, dark purple), and the histidine base (B, purple). Potential epoxide ring-opening residues (RO_1 & RO_2) and residues of the halide pocket (HP) are shown in yellow. Potential halide-stabilising residues and carboxylate-binding arginine residues (CB_1 & CB_2) are shown in orange. B) Alignment with an epoxide hydrolase (PaeCIF[89]), a haloalkane dehalogenase (DhlA[90]) and a haloacetate dehalogenases (RpaHacD[149]). Epoxide ring-opening residues can be a histidine-tyrosine or tyrosine-tyrosine pair. The halide pocket consists of a histidine-tryptophan pair ($HP_{1/2}$) and tyrosine (HP_3) and overlaps with the epoxide ring-opening residues. The primary halide-stabilising residue (HS_1) is a tryptophan and the secondary halide-stabilising residue (HS_2 or HS_3) can be an asparagine or a tryptophan respectively. Full sequences can be found in Appendix A3.4. Details of the homology models are listed in Appendix A1.4 Table S2.

Neither of the halide-stabilising pairs were present in Brno119, so these residues were introduced by changing the phenylalanine (F39) in the HGxP-motif to an asparagine (N39) and the leucine (L152) to a tryptophan. Brno157 already has a ring-opening pair (H149/Y120), but no halide-stabilising pairs. Two pairs were introduced by changing the phenylalanine (F39) to an asparagine (N39) and the histidine (H150) to a tryptophan (W150). Both Brno119 and Brno157 now have both halide-stabilising pairs; the asparagine-tryptophan pair commonly found in subfamilies HLD-II and HLD-III of the haloalkane dehalogenases and the tryptophan-tryptophan pair commonly found in subfamily HLD-I.

3.3.5 Expression and purification of the ancestral sequences

The ancestral sequences for Brno86, Brno119 and Brno157 were also ordered codon optimized for expression in *Escherichia coli* and cloned into a pET-28a(+) vector. The plasmids were transformed into *E. coli* BL21(DE3) and expression was tested under several expression conditions. However, also for this set of ancestral proteins expression proved challenging (Figure 19A). Regardless of the difficulties with protein expression, the His_6-tagged proteins for all ancestral sequences were purified using immobilised metal-affinity chromatography (Figure 19B). Due to the low soluble expression of the target proteins, the purified samples on the SDS-gel also show other protein bands.

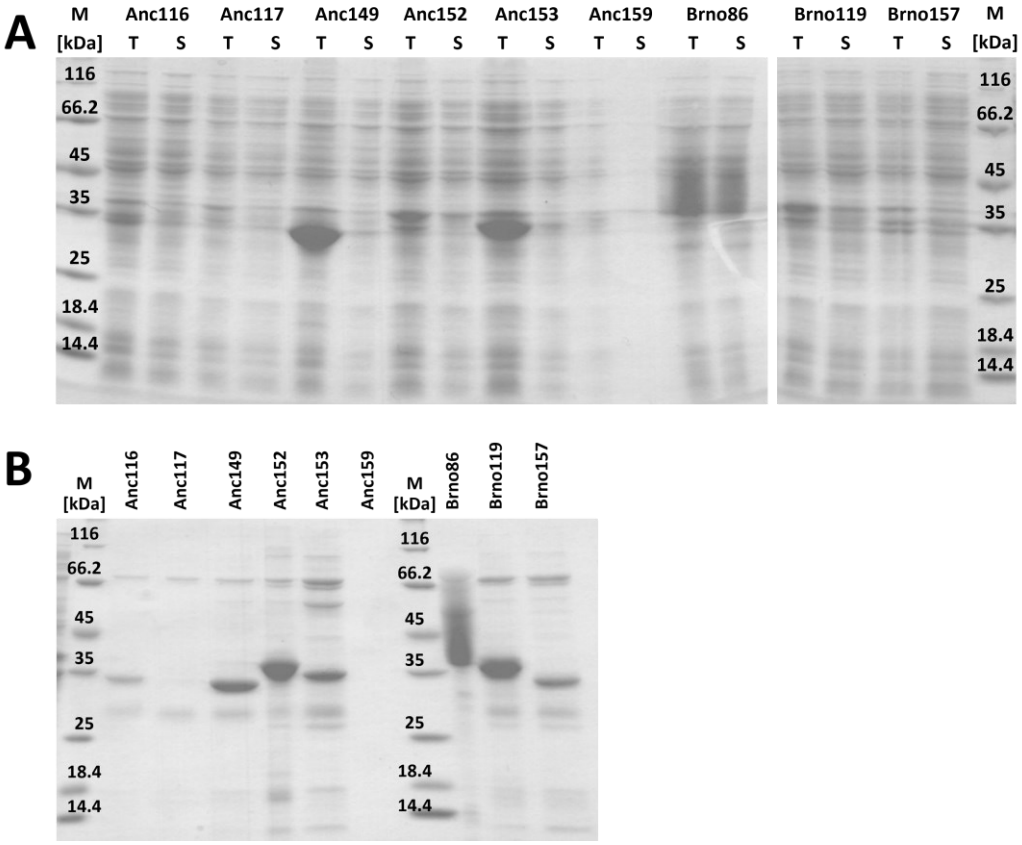

Figure 19. SDS-PAGE. A) Example of a protein expression experiment with the ancestral sequences. Normalised total (T) and soluble (S) fractions taken from ZYM-5052[161] autoinduction cultures. B) Samples of the His6-tagged ancestral proteins purified by immobilised metal-affinity chromatography. Target proteins are expected between 30 and 40 kDa: Anc116 (36 kDa), Anc117 (37 kDa), Anc149 (35 kDa), Anc152 (34 kDa), Anc153 (34 kDa), Anc159 (35 kDa), Brno86 (36 kDa), Brno119 (36 kDa) and Brno157 (35 kDa).

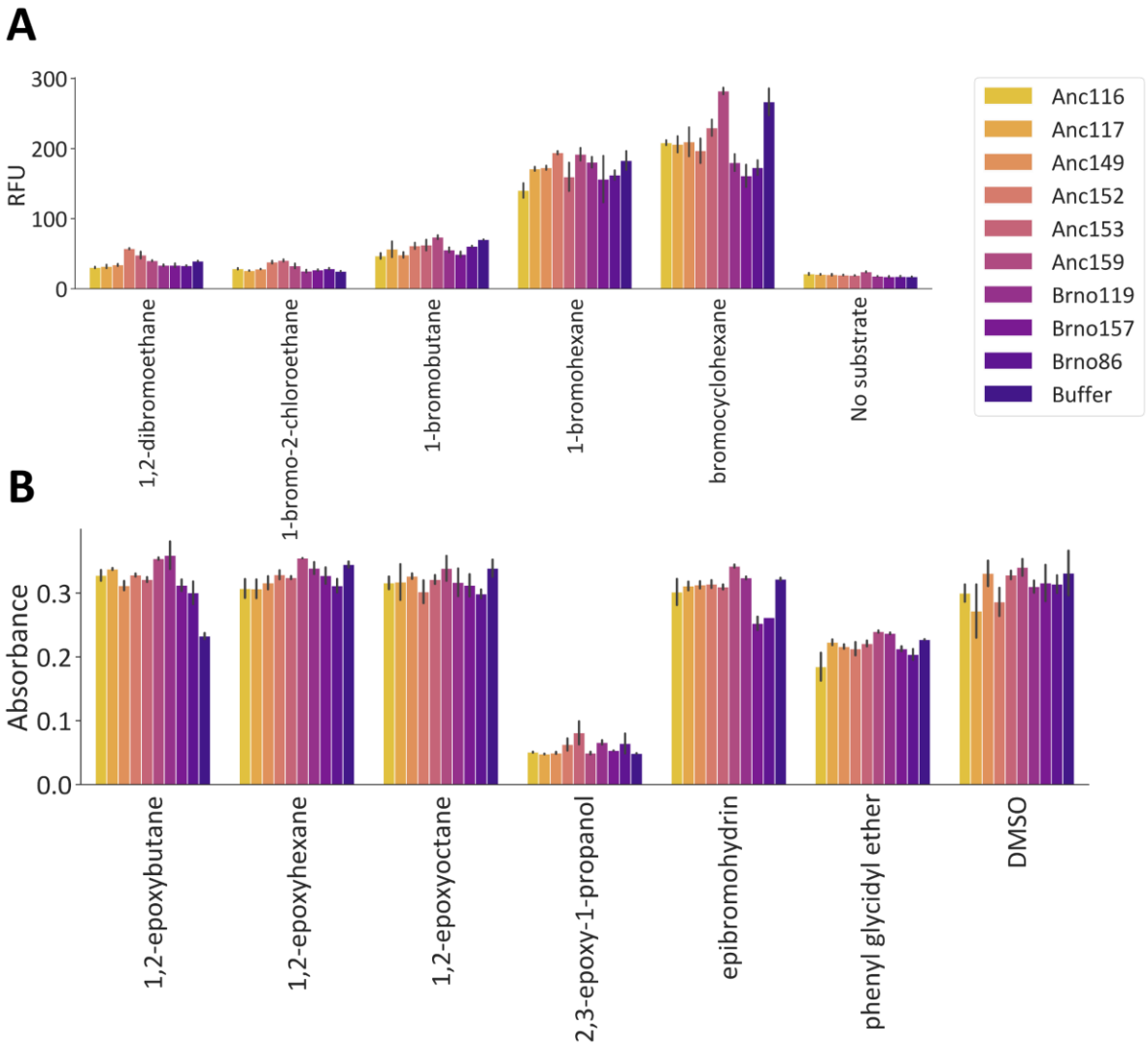

Figure 20. Screening results of reactions with the ancestral proteins and several epoxide and halogenated substrates. A) Screening for dehalogenase activity using the halide oxidation (HOX) assay for several halogenated substrates. The relative fluorescence units (RFU) are a measure for determining the halide release. Reactions were performed at room temperature in 50 mM NaH_2PO_4 at pH 8.0 with 0.15 mg/mL enzyme sample and 10 mM substrate for 4.5 hours. Undiluted reaction sample (2 µL) was added to the HOX assay reaction buffer (total volume of 40 µL) containing 2 mM H_2O_2, 25 µM aminophenyl fluorescein, 1 mM orthovanadate, 2.5 U/mL *Curvularia inaequalis* vanadium-dependent chloroperoxidase (*Ci*VCPO) at pH 6.0. Reactions were incubated in black 384-well plates for 40 min at room temperature before measuring fluorescence at 525 nm (excitation at 488 nm). B) Screening for epoxide hydrolysis using the adrenaline assay[163,164] for several epoxide substrates. The absorbance at 490 nm is an indirect measure for determining the formation of diols. A lower absorbance compared to the negative control indicates activity. The reactions (total volume of 100 µL) were performed with 0.15 mg/mL enzyme and 10 mM substrate in 50 mM NaH_2PO_4 at pH 8.0 containing 1.25 mM $NaIO_4$. The reactions were incubated at 37 °C for at least 30 min. A sample of the reactions (42.5 µL) was added to 7.5 µL 10 mM L-adrenaline in a 384-well plate and the absorbance was measured at 490 nm. The 10 mM substrate stocks were prepared in DMSO.

3.3.6 Screening ancestral proteins for dehalogenation and epoxide hydrolysis

The purified protein samples were screened for epoxide hydrolysis with several epoxide substrates using the adrenaline assay[163,164]. Epoxide hydrolysis produces 1,2-diols that can be oxidised by periodate. Back-titration of the oxidant with adrenaline to produce the red adrenochrome allows for quantification of the diols by measuring the absorbance at 490nm. Execution of the adrenaline assay is described in detail in Appendix A2.7. Dehalogenase activity was screened using the HOX assay (see Chapter 2). No significant activity was detected in any of the activity screenings (Figure 20). Despite our best efforts, it was not possible to obtain reliable and reproducible results. Purer and more protein is needed to improve the reliability of the screening. However, instead of trying to improve protein expression and purification protocols for these ancestral sequences, we decided to focus on screening extant sequences with the newly developed halide oxidation assay to find a promiscuous epoxide hydrolase-dehalogenase.

Chapter 4

Searching for promiscuity

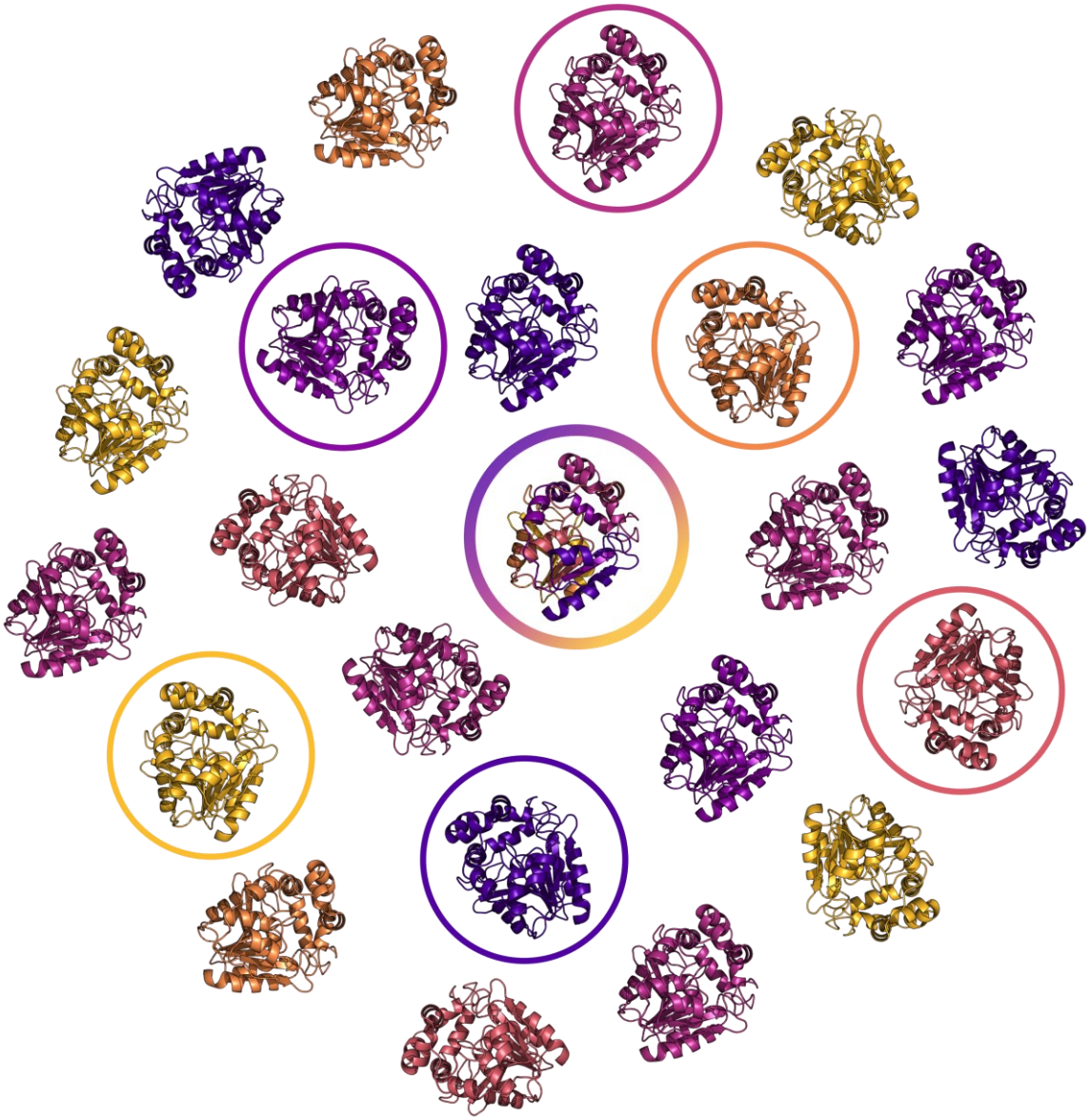

Adapted from:

'Promiscuous Dehalogenase Activity of the Epoxide Hydrolase CorEH from Corynebacterium sp. C12'

E.D. Schuiten, C.P.S. Badenhorst, G.J. Palm, L. Berndt, M. Lammers, J. Mican, D. Bednar, J. Damborský, U.T. Bornscheuer, *ACS Catalysis* 2021, *11* (10), 6113-6120

4.1 Selected epoxide hydrolases

The phylogenetic analysis described in Chapter 3 resulted in a phylogenetic tree containing 45 epoxide hydrolases, 30 haloalkane dehalogenases and 7 haloacetate dehalogenases from a variety of different organisms (Figure 21). From this tree, eight extant epoxide hydrolases were selected as promising potential engineering scaffolds and for screening towards dehalogenase activity. Due to their relatively close relation to the dehalogenase sequences in the data set, these sequences were thought to be more likely to possess promiscuous dehalogenase activity than the other epoxide hydrolases.

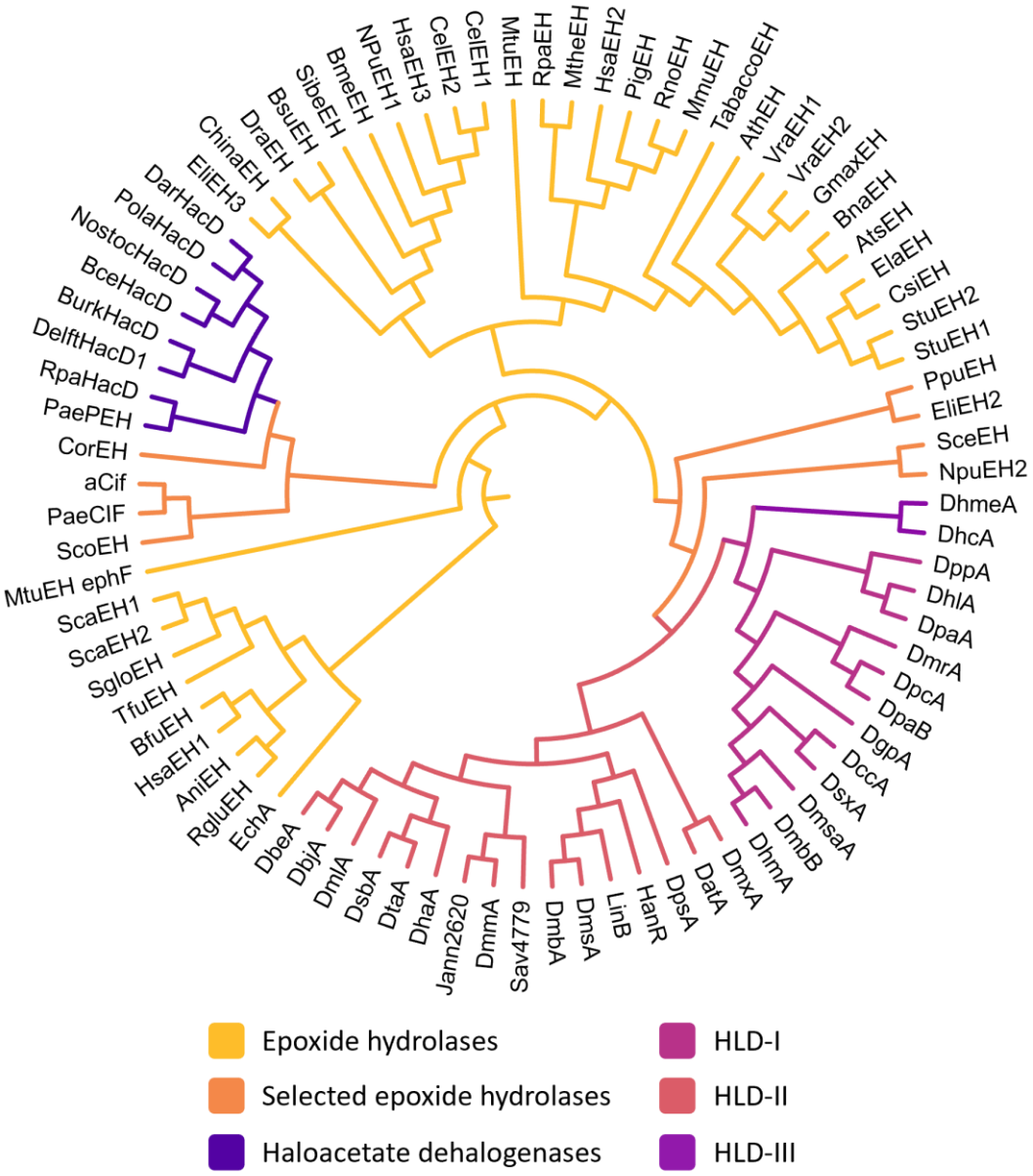

Figure 21. Phylogenetic tree based on characterized epoxide hydrolases, haloacetate dehalogenases and haloalkane dehalogenases. Epoxide hydrolase branches are shown in yellow, except the branches connected to the 8 extant epoxide hydrolases selected for screening, which are shown in orange. The haloacetate dehalogenase branches are shown in dark purple. The haloalkane dehalogenase branches are shown in a different colour for each subfamily: HLD-I in dark pink, HLD-II in pink and HLD-III in purple. As branch length is not important for the purpose of this figure, it was ignored for clarity.

Four of the selected epoxide hydrolases form a distinct group that utilise a histidine-tyrosine ring-opening pair[89] instead of the canonical tyrosine-tyrosine pair (Figure 22). This group is close to haloacetate dehalogenases in the phylogenetic tree and includes PaeCIF from *Pseudomonas Aeruginosa*[85], aCIF from *Acinetobacter nosocomialis*[165], ScoEH from *Streptomyces coelicor*[63], and CorEH from *Corynebacterium* sp. C12[153,154].

PaeCIF is known as a virulence factor in lung infections and is usually referred to as CFTR inhibitory factor (CIF). PaeCIF has been reported to decrease the concentration of the cystic fibrosis transmembrane conductance regulator (CFTR) on the apical surface of lung epithelial cells, disrupt inflammation resolution signalling, and slow down mucociliary clearance of bacteria[166–168]. PaeCIF can convert polyunsaturated fatty acid epoxides[169] and is known to accept epibromohydrin as a substrate[85]. Due to the high sequence similarity and close relation between PaeCIF and haloacetate dehalogenases, PaeCIF has been tested for both haloacetate and haloalkane dehalogenase activity, but none was reported[110]. Interestingly, Bahl *et al*. observed some dehalogenation of epibromohydrin by a charge relay acid mutant of PaeCIF (E153Q) in mass spectrometry experiments[85]. Due to the mutation of the charge relay acid, this variant is unable to hydrolyse the covalently attached alkyl-enzyme intermediate. Although PaeCIF is similar to haloacetate dehalogenases, it does not have the arginine-rich nucleophilic aspartate motif found in haloacetate dehalogenases[111] (see Figure 24B).

Like PaeCIF, aCIF is also a CFTR inhibitory factor and was shown to catalyse the hydrolysis of multiple epoxides, including (*S*)-styrene-oxide, epoxycyclohexene and nitrostyrene oxide[165]. Unlike PaeCIF, which utilises a glutamate (E153) as the charge relay acid, aCIF uses an aspartate (D182). Recently, and after we constructed the phylogenetic tree in Figure 21, two other CIF-like epoxide hydrolases from *Burkholderia cenocepacia* were identified by Taher *et al*.[170].

Carter *et al*. isolated CorEH from *Corynebacterium* sp. C12, as strain that grows on cyclohexene oxide as the sole carbon source[153]. CorEH was first described by Misawa *et al*. as the enzyme responsible for epoxide hydrolysis by *Corynebacterium* sp. C12 in 1998[154]. Although CorEH is expressed at low levels under normal circumstances, expression is induced to much higher levels by growth on potential epoxide substrates like cyclohexene oxide and the hydrolysis product 1,2-dihydroxy cyclohexane, indicating a specific function for the enzyme in the catabolism of epoxides. Misawa *et al*. observed the highest activity with C_6 and C_7 carbocyclic epoxides, while C_5 and C_8 carbocyclic epoxides were hydrolysed with less than 20% of the activity against cyclohexene oxide. CorEH also hydrolysed linear 1,2-epoxyalkanes, with notable preference for substrates with long alkyl chains, suggesting hydrophobic interactions might play an important role in substrate binding. In addition, CorEH was also reported to hydrolyse several other epoxides, including epichlorohydrin and epibromohydrin, and displays a diverse substrate scope[63]. CorEH's putative ring-opening residues were reported as a tyrosine pair by van Loo *et al*. (Y167 and Y209). However, Y167 is located in helix α6 in the cap-domain, while the epoxide ring-opening residues are always found in helix α4b and helix α8 (Figure 24A). Instead of a tyrosine pair, CorEH uses a histidine-tyrosine pair (H145 and Y209).

Several *Streptomyces* strains[171] have been reported to hydrolyse epoxides and ScoEH was reported by van Loo *et al*.[63] to have minimal activity with *para*-nitrostyrene oxide and *para*-nitrophenyl glycidyl ether. van Loo *et al*. identified two potential ring-opening tyrosine residues (Y158 and Y215) but the alignment, phylogenetic tree, and a comparison of active sites (Figure 22) suggest that ScoEH uses a histidine-tyrosine pair (H154 and Y215).

It should be noted that the homology models for the selected epoxide hydrolases (Figure 22 and Figure 23), have relatively low sequence identity and sequence similarity, and the models should therefore be interpreted carefully (Appendix A1.4 Table S2).

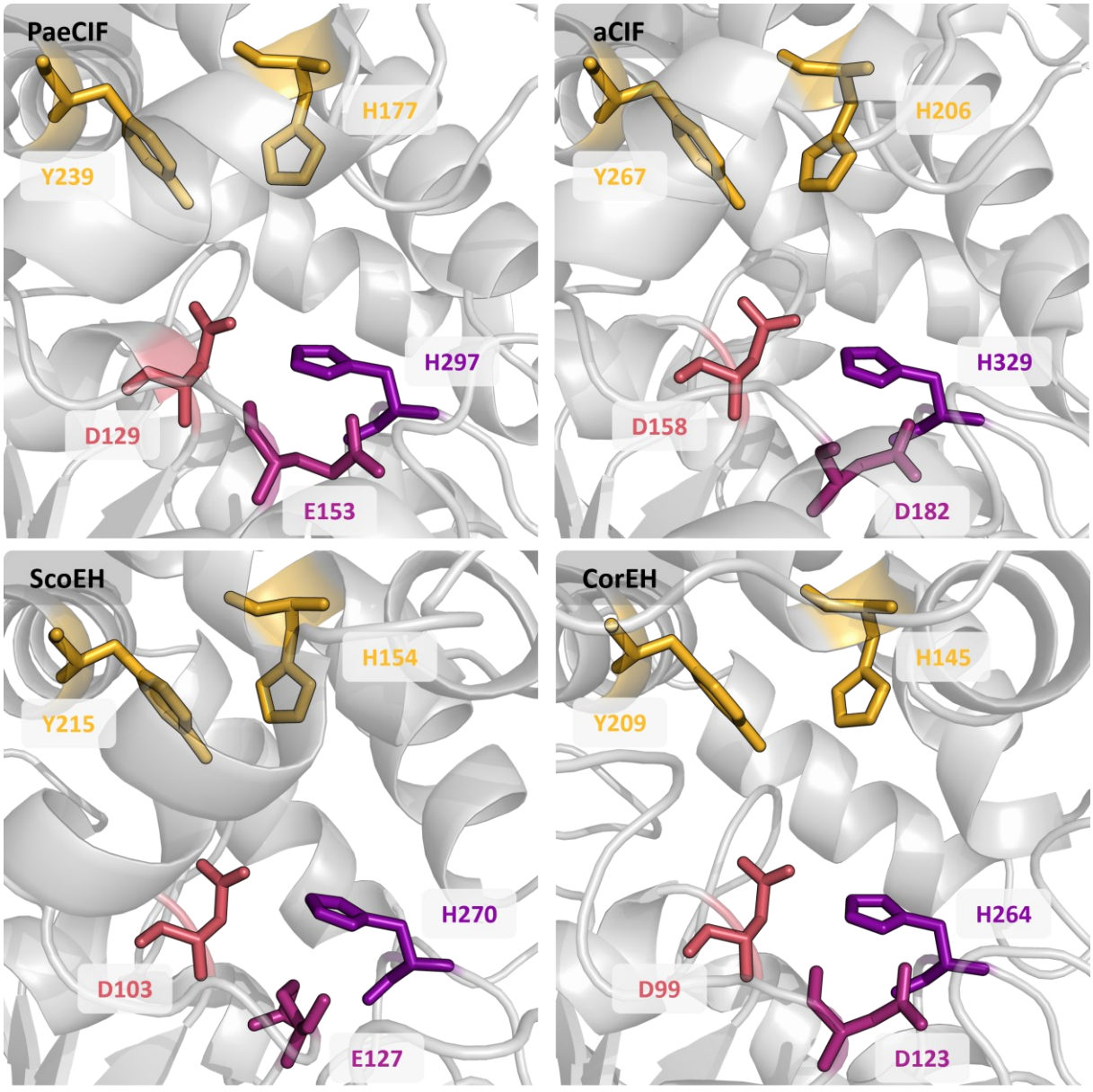

Figure 22. Comparison of the epoxide hydrolase active sites with a histidine-tyrosine epoxide ring-opening pair. Crystal structures were used for PaeCIF from *Pseudomonas aeruginosa* (PDB ID: 3KD2), aCIF from *Acinetobacter nosocomialis* (PDB ID: 4MEA) and CorEH from *Corynebacterium* sp. C12 (PDB ID: 7AC0). A SWISS-MODEL[172] homology model was used for ScoEH from *Streptomyces coelicor* (Appendix A1.4 Table S2). The catalytic nucleophile (pink), the charge-relay acid at position 1 (dark pink), and the histidine base (B, purple) are shown. The histidine-tyrosine ring-opening pair characteristic for this group of epoxide hydrolases is shown in yellow.

The other group of selected epoxide hydrolases is close to the haloalkane dehalogenase branches and includes NpuEH2 from *Nostoc punctiforme*[63], SceEH from *Saccharomyces cerevisiae*[156], EliEH2 from *Eryhtrobacter litoralis*[155] and PpuEH from *Pseudomonas putida*[63]. They are separated into two distinct branches in Figure 21, with SceEH and NpuEH2 in the branch closest to the haloalkane dehalogenases, and EliEH2 and PpuEH in the next branch.

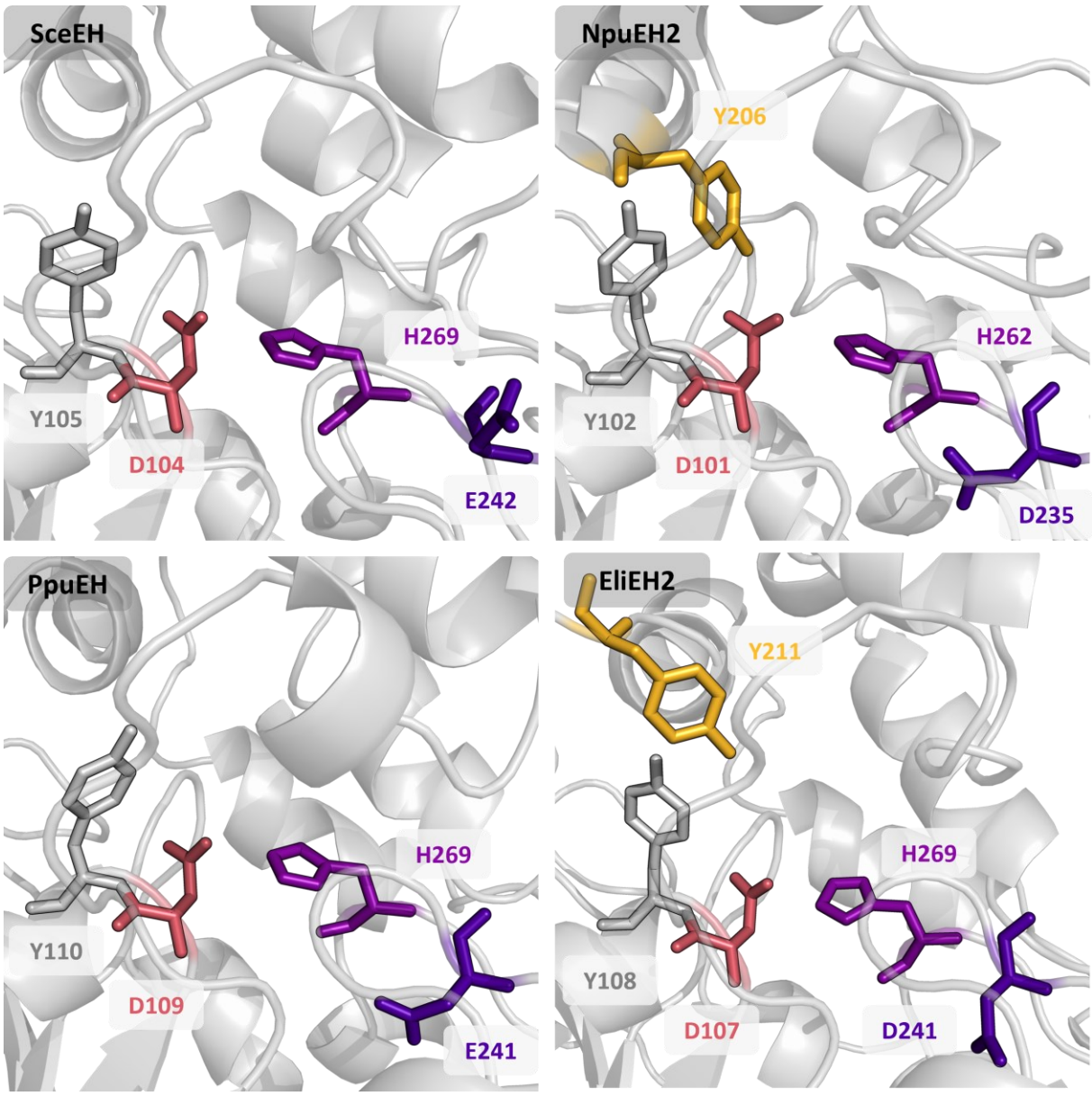

Figure 23. Comparison of active sites of the epoxide hydrolases SceEH from *Saccharomyces cerevisiae*, NpuEH2 from *Nostoc punctiforme*, PpuEH from *Pseudomonas putida*, and EliEH2 from *Erythrobacter litoralis*. SWISS-MODEL[172] homology models were used, but the accuracy of the models with these protein sequences was low (Appendix A1.4 Table S2). The catalytic nucleophile (pink), the charge-relay acid at position 2 (dark purple), and the histidine base (B, purple) are shown. The histidine-tyrosine ring-opening pair characteristic for this group of epoxide hydrolases is shown in yellow.

SceEH was first identified as an epoxide hydrolase by Elfström *et al*.[156]. Compared to other epoxide hydrolases, the hydrolase activity of SceEH was low, but reproducible, and activity was detected with racemic phenanthrene 9,10-oxide, and *trans*- and *cis*-stilbene oxide. As SceEH was originally annotated as a putative dehalogenase, Elfström *et al*. also tested the dehalogenation with dichloroethane, but no dehalogenation could be detected. The authors called SceEH an 'orphaned' epoxide hydrolase, meaning that they assigned an enzymatic activity by assaying with a standard substrate while no physiologically relevant substrate has been identified. The low activity of SceEH with standard substrates can indicate that the physiologically relevant substrate is another epoxide, or that the epoxide hydrolase activity is not physiologically relevant. According to the alignment in Figure 24B, SceEH has two ring-opening residues (FP_1: Y147 and FP_2: Y213), but neither residue is oriented towards the active site in the homology model (Figure 23).

Not much is known about the enzymes NpuEH2 and PpuEH. While both enzymes are treated as known epoxide hydrolases by van Loo *et al*.[63], their epoxide hydrolase activity was extremely low with all of the tested substrates. The only substrate for which NpuEH2 clearly shows some activity is *para*-nitrophenyl glycidyl ether. According to the alignment (Figure 24B), NpuEH2 has two ring-opening residues (FP_1: Y143 and FP_2: Y206), but Y143 is not properly positioned in the homology model (Figure 23). PpuEH has one ring-opening residue (FP_2: Y211) according to the alignment, but no clearly identifiable residue is visible in the structure model as Y211 is positioned away from the active site. Nevertheless, during screening, both NpuEH2 and PpuEH were treated as epoxide hydrolases with potential dehalogenase activity.

Several epoxide hydrolases with different phylogenetic origins and different enantioselectivities were identified from *Erythrobacter litoralis*[155]. While EliEH3 is enantioselective towards (*S*)-styrene oxide and EliEH1 is selective towards (*R*)-styrene oxide, EliEH2 is not selective towards either of the two enantiomers. In addition to styrene oxide, EliEH2 had low but detectable hydrolysis activity with phenyl glycidyl ether, 1,2-epoxyhexane, and 1,2-epoxybutane. The hydrolysis activity of EliEH1 was overall superior to EliEH2 and EliEH3, so why does *Erythrobacter litoralis* have three different epoxide hydrolases? Woo *et al*. suggested that the different enantioselectivities might fulfil different physiological roles in the organism, but it is not certain if all three genes are expressed in the original strain. EliEH2 and EliEH3 were included in the alignment for the phylogenetic tree in Figure 21, while EliEH1 was not. Based on the phylogenetic analysis of Woo *et al*., EliEH1 would have appeared in the second largest epoxide hydrolase branch in the phylogenetic tree in Figure 21, close to epoxide hydrolases like the human HsaEH1[173] and AniEH from *Aspergillus niger*[174]. EliEH3 is included in the largest epoxide hydrolase branch (Figure 21,) and thus only EliEH2 appears close to a dehalogenase branch. Only one of the ring-opening residues of EliEH2 can easily be identified (RO_2: Y211) (Figure 23). Woo *et al*. suggested that this might explain the low hydrolysis activity of EliEH2 compared to EliEH1 and EliEH3.

For all four of these epoxide hydrolases, the tyrosine residue next to the nucleophile is close enough to be catalytically relevant. However, no epoxide hydrolase has been reported to use this residue for the opening of the epoxide ring.

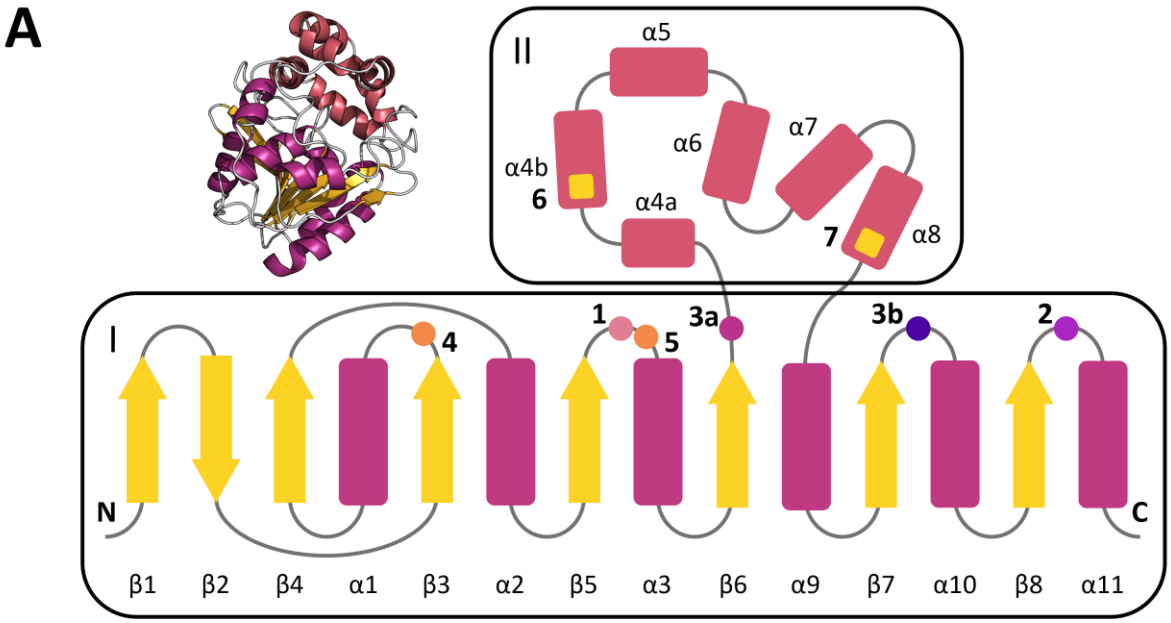

B

Enzyme	HS_2	$CN/HS_1/CB_{1/2}$	CRA_1	$RO_1/HP_{1/2}$	HS_3	RO_2/HP_3	CRA_2	B
CorEH	HGWP	GHDWGGSVA	ILDMI	INHIFF	-----	QWYAT	AWGGS	CGHFV
PaeCIF	HGFG	AHDIGIWNT	YMEAP	VWHFSF	-----	-YYRA	GGH--	CGHWL
AciCIF	HGFG	SHDLGNTAS	FMDSP	GWHFGY	-----	-YYRS	QKG--	TGHWM
ScoEH	HGVP	GEDWGAVIG	FAEAL	LWHLGF	-----	-VYRA	SAF--	AGHDL
EliEH2	HGYP	VHDYGVGVS	LGQTV	------	-----	-HYIA	ALDPV	VGHYP
PpuEH	HGFP	AHDYGGSVA	FLNSG	------	-----	-GYMP	VVDPL	IGHYP
NpuEH2	HGFP	VMDYGAPIG	VQNGN	------	KAY--	-LYSY	KND--	TGHFA
SceEH	HGFP	IFDYGSPVG	TQNGN	------	KEY--	-DYQN	ANDTI	TGHFA
DhlA	HGEP	VQDWGGFLG	IMNA-	------	TAW--	-FPKM	MKDKL	AGHFV
RpaHacD	HGFP	GHDRGARVS	VLDIL	IYHWSF	-----	-DYRA	ASG--	SGHFL

Figure 24. General topology and structure of α/β-hydrolase-fold epoxide hydrolases, haloacetate dehalogenases and haloalkane dehalogenases. A) Topology scheme highlighting important catalytic residues (numbered dots) in the highly conserved main domain (I) and the variable cap domain (II). B) Alignment of the active site of the selected epoxide hydrolases with the haloalkane dehalogenase DhlA[90] and the haloacetate dehalogenases RpaHacD[149]. The catalytic nucleophile (CN/1, pink), the histidine base (B/2, purple) and the charge-relay acid (CRA/3, hot pink) are shown. The charge relay acid can be located at two different positions in the sequence, either before the cap-domain after β-strand β6 (CRA_1/3a) or after the cap-domain between β-strand β7 and helix α10 (CRA_2/3b). In epoxide hydrolases, both supporting residues are in the cap domain (RO_1/6 and RO_2/7, yellow). The Tyr-Tyr[88] or His-Tyr[89] pair assists with the opening of the epoxide ring. In haloalkane dehalogenases, a primary halide-stabilising tryptophan is directly next to the catalytic nucleophile (HS_1/5, orange). Generally, this residue is supported by a secondary halide-stabilising residue, either an asparagine in the HGxP-motif in the main domain (HS_2/4, orange) for dehalogenase subfamilies HLD-II and HLD-III[62,91] or another tryptophan in the cap-domain (HS_3/6, yellow in A, orange in B) in subfamily HLD-I[90]. Haloacetate dehalogenases have two carboxylate-binding arginine residues next to the catalytic nucleophile ($CB_{1/2}$/5, orange) and a halide pocket. The halide pocket includes a histidine and tryptophan residue ($HP_{1/2}$/6, yellow) and a tyrosine (HP_3/7, yellow). The HP_1 and HP_3 residues overlap with the RO_1 and RO_2 residues in epoxide hydrolases.

4.1.1 Potential dehalogenase residues

Epoxide hydrolases, haloacetate dehalogenases, and haloalkane dehalogenases all use an Asp-His-Asp/Glu catalytic triad but have different supporting residues. Interestingly, the position of the charge relay acid differs between the two groups of selected epoxide hydrolases. In haloacetate dehalogenases, dehalogenases of subfamily HLD-II and some epoxide hydrolases, including PaeCIF, aCIF, ScoEH and CorEH, the charge relay acid is located after the β-strand β6, just before the cap-domain (3a in Figure 24A). Like in most epoxide hydrolases and dehalogenases of subfamilies HLD-I and HLD-III, the charge relay acid in NpuEH2, SceEH, EliEH2, and PpuEH is found at the second possible position between sheet β7 and helix α10 (3b in Figure 24A).

In addition to the catalytic triad, epoxide hydrolases use either a tyrosine-tyrosine[88] or a histidine-tyrosine pair to open the epoxide ring[89]. Both of these epoxide hydrolase residues are positioned in the variable cap domain (6 and 7 in Figure 24A) and overlap with the halide pocket of haloacetate dehalogenases. This pocket is formed by three important residues: a histidine and a tryptophan in helix α4b and a tyrosine in helix α8[112]. Because the histidine and tyrosine in the halide pocket overlap with the epoxide ring-opening residues, epoxide hydrolases like PaeCIF that utilise a histidine-tyrosine pair could, in theory, also facilitate a halide pocket. However, the third residue of the halide pocket, the tryptophan, is missing in all of the selected epoxide hydrolases. In addition to the halide pocket, haloacetate dehalogenases have two carboxylate-binding arginine residues close to the catalytic nucleophile (5 in Figure 24A). None of the selected epoxide hydrolases have these carboxylate-binding arginine residues.

Most haloalkane dehalogenases have a primary and a secondary halide-stabilising residue (4 and 5 in Figure 24A). As shown in the alignment (Figure 24B), two of the selected epoxide hydrolases have a tryptophan at the primary halide-stabilising position; CorEH and ScoEH (W100 and W104 respectively). However, neither of these two epoxide hydrolases possess a canonical secondary halide-stabilising residue. CorEH does have a tryptophan in the HGxP-motif (W34), but no haloalkane dehalogenase that utilises a tryptophan in the HGxP-motif has been reported. ScoEH has a tryptophan residue directly next to its histidine ring-opening residue (W153), but in the structural model this residue is oriented outwards, away from the active site. However, DatA from *Agrobacterium tumefaciens* has been reported to utilise a special asparagine-tyrosine pair[92,93] and some dehalogenases, such as DmxA[94], DsaA[82], DmrB[78] and DsvA[95], have been reported to have only one halide-stabilising residue. This suggests that some flexibility is possible when it comes to the halide-stabilising residues.

4.1.2 Ylehd from *Yarrowia lipolytica*

In 2017, Bendigiri *et al*. reported the discovery of an epoxide hydrolase, Ylehd from the tropical marine yeast *Yarrowia lipolytica*, with promiscuous haloalkane dehalogenase activity[175]. Supposedly, Ylehd catalyses the hydrolysis of epoxides at pH 8, while catalysing the dehalogenation of several haloalkanes at pH 4. Unfortunately, the publication lacked proper controls for autohydrolysis. We tried to reproduce the dehalogenase activity as claimed by Bendigiri *et al.* and therefore Ylehd was included in our screening efforts.

4.2 Methods

4.2.1 Expression and Purification

The selected epoxide hydrolase sequences were codon optimised for expression in *Escherichia coli* and ordered cloned into pET-28a(+) with N-terminal His_6-tag. The plasmids were transformed into *E. coli* BL21(DE3) and expression was tested under several expression conditions. After some testing, all epoxide hydrolases were expressed in the autoinduction medium ZYM-5052[161] without the optional trace metal solution. After inoculation from an overnight LB pre-culture, the culture is grown for 1h at 37 °C, followed by another 40 h at 20 °C. The cells were harvested by centrifugation, lysed through ultrasonication, and the proteins were purified by immobilised metal-affinity chromatography. Concentrations of the purified protein samples were determined using a NanoDrop™ device and protein concentrations were normalised for the screening reactions. Theoretical extinction coefficients and molecular weights are listed in Table S6 in Appendix A2.6.

4.2.2 Screening substrates

Epoxide hydrolase activity was determined using the adrenaline assay[164] for the selected epoxide hydrolases with several epoxide substrates (Figure 25A). Epoxide hydrolysis produces 1,2-diols that can be oxidised by periodate. Using back-titration of the oxidant with adrenaline to produce the red adrenochrome allows for quantification of the diols by measuring the absorbance at 490nm. Signals were corrected for autohydrolysis by subtracting the background signal from reactions without enzyme. The background signal of the enzyme solution was also considered by performing reactions without substrate. Dehalogenase activity for several haloalkanes (Figure 25A) was determined using the HOX assay (Chapter 2).

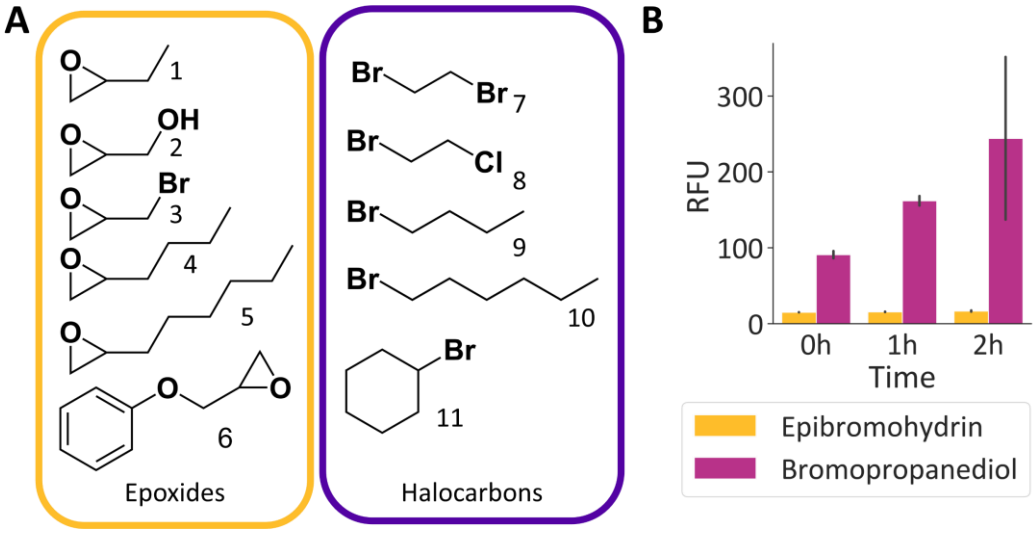

Figure 25. A) Screening substrates. **1**: 1,2-epoxybutane; **2**: 1,2-epoxyhexane; **3**: 1,2-epoxyoctane; **4**: 2,3-epoxy-1-propanol (glycidol); **5**: epibromohydrin; **6**: 1,2-epoxy-3-phenoxypropane (phenyl glycidyl ether); **7**: 1,2-dibromoethane; **8**: 1-bromo-2-chloroethane; **9**: 1-bromobutane; **10**: 1-bromohexane; **11**: 1-bromohexane. B) Fluorescence signal at 525 nm (excitation at 488 nm) for time samples of epibromohydrin and 3-bromo-1,2-propanediol. Samples were taken from 25 mM DMSO stocks, diluted 100-fold into HOX reaction buffer and incubated at 22 ˚C and 1200 rpm. Samples for the HOX assay were taken in triplicate.

Epihalohydrins like epibromohydrin can act as substrates for both epoxide hydrolases and dehalogenases. While epoxide hydrolases attack the C-O bond of the epoxide ring, haloalkane dehalogenases will instead attack the C-X bond. The epoxide hydrolysis of epibromohydrin produces 3-bromo-1,2-propanediol, and it is possible that 3-bromo-1,2-propanediol spontaneously hydrolyses in buffer, leading to the release of the halide without enzymatic catalysis. To verify this, we tested the stability of 3-bromo-1,2-propanediol in buffer by measuring the release of halides using the HOX assay (Figure 25B). While there was no significant change in the fluorescence signal over time for epibromohydrin in the absence of enzyme, the signal for 3-bromo-1,2-propanediol increased considerably. We assume that the epoxide hydrolysis activity of the epoxide hydrolases would be faster than any (promiscuous) dehalogenation activity, which implies that the release of halides as detected with the HOX assay for epibromohydrin does not indicate dehalogenation but instead is a side effect of epoxide hydrolysis.

4.3 Results and discussion

4.3.1 Hydrolysis of epoxides

Epoxide hydrolase activity with several epoxides was determined using the adrenaline assay[164] (Figure 26A). Significant hydrolysis of epoxides was found for CorEH, PaeCIF, PpuEH, and Ylehd. Some activity was detected for EliEH2 with 1,2-epoxybutane (0.019 ± 0.013 $\mu mol \cdot min^{-1} \cdot mg^{-1}$), for NpuEH2 with 1,2-epoxybutane (0.014 ± 0.006 $\mu mol \cdot min^{-1} \cdot mg^{-1}$), for SceEH with 1,2-epoxyoctane (0.023 ± 0.012 $\mu mol \cdot min^{-1} \cdot mg^{-1}$) and for ScoEH with 1,2-epoxy-3-phenoxypropane (0.024 ± 0.003 $\mu mol \cdot min^{-1} \cdot mg^{-}$), but no epoxide hydrolysis was detected for aCIF under these assay conditions.

4.3.2 Dehalogenation

The epoxide hydrolases were screened for dehalogenation using the newly developed HOX assay (Figure 26B). Most epoxide hydrolases showed no sign of halide release above autohydrolysis, but a significant signal was detected for the epoxide hydrolase CorEH from *Corynebacterium* sp. C12. Halide release was detected for 1-bromobutane and 1-bromohexane, both standard haloalkane dehalogenase substrates. The specific activity determined in this initial screening is about 10,000-fold lower than the average activity of several known haloalkane dehalogenases. The haloalkane dehalogenases DbjA, DhaA, DhlA and DmbA average a specific activity of 1 $\mu mol \cdot min^{-1} \cdot mg^{-1}$ with 1-bromobutane[62]. Both PpuEH and SceEH also show a slight signal above autohydrolysis for 1,2-dibromoethane and in the case of SceEH also for 1-bromo-2-chloroethane (Figure 25D). However, it proved difficult to reliably reproduce the very low signal for PpuEH and SceEH. Therefore, we decided to focus on confirming and further investigating the supposed dehalogenation by the epoxide hydrolase CorEH.

Interestingly, the measured concentrations of bromide were only 150-250 nM, well below the lowest detection limit of 20 µM achievable in microtiter plate format with the Iwasaki assay[107]. This means that the dehalogenase activity of CorEH would probably not have been detected were it not for the development of the sensitive halide oxidation assay with a detection limit of 20 nM for bromide (Chapter 2).

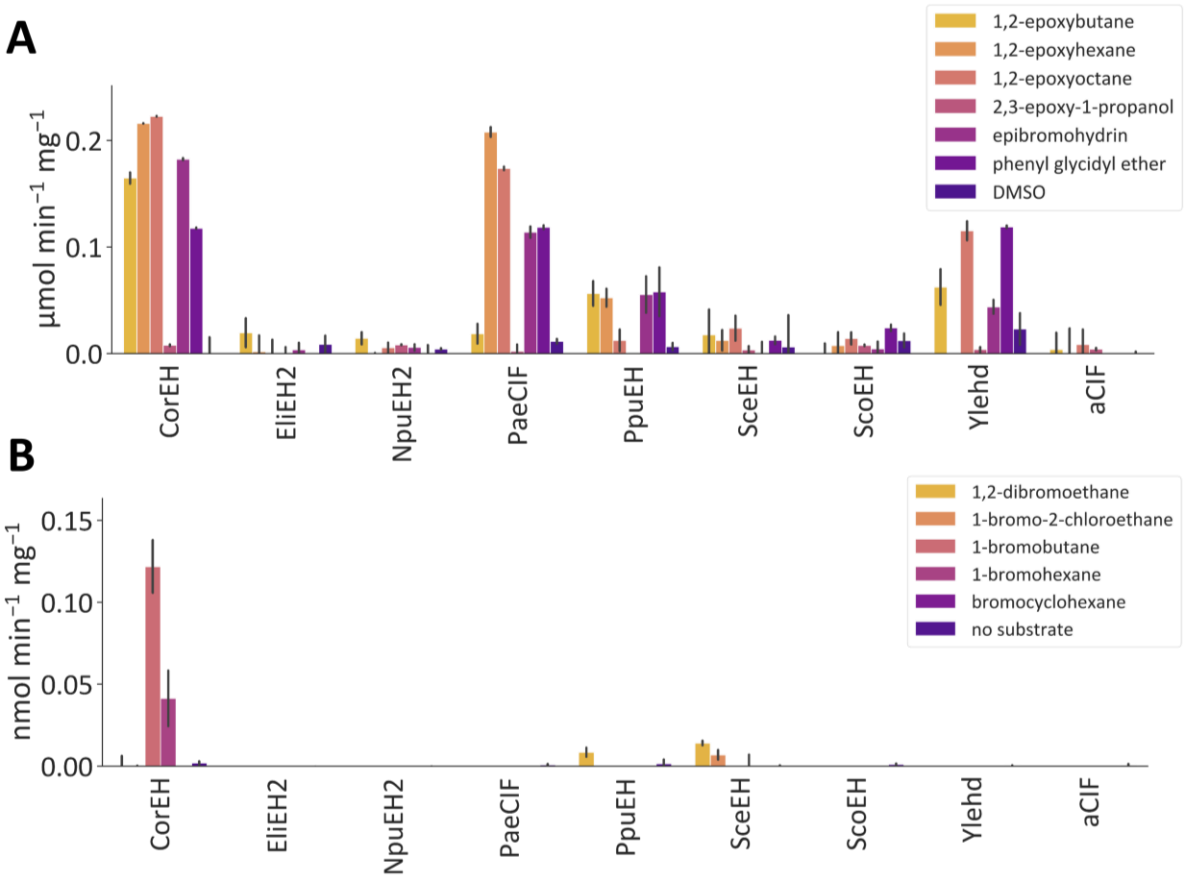

Figure 26. Screening results of reactions with the elected epoxide hydrolases with several epoxide and halogenated substrates A) Screening for epoxide hydrolysis using the adrenaline assay. Signal was corrected for autohydrolysis. Reactions with 10 mM substrate were performed at 37 °C and pH 8.0 for 45 min. B) Screening for dehalogenase activity using the HOX assay. Reactions with 20 mM substrate were incubated at 30 °C and pH 8.0 for 4 h. All reactions were performed in triplicate and standard deviations are shown.

4.3.4 CorEH catalyses epoxide hydrolysis and dehalogenation

Using the HOX assay, wild-type CorEH was reproducibly shown to exhibit significant dehalogenase activity with 1-bromobutane, with a specific activity of 0.25 nmol·min^{-1}·mg^{-1}. This was confirmed by gas chromatography-mass spectrometry (GC-MS, Figure 27A, C, and D), where instead of monitoring the bromide release, the production of 1-butanol is used to identify dehalogenase activity. In addition to the activity with 1-bromobutane, dehalogenase activity was detected with other substrates like 1-bromohexane, 1,2-dibromoethane, 1-iodobutane, and 1-iodohexane (Figure 27B).

To exclude unspecific reactions of substrates with the protein, two catalytic triad variants of CorEH, D123N (catalytic acid) and H264F (catalytic base), were also tested for dehalogenase activity. These variants alter the charge-relay acid and the histidine base, respectively, and consequently the alkyl-enzyme intermediate formed during the reactions cannot be hydrolysed by an activated water molecule[85,176]. The loss of activity in the reactions with these variants confirms that CorEH is actively converting 1-bromobutane to 1-butanol and that the reaction is an enzymatically catalysed reaction rather than a non-enzymatic conversion.

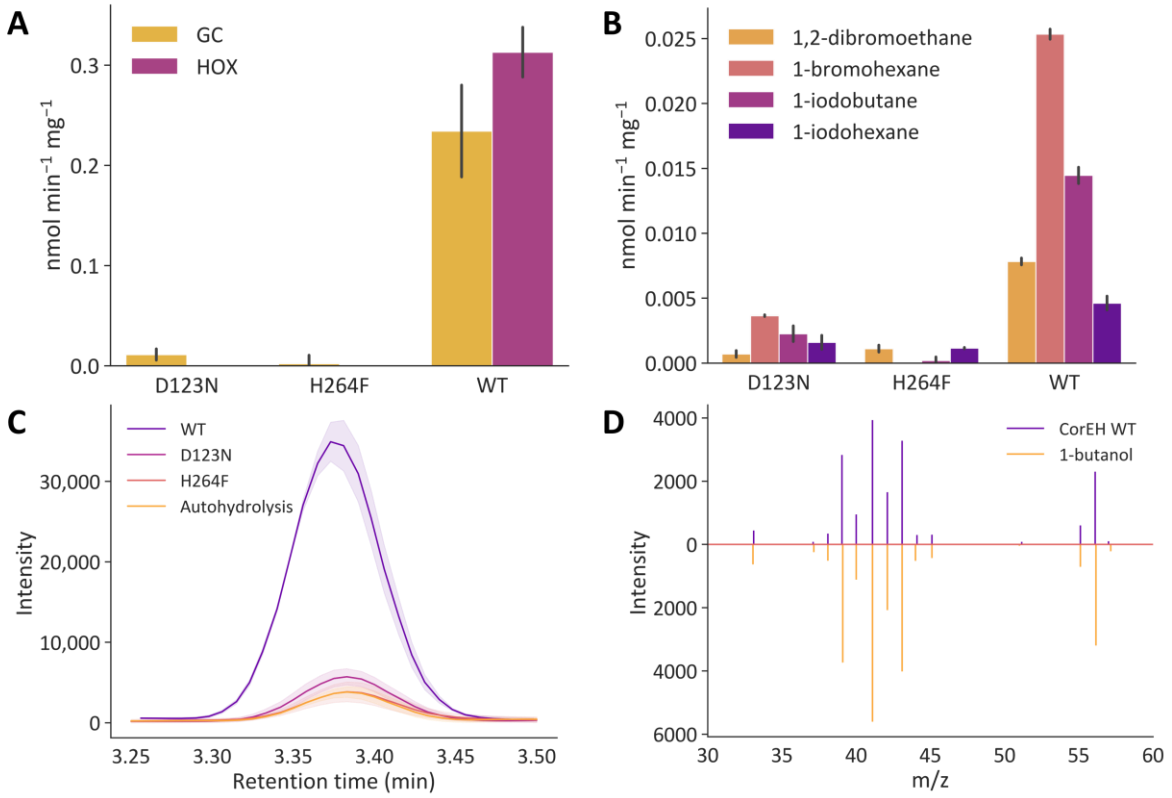

Figure 27. Dehalogenase activity of CorEH and the catalytic triad variants D132N and H264F. A) Specific activity of CorEH for 1-bromobutane. Activity was determined using the halide oxidation (HOX) assay, for bromide formation, and gas chromatography (GC), for the production of butanol. B) Specific activities of CorEH towards several other halogenated compounds. C) Overlay of gas chromatograms for the peak identified as butanol, clearly showing the difference between CorEH and autohydrolysis. The differences between the catalytic triad variants D123N and H264F and autohydrolysis are small. The peak of H264F is almost exactly the same as autohydrolysis. D) Mass spectra of the peak in (C) compared to a butanol standard (500 µM). To easily compare the two spectra, the standard spectrum is inversed. All reactions were performed in triplicate and standard deviations are shown (A/B/C). Experiments were repeated multiple times, resulting in similar values.

4.3.5 Failure to verify the claim that Ylehd has dehalogenase activity

From the screening in Figure 25C/D, it is clear that Ylehd from *Yarrowia lipolytica* can catalyse epoxide hydrolysis. However, no dehalogenase activity could be detected under the tested conditions. Bendigiri *et al*. claimed that Ylehd showed pH-dependent dual activity, with epoxide hydrolase activity at pH 8.0 and dehalogenase activity at pH 4.0[175]. The authors claimed dehalogenase activity of approximately 0.8 nmol·s^{-1}·mg^{-1} with 1-bromobutane and 1 nmol·s^{-1}·mg^{-1} with 1-bromohexane, but no controls for autohydrolysis are mentioned[80]. Therefore, the dehalogenase activity of Ylehd was compared to CorEH at pH 4.0 and pH 8.0 while correcting for autohydrolysis using controls without enzyme (Figure 28). No activity above autohydrolysis was detected for Ylehd at pH 4.0 or at pH 8.0. The epoxide hydrolysis by Ylehd could be confirmed with several epoxides (Figure 25A). The specific activities for hydrolysis of these epoxides are 10-fold lower than reported by Bendigiri *et al.* However, even a 10-fold lower dehalogenase activity of approximately 0.1 nmol·s^{-1}·mg^{-1} is easily within the detection limits of the HOX assay and should have been detected. Thus, we were unable to reproduce the dehalogenase activity claimed by Bendigiri *et al*.

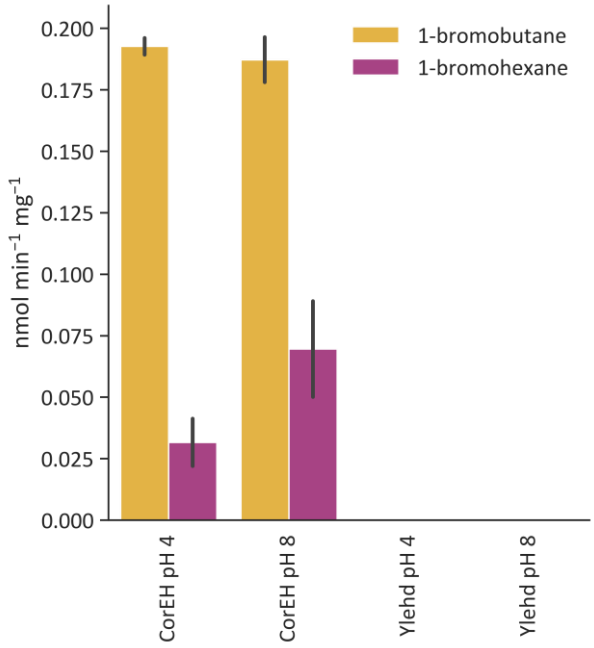

Figure 28. Comparing specific dehalogenase activities in nmol·min^{-1}·mg^{-1} for CorEH and Ylehd with 1-bromobutane and 1-bromohexane. Reactions were performed over 2 h at 30 °C, using 20 mM substrate at both pH 4.0 and pH 8.0. Activities were determined using the HOX assay.

Chapter 5

Characterisation of CorEH

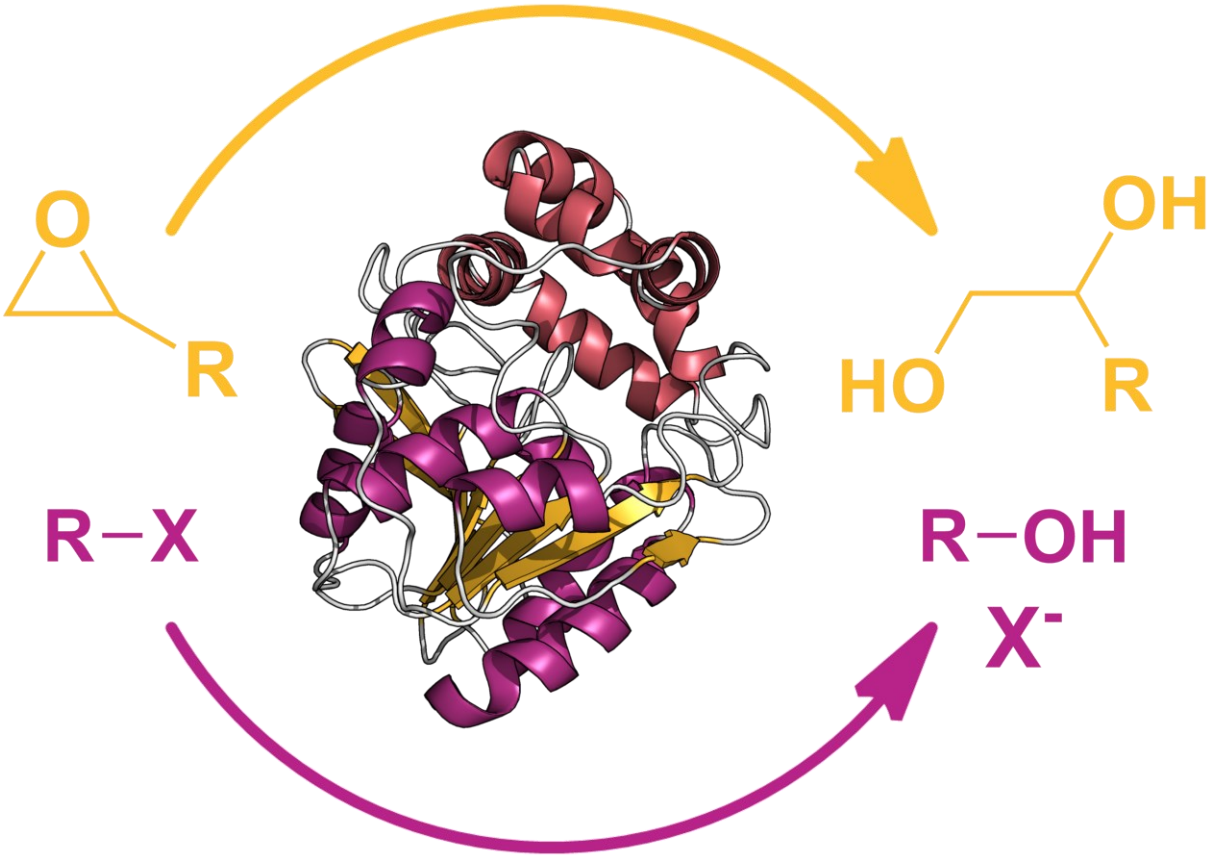

Adapted from:

'Promiscuous Dehalogenase Activity of the Epoxide Hydrolase CorEH from Corynebacterium sp. C12'

E.D. Schuiten, C.P.S. Badenhorst, G.J. Palm, L. Berndt, M. Lammers, J. Mican, D. Bednar, J. Damborský, U.T. Bornscheuer, *ACS Catalysis* 2021, *11* (10), 6113-6120

5.1 An epoxide hydrolase with dehalogenase activity

Promiscuity is often observed within the class of α/β-hydrolase fold enzymes, but despite the mechanistic similarities of epoxide hydrolases and dehalogenases, no α/β-hydrolases that exhibit both epoxide hydrolase and dehalogenase activity were previously known. Epoxide hydrolases and dehalogenases even share the same catalytic triad and form similar covalent reaction intermediates, yet they are known for attacking either epoxides or C-X bonds with perfect chemoselectivity, even when the substrate molecule possesses both an epoxide ring and a halogen atom. We screened a subset of epoxide hydrolases, closely related to dehalogenases, for dehalogenase activity and found that the epoxide hydrolase CorEH from *Corynebacterium* sp. C12 exhibits promiscuous dehalogenase activity (Chapter 4).

CorEH catalyses the dehalogenation of 1-bromobutane, 1-bromohexane, 1,2-dibromoethane, 1-iodobutane and 1-iodohexane. The highest specific activity was measured with 1-bromobutane (0.25 $nmol \cdot min^{-1} \cdot mg^{-1}$). These haloalkanes add to the already diverse set of epoxide substrates that are hydrolysed by CorEH (Figure 29). The promiscuous dehalogenase activity of CorEH with 1-bromobutane is approximately 5,000-fold lower compared to the highest reported primary activity of CorEH with cyclohexene oxide (1.41 $\mu mol \cdot min^{-1}$ mg^{-1})[154] but only 1,000-fold lower when compared to the activity with other epoxides like 1,2-epoxyoctane (0.22 $\mu mol \cdot min^{-1} \cdot mg^{-1}$). The highest epoxide hydrolase activity for CorEH was reported with C_6 and C_7 carbocyclic epoxides, while C_5 and C_8 carbocyclic epoxides were hydrolysed with less than 20% of the activity against cyclohexene oxide[154]. CorEH also hydrolyses linear 1,2-epoxyalkanes, like 1,2-epoxyhexane and 1,2-epoxyoctane, and epihalohydrins, like epichlorohydrin and epibromohydrin (Figure 29)[63]. CorEH seems to prefer substrates with longer alkyl chains, such as 1,2-epoxydecane, suggesting that hydrophobic interactions might play an important role in substrate binding[154].

To gain insight into the possible mechanism behind the promiscuous activity of CorEH, we determined the crystal structure and performed docking studies for several substrates. To prove the formation of alkyl-enzyme intermediates by CorEH for both epoxide hydrolysis and dehalogenation, two CorEH variants were designed to trap the enzyme in the alkyl-enzyme intermediate form. Substitution of the charge relay acid or catalytic base inhibits the hydrolysis of the alkyl-enzyme intermediate. This method has been used to investigate the mechanisms of both epoxide hydrolases[85] and dehalogenases[177]. In addition, three other CorEH variants were screened for epoxide hydrolysis and dehalogenation to investigate the involvement of two potential halide-stabilising residues in the promiscuous activity.

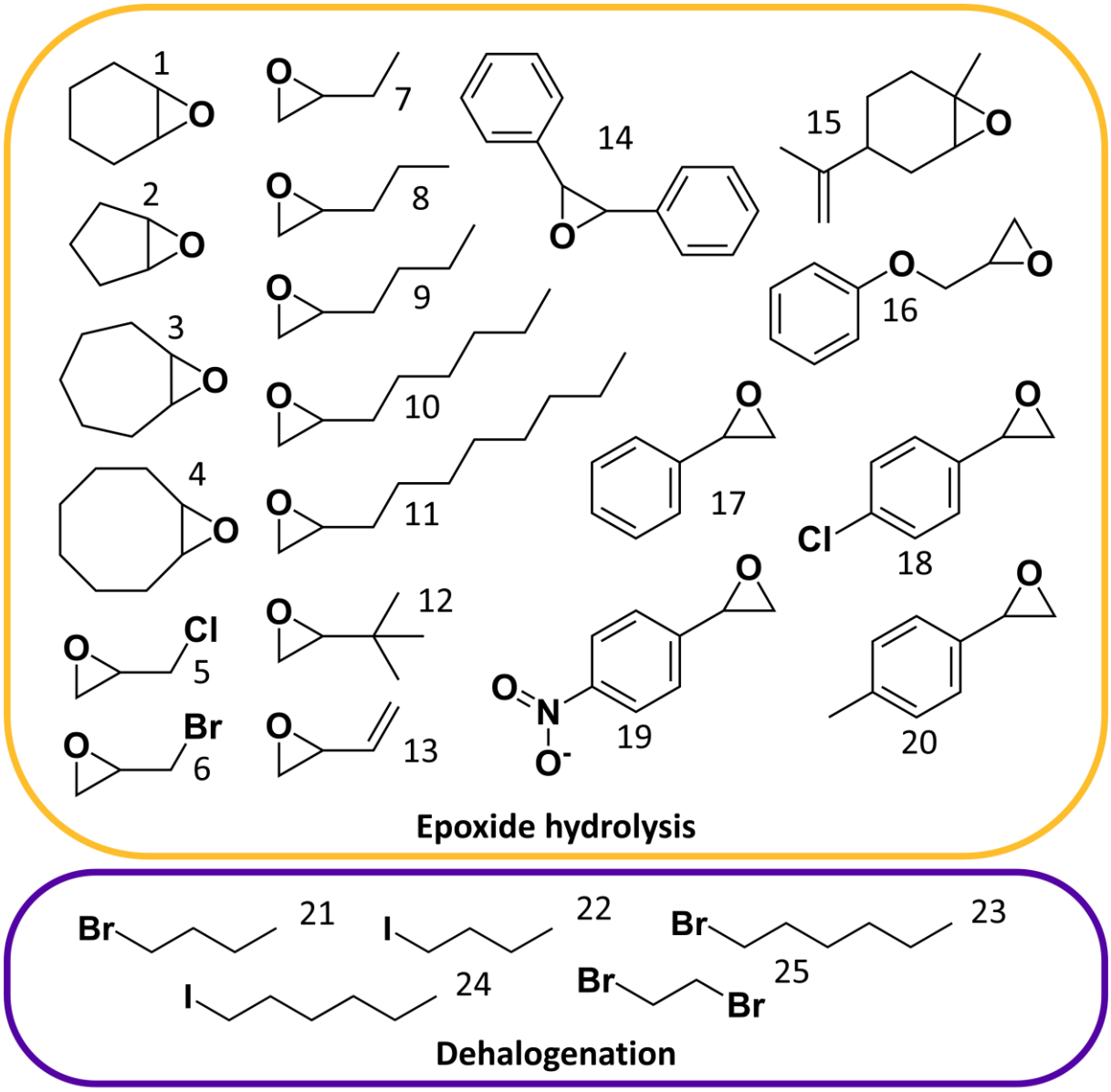

Figure 29. Epoxide and halogenated substrates accepted by the epoxide hydrolase CorEH from *Corynebacterium* sp. C12 with promiscuous dehalogenase activity. **1**: cyclohexene oxide; **2**: cyclopentene oxide; **3**: cycloheptene oxide; **4**: cyclooctene oxide; **5**: epichlorohydrin; **6**: epibromohydrin; **7**: 1,2-epoxybutane; **8**: 1,2-epoxypentane; **9**: 1,2-epoxyhexane; **10**: 1,2-epoxyoctane; **11**: 1,2-epoxydecane; **12**: vinyloxirane; **13**: *tert*-butyloxirane; **14**: *cis*-stilbene oxide; **15**: limonene-1,2-epoxide; **16**: 1,2-epoxy-3-phenoxypropane; **17**: styrene oxide; **18**: chlorostyrene oxide; **19**: *para*-nitrostyrene oxide; **20**: *para*-methylstyrene oxide; **21**: 1-bromobutane; **22**: 1-iodobutane; **23**: 1-bromohexane; **24**: 1-iodohexane; **25**: 1,2-dibromoethane.

5.2 Results & discussion

5.2.1 Analysing structure & function

The crystal structure of wild-type CorEH was determined to 2.2 Å resolution (Figure 30A). Technical details of the crystallisation are described in Appendix A2.10. As is typical for α/β-hydrolase enzymes, the main domain of CorEH is formed by a mostly parallel 8-stranded β-sheet connected through 6 α-helices (Figure 30C). Aside from the main domain, CorEH also possesses a cap domain that consists of 5 short α-helices. The active site of CorEH (Figure 30B) includes the catalytic triad used by both epoxide hydrolases and dehalogenases of the α/β-hydrolase family. The triad consists of the catalytic nucleophile D99, the charge relay acid D123 and the histidine base H264. Unlike most other epoxide hydrolases, the charge-relay acid of CorEH is located at the first position after β-sheet β6 before the cap-domain. Like other closely related epoxide hydrolases, such as PaeCIF, the epoxide ring-opening in CorEH is assisted by a non-canonical His-Tyr pair (H145 and Y209; Figure 30B).

Although CorEH is close to haloacetate dehalogenases in our phylogenetic tree (Chapter 3, Figure 14), CorEH does not have the catalytic motifs typical for haloacetate dehalogenases, such as the carboxylate-binding arginine residues around the catalytic nucleophile or halide pocket. In addition to the catalytic triad, most natural haloalkane dehalogenases have two halide-stabilising residues (Figure 31). These residues assist with the positioning of the substrate required for the S_N2 reaction and stabilise the transition state and the halide ion that is released during the cleavage of the carbon-halogen bond. The primary halide-stabilising residue is a tryptophan directly next to the catalytic nucleophile. This tryptophan residue is very conserved among haloalkane dehalogenases and is also found in many epoxide hydrolases (~70%). Aside from the halide-stabilisation in dehalogenases, the tryptophan also assists to position the catalytic nucleophile in the correct orientation for nucleophilic attack[178]. Instead of a tryptophan, some epoxide hydrolases have a leucine, isoleucine, phenylalanine, or tyrosine residue at this position. CorEH has a tryptophan, W100, at the primary halide-stabilising position, but lacks other canonical stabilising residues (Figure 30C). Aside from CorEH, only ScoEH, the epoxide hydrolase from *Streptomyces coelicolor*[63], has a tryptophan in the primary halide-stabilising position, but no dehalogenase activity was detected with ScoEH.

In dehalogenase subfamilies HLD-II and HLD-III, the primary halide-stabilising residue is paired with an asparagine located in the HGxP-motif (Figure 31). The HGxP-motif of CorEH includes a tryptophan residue (W34), which is not uncommon among epoxide hydrolases (approximately 24% in the characterised dataset), but it is not found in any of the dehalogenases. Tryptophan halide-stabilising pairs are characteristic for dehalogenases of subfamily HLD-I, but the halide-stabilisation pair is completed by a tryptophan in the variable cap-domain (Figure 31) instead of in the HGxP-motif. The sequence in this region of the variable cap-domain does not align with epoxide hydrolases, but when comparing crystal structures, the tryptophan residue at HS_3 nevertheless appears to overlap with one of the epoxide ring-opening residues (Chapter 2, Figure 12).

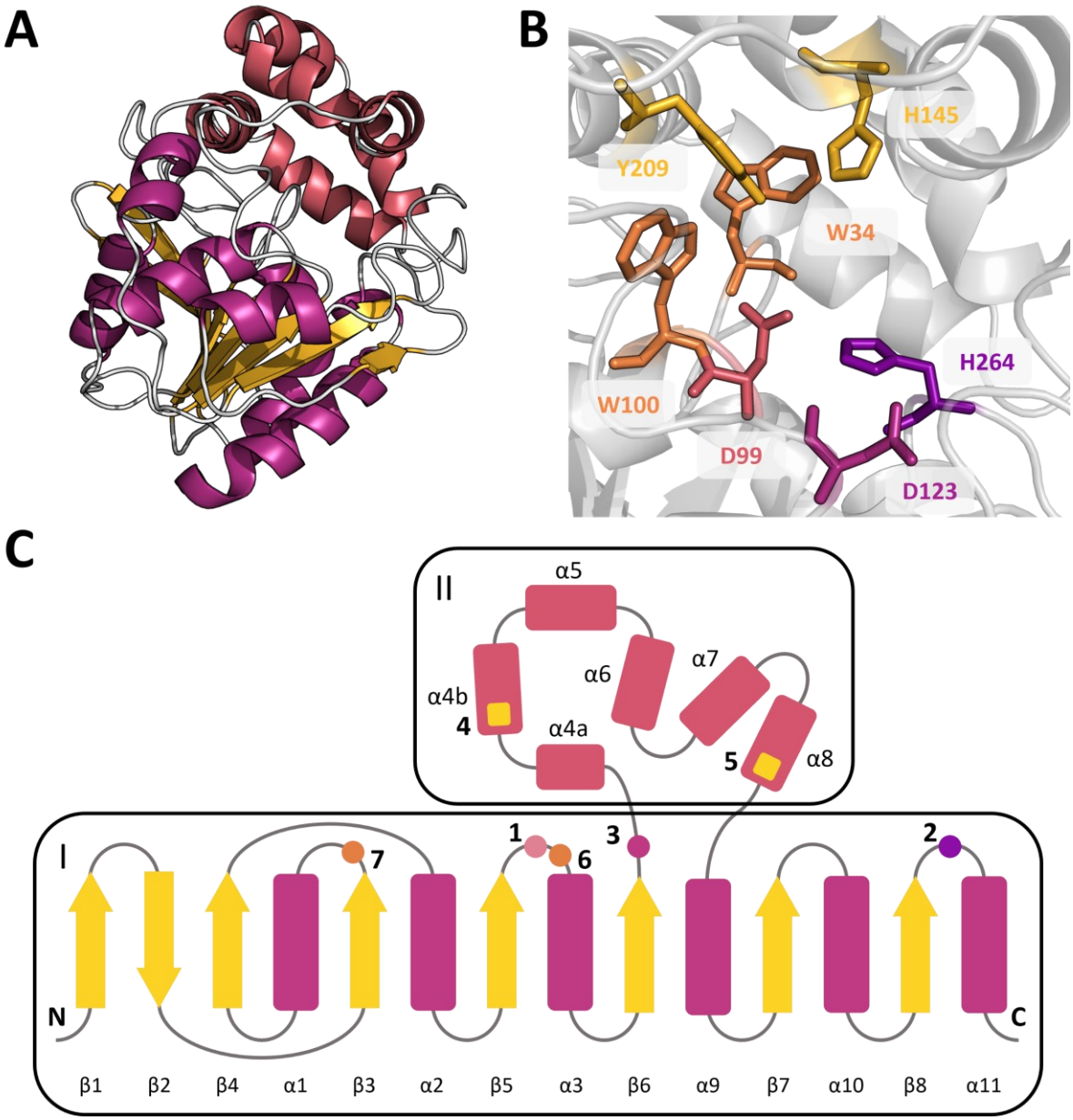

Figure 30. Structure and active site of CorEH. A) A single monomer of CorEH highlighting the highly conserved main domain consisting of a mostly parallel β-sheet (yellow) surrounded by α-helices (hot pink) and the variable cap domain (pink) typical for members of the α/β-hydrolase fold superfamily. The crystal structure of CorEH is available in the Protein Data Bank with PDB ID 7AC0. B) Close-up of the active site of CorEH showing the catalytic triad and supporting residues. C) Topology scheme highlighting the position of important catalytic residues with numbered dots in the main domain (I) and squares in the cap domain (II) of CorEH. The catalytic nucleophile D99 (1, pink), the histidine base H188 (2, purple), and the charge-relay acid D123 (3, hot pink) are shown. H145 and Y209 (4 and 5 respectively, yellow) form the non-canonical epoxide ring-opening pair. Two potential halide-stabilising residues are shown in orange: W100 in the primary halide-stabilising position (6) and W34 at the secondary halide-stabilising position in the HGxP-motif (7).

5.2.2 Special halide-stabilising residues

Although most haloalkane dehalogenases have a standard halide-stabilising pair, there are some dehalogenases that deviate from this standard. DatA from *Agrobacterium tumefaciens* has been reported to utilise a special pair consisting of an asparagine and a tyrosine[77,92,93] (Figure 31A). Like the dehalogenases from the HLD-II subfamily, DatA has an asparagine residue (N43) in the HGxP-motif. However, unlike members of the HLD-II subfamily, DatA has a tyrosine residue (Y109) next to the catalytic nucleophile instead of the usual tryptophan. In a study by Guan *et al*., docking experiments in the crystal structure of DatA showed a long distance (5.7 Å) between the hydroxyl group of Y109 and the substrate, indicating that the hydroxyl group is probably not involved in halide-stabilisation in DatA. They speculate that N43 is the primary halide-stabilising residue in DatA, and that Y109 may function as a secondary halide-stabilisation residue through the interaction of the halogen atom and positively charged hydrogen atoms at the edge of the aromatic ring[93], but this hypothesis is not supported by experimental data or literature. The highest reported activity for DatA was 50 nmol·min^{-1}·mg^{-1} with 1,3-dibromopropane and similar specific activities were reported with 1-bromohexane and 1-bromobutane (around 45 nmol·min^{-1}·mg^{-1}).

Introducing a standard halide-stabilising pair by mutation of the tyrosine residue to a tryptophan (Y109W) reportedly stabilised the enzyme-halide complex, but overall the variant was less active towards most of the tested substrates[92]. The tryptophan-selective fluorescence spectrum of DatA Y109W confirmed that the mutated residue interacts specifically with the halide ion during bromide binding and semi-empirical quantum mechanics (QM) calculations and molecular dynamics (MD) simulations indicated the formation of a second hydrogen bond that helps stabilise the partial negative charge on the halide ion as the carbon-halide bond is broken. Pre-steady-state kinetics revealed clear burst for substrate depletion and the formation of bromide ions with both the wild-type and the variant, but no burst in alcohol formation was observed. This indicated that substrate binding and cleavage of the carbon-halogen bond are fast steps in the reaction, while the hydrolysis of the alkyl-enzyme intermediate is the rate limiting step. DatA Y109W had a higher burst rate compared to the wild type, suggesting that the second hydrogen bond decreases the activation energy of the first step of the reaction. However, this is counteracted by a negative effect on the hydrolysis of the alkyl-enzyme intermediate, which explains why DatA could tolerate changing of the primary halide-stabilising residue without losing its catalytic activity towards most substrates[92].

DmxA[94], DsaA[82], DmrB[78], and DsvA[95] have been reported to have only the primary halide-stabilising tryptophan (Figure 31A). All four of these special dehalogenases have relatively low activity when compared to dehalogenases with a canonical halide-stabilising pair. The highest specific activity for DmxA was reported with 1,3-dibromopropane at 300 nmol·min^{-1}·mg^{-1}. The highest activities for DsaA (65 nmol·min^{-1}·mg^{-1}), DmrB (90 nmol·min^{-1}·mg^{-1}) and DsvA (68 nmol·min^{-1}·mg^{-1}) were reported with 1-bromohexane. In comparison, the average specific activity for DbjA, DhaA, DhlA, and DmbA is around 1 µmol·min^{-1}·mg^{-1} with 1-bromohexane[62] and 2.2 µmol·min^{-1}·mg^{-1} with 1,2-dibromopropane[62].

Although the halide-stabilising pair is generally considered a requirement for dehalogenation by haloalkane dehalogenases, these examples show that there is some flexibility, and one single halide-stabilising residue can be enough for catalysis to occur. It is possible that, like the dehalogenases with a single primary halide-stabilising tryptophan, CorEH uses only one halide-stabilising residue. The dehalogenase activity of wild-type CorEH with 1-bromobutane (0.25 $nmol \cdot min^{-1} \cdot mg^{-1}$) is about 4000-fold lower than the average activity of several natural dehalogenases with two halide-stabilising residues (1 $\mu mol \cdot min^{-1} \cdot mg^{-1}$)[62] and approximately 400-fold lower compared to the dehalogenases with a single halide-stabilising residue. The lack of a canonical secondary halide-stabilising residue in CorEH could partially explain the low dehalogenase activity compared to other dehalogenases.

5.2.3 Docking studies with typical substrates

Docking calculations were performed to study the binding of substrates typical for both epoxide hydrolysis and dehalogenation by CorEH. The formation of reactive Michaelis-Menten complexes indicated by favourable binding energies was compared with experimental results for CorEH, the closely related epoxide hydrolase PaeCIF, and the haloalkane dehalogenase DhlA (Appendix A1.3 TableS1). Plausible binding poses were identified for CorEH with both epoxides and bromoalkanes (Figure 31B).

As shown in Figure 31B, the distance of the oxygen atom of the nucleophile D99 to the attacked carbon atom is 3.4 Å for 1,2-epoxyhexane and 4.0 Å for 1-bromobutane. The epoxide ring of 1,2-epoxyhexane is stabilised by hydrogen bonds to the Y209 and H145 residues. The bromine atom of 1-bromobutane can be stabilised by the tryptophan W100 and possibly also by a hydrogen bond with the hydroxyl group of the epoxide ring-opening tyrosine Y209. The orientation of the sidechain of W34 in the crystal structure makes it unlikely that this residue is able to form hydrogen bonds with the substrate to stabilise the leaving halide. The iodinated substrates could bind with favourable energies, but no stabilisation of the leaving halogen was observed.

5.2.4 Capturing the alkyl-enzyme intermediate by mass spectrometry

To prove by mass spectrometry that the alkyl-enzyme intermediate is formed during the reaction, two CorEH variants were designed to trap the enzyme in the alkyl-enzyme intermediate form. In D123N, the charge relay acid is changed from an aspartic acid to an asparagine, and in H264F the histidine base is substituted by a phenylalanine. The mass spectrometry experiments were performed at Loschmidt Laboratories in Brno, Czech Republic. Unfortunately, the purity of the protein samples was insufficient, complicating the confirmation of the formation of the alkyl-enzyme intermediate (Appendix A1.1 Figure S1).

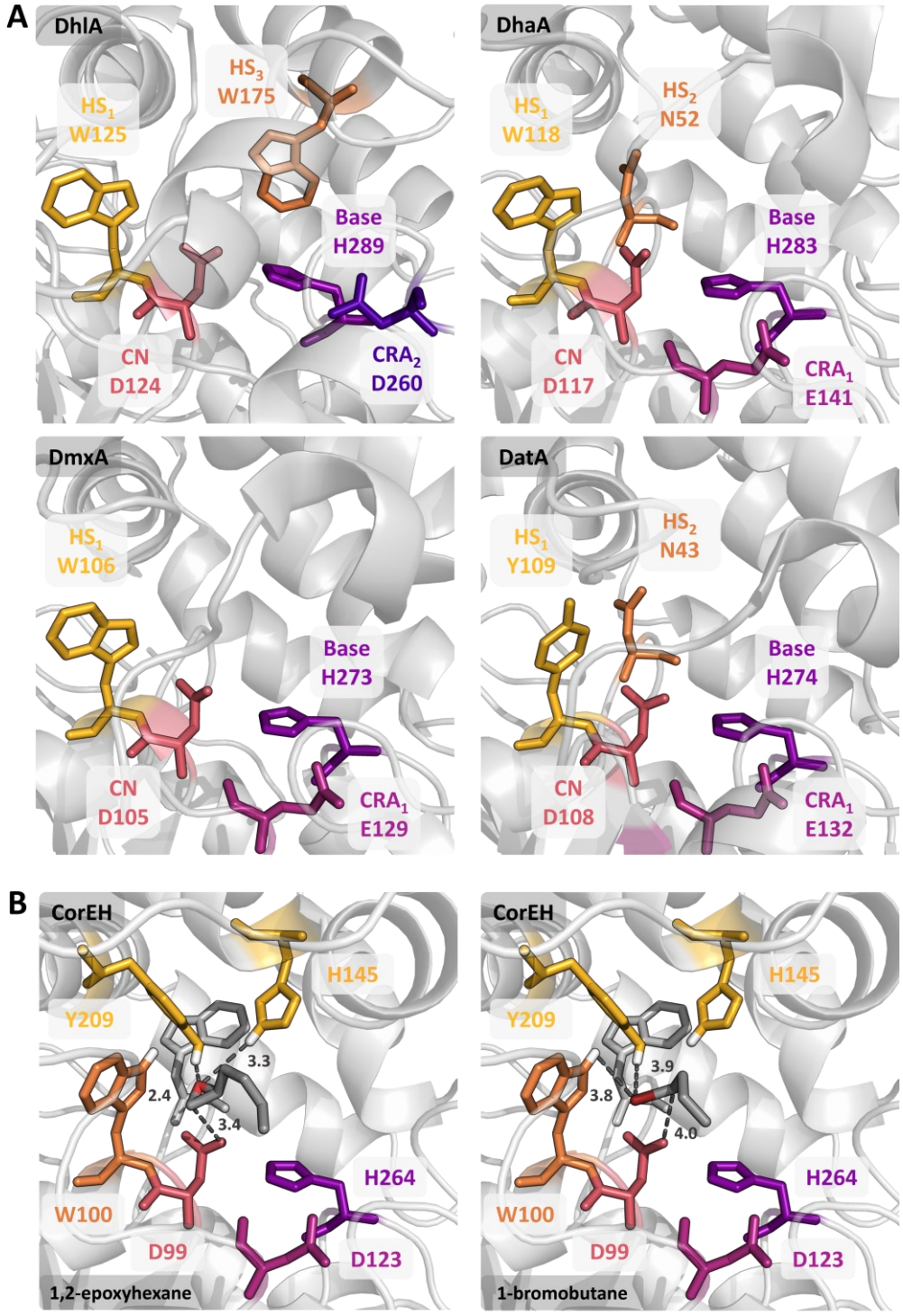

Figure 31. Overview of the active site. The catalytic triad is shown with the catalytic nucleophile (CN, pink), the charge-relay acid (CRA) at position 1 (CRA_1, dark pink) or 2 (CRA_2, dark purple), and the histidine base (B, purple). A) Active sites of four haloalkane dehalogenases: DhlA of subfamily HLD-I (PDB ID: 2HAD)[90], DhaA of subfamily HLD-II (PDB ID: 1BN6)[80], DmxA (PDB ID: 5MXP)[94] and DatA (PDB ID: 3WI7)[77,93]. The primary halide-stabilising residue is shown in yellow (HS_1) and the secondary stabilising residues in orange ($HS_{2/3}$). B) Predicted binding mode for 1,2-epoxyhexane and 1-bromobutane in CorEH (PDB ID: 7AC0). Epoxide ring-opening residues are shown in yellow and a potential halide-stabilising residue in orange. Distances (in Å) between the catalytic nucleophile and the attacked carbon atom, between the stabilising residues and the oxygen atom of the epoxide ring (red), and between stabilising residues and the bromide atom (dark red) are shown with dashes.

5.2.5 Mutational studies of CorEH

To investigate the involvement of the two tryptophan residues in the dehalogenase activity of CorEH, three variants were created and tested for epoxide hydrolysis and dehalogenation: W34F, W34N and W100A.

Two of the three variants target the tryptophan in the HGxP-motif (W34). In W34F, this tryptophan is changed to a phenylalanine, because this is the most common residue in the HGxP-motif for epoxide hydrolases in the characterised dataset (approximately 70%). Thus, W34F seemed to be a good substitution in the oxyanion hole to investigate the role of the tryptophan residue in the dehalogenation activity of CorEH without losing the epoxide hydrolase activity. In W34N, the tryptophan was changed to an asparagine to establish a canonical halide-stabilising pair commonly found in members of the HLD-II and HLD-III subfamilies. In the haloalkane dehalogenase DmxA, mutation of the equivalent residue to asparagine (Q40N) increased the activity towards 11 of 30 tested substrates, in some cases even doubling the specific activity[94]. Glutamine and asparagine are similar amino acids, while tryptophan and asparagine have very different properties. Thus, the mutation Q40N in DmxA is much more conservative than W34N in CorEH.

Lastly, in W100A the potential primary halide-stabilising residue is targeted and changed from a tryptophan to an alanine to remove the halide-stabilising function. Alanine scanning is a technique widely used to determine the contribution of a specific residue to the stability or function of a protein[179]. Interesting residues are mutated to alanine, because it has a non-bulky, chemically inert methyl sidechain and mimics the secondary structure preferences of many other amino acids. We wanted to remove the potential halide-stabilising function of W100 completely and thus alanine was chosen. The three variants, W34F, W34N and W100A, were screened together with wild-type CorEH and the two catalytic triad variants, D123N and H264F. The catalytic variants alter the charge-relay acid and the histidine base and are expected to prevent the hydrolysis of the alkyl-enzyme intermediate by an activated water molecule[85,176].

Compared to wild-type CorEH, the three variants lost most of both the dehalogenase and epoxide hydrolase activities. The W34F variant retained most of the dehalogenase activity, except towards 1-bromobutane, for which 45% of the wild-type activity was retained. However, the W34F variant lost most of the epoxide hydrolase activity. The W34F variant has the highest relative activity towards 1,2-epoxyoctane at approximately 24% of the wild-type activity. As the tryptophan W34 did not seem to be directly involved in the reaction mechanism based on the crystal structure, the loss in activity seems to indicate that the tryptophan is important for the overall structure of the CorEH active site.

The variant W34N loses almost all activity towards 1,2-epoxyoctane (5% of the wild-type activity) and most activity towards 1-bromobutane (10% of the wild-type activity). In W34N, the large hydrophobic tryptophan residue is substituted by a much smaller polar residue, while in W34F it is replaced by another large hydrophobic residue. Misawa *et al*. already proposed that hydrophobic interactions might be important for substrate binding[154] and it is possible that the change in hydrophobicity causes the more severe loss of activity for W34N.

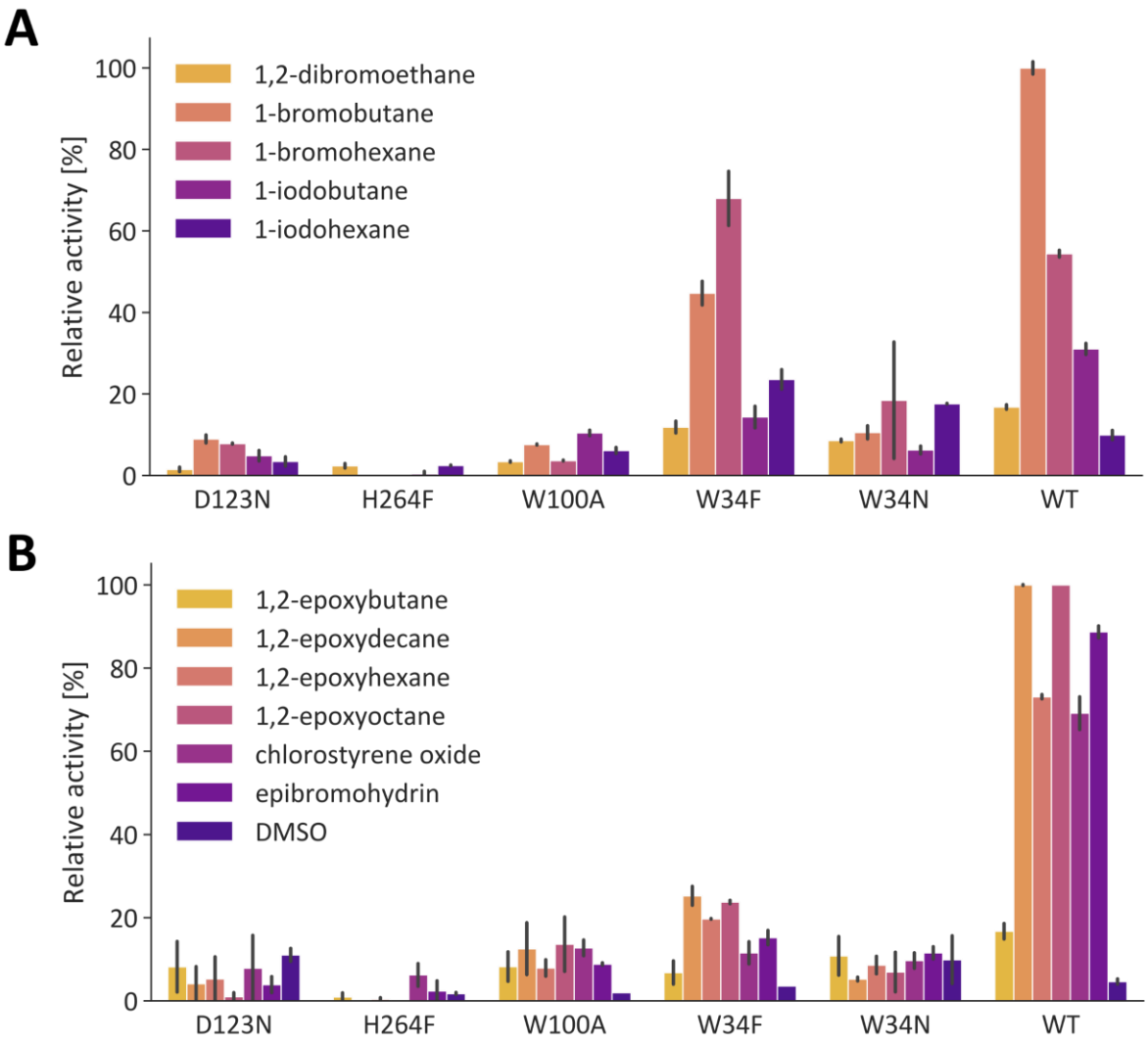

Figure 32. Relative activity of CorEH variants with several halogenated substrates. A) Relative dehalogenation as a percentage of the wild-type activity with 1-bromobutane (0.12 nmol·min^{-1}·mg^{-1} in this assay). Reactions with 20 mM substrate performed at pH 8 and 30 °C for 20 h. Activity determined using the HOX assay for the bromoalkanes and with the iodide assay for the iodoalkanes. B) Relative epoxide hydrolysis as a percentage of the wild-type activity with 1,2-epoxyoctane (0.22 ± 0.0 µmol·min^{-1}·mg^{-1}). Reactions with 10 mM substrate performed at pH 8 and 30 °C for 2 h. Activity was determined using the adrenaline assay. All reactions were performed in triplicate and standard deviations are shown.

Like W34N, the variant W100A loses most of the wild-type activity, exhibiting only 13% of the wild-type activity towards 1,2-epoxyoctane and 8% of the wild-type activity towards 1-bromobutane. The equivalent loss of epoxide hydrolysis and dehalogenation means it is difficult to conclude if W100 is specifically involved in the dehalogenation. The loss of both activities for the W100A variant can possibly be explained by the secondary function of the tryptophan[178]; removal of W100 might lead to the incorrect positioning of the catalytic nucleophile for the nucleophilic attack involved in both epoxide hydrolysis and dehalogenation. W100A also introduces a large change in hydrophobicity in the active site, exchanging a large amino acid with a very small amino acid. In future studies, other mutations could be tried that might not cause the loss of both activities simultaneously. For example, the tryptophan could be substituted by similarly sized non-polar residues such as tyrosine or phenylalanine, or the slightly smaller leucine or isoleucine, which are common in epoxide hydrolases that do not have this tryptophan. Especially phenylalanine would be a promising choice as it is similar in size to tryptophan but does not have the potential to form the hydrogen bond for stabilising the halide. Regardless, both W34 and W100 seem to be important for substrate binding to the active site, but it is currently unclear whether they are directly involved in halide-stabilisation.

5.2.6 Mechanism of CorEH

The catalytic mechanism for both epoxide hydrolysis and dehalogenation by α/β-hydrolases is very similar, but despite using the same catalytic triad and performing a S_N2 attack with the same nucleophilic aspartate, both reactions go through different transition states. In CorEH the catalytic nucleophile D99 can perform a nucleophilic attack on both the primary carbon of the epoxide or the halocarbon to presumably form an alkyl-enzyme intermediate (Figure 33). The nucleophilic attack is enabled by several supporting residues that help position the substrate in the active site. For the epoxide hydrolysis, a histidine (H145) and tyrosine (Y209) pair help with the opening of the epoxide ring by forming hydrogen bonds with the oxygen of the epoxide. These residues also help stabilise the alkyl-enzyme intermediate through hydrogen bonds with the hydroxyl group, before the intermediate is hydrolysed by the water molecule activated by the charge relay acid and histidine base pair. For dehalogenation, CorEH probably uses the tryptophan residue W100 right next to the catalytic aspartate to position the haloalkane substrate correctly for the S_N2 reaction and to stabilise the transition state and halide ion that is released during the cleavage of the carbon-halogen bond (Figure 33). Based on the docking studies (Figure 31), this tryptophan could be involved in the stabilisation of the halide by the epoxide ring-opening tyrosine (Y209), as it is close enough to be able to form hydrogen bonds to stabilise the substrate. However, it is also possible that CorEH only uses a single residue to stabilise the halide like several haloalkane dehalogenase have been reported to do (Section 5.2.2).

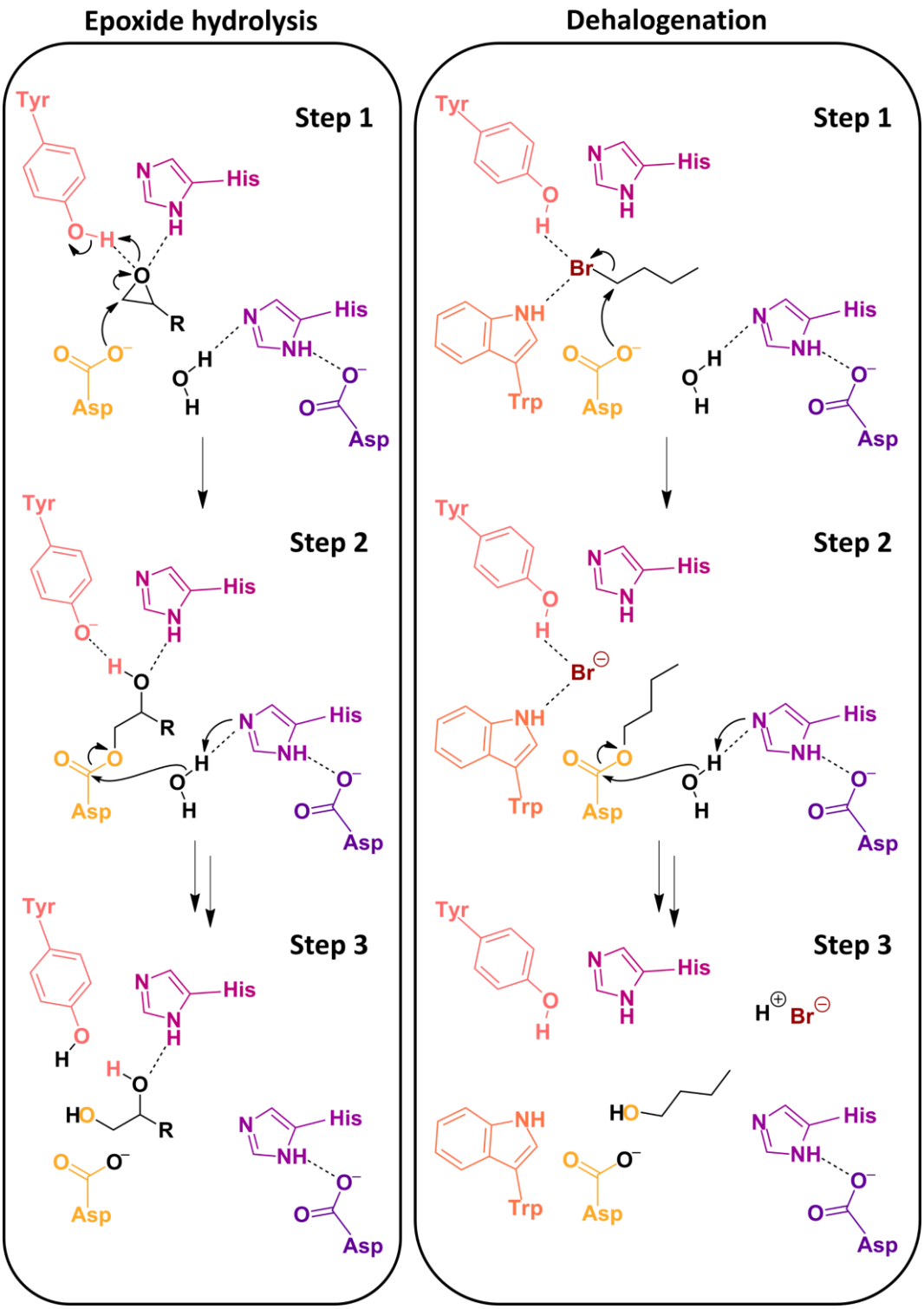

Figure 33. Simplified catalytic mechanism for epoxide hydrolysis by CorEH and proposed mechanism for dehalogenation by CorEH. Both reactions start with a nucleophilic attack on the epoxide or halocarbon by the nucleophilic aspartate (yellow), which results in the formation of an alkyl-enzyme intermediate. The alkyl-enzyme intermediate is hydrolysed by a water molecule activated by the histidine-aspartate pair (purple). This leads to the release of a vicinal diol after epoxide hydrolysis or the release of an alcohol in the case of dehalogenation. Possible further intermediates and transition states between step 2 and step 3 were omitted for clarity. Epoxide ring-opening is assisted by a histidine-tyrosine pair (pink). The halide is probably stabilised by hydrogen bonds with the tryptophan (orange) and potentially also by a hydrogen bond with the tyrosine (pink).

Chapter 6

Summary & Outlook

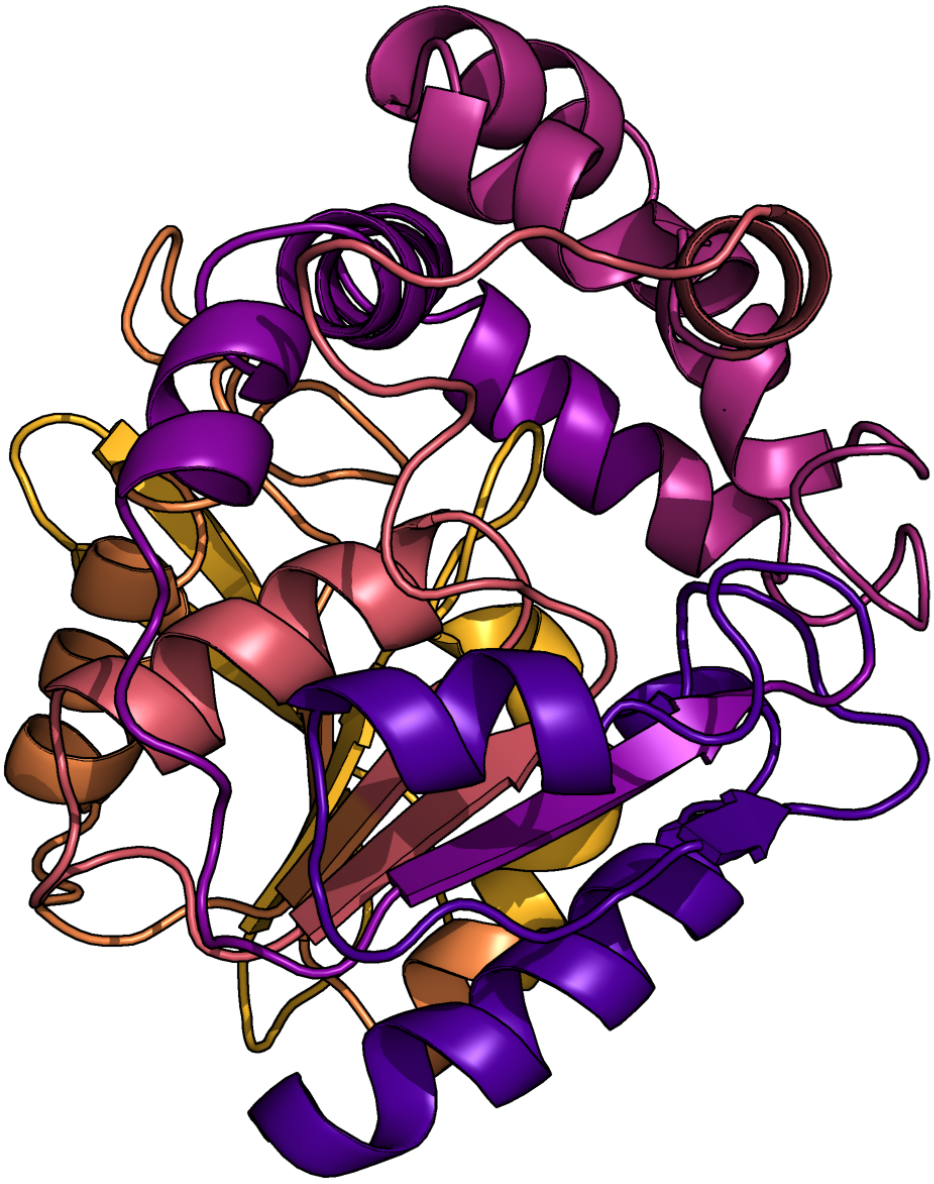

Enzymes are well-known for being remarkably selective catalysts. They are often able to catalyse reactions for certain molecules while leaving other similar molecules completely unchanged. Nevertheless, many enzymes are capable of catalysing other reactions and/or transforming other substrates than their physiologically relevant activities. This phenomenon is referred to as enzyme promiscuity and it is thought to play an important role in the emergence of novel functions by providing a starting point for divergent evolution towards different enzymatic activities[41–46]. It is important for enzymes to be selective to avoid harmful side-products and increase reaction efficiency, but often catalysts are not optimised beyond what is required for their function. Life profits from the cross-reactivity and enzyme promiscuity through accidental discovery of new helpful molecules and pathways, while using regulation to quickly adapt to changing circumstances.

Enzymes are grouped together with other similar proteins into structural families and superfamilies. Members of a structural family share significant structural elements and often have similar catalytic mechanisms. However, they often catalyse very different chemical reactions and accept a variety of different substrates. Promiscuous activities are common within superfamilies, where the primary function of one family member is often found as promiscuous activity in other family members[36,40]. Together with the structural similarities, this prevalent cross-reactivity suggests a common evolutionary origin. One of the largest structural superfamilies is the α/β-hydrolase-fold family. Despite sharing a highly conserved core structure, this superfamily is catalytically diverse and spans several distinct enzyme classes including hydrolases, acyltransferases, oxidoreductases, lyases, and isomerases[58,59]. Epoxide hydrolases and dehalogenases of the α/β-hydrolase-fold family even share the same Asp/Glu-His-Asp catalytic triad and form similar covalent alkyl-enzyme reaction intermediates, yet they are known for attacking either epoxides or C-X bonds with perfect chemoselectivity. Although promiscuity is often observed within the α/β-hydrolase fold family and despite their mechanistic similarities, no α/β-hydrolases were known that exhibit both epoxide hydrolase and dehalogenase activity simultaneously.

The versatility of the catalytic triads used by α/β-hydrolases makes these enzymes attractive targets for the conversion of catalytic activity through protein engineering[28,29,102,103]. Several attempts were made to introduce dehalogenase activity in an epoxide hydrolase, and after several rounds of designing and screening different variants of the epoxide hydrolase PaeCIF from *Pseudomonas aeruginosa*, minor dehalogenase activity was detected for some of the variants. However, despite promising first results it proved extremely difficult to reliably reproduce the results, primarily due to expression problems and low sensitivity of the halide detection assays that were available at the time. Since the conversion proved to be more difficult than expected (unpublished data), it was decided to investigate other potential protein scaffolds.

Considering the prevalence of catalytic promiscuity among members of the α/β-hydrolase-fold superfamily[58], and the close relationship and catalytic similarities between epoxide hydrolases and dehalogenases, it seemed odd that no enzyme is known to have both epoxide hydrolase and dehalogenase activity. We argued that it is highly probable that a promiscuous epoxide hydrolase-dehalogenase enzyme exists, but it simply has not been found yet due to the absence of sensitive high-throughput halide assays and not screening the right set of enzymes. Although several established assays were available for the determination of dehalogenase activity, these assays suffer major drawbacks. For example, one of the most popular assays, the Iwasaki assay, is not very sensitive and uses extremely toxic chemicals, while pH assays like the phenol red assay are inherently unreliable and insensitive due to the low buffer concentrations employed[107,114]. Thus, a new assay for the screening of dehalogenase activity through the selective detection of halides was developed[115]. The halide oxidation assay provides a safer, more reliable, and most importantly, much more sensitive method to detect dehalogenase activity.

Using molecular phylogenetics, we studied the evolutionary relationship between epoxide hydrolases and dehalogenases to identify interesting extant epoxide hydrolases. Molecular phylogenetics uses a multiple sequence alignment of the amino acid or nucleotide sequences of extant enzymes to construct a phylogenetic tree. At first, we tried using a large dataset with almost 3,500 putative epoxide hydrolase and dehalogenase sequences, but we quickly realised the resulting phylogenetic tree was impractical. Most of the sequences in this large dataset were not characterised experimentally but annotated automatically based on their sequence similarity to a rather limited number of characterised sequences. Although automated annotations can be used as predictions for catalytic activity, they are often wrong. As we were particularly interested in the interface of both epoxide hydrolase and dehalogenase activities, we needed more certainty and a change in direction was necessary.

Instead of trying to filter the α/β-hydrolase fold database, experimentally characterised sequences were collected through literature research. This smaller dataset consisting of characterised sequences resulted in a phylogenetic tree containing 45 epoxide hydrolases, 30 haloalkane dehalogenases and 7 haloacetate dehalogenases from a variety of different organisms. Ancestral sequence reconstruction was attempted for several interesting nodes in this phylogenetic tree. By combining the multiple sequence alignment, the evolutionary relationships from the phylogenetic tree, and evolutionary models, a hypothetical sequence of the theoretical ancestor can be determined. Unfortunately, it was difficult to get good soluble protein expression with the ancestral sequences and despite our best efforts it was not possible to obtain reliable and reproducible screening results. Instead of trying to improve protein expression and purification protocols for the ancestral sequences, we decided to focus on screening extant sequences with the newly developed halide oxidation assay to find a promiscuous epoxide hydrolase-dehalogenase.

In addition to reconstructing ancestral sequences, eight extant epoxide hydrolases could be selected for screening towards dehalogenase activity and as promising potential engineering scaffolds from this phylogenetic tree. The eight selected epoxide hydrolases were screened for dehalogenase activity with several haloalkane substrates and the epoxide hydrolase CorEH from *Corynebacterium* sp. C12 was found to exhibit promiscuous dehalogenase activity. Interestingly, the measured concentrations of bromide for the initial hit with CorEH were only 150-250 nM, well below the lowest detection limit of 20 µM achievable in microtiter plate format with the Iwasaki assay[107]. This means that the dehalogenase activity of CorEH would probably not have been detected were it not for the development of the sensitive halide oxidation assay.

CorEH is an epoxide hydrolase that can also catalyse the dehalogenation of haloalkanes, particularly bromoalkanes such as 1-bromobutane and 1-bromohexane. The dehalogenase activity of wild-type CorEH with 1-bromobutane (0.25 $nmol \cdot min^{-1} \cdot mg^{-1}$) is about 4,000-fold lower than the average activity of several natural dehalogenases with two halide-stabilising residues (1 $\mu mol \cdot min^{-1} \cdot mg^{-1}$)[62] and approximately 400-fold lower compared to the dehalogenases with a single halide-stabilising residue. The crystal structure of CorEH was determined to 2.2 Å. Our structure-function studies suggest that the dehalogenase activity of CorEH probably stems from the presence of at least one halide-stabilising residue. Unfortunately, this could not be confirmed experimentally via mutagenesis as the W100A variant lost both the dehalogenase and epoxide hydrolase activity in equal measure, making it difficult to demonstrate that W100 is involved in halide stabilisation. The loss of both activities for variant W100A can possibly be explained by the secondary function of the tryptophan[178]; removal of W100 might lead to the incorrect positioning of the catalytic nucleophile for the nucleophilic attack involved in both epoxide hydrolysis and dehalogenation. Nevertheless, computational modelling of Michaelis-Menten complexes, utilising the crystal structure of CorEH, supports the hypothesis that the tryptophan W100 is involved in halide stabilisation in CorEH. Based on docking studies, the epoxide ring-opening tyrosine is also close enough to form hydrogen bonds to stabilise the substrate. However, it is also possible that like several characterised haloalkane dehalogenases, CorEH only uses a single residue to stabilise the halide. Removal of the tryptophan at the primary halide-stabilising position resulted in the loss of both activities, likely due to the loss of its secondary function to properly position the catalytic nucleophile[178]. Substitution of the uncommon tryptophan in the HGxP-motif with phenylalanine does not completely remove the dehalogenase activity. Nevertheless, it causes a significant drop in both haloalkane dehalogenase and epoxide hydrolase activities, indicating that this residue is important for catalysis or the structural integrity of CorEH.

Enzyme promiscuity plays an important role in enzyme evolution and the diversification of enzymes. Several researchers have attempted to interconvert epoxide hydrolase and dehalogenase activity, or to find an enzyme with both activities, without success. It would be hard to maintain the view that promiscuity is a fundamental property crucial to enzyme evolution if we could not observe promiscuity between two enzyme classes with such similar reaction mechanisms. Our findings show that dual epoxide hydrolase and dehalogenase activity can occur in one natural protein scaffold. We believe that we succeeded because we used a phylogenetic analysis of characterised sequences to select the right subset of epoxide hydrolases to investigate and due to the much more sensitive halide assays not available to those before us. The versatility of the catalytic triad in α/β-hydrolases combined with the variety of possible supporting residues found in both epoxide hydrolases and dehalogenases shows that catalytic mechanisms can be flexible. This flexibility allows space for diversification of catalytic residues without loss of function, giving rise to novel (promiscuous) functions and new cross-reactivities.

References

(1) Nelson, D. L.; Cox, M. M. *Lehninger Principles of Biochemistry*, 5th ed.; W.H. Freeman and Company, 2008.

(2) Whitford, D. *Proteins Structure and Function*; John Wiley & Sons Ltd, 2005.

(3) Bornscheuer, U. T.; Huisman, G. W.; Kazlauskas, R. J.; Lutz, S.; Moore, J. C.; Robins, K. Engineering the Third Wave of Biocatalysis. *Nature* **2012**, *485* (7397), 185–194. https://doi.org/10.1038/NATURE11117.

(4) Cohen, S. N.; Chang, A. C. Y.; Boyer, H. W.; Helling, R. B. Construction of Biologically Functional Bacterial Plasmids In Vitro. *Proc Natl Acad Sci U S A* **1973**, *70* (11), 3240. https://doi.org/10.1073/PNAS.70.11.3240.

(5) Arnold, F. H. Directed Evolution: Creating Biocatalysts for the Future. *Chemical Engineering Science* **1996**, *51* (23), 5091–5102. https://doi.org/10.1016/S0009-2509(96)00288-6.

(6) Schmidt-Dannert, C.; Arnold, F. H. Directed Evolution of Industrial Enzymes. *Trends in Biotechnology* **1999**, *17* (4), 135–136. https://doi.org/10.1016/S0167-7799(98)01283-9.

(7) Jochens, H.; Bornscheuer, U. T. Natural Diversity to Guide Focused Directed Evolution. *ChemBioChem* **2010**, *11* (13), 1861–1866. https://doi.org/10.1002/cbic.201000284.

(8) Zuckerkandl, E.; Pauling, L. Evolutionary Divergence and Convergence in Proteins. *Evolving Genes and Proteins* **1965**, 97–166. https://doi.org/10.1016/B978-1-4832-2734-4.50017-6.

(9) Pauling, L.; Zuckerkandl, E.; Henriksen, T.; Lövstad, R. Chemical Paleogenetics. Molecular "Restoration Studies" of Extinct Forms of Life. *Acta Chemica Scandinavica* **1963**, *17 supl.* (9–16), 9–16. https://doi.org/10.3891/acta.chem.scand.17s-0009.

(10) NCBI Resource Coordinators. Database Resources of the National Center for Biotechnology Information. *Nucleic Acids Res* **2016**, *44* (D1), D7-19. https://doi.org/10.1093/nar/gkv1290.

(11) The Uniprot Consortium. UniProt: The Universal Protein Knowledgebase in 2021. *Nucleic Acids Research* **2021**, *49* (D1), D480–D489. https://doi.org/10.1093/nar/gkaa1100.

(12) Altschul, S. F.; Gish, W.; Miller, W.; Myers, E. W.; Lipman, D. J. Basic Local Alignment Search Tool. *Journal of Molecular Biology* **1990**, *215* (3), 403–410. https://doi.org/10.1016/S0022-2836(05)80360-2.

(13) Larkin, M. A.; Blackshields, G.; Brown, N. P.; Chenna, R.; McGettigan, P. A.; McWilliam, H.; Valentin, F.; Wallace, I. M.; Wilm, A.; Lopez, R.; Thompson, J. D.; Gibson, T. J.; Higgins, D. G. Clustal W and Clustal X Version 2.0. *Bioinformatics* **2007**, *23* (21), 2947–2948. https://doi.org/10.1093/bioinformatics/btm404.

(14) Katoh, K.; Standley, D. M. MAFFT Multiple Sequence Alignment Software Version 7: Improvements in Performance and Usability. *Molecular Biology and Evolution* **2013**, *30* (4), 772–780. https://doi.org/10.1093/molbev/mst010.

(15) Edgar, R. C. MUSCLE: A Multiple Sequence Alignment Method with Reduced Time and Space Complexity. *BMC Bioinformatics* **2004**, *5* (1), 113. https://doi.org/10.1186/1471-2105-5-113.

(16) Notredame, C.; Higgins, D. G.; Heringa, J. T-Coffee: A Novel Method for Fast and Accurate Multiple Sequence Alignment. *Journal of Molecular Biology* **2000**, *302* (1), 205–217. https://doi.org/10.1006/jmbi.2000.4042.

(17) Fitch, W. M. Toward Defining the Course of Evolution: Minimum Change for a Specific Tree Topology. *Systematic Zoology* **1971**, *20* (4), 406–416. https://doi.org/10.2307/2412116.

(18) Yang, Z.; Rannala, B. Molecular Phylogenetics: Principles and Practice. *Nature Reviews Genetics* **2012**, *13* (5), 303–314. https://doi.org/10.1038/nrg3186.

(19) Yang, Z.; Kumar, S.; Nei, M. A New Method of Inference of Ancestral Nucleotide and Amino Acid Sequences. *Genetics* **1995**, *141* (4), 1641–1650. https://doi.org/10.1093/genetics/141.4.1641.

(20) Abascal, F.; Zardoya, R.; Posada, D. ProtTest: Selection of Best-Fit Models of Protein Evolution. *Bioinformatics* **2005**, *21* (9), 2104–2105. https://doi.org/10.1093/bioinformatics/bti263.

(21) Nguyen, L. T.; Schmidt, H. A.; von Haeseler, A.; Minh, B. Q. IQ-TREE: A Fast and Effective Stochastic Algorithm for Estimating Maximum-Likelihood Phylogenies. *Molecular Biology and Evolution* **2015**, *32* (1), 268–274. https://doi.org/10.1093/molbev/msu300.

(22) Pauling, L.; Zuckerkandl, E.; Henriksen, T.; Lövstad, R. Chemical Paleogenetics. Molecular "Restoration Studies" of Extinct Forms of Life. *Acta Chemica Scandinavica* **1963**, *17 supl.*, 9–16. https://doi.org/10.3891/acta.chem.scand.17s-0009.

(23) Adey, N. B.; Tollefsbol, T. O.; Sparks, A. B.; Edgell, M. H.; Hutchison, C. A. Molecular Resurrection of an Extinct Ancestral Promoter for Mouse L1. *Proceedings of the National Academy of Sciences* **1994**, *91* (4), 1569 LP – 1573. https://doi.org/10.1073/pnas.91.4.1569.

(24) Lu, Q.; Fox, G. E. Resurrection of an Ancestral 5S RRNA. *BMC Evolutionary Biology* **2011**, *11* (1), 218. https://doi.org/10.1186/1471-2148-11-218.

(25) Ducatez, M. F.; Bahl, J.; Griffin, Y.; Stigger-Rosser, E.; Franks, J.; Barman, S.; Vijaykrishna, D.; Webb, A.; Guan, Y.; Webster, R. G.; Smith, G. J. D.; Webby, R. J. Feasibility of Reconstructed Ancestral H5N1 Influenza Viruses for Cross-Clade Protective Vaccine Development. *Proceedings of the National Academy of Sciences* **2011**, *108* (1), 349 LP – 354. https://doi.org/10.1073/pnas.1012457108.

(26) Blanchette, M.; Diallo, A. B.; Green, E. D.; Miller, W.; Haussler, D. Computational Reconstruction of Ancestral DNA Sequences. *Methods Mol Biol* **2008**, *422*, 171–184. https://doi.org/10.1007/978-1-59745-581-7_11.

(27) Gumulya, Y.; Baek, J.-M.; Wun, S.-J.; Thomson, R. E. S.; Harris, K. L.; Hunter, D. J. B.; Behrendorff, J. B. Y. H.; Kulig, J.; Zheng, S.; Wu, X.; Wu, B.; Stok, J. E.; de Voss, J. J.; Schenk, G.; Jurva, U.; Andersson, S.; Isin, E. M.; Bodén, M.; Guddat, L.; Gillam, E. M. J.; Voss, J. J. de; Schenk, G.; Jurva, U.; Andersson, S.; Isin, E. M.; Bodén, M.; Guddat, L.; Gillam, E. M. J.; de Voss, J. J.; Schenk, G.; Jurva, U.; Andersson, S.; Isin, E. M.; Bodén, M.; Guddat, L.; Gillam, E. M. J. Engineering Highly Functional Thermostable Proteins Using Ancestral Sequence Reconstruction. *Nature Catalysis* **2018**, *1* (11), 878–888. https://doi.org/10.1038/s41929-018-0159-5.

(28) Chaloupkova, R.; Liskova, V.; Toul, M.; Markova, K.; Sebestova, E.; Hernychova, L.; Marek, M.; Pinto, G. P.; Pluskal, D.; Waterman, J.; Prokop, Z.; Damborsky, J. Light-Emitting Dehalogenases: Reconstruction of Multifunctional Biocatalysts. *ACS Catalysis* **2019**, *9* (6), 4810–4823. https://doi.org/10.1021/acscatal.9b01031.

(29) Jones, B. J.; Evans, R. L.; Mylrea, N. J.; Chaudhury, D.; Luo, C.; Guan, B.; Pierce, C. T.; Gordon, W. R.; Wilmot, C. M.; Kazlauskas, R. J. Larger Active Site in an Ancestral Hydroxynitrile Lyase Increases Catalytically Promiscuous Esterase Activity. *PLoS One* **2020**, *15* (6). https://doi.org/10.1371/journal.pone.0235341.

(30) Babkova, P.; Sebestova, E.; Brezovsky, J.; Chaloupkova, R.; Damborsky, J. Ancestral Haloalkane Dehalogenases Show Robustness and Unique Substrate Specificity. *ChemBioChem* **2017**, *18* (14), 1448–1456. https://doi.org/10.1002/cbic.201700197.

(31) Kaltenbach, M.; Burke, J. R.; Dindo, M.; Pabis, A.; Munsberg, F. S.; Rabin, A.; Kamerlin, S. C. L.; Noel, J. P.; Tawfik, D. S. Evolution of Chalcone Isomerase from a Noncatalytic Ancestor. *Nature Chemical Biology* **2018**, *14* (6), 548–555. https://doi.org/10.1038/s41589-018-0042-3.

(32) Clifton, B. E.; Kaczmarski, J. A.; Carr, P. D.; Gerth, M. L.; Tokuriki, N.; Jackson, C. J. Evolution of Cyclohexadienyl Dehydratase from an Ancestral Solute-Binding Protein. *Nature Chemical Biology* **2018**, *14* (6), 542–547. https://doi.org/10.1038/s41589-018-0043-2.

(33) Huang, H.; Pandya, C.; Liu, C.; Al-Obaidi, N. F.; Wang, M.; Zheng, L.; Keating, S. T.; Aono, M.; Love, J. D.; Evans, B.; Seidel, R. D.; Hillerich, B. S.; Garforth, S. J.; Almo, S. C.; Mariano, P. S.; Dunaway-Mariano, D.; Allen, K. N.; Farelli, J. D. Panoramic View of a Superfamily of Phosphatases through Substrate Profiling. *Proc Natl Acad Sci U S A* **2015**, *112* (16), E1974–E1983. https://doi.org/10.1073/PNAS.1423570112.

(34) Chen, R.; Gao, B.; Liu, X.; Ruan, F.; Zhang, Y.; Lou, J.; Feng, K.; Wunsch, C.; Li, S.-M.; Dai, J.; Sun, F. Molecular Insights into the Enzyme Promiscuity of an Aromatic Prenyltransferase. *Nature Chemical Biology* **2017**, *13* (2), 226–234. https://doi.org/10.1038/nchembio.2263.

(35) Baier, F.; Tokuriki, N. Connectivity between Catalytic Landscapes of the Metallo-β-Lactamase Superfamily. *Journal of Molecular Biology* **2014**, *426* (13), 2442–2456. https://doi.org/10.1016/J.JMB.2014.04.013.

(36) Tawfik, D. S.; Khersonsky, O. Enzyme Promiscuity: A Mechanistic and Evolutionary Perspective. *Annual Review of Biochemistry* **2010**, *79* (1), 471–505. https://doi.org/10.1146/annurev-biochem-030409-143718.

(37) Copley, S. D. Enzymes with Extra Talents: Moonlighting Functions and Catalytic Promiscuity. *Current Opinion in Chemical Biology* **2003**, *7* (2), 265–272. https://doi.org/10.1016/S1367-5931(03)00032-2.

(38) D'Ari, R.; Casadesús, J. Underground Metabolism. *BioEssays* **1998**, *20* (2), 181–186. https://doi.org/10.1002/(SICI)1521-1878(199802)20:2<181::AID-BIES10>3.0.CO;2-0.

(39) Jensen, R. A. *Enzyme Recruitment in Evolution of New Function*; 1976; Vol. 30, pp 409–434. https://doi.org/10.1146/annurev.mi.30.100176.002205.

(40) Müller, H.; Becker, A. K.; Palm, G. J.; Berndt, L.; Badenhorst, C. P. S. S.; Godehard, S. P.; Reisky, L.; Lammers, M.; Bornscheuer, U. T. Sequence-Based Prediction of Promiscuous Acyltransferase Activity in Hydrolases. *Angew. Chem. Int. Ed* **2020**, *59* (28), 11704–11709. https://doi.org/10.1002/anie.202003635.

(41) Pandya, C.; Farelli, J. D.; Dunaway-mariano, D.; Allen, K. N. Enzyme Promiscuity : Engine of Evolutionary Innovation. *The Journal of Biological Chemistry* **2014**, *289* (44), 30229–30236. https://doi.org/10.1074/jbc.R114.572990.

(42) Khersonsky, O.; Roodveldt, C.; Tawfik, D. Enzyme Promiscuity: Evolutionary and Mechanistic Aspects. *Current Opinion in Chemical Biology* **2006**, *10* (5), 498–508. https://doi.org/10.1016/j.cbpa.2006.08.011.

(43) Leveson-Gower, R. B.; Mayer, C.; Roelfes, G. The Importance of Catalytic Promiscuity for Enzyme Design and Evolution. *Nature Reviews Chemistry* **2019**, *3* (12), 687–705. https://doi.org/10.1038/s41570-019-0143-x.

(44) Bornscheuer, U. T.; Kazlauskas, R. J. Catalytic Promiscuity in Biocatalysis: Using Old Enzymes to Form New Bonds and Follow New Pathways. *Angewandte Chemie - International Edition* **2004**, *43* (45), 6032–6040. https://doi.org/10.1002/anie.200460416.

(45) Kazlauskas, R. J. Enhancing Catalytic Promiscuity for Biocatalysis. *Current Opinion in Chemical Biology* **2005**, *9* (2), 195–201. https://doi.org/10.1016/j.cbpa.2005.02.008.

(46) Jensen, R. A. *Enzyme Recruitment in Evolution of New Function*; 1976; Vol. 30. https://doi.org/10.1146/annurev.mi.30.100176.002205.

(47) Ohno, S. *Evolution by Gene Duplication*; Springer-Verlag New York Inc., 1970. https://doi.org/10.1007/978-3-642-86659-3.

(48) Scannell, D. R.; Wolfe, K. H. A Burst of Protein Sequence Evolution and a Prolonged Period of Asymmetric Evolution Follow Gene Duplication in Yeast. *Genome Res* **2008**, *18* (1), 137–147. https://doi.org/10.1101/GR.6341207.

(49) Dekel, E.; Alon, U. Optimality and Evolutionary Tuning of the Expression Level of a Protein. *Nature* **2005**, *436* (7050), 588–592. https://doi.org/10.1038/NATURE03842.

(50) Stoebel, D. M.; Dean, A. M.; Dykhuizen, D. E. The Cost of Expression of *Escherichia Coli* Lac Operon Proteins Is in the Process, Not in the Products. *Genetics* **2008**, *178* (3), 1653–1660. https://doi.org/10.1534/GENETICS.107.085399.

(51) Wagner, A. Energy Constraints on the Evolution of Gene Expression. *Mol Biol Evol* **2005**, *22* (6), 1365–1374. https://doi.org/10.1093/MOLBEV/MSI126.

(52) Tokuriki, N.; Stricher, F.; Schymkowitz, J.; Serrano, L.; Tawfik, D. S. The Stability Effects of Protein Mutations Appear to Be Universally Distributed. *Journal of Molecular Biology* **2007**, *369* (5), 1318–1332. https://doi.org/10.1016/J.JMB.2007.03.069.

(53) Camps, M.; Herman, A.; Loh, E.; Loeb, L. A. Genetic Constraints on Protein Evolution. *Crit Rev Biochem Mol Biol* **2007**, *42* (5), 313–326. https://doi.org/10.1080/10409230701597642.

(54) Bershtein, S.; Tawfik, D. S. Ohno's Model Revisited: Measuring the Frequency of Potentially Adaptive Mutations under Various Mutational Drifts. *Molecular Biology and Evolution* **2008**, *25* (11), 2311–2318. https://doi.org/10.1093/MOLBEV/MSN174.

(55) Näsvall, J.; Sun, L.; Roth, J. R.; Andersson, D. I. Real-Time Evolution of New Genes by Innovation, Amplification, and Divergence. *Science* **2012**, *338* (6105), 384–387. https://doi.org/10.1126/SCIENCE.1226521.

(56) des Marais, D. L.; Rausher, M. D. Escape from Adaptive Conflict after Duplication in an Anthocyanin Pathway Gene. *Nature* **2008**, *454* (7205), 762–765. https://doi.org/10.1038/NATURE07092.

(57) Bergthorsson, U.; Andersson, D. I.; Roth, J. R. Ohno's Dilemma: Evolution of New Genes under Continuous Selection. *Proceedings of the National Academy of Sciences* **2007**, *104* (43), 17004–17009. https://doi.org/10.1073/pnas.0707158104.

(58) Rauwerdink, A.; Kazlauskas, R. J. How the Same Core Catalytic Machinery Catalyzes 17 Different Reactions: The Serine-Histidine-Aspartate Catalytic Triad of α/β-Hydrolase Fold Enzymes. *ACS Catalysis* **2015**, *5* (10), 6153–6176. https://doi.org/10.1021/acscatal.5b01539.

(59) Nardini, M.; Dijkstra, B. W. α/β Hydrolase Fold Enzymes: The Family Keeps Growing. *Current Opinion in Structural Biology* **1999**, *9* (6), 732–737. https://doi.org/10.1016/S0959-440X(99)00037-8.

(60) Denesyuk, A.; Dimitriou, P. S.; Johnson, M. S.; Nakayama, T.; Denessiouk, K. The Acid-Base-Nucleophile Catalytic Triad in ABH-Fold Enzymes Is Coordinated by a Set of Structural Elements. *PLoS ONE* **2020**, *15* (2), 1–28. https://doi.org/10.1371/journal.pone.0229376.

(61) Dimitriou, P. S.; Denesyuk, A. I.; Nakayama, T.; Johnson, M. S.; Denessiouk, K. Distinctive Structural Motifs Co-Ordinate the Catalytic Nucleophile and the Residues of the Oxyanion Hole in the Alpha/Beta-Hydrolase Fold Enzymes. *Protein Science* **2019**, *28* (2), 344–364. https://doi.org/10.1002/pro.3527.

(62) Koudelakova, T.; Chovancova, E.; Brezovsky, J.; Monincova, M.; Fortova, A.; Jarkovsky, J.; Damborsky, J. Substrate Specificity of Haloalkane Dehalogenases. *Biochemical Journal* **2011**, *435* (2), 345–354. https://doi.org/10.1042/BJ20101405.

(63) van Loo, B.; Kingma, J.; Arand, M.; Wubbolts, M. G.; Janssen, D. B. Diversity and Biocatalytic Potential of Epoxide Hydrolases Identified by Genome Analysis. *Applied and Environmental Microbiology* **2006**, *72* (4), 2905–2917. https://doi.org/10.1128/AEM.72.4.2905–2917.2006.

(64) Hackenschmidt, S.; Moldenhauer, E. J.; Behrens, G. A.; Gand, M.; Pavlidis, I. v.; Bornscheuer, U. T. Enhancement of Promiscuous Amidase Activity of a *Bacillus Subtilis* Esterase by Formation of a π-π Network. *ChemCatChem* **2014**, *6* (4), 1015–1020. https://doi.org/10.1002/cctc.201300837.

(65) van der Werf, M. J.; Overkamp, K. M.; de Bont, J. A. M. Limonene-1,2-Epoxide Hydrolase from *Rhodococcus Erythropolis* DCL14 Belongs to a Novel Class of Epoxide Hydrolases. *Journal of Bacteriology* **1998**, *180* (19), 5052. https://doi.org/10.1128/JB.180.19.5052-5057.1998.

(66) Menon, B. R. K.; Richmond, D.; Menon, N. Halogenases for Biosynthetic Pathway Engineering: Toward New Routes to Naturals and Non-Naturals. *Catalysis Reviews* **2020**, 1–59. https://doi.org/10.1080/01614940.2020.1823788.

(67) Janssen, D. B.; Stucki, G. Perspectives of Genetically Engineered Microbes for Groundwater Bioremediation. *Environmental Science: Processes & Impacts* **2020**, *22* (3), 487–499. https://doi.org/10.1039/C9EM00601J.

(68) Koudelakova, T.; Bidmanova, S.; Dvorak, P.; Pavelka, A.; Chaloupkova, R.; Prokop, Z.; Damborsky, J. Haloalkane Dehalogenases: Biotechnological Applications. *Biotechnology Journal* **2013**, *8* (1), 32–45. https://doi.org/10.1002/biot.201100486.

(69) Rhew, R. C.; Miller, B. R.; Weiss, R. F. Natural Methyl Bromide and Methyl Chloride Emissions from Coastal Salt Marshes. *Nature* **2000**, *403* (6767), 292–295. https://doi.org/10.1038/35002043.

(70) Wuosmaa, A. M.; Hager, L. P. Methyl Chloride Transferase: A Carbocation Route for Biosynthesis of Halometabolites. *Science (1979)* **1990**, *249* (4965), 160–162. https://doi.org/10.1126/science.2371563.

(71) Janssen, D. B.; Scheper, A.; Dijkhuizen, L.; Witholt, B. Degradation of Halogenated Aliphatic Compounds by *Xanthobacter Autotrophicus* GJ10. *Applied and Environmental Microbiology* **1985**, *49* (3), 673–677. https://doi.org/10.1128/aem.49.3.673-677.1985.

(72) Jensen, H. L. Decomposition of Chloroacetates and Chloropropionates by Bacteria. *Acta Agriculturae Scandinavica* **1960**, *10* (1), 83–103. https://doi.org/10.1080/00015126009435651.

(73) Jesenská, A.; Bartoš, M.; Czerneková, V.; Rychlìk, I.; Pavlìk, I.; Damborský, J. Cloning and Expression of the Haloalkane Dehalogenase Gene DhmA from *Mycobacterium Avium* N85 and Preliminary Characterization of DhmA. *Applied and Environmental Microbiology* **2002**, *68* (8), 3724. https://doi.org/10.1128/AEM.68.8.3724-3730.2002.

(74) Jesenská, A.; Pavlová, M.; Strouhal, M.; Chaloupková, R.; Těšínská, I.; Monincová, M.; Prokop, Z.; Bartoš, M.; Pavlík, I.; Rychlík, I.; Möbius, P.; Nagata, Y.; Damborský, J. Cloning, Biochemical Properties, and Distribution of Mycobacterial Haloalkane Dehalogenases. *Applied and Environmental Microbiology* **2005**, *71* (11), 6736. https://doi.org/10.1128/AEM.71.11.6736-6745.2005.

(75) Sato, Y.; Monincová, M.; Chaloupková, R.; Prokop, Z.; Ohtsubo, Y.; Minamisawa, K.; Tsuda, M.; Damborsky, J.; Nagata, Y. Two Rhizobial Strains, *Mesorhizobium Loti* MAFF303099 and *Bradyrhizobium Japonicum* USDA110, Encode Haloalkane Dehalogenases with Novel Structures and Substrate Specificities. *Applied and Environmental Microbiology* **2005**, *71* (8), 4372. https://doi.org/10.1128/AEM.71.8.4372-4379.2005.

(76) Hesseler, M.; Bogdanović, X.; Hidalgo, A.; Berenguer, J.; Palm, G. J.; Hinrichs, W.; Bornscheuer, U. T. Cloning, Functional Expression, Biochemical Characterization, and Structural Analysis of a Haloalkane Dehalogenase from <i>Plesiocystis Pacifica<i> SIR-1. *Appl Microbiol Biotechnol* **2011**, *91* (4), 1049–1060. https://doi.org/10.1007/S00253-011-3328-X.

(77) Hasan, K.; Fortova, A.; Koudelakova, T.; Chaloupkova, R.; Ishitsuka, M.; Nagata, Y.; Damborsky, J.; Prokop, Z. Biochemical Characteristics of the Novel Haloalkane Dehalogenase DatA, Isolated from the Plant Pathogen *Agrobacterium Tumefaciens* C58. *Applied and Environmental Microbiology* **2011**, *77* (5), 1881–1884. https://doi.org/10.1128/AEM.02109-10.

(78) Fung, H. K. H.; Gadd, M. S.; Drury, T. A.; Cheung, S.; Guss, J. M.; Coleman, N. v.; Matthews, J. M. Biochemical and Biophysical Characterisation of Haloalkane Dehalogenases DmrA and DmrB in *Mycobacterium* Strain JS60 and Their Role in Growth on Haloalkanes. *Molecular Microbiology* **2015**, *97* (3), 439–453. https://doi.org/10.1111/mmi.13039.

(79) Fortova, A.; Sebestova, E.; Stepankova, V.; Koudelakova, T.; Palkova, L.; Damborsky, J.; Chaloupkova, R. DspA from *Strongylocentrotus Purpuratus*: The First Biochemically Characterized Haloalkane Dehalogenase of Non-Microbial Origin. *Biochimie* **2013**, *95* (11), 2091–2096. https://doi.org/10.1016/J.BIOCHI.2013.07.025.

(80) Vanacek, P.; Sebestova, E.; Babkova, P.; Bidmanova, S.; Daniel, L.; Dvorak, P.; Stepankova, V.; Chaloupkova, R.; Brezovsky, J.; Prokop, Z.; Damborsky, J. Exploration of Enzyme Diversity by Integrating Bioinformatics with Expression Analysis and Biochemical Characterization. *ACS Catalysis* **2018**, *8* (3), 2402–2412. https://doi.org/10.1021/acscatal.7b03523.

(81) Novak, H. R.; Sayer, C.; Isupov, M. N.; Gotz, D.; Spragg, A. M.; Littlechild, J. A. Biochemical and Structural Characterisation of a Haloalkane Dehalogenase from a Marine Rhodobacteraceae. *FEBS Letters* **2014**, *588* (9), 1616–1622. https://doi.org/10.1016/j.febslet.2014.02.056.

(82) Carlucci, L.; Zhou, E.; Malashkevich, V. N.; Almo, S. C.; Mundorff, E. C. Biochemical Characterization of Two Haloalkane Dehalogenases: DccA from *Caulobacter Crescentus* and DsaA from *Saccharomonospora Azurea*. *Protein Science* **2016**, *25* (4), 877–886. https://doi.org/10.1002/pro.2895.

(83) Chovancová, E.; Kosinski, J.; Bujnicki, J. M.; Damborský, J. Phylogenetic Analysis of Haloalkane Dehalogenases. *Proteins: Structure, Function, and Bioinformatics* **2007**, *67* (2), 305–316. https://doi.org/10.1002/prot.21313.

(84) Kunka, A.; Damborsky, J.; Prokop, Z. Haloalkane Dehalogenases From Marine Organisms. *Methods in Enzymology* **2018**, *605*, 203–251. https://doi.org/10.1016/BS.MIE.2018.03.005.

(85) Bahl, C. D.; Hvorecny, K. L.; Morisseau, C.; Gerber, S. A.; Madden, D. R. Visualizing the Mechanism of Epoxide Hydrolysis by the Bacterial Virulence Enzyme Cif. *Biochemistry* **2016**, *55* (5), 788–797. https://doi.org/10.1021/acs.biochem.5b01229.

(86) Rink, R.; Fennema, M.; Smids, M.; Dehmel, U.; Janssen, D. B. Primary Structure and Catalytic Mechanism of the Epoxide Hydrolase from *Agrobacterium Radiobacter* AD1. *Journal of Biological Chemistry* **1997**, *272* (23), 14650–14657. https://doi.org/10.1074/jbc.272.23.14650.

(87) Damborský, J.; Rorije, E.; Jesenská, A.; Nagata, Y.; Klopman, G.; Peijnenburg, W. J. G. M. Structure-Specificity Relationships for Haloalkane Dehalogenases. *Environmental Toxicology and Chemistry* **2001**, *20* (12), 2681–2689. https://doi.org/10.1002/etc.5620201205.

(88) Yamada, T.; Morisseau, C.; Maxwell, J. E.; Argiriadi, M. A.; Christianson, D. W.; Hammock, B. D. Biochemical Evidence for the Involvement of Tyrosine in Epoxide Activation during the Catalytic Cycle of Epoxide Hydrolase. *Journal of Biological Chemistry* **2000**, *275* (30), 23082–23088. https://doi.org/10.1074/jbc.M001464200.

(89) Bahl, C. D.; Madden, D. R. *Pseudomonas Aeruginosa* Cif Defines a Distinct Class of α/β Epoxide Hydrolases Utilizing a His/Tyr Ring-Opening Pair. *Protein & Peptide Letters* **2012**, *19* (2), 186–193. https://doi.org/10.2174/092986612799080392.

(90) Verschueren, K. H. G.; Franken, S. M.; Rozeboom, H. J.; Kalk, K. H.; Dijkstra, B. W. Refined X-Ray Structures of Haloalkane Dehalogenase at PH 6.2 and PH 8.2 and Implications for the Reaction Mechanism. *Journal of Molecular Biology* **1993**, *232*.

(91) Boháč, M.; Nagata, Y.; Prokop, Z.; Prokop, M.; Monincová, M.; Tsuda, M.; Koča, J.; Damborský, J. Halide-Stabilizing Residues of Haloalkane Dehalogenases Studied by Quantum Mechanic Calculations and Site-Directed Mutagenesis. *Biochemistry* **2002**, *41* (48), 14272–14280. https://doi.org/10.1021/bi026427v.

(92) Hasan, K.; Gora, A.; Brezovsky, J.; Chaloupkova, R.; Moskalikova, H.; Fortova, A.; Nagata, Y.; Damborsky, J.; Prokop, Z. The Effect of a Unique Halide-Stabilizing Residue on the Catalytic Properties of Haloalkane Dehalogenase DatA from Agrobacterium Tumefaciens C58. *FEBS Journal* **2013**, *280* (13), 3149–3159. https://doi.org/10.1111/febs.12238.

(93) Guan, L.; Yabuki, H.; Okai, M.; Ohtsuka, J.; Tanokura, M. Crystal Structure of the Novel Haloalkane Dehalogenase DatA from *Agrobacterium Tumefaciens* C58 Reveals a Special Halide-Stabilizing Pair and Enantioselectivity Mechanism. *Applied Microbiology and Biotechnology* **2014**, *98* (20), 8573–8582. https://doi.org/10.1007/s00253-014-5751-2.

(94) Chrast, L.; Tratsiak, K.; Planas-Iglesias, J.; Daniel, L.; Prudnikova, T.; Brezovsky, J.; Bednar, D.; Smatanova, I. K.; Chaloupkova, R.; Damborsky, J. Deciphering the Structural Basis of High Thermostability of Dehalogenase from Psychrophilic Bacterium *Marinobacter* Sp. ELB17. *Microorganisms* **2019**, *7* (11). https://doi.org/10.3390/microorganisms7110498.

(95) Chmelova, K.; Sebestova, E.; Liskova, V.; Beier, A.; Bednar, D.; Prokop, Z.; Chaloupkova, R.; Damborsky, J. A Haloalkane Dehalogenase from *Saccharomonospora Viridis* Strain DSM 43017, a Compost Bacterium with Unusual Catalytic Residues, Unique (S)-Enantiopreference, and High Thermostability. *Applied and Environmental Microbiology* **2020**, *86* (17), 1–12. https://doi.org/10.1128/AEM.02820-19.

(96) Lutje Spelberg, J. H.; Tang, L.; van Gelder, M.; Kellogg, R. M.; Janssen, D. B. Exploration of the Biocatalytic Potential of a Halohydrin Dehalogenase Using Chromogenic Substrates. *Tetrahedron: Asymmetry* **2002**, *13* (10), 1083–1089. https://doi.org/10.1016/S0957-4166(02)00222-7.

(97) Schallmey, A.; Schallmey, M. Recent Advances on Halohydrin Dehalogenases—from Enzyme Identification to Novel Biocatalytic Applications. *Applied Microbiology and Biotechnology* **2016**, *100* (18), 7827–7839. https://doi.org/10.1007/s00253-016-7750-y.

(98) van Hylckama Vlieg, J. E. T.; Tang, L.; Lutje Spelberg, J. H.; Smilda, T.; Poelarends, G. J.; Bosma, T.; van Merode, A. E. J.; Fraaije, M. W.; Janssen, D. B. Halohydrin Dehalogenases Are Structurally and Mechanistically Related to Short-Chain Dehydrogenases/Reductases. *Journal of Bacteriology* **2001**, *183* (17), 5058–5066. https://doi.org/10.1128/JB.183.17.5058-5066.2001.

(99) Archelas, A.; Iacazio, G.; Kotik, M. Epoxide Hydrolases and Their Application in Organic Synthesis. In *Green Biocatalysis*; Patel, R. N., Ed.; 2016. https://doi.org/10.1002/9781118828083.ch8.

(100) Bahl, C. D.; Hvorecny, K. L.; Bomberger, J. M.; Stanton, B. A.; Hammock, B. D.; Morisseau, C.; Madden, D. R. Inhibiting an Epoxide Hydrolase Virulence Factor from *Pseudomonas Aeruginosa* Protects CFTR. *Angew. Chem. Int. Ed* **2015**, *54* (34), 9881–9885. https://doi.org/10.1002/anie.201503983.

(101) Jochens, H.; Hesseler, M.; Stiba, K.; Padhi, S. K.; Kazlauskas, R. J.; Bornscheuer, U. T. Protein Engineering of α/β-Hydrolase Fold Enzymes. *ChemBioChem* **2011**, *12* (10), 1508–1517. https://doi.org/10.1002/cbic.201000771.

(102) Padhi, S. K.; Fujii, R.; Legatt, G. A.; Fossum, S. L.; Berchtold, R.; Kazlauskas, R. J. Switching from an Esterase to a Hydroxynitrile Lyase Mechanism Requires Only Two Amino Acid Substitutions. *Chemistry and Biology* **2010**, *17* (8), 863–871. https://doi.org/10.1016/j.chembiol.2010.06.013.

(103) Jochens, H.; Stiba, K.; Savile, C.; Fujii, R.; Yu, J. G.; Gerassenkov, T.; Kazlauskas, R. J.; Bornscheuer, U. T. Converting an Esterase into an Epoxide Hydrolase. *Angew. Chem. Int. Ed* **2009**, *48* (19), 3532–3535. https://doi.org/10.1002/anie.200806276.

(104) Nardini, M.; Ridder, I. S.; Rozeboom, H. J.; Kalk, K. H.; Rink, R.; Janssen, D. B.; Dijkstra, B. W. The X-Ray Structure of Epoxide Hydrolase from *Agrobacterium Radiobacter* AD1. *The Journal of Biological Chemistry* **1999**, *274* (21), 14579–14586. https://doi.org/10.1016/S1381-1177(00)00049-7.

(105) Arand, M.; Grant, D. F.; Beetham, J. K.; Friedberg, T.; Oesch, F.; Hammock, B. D. Sequence Similarity of Mammalian Epoxide Hydrolases to the Bacterial Haloalkane Dehalogenase and Other Related Proteins. Implication for the Potential Catalytic Mechanism of Enzymatic Epoxide Hydrolysis. *FEBS Letters* **1994**, *338* (3), 251–256. https://doi.org/10.1016/0014-5793(94)80278-5.

(106) Nardini, M.; Rink, R.; Janssen, D. B.; Dijkstra, B. W. Structure and Mechanism of the Epoxide Hydrolase from *Agrobacterium Radiobacter* AD1. *Journal of Molecular Catalysis B: Enzymatic* **2001**, *11* (4–6), 1035–1042. https://doi.org/10.1016/S1381-1177(00)00049-7.

(107) Iwasaki, I.; Utsumi, S.; Hagino, K.; Ozawa, T. A New Spectrophotometric Method for the Determination of Small Amounts of Chloride Using the Mercury Thiocyanate Method. *Bull Chem Soc Jpn* **1956**, *29* (8), 860–864. https://doi.org/10.1246/bcsj.29.860.

(108) Phillips, T. M.; Seech, A. G.; Lee, H.; Trevors, J. T. Colorimetric Assay for Lindane Dechlorination by Bacteria. *Journal of Microbiological Methods* **2001**, *47* (2), 181–188. https://doi.org/10.1016/S0167-7012(01)00299-8.

(109) Newman, J.; Peat, T. S.; Richard, R.; Kan, L.; Swanson, P. E.; Affholter, J. A.; Holmes, I. H.; Schindler, J. F.; Unkefer, C. J.; Terwilliger, T. C. Haloalkane Dehalogenases: Structure of a *Rhodococcus* Enzyme. *Biochemistry* **1999**, *38* (49), 16105–16114. https://doi.org/10.1021/BI9913855.

(110) Bahl, C. D.; Morisseau, C.; Bomberger, J. M.; Stanton, B. A.; Hammock, B. D.; O'Toole, G. A.; Madden, D. R. Crystal Structure of the Cystic Fibrosis Transmembrane Conductance Regulator Inhibitory Factor Cif Reveals Novel Active-Site Features of an Epoxide Hydrolase Virulence Factor. *Journal of Bacteriology* **2010**, *192* (7), 1785–1795. https://doi.org/10.1128/JB.01348-09.

(111) Jitsumori, K.; Omi, R.; Kurihara, T.; Kurata, A.; Mihara, H.; Miyahara, I.; Hirotsu, K.; Esaki, N. X-Ray Crystallographic and Mutational Studies of Fluoroacetate Dehalogenase from *Burkholderia* Sp. Strain FA1. *Journal of Bacteriology* **2009**, *191* (8), 2630–2637. https://doi.org/10.1128/JB.01654-08.

(112) Kamachi, T.; Nakayama, T.; Shitamichi, O.; Jitsumori, K.; Kurihara, T.; Esaki, N.; Yoshizawa, K. The Catalytic Mechanism of Fluoroacetate Dehalogenase: A Computational Exploration of Biological Dehalogenation. *Chemistry - A European Journal* **2009**, *15* (30), 7394–7403. https://doi.org/10.1002/chem.200801813.

(113) Aslan-Üzel, A. S. Protein Engineering and Studies on the Catalytic Promiscuity of Haloalkane Dehalogenases. PhD-Thesis, Universität Greifswald, 2021.

(114) Holloway, P.; Trevors, J. T.; Lee, H. A Colorimetric Assay for Detecting Haloalkane Dehalogenase Activity. *Journal of Microbiological Methods* **1998**, *32* (1), 31–36. https://doi.org/10.1016/S0167-7012(98)00008-6.

(115) Aslan-Üzel, A. S.; Beier, A.; Kovář, D.; Cziegler, C.; Padhi, S. K.; Schuiten, E. D.; Dörr, M.; Böttcher, D.; Hollmann, F.; Rudroff, F.; Mihovilovic, M. D.; Buryška, T.; Damborský, J.; Prokop, Z.; Badenhorst, C. P. S.; Bornscheuer, U. T. An Ultrasensitive Fluorescence Assay for the Detection of Halides and Enzymatic Dehalogenation. *ChemCatChem* **2020**, *12* (7), 2032–2039. https://doi.org/10.1002/cctc.201901891.

(116) Tang, Q.; Grathwol, C. W.; Aslan-Üzel, A. S.; Wu, S.; Link, A.; Pavlidis, I. v.; Badenhorst, C. P. S. S.; Bornscheuer, U. T.; Aslan-Üzel, A. S.; Wu, S.; Link, A.; Pavlidis, I. v.; Badenhorst, C. P. S. S.; Bornscheuer, U. T. Directed Evolution of a Halide Methyltransferase Enables Biocatalytic Synthesis of Diverse SAM Analogs. *Angew. Chem. Int. Ed* **2021**, *60* (3), 1524–1527. https://doi.org/10.1002/anie.202013871.

(117) Menon, B. R. K. K.; Richmond, D.; Menon, N. Halogenases for Biosynthetic Pathway Engineering: Toward New Routes to Naturals and Non-Naturals. **2020**, 1–59. https://doi.org/10.1080/01614940.2020.1823788.

(118) Crowe, C.; Molyneux, S.; Sharma, S. v.; Zhang, Y.; Gkotsi, D. S.; Connaris, H.; Goss, R. J. M. Halogenases: A Palette of Emerging Opportunities for Synthetic Biology-Synthetic Chemistry and C-H Functionalisation. *Chemical Society Reviews* **2021**, *50* (17), 9443–9481. https://doi.org/10.1039/d0cs01551b.

(119) Dong, C.; Huang, F.; Deng, H.; Schaffrath, C.; Spencer, J. B.; O'Hagan, D.; Naismith, J. H. Crystal Structure and Mechanism of a Bacterial Fluorinating Enzyme. *Nature* **2004**, *427* (6974), 561–565. https://doi.org/10.1038/nature02280.

(120) Eustáquio, A. S.; Pojer, F.; Noel, J. P.; Moore, B. S. Discovery and Characterization of a Marine Bacterial SAM-Dependent Chlorinase. *Nature Chemical Biology* **2008**, *4* (1), 69–74. https://doi.org/10.1038/nchembio.2007.56.

(121) Neubauer, P. R.; Widmann, C.; Wibberg, D.; Schröder, L.; Frese, M.; Kottke, T.; Kalinowski, J.; Niemann, H. H.; Sewald, N. A Flavin-Dependent Halogenase from Metagenomic Analysis Prefers Bromination over Chlorination. *PLOS ONE* **2018**, *13* (5), e0196797. https://doi.org/10.1371/journal.pone.0196797.

(122) Gkotsi, D. S.; Ludewig, H.; Sharma, S. v.; Connolly, J. A.; Dhaliwal, J.; Wang, Y.; Unsworth, W. P.; Taylor, R. J. K.; McLachlan, M. M. W.; Shanahan, S.; Naismith, J. H.; Goss, R. J. M. A Marine Viral Halogenase That Iodinates Diverse Substrates. *Nature Chemistry* **2019**, *11* (12), 1091–1097. https://doi.org/10.1038/s41557-019-0349-z.

(123) Hayashi, T.; Ligibel, M.; Sager, E.; Voss, M.; Hunziker, J.; Schroer, K.; Snajdrova, R.; Buller, R. Evolved Aliphatic Halogenases Enable Regiocomplementary C−H Functionalization of a Pharmaceutically Relevant Compound. *Angewandte Chemie International Edition* **2019**, *58* (51), 18535–18539. https://doi.org/10.1002/anie.201907245.

(124) Voss, M.; Honda Malca, S.; Buller, R. Exploring the Biocatalytic Potential of Fe/A-Ketoglutarate-Dependent Halogenases. *Chemistry – A European Journal* **2020**, *26* (33), 7336–7345. https://doi.org/10.1002/chem.201905752.

(125) Marvanová, S.; Nagata, Y.; Wimmerová, M.; Sýkorová, J.; Hynková, K.; Damborský, J. Biochemical Characterization of Broad-Specificity Enzymes Using Multivariate Experimental Design and a Colorimetric Microplate Assay: Characterization of the Haloalkane Dehalogenase Mutants. *Journal of Microbiological Methods* **2001**, *44* (2), 149–157. https://doi.org/10.1016/S0167-7012(00)00250-5.

(126) Nevolova, S.; Manaskova, E.; Mazurenko, S.; Damborsky, J.; Prokop, Z. Development of Fluorescent Assay for Monitoring of Dehalogenase Activity. *Biotechnology Journal* **2019**, *14* (3), 1–6. https://doi.org/10.1002/biot.201800144.

(127) Merchant, M. Miniaturization of a Chloride Ion Assay for Use in a Microtiter Format. *Microchemical Journal* **2009**, *92* (1), 80–82. https://doi.org/10.1016/J.MICROC.2009.01.002.

(128) Brestel, E. P. Co-Oxidation of Luminol by Hypochlorite and Hydrogen Peroxide Implications for Neutrophil Chemiluminescence. *Biochemical and Biophysical Research Communications* **1985**, *126* (1), 482–488. https://doi.org/10.1016/0006-291X(85)90631-X.

(129) Flemmig, J.; Remmler, J.; Zschaler, J.; Arnhold, J. Detection of the Halogenating Activity of Heme Peroxidases in Leukocytes by Aminophenyl Fluorescein. *Free Radical Research* **2015**, *49* (6), 768–776. https://doi.org/10.3109/10715762.2014.999676.

(130) Colin, C.; Leblanc, C.; Wagner, E.; Delage, L.; Leize-Wagner, E.; van Dorsselaer, A.; Kloareg, B.; Potin, P. The Brown Algal Kelp *Laminaria Digitata* Features Distinct Bromoperoxidase and Iodoperoxidase Activities. *Journal of Biological Chemistry* **2003**, *278* (26), 23545–23552. https://doi.org/10.1074/JBC.M300247200.

(131) Hager, L. P.; Morris, D. R.; Brown, F. S.; Eberwein, H. Chloroperoxidase: II. UTILIZATION OF HALOGEN ANIONS. *Journal of Biological Chemistry* **1966**, *241* (8), 1769–1777. https://doi.org/10.1016/S0021-9258(18)96702-5.

(132) Chen, X.; Lee, K.-A.; Ren, X.; Ryu, J.-C.; Kim, G.; Ryu, J.-H.; Lee, W.-J.; Yoon, J. Synthesis of a Highly HOCl-Selective Fluorescent Probe and Its Use for Imaging HOCl in Cells and Organisms. *Nature Protocols* **2016**, *11* (7), 1219–1228. https://doi.org/10.1038/nprot.2016.062.

(133) Sokolov, A. v.; Kostevich, V. A.; Kozlov, S. O.; Donskyi, I. S.; Vlasova, I. I.; Rudenko, A. O.; Zakharova, E. T.; Vasilyev, V. B.; Panasenko, O. M. Kinetic Method for Assaying the Halogenating Activity of Myeloperoxidase Based on Reaction of Celestine Blue B with Taurine Halogenamines. *Free Radical Research* **2015**, *49* (6), 777–789. https://doi.org/10.3109/10715762.2015.1017478.

(134) Albrett, A. M.; Ashby, L. v.; Dickerhof, N.; Kettle, A. J.; Winterbourn, C. C. Heterogeneity of Hypochlorous Acid Production in Individual Neutrophil Phagosomes Revealed by a Rhodamine-Based Probe. *J Biol Chem* **2018**, *293* (40), 15715–15724. https://doi.org/10.1074/JBC.RA118.004789.

(135) Josephy, P. D.; Eling, T.; Mason, R. P. The Horseradish Peroxidase-Catalyzed Oxidation of 3,5,3',5'-Tetramethylbenzidine. Free Radical and Charge-Transfer Complex Intermediates. *Journal of Biological Chemistry* **1982**, *257* (7), 3669–3675. https://doi.org/10.1016/S0021-9258(18)34832-4.

(136) Tang, Q.; Grathwol, C. W.; Aslan-Üzel, A. S.; Wu, S.; Link, A.; Pavlidis, I. v.; Badenhorst, C. P. S.; Bornscheuer, U. T. Directed Evolution of a Halide Methyltransferase Enables Biocatalytic Synthesis of Diverse SAM Analogs. *Angew. Chem. Int. Ed* **2020**, 1–5. https://doi.org/10.1002/anie.202013871.

(137) Bozeman, P. M.; Learn, D. B.; Thomas, E. L. Assay of the Human Leukocyte Enzymes Myeloperoxidase and Eosinophil Peroxidase. *Journal of Immunological Methods* **1990**, *126* (1), 125–133. https://doi.org/10.1016/0022-1759(90)90020-V.

(138) Senthilmohan, R.; Kettle, A. J. Bromination and Chlorination Reactions of Myeloperoxidase at Physiological Concentrations of Bromide and Chloride. *Archives of Biochemistry and Biophysics* **2006**, *445* (2), 235–244. https://doi.org/10.1016/j.abb.2005.07.005.

(139) Tang, Q.; Aslan-Üzel, A. S.; Schuiten, E. D.; Badenhorst, C. P. S.; Pavlidis, I. v.; Bornscheuer, U. T. Enzymatic Photometric Assays for the Selective Detection of Halides. In *Multienzymatic Assemblies: Methods and Protocols*; Springer-Verlag New York Inc., 2022; pp 361–375. https://doi.org/10.1007/978-1-0716-2269-8_22.

(140) Archer, S. D.; Posman, K. M.; DeStefano, J.; Harrison, A. O.; Ladina, A.; Cheff, E. A.; Witt, D. P. Fluorescent Detection of Bromoperoxidase Activity in Microalgae and Planktonic Microbial Communities Using Aminophenyl Fluorescein. *Front Mar Sci* **2019**, *6* (FEB), 68. https://doi.org/10.3389/FMARS.2019.00068/BIBTEX.

(141) Prütz, W. A.; Kissner, R.; Koppenol, W. H.; Rüegger, H. On the Irreversible Destruction of Reduced Nicotinamide Nucleotides by Hypohalous Acids. *Archives of Biochemistry and Biophysics* **2000**, *380* (1), 181–191. https://doi.org/10.1006/ABBI.2000.1914.

(142) Prütz, W. A.; Kissner, R.; Nauser, T.; Koppenol, W. H. On the Oxidation of Cytochrome c by Hypohalous Acids. *Arch Biochem Biophys* **2001**, *389* (1), 110–122. https://doi.org/10.1006/ABBI.2001.2321.

(143) Chapman, A. L. P.; Skaff, O.; Senthilmohan, R.; Kettle, A.; Davies, M. J. Hypobromous Acid and Bromamine Production by Neutrophils and Modulation by Superoxide. *Biochemical Journal* **2009**, *417* (3), 773–781. https://doi.org/10.1042/BJ20071563.

(144) Bosma, T.; Pikkemaat, M. G.; Kingma, J.; Dijk, J.; Janssen, D. B. Steady-State and Pre-Steady-State Kinetic Analysis of Halopropane Conversion by a Rhodococcus Haloalkane Dehalogenase. *Biochemistry* **2003**, *42* (26), 8047–8053. https://doi.org/10.1021/BI026907M.

(145) Tang, Q.; Aslan-Üzel, A. S.; Schuiten, E. D.; Badenhorst, C. P. S.; Pavlidis, I. v.; Bornscheuer, U. T. Enzymatic Photometric Assays for the Selective Detection of Halides. In *Multienzymatic Assemblies: Methods and Protocols*; Springer-Verlag New York Inc., 2022; pp 361–375. https://doi.org/10.1007/978-1-0716-2269-8_22.

(146) Hasan, Z.; Renirie, R.; Kerkman, R.; Ruijssenaars, H. J.; Hartog, A. F.; Wever, R. Laboratory-Evolved Vanadium Chloroperoxidase Exhibits 100-Fold Higher Halogenating Activity at Alkaline PH. *Journal of Biological Chemistry* **2006**, *281* (14), 9738–9744. https://doi.org/10.1074/jbc.M512166200.

(147) Carter, J. N.; Beatty, K. E.; Simpson, M. T.; Butler, A. Reactivity of Recombinant and Mutant Vanadium Bromoperoxidase from the Red Alga *Corallina Officinalis*. *Journal of Inorganic Biochemistry* **2002**, *91* (1), 59–69. https://doi.org/10.1016/S0162-0134(02)00400-2.

(148) Kourist, R.; Jochens, H.; Bartsch, S.; Kuipers, R.; Padhi, S. K.; Gall, M.; Böttcher, D.; Joosten, H. J.; Bornscheuer, U. T. The α/β-Hydrolase Fold 3DM Database (ABHDB) as a Tool for Protein Engineering. *ChemBioChem* **2010**, *11* (12), 1635–1643. https://doi.org/10.1002/cbic.201000213.

(149) Chan, P. W. Y.; Yakunin, A. F.; Edwards, E. A.; Pai, E. F. Mapping the Reaction Coordinates of Enzymatic Defluorination. *J Am Chem Soc* **2011**, *133* (19), 7461–7468. https://doi.org/10.1021/ja200277d.

(150) Fu, L.; Niu, B.; Zhu, Z.; Wu, S.; Li, W. CD-HIT: Accelerated for Clustering the next-Generation Sequencing Data. *Bioinformatics* **2012**, *28* (23), 3150–3152. https://doi.org/10.1093/bioinformatics/bts565.

(151) Kalyaanamoorthy, S.; Minh, B. Q.; Wong, T. K. F.; von Haeseler, A.; Jermiin, L. S. ModelFinder: Fast Model Selection for Accurate Phylogenetic Estimates. *Nature Methods* **2017**, *14* (6), 587–589. https://doi.org/10.1038/nmeth.4285.

(152) Barth, S.; Fischer, M.; Schmid, R. D.; Pleiss, J. Sequence and Structure of Epoxide Hydrolases: A Systematic Analysis. *Proteins: Structure, Function, and Bioinformatics* **2004**, *55* (4), 846–855. https://doi.org/10.1002/PROT.20013.

(153) Carter, S. F.; Leak, D. J. The Isolation and Characterisation of a Carbocyclic Epoxide-Degrading *Corynebacterium* Sp. *Biocatalysis and Biotransformation* **1995**, *13* (2), 111–129. https://doi.org/10.3109/10242429509015217.

(154) Misawa, E.; Chan Kwo Chion, C. K. C.; Archer, I. v.; Woodland, M. P.; Zhou, N. Y.; Carter, S. F.; Widdowson, D. A.; Leak, D. J. Characterisation of a Catabolic Epoxide Hydrolase from a *Corynebacterium* Sp. *European Journal of Biochemistry* **1998**, *253* (1), 173–183. https://doi.org/10.1046/j.1432-1327.1998.2530173.x.

(155) Woo, J. H.; Hwang, Y. O.; Kang, S. G.; Lee, H. S.; Cho, J. C.; Kim, S. J. Cloning and Characterization of Three Epoxide Hydrolases from a Marine Bacterium, *Erythrobacter Litoralis* HTCC2594. *Applied Microbiology and Biotechnology* **2007**, *76* (2), 365–375. https://doi.org/10.1007/s00253-007-1011-z.

(156) Elfström, L. T.; Widersten, M. The *Saccharomyces Cerevisiae* ORF YNR064c Protein Has Characteristics of an "orphaned" Epoxide Hydrolase. *Biochimica et Biophysica Acta - Proteins and Proteomics* **2005**, *1748* (2), 213–221. https://doi.org/10.1016/j.bbapap.2005.01.005.

(157) Stamatakis, A. RAxML Version 8: A Tool for Phylogenetic Analysis and Post-Analysis of Large Phylogenies. *Bioinformatics* **2014**, *30* (9), 1312–1313. https://doi.org/10.1093/bioinformatics/btu033.

(158) Gregory, T. R. Insertion–Deletion Biases and the Evolution of Genome Size. *Gene* **2004**, *324*, 15–34. https://doi.org/10.1016/j.gene.2003.09.030.

(159) Hall, T. A. BioEdit: A User-Friendly Biological Sequence Alignment Editor and Analysis Program for Windows 95/98/NT. *Nucleic Acids Symposium Series* **1999**, *41*.

(160) Waterhouse, A.; Bertoni, M.; Bienert, S.; Studer, G.; Tauriello, G.; Gumienny, R.; Heer, F. T.; de Beer, T. A. P.; Rempfer, C.; Bordoli, L.; Lepore, R.; Schwede, T. SWISS-MODEL: Homology Modelling of Protein Structures and Complexes. *Nucleic Acids Research* **2018**, *46* (W1), W296–W303. https://doi.org/10.1093/nar/gky427.

(161) Studier, F. W. Protein Production by Auto-Induction in High-Density Shaking Cultures. *Protein Expression &* **2005**, *41*, 207–234. https://doi.org/10.1016/j.pep.2005.01.016.

(162) Khan, R. T.; Musil, M.; Stourac, J.; Damborsky, J.; Bednar, D. Fully Automated Ancestral Sequence Reconstruction Using FireProt^{ASR}. *Current Protocols* **2021**, *1* (2). https://doi.org/10.1002/cpz1.30.

(163) Wahler, D.; Reymond, J. L. The Adrenaline Test for Enzymes. *Angewandte Chemie - International Edition* **2002**, *41* (7), 1229–1232. https://doi.org/10.1002/1521-3773(20020402)41:7<1229::AID-ANIE1229>3.0.CO;2-5.

(164) Fluxá, V. S.; Wahler, D.; Reymond, J. L. Enzyme Assay and Activity Fingerprinting of Hydrolases with the Red-Chromogenic Adrenaline Test. *Nature Protocols* **2008**, *3* (8), 1270–1277. https://doi.org/10.1038/nprot.2008.106.

(165) Bahl, C. D.; Hvorecny, K. L.; Bridges, A. A.; Ballok, A. E.; Bomberger, J. M.; Cady, K. C.; O'Toole, G. A.; Madden, D. R. Signature Motifs Identify an *Acinetobacter* Cif Virulence Factor with Epoxide Hydrolase Activity. *Journal of Biological Chemistry* **2014**, *289* (11), 7460–7469. https://doi.org/10.1074/jbc.M113.518092.

(166) Flitter, B. A.; Hvorecny, K. L.; Ono, E.; Eddens, T.; Yang, J.; Kwak, D. H.; Bahl, C. D.; Hampton, T. H.; Morisseau, C.; Hammock, B. D.; Liu, X.; Lee, J. S.; Kolls, J. K.; Levy, B. D.; Madden, D. R.; Bomberger, J. M. *Pseudomonas Aeruginosa* Sabotages the Generation of Host Proresolving Lipid Mediators. *Proceedings of the National Academy of Sciences* **2017**, *114* (1), 136–141. https://doi.org/10.1073/pnas.1610242114.

(167) Hvorecny, K. L.; Dolben, E.; Moreau-Marquis, S.; Hampton, T. H.; Shabaneh, T. B.; Flitter, B. A.; Bahl, C. D.; Bomberger, J. M.; Levy, B. D.; Stanton, B. A.; Hogan, D. A.; Madden, D. R. An Epoxide Hydrolase Secreted by *Pseudomonas Aeruginosa* Decreases Mucociliary Transport and Hinders Bacterial Clearance from the Lung. *American Journal of Physiology-Lung Cellular and Molecular Physiology* **2018**, *314* (1), L150–L156. https://doi.org/10.1152/ajplung.00383.2017.

(168) MacEachran, D. P.; Ye, S.; Bomberger, J. M.; Hogan, D. A.; Swiatecka-Urban, A.; Stanton, B. A.; O'Toole, G. A. The *Pseudomonas Aeruginosa* Secreted Protein PA2934 Decreases Apical Membrane Expression of the Cystic Fibrosis Transmembrane Conductance Regulator. *Infection and Immunity* **2007**, *75* (8), 3902–3912. https://doi.org/10.1128/IAI.00338-07.

(169) Hvorecny, K. L.; Bahl, C. D.; Kitamura, S.; Lee, K. S. S.; Hammock, B. D.; Morisseau, C.; Madden, D. R. Active-Site Flexibility and Substrate Specificity in a Bacterial Virulence Factor: Crystallographic Snapshots of an Epoxide Hydrolase. *Structure* **2017**, *25* (5), 697-707.e4. https://doi.org/10.1016/j.str.2017.03.002.

(170) Taher, N. M.; Hvorecny, K. L.; Burke, C. M.; Gilman, M. S. A.; Heussler, G. E.; Adolf-Bryfogle, J.; Bahl, C. D.; O'Toole, G. A.; Madden, D. R. Biochemical and Structural Characterization of Two Cif-like Epoxide Hydrolases from *Burkholderia Cenocepacia*. *Current Research in Structural Biology* **2021**, *3*, 72–84. https://doi.org/10.1016/j.crstbi.2021.02.002.

(171) Zocher, F.; Enzelberger, M. M.; Bornscheuer, U. T.; Hauer, B.; Wohlleben, W.; Schmid, R. D. Epoxide Hydrolase Activity of Streptomyces Strains. *Journal of Biotechnology* **2000**, *77* (2–3), 287–292. https://doi.org/10.1016/S0168-1656(99)00225-4.

(172) Waterhouse, A.; Bertoni, M.; Bienert, S.; Studer, G.; Tauriello, G.; Gumienny, R.; Heer, F. T.; de Beer, T. A. P.; Rempfer, C.; Bordoli, L.; Lepore, R.; Schwede, T.; de Beer, T. A. P.; Rempfer, C.; Bordoli, L.; Lepore, R.; Schwede, T. SWISS-MODEL: Homology Modelling of Protein Structures and Complexes. *Nucleic Acids Research* **2018**, *46* (W1), W296–W303. https://doi.org/10.1093/nar/gky427.

(173) Barnych, B.; Singh, N.; Negrel, S.; Zhang, Y.; Magis, D.; Roux, C.; Hua, X.; Ding, Z.; Morisseau, C.; Tantillo, D. J.; Siegel, J. B.; Hammock, B. D. Development of Potent Inhibitors of the Human Microsomal Epoxide Hydrolase. *European Journal of Medicinal Chemistry* **2020**, *193*, 112206. https://doi.org/10.1016/J.EJMECH.2020.112206.

(174) Zou, J.; Hallberg, B. M.; Bergfors, T.; Oesch, F.; Arand, M.; Mowbray, S. L.; Jones, T. A. Structure of *Aspergillus Niger* Epoxide Hydrolase at 1.8 Å Resolution: Implications for the Structure and Function of the Mammalian Microsomal Class of Epoxide Hydrolases. *Structure* **2000**, *8* (2), 111–122. https://doi.org/10.1016/S0969-2126(00)00087-3.

(175) Bendigiri, C.; Zinjarde, S.; RaviKumar, A. Ylehd, an Epoxide Hydrolase with Promiscuous Haloalkane Dehalogenase Activity from Tropical Marine Yeast *Yarrowia Lipolytica* Is Induced upon Xenobiotic Stress. *Scientific Reports* **2017**, *7* (1), 1–27. https://doi.org/10.1038/s41598-017-12284-9.

(176) Pries, F.; Kingma, J.; Krooshof, G. H.; Jeronimus-Stratingh, C. M.; Bruins, A. P.; Janssen, D. B. Histidine 289 Is Essential for Hydrolysis of the Alkyl-Enzyme Intermediate of Haloalkane Dehalogenase. *Journal of Biological Chemistry* **1995**, *270* (18), 10405–10411. https://doi.org/10.1074/JBC.270.18.10405.

(177) Beier, A.; Damborsky, J.; Prokop, Z. Transhalogenation Catalysed by Haloalkane Dehalogenases Engineered to Stop Natural Pathway at Intermediate. *Advanced Synthesis and Catalysis* **2019**, *361* (11), 2438–2442. https://doi.org/10.1002/adsc.201900132.

(178) Kennes, C.; Pries, F.; Krooshof, G. H.; Bokma, E.; Kingma, J.; Janssen, D. B. Replacement of Tryptophan Residues in Haloalkane Dehalogenase Reduces Halide Binding and Catalytic Activity. *European Journal of Biochemistry* **1995**, *228* (2), 403–407. https://doi.org/10.1111/j.1432-1033.1995.00403.x.

(179) Morrison, K. L.; Weiss, G. A. Combinatorial Alanine-Scanning. *Current Opinion in Chemical Biology* **2001**, *5* (3), 302–307. https://doi.org/10.1016/S1367-5931(00)00206-4.

(180) Chan, W. Y.; Wong, M.; Guthrie, J.; Savchenko, A. v.; Yakunin, A. F.; Pai, E. F.; Edwards, E. A. Sequence- and Activity-Based Screening of Microbial Genomes for Novel Dehalogenases. *Microbial Biotechnology* **2010**, *3* (1), 107–120. https://doi.org/10.1111/j.1751-7915.2009.00155.x.

(181) Kurihara, T.; Yamauchi, T.; Ichiyama, S.; Takahata, H.; Esaki, N. Purification, Characterization, and Gene Cloning of a Novel Fluoroacetate Dehalogenase from *Burkholderia* Sp. FA1. *Journal of Molecular Catalysis B: Enzymatic* **2003**, *23* (2–6), 347–355. https://doi.org/10.1016/S1381-1177(03)00098-5.

(182) Nakayama, T.; Kamachi, T.; Jitsumori, K.; Omi, R.; Hirotsu, K.; Esaki, N.; Kurihara, T.; Yoshizawa, K. Substrate Specificity of Fluoroacetate Dehalogenase: An Insight from Crystallographic Analysis, Fluorescence Spectroscopy, and Theoretical Computations. *Chemistry - A European Journal* **2012**, *18* (27), 8392–8402. https://doi.org/10.1002/chem.201103369.

(183) Liu, J. Q.; Kurihara, T.; Ichiyama, S.; Miyagi, M.; Tsunasawa, S.; Kawasaki, H.; Soda, K.; Esaki, N. Reaction Mechanism of Fluoroacetate Dehalogenase from *Moraxella* Sp. B. *Journal of Biological Chemistry* **1998**, *273* (47), 30897–30902. https://doi.org/10.1074/jbc.273.47.30897.

(184) Ichiyama, S.; Kurihara, T.; Miyagi, M.; Galkin, A.; Tsunasawa, S.; Kawasaki, H.; Esaki, N. Catalysis-Linked Inactivation of Fluoroacetate Dehalogenase by Ammonia: A Novel Approach to Probe the Active-Site Environment. *Journal of Biochemistry* **2002**, *131* (5), 671–677. https://doi.org/10.1093/oxfordjournals.jbchem.a003150.

(185) Kawasaki, H.; Tsuda, K.; Matsushita, I.; Tonomura, K. Lack of Homology between Two Haloacetate Dehalogenase Genes Encoded on a Plasmid from *Moraxella* Sp. Strain B. *Journal of General Microbiology* **1992**, *138* (7), 1317–1323. https://doi.org/10.1099/00221287-138-7-1317.

(186) Kim, T. H.; Mehrabi, P.; Ren, Z.; Sljoka, A.; Ing, C.; Bezginov, A.; Ye, L.; Pomès, R.; Prosser, R. S.; Pai, E. F. The Role of Dimer Asymmetry and Protomer Dynamics in Enzyme Catalysis. *Science (1979)* **2017**, *355* (6322). https://doi.org/10.1126/science.aag2355.

(187) Zheng, H.; Kahakeaw, D.; Acevedo, J. P.; Reetz, M. T. Directed Evolution of Enantioconvergency: The Case of an Epoxide Hydrolase-Catalyzed Reaction of a Racemic Epoxide. *ChemCatChem* **2010**, *2* (8), 958–961. https://doi.org/10.1002/cctc.201000122.

(188) Pineau, E.; Xu, L.; Renault, H.; Trolet, A.; Navrot, N.; Ullmann, P.; Légeret, B.; Verdier, G.; Beisson, F.; Pinot, F. *Arabidopsis Thaliana* EpoxideHydrolase1 (AtEH1) Is a Cytosolic Epoxide Hydrolase Involved in the Synthesis of Poly-Hydroxylated Cutin Monomers. *New Phytologist* **2017**, *215* (1), 173–186. https://doi.org/10.1111/nph.14590.

(189) Kiyosue, T.; Beetham, J. K.; Pinot, F.; Hammock, B. D.; Yamaguchi-Shinozaki, K.; Shinozaki, K. Characterization of an *Arabidopsis* CDNA for a Soluble Epoxide Hydrolase Gene That Is Inducible by Auxin and Water Stress. *The Plant Journal* **1994**, *6* (2), 259–269. https://doi.org/10.1046/j.1365-313X.1994.6020259.x.

(190) Kong, X.-D.; Yuan, S.; Li, L.; Chen, S.; Xu, J.-H.; Zhou, J. Engineering of an Epoxide Hydrolase for Efficient Bioresolution of Bulky Pharmaco Substrates. *Proceedings of the National Academy of Sciences* **2014**, *111* (44), 15717–15722. https://doi.org/10.1073/pnas.1404915111.

(191) Gong, P. F.; Xu, J. H. Bio-Resolution of a Chiral Epoxide Using Whole Cells of Bacillus Megaterium ECU1001 in a Biphasic System. *Enzyme and Microbial Technology* **2005**, *36* (2–3), 252–257. https://doi.org/10.1016/j.enzmictec.2004.07.014.

(192) Bellevik, S.; Zhang, J.; Meijer, J. *Brassica Napus* Soluble Epoxide Hydrolase (BNSEH1): Cloning and Characterization of the Recombinant Enzyme Expressed in *Pichia Pastoris*. *European Journal of Biochemistry* **2002**, *269* (21), 5295–5302. https://doi.org/10.1046/j.1432-1033.2002.03247.x.

(193) Harris, T. R.; Aronov, P. A.; Jones, P. D.; Tanaka, H.; Arand, M.; Hammock, B. D. Identification of Two Epoxide Hydrolases in *Caenorhabditis Elegans* That Metabolize Mammalian Lipid Signaling Molecules. *Archives of Biochemistry and Biophysics* **2008**, *472* (2), 139–149. https://doi.org/10.1016/j.abb.2008.01.016.

(194) Ferrandi, E. E.; Sayer, C.; de Rose, S. A.; Guazzelli, E.; Marchesi, C.; Saneei, V.; Isupov, M. N.; Littlechild, J. A.; Monti, D. New Thermophilic α/β Class Epoxide Hydrolases Found in Metagenomes From Hot Environments. *Frontiers in Bioengineering and Biotechnology* **2018**, *6* (October), 1–16. https://doi.org/10.3389/fbioe.2018.00144.

(195) Gomi, K.; Yamamato, H.; Akimitsu, K. Epoxide Hydrolase: A MRNA Induced by the Fungal Pathogen *Alternaria Alternata* on Rough Lemon (*Citrus Jambhiri* Lush). *Plant Molecular Biology* **2003**, *53* (1–2), 189–199. https://doi.org/10.1023/B:PLAN.0000009287.95682.24.

(196) Edqvist, J.; Farbos, I. A Germination-Specific Epoxide Hydrolase from *Euphorbia Lagascae*. *Planta* **2003**, *216* (3), 403–412. https://doi.org/10.1007/s00425-002-0876-4.

(197) Arahira, M.; Nong, V. H.; Udaka, K.; Fukazawa, C. Purification, Molecular Cloning and Ethylene-Inducible Expression of a Soluble-Type Epoxide Hydrolase from Soybean. *European Journal of Biochemistry* **2000**, *267* (9), 2649–2657. https://doi.org/10.1046/j.1432-1327.2000.01276.x.

(198) Gomez, G. A.; Morisseau, C.; Hammock, B. D.; Christianson, D. W. Structure of Human Epoxide Hydrolase Reveals Mechanistic Inferences on Bifunctional Catalysis in Epoxide and Phosphate Ester Hydrolysis. *Biochemistry* **2004**, *43* (16), 4716–4723. https://doi.org/10.1021/bi036189j.

(199) Beetham, J. K.; Tian, T. G.; Hammock, B. D. CDNA Cloning and Expression of a Soluble Epoxide Hydrolase from Human Liver. *Archives of Biochemistry and Biophysics*. 1993, pp 197–201. https://doi.org/10.1006/abbi.1993.1411.

(200) Argiriadi, M. A.; Morisseau, C.; Hammock, B. D.; Christianson, D. W. Detoxification of Environmental Mutagens and Carcinogens: Structure, Mechanism, and Evolution of Liver Epoxide Hydrolase. *Proceedings of the National Academy of Sciences* **1999**, *96* (19), 10637–10642. https://doi.org/10.1073/pnas.96.19.10637.

(201) Biswal, B. K.; Morisseau, C.; Garen, G.; Cherney, M. M.; Garen, C.; Niu, C.; Hammock, B. D.; James, M. N. G. The Molecular Structure of Epoxide Hydrolase B from *Mycobacterium Tuberculosis* and Its Complex with a Urea-Based Inhibitor. *Journal of Molecular Biology* **2008**, *381* (4), 897–912. https://doi.org/10.1016/j.jmb.2008.06.030.

(202) Newman, J. W.; Stok, J. E.; Vidal, J. D.; Corbin, C. J.; Huang, Q.; Hammock, B. D.; Conley, A. J. Cytochrome P450-Dependent Lipid Metabolism in Preovulatory Follicles. *Endocrinology* **2004**, *145* (11), 5097–5105. https://doi.org/10.1210/en.2004-0710.

(203) Visser, H.; Vreugdenhil, S.; de Bont, J. A. M.; Verdoes, J. C. Cloning and Characterization of an Epoxide Hydrolase-Encoding Gene from *Rhodotorula Glutinis*. *Applied Microbiology and Biotechnology* **2000**, *53* (4), 415–419. https://doi.org/10.1007/s002530051635.

(204) Knehr, M.; Thomas, H.; Arand, M.; Gebel, T.; Zeller, H. D.; Oesch, F. Isolation and Characterization of a CDNA Encoding Rat Liver Cytosolic Epoxide Hydrolase and Its Functional Expression in *Escherichia Coli*. *Journal of Biological Chemistry* **1993**, *268* (23), 17623–17627.

(205) Lin, S.; Horsman, G. P.; Chen, Y.; Li, W.; Shen, B. Characterization of the SgcF Epoxide Hydrolase Supporting an (R)-Vicinal Diol Intermediate for Enediyne Antitumor Antibiotic C-1027 Biosynthesis. *J Am Chem Soc* **2009**, *131* (45), 16410–16417. https://doi.org/10.1021/ja901242s.

(206) Horsman, G. P.; Lechner, A.; Ohnishi, Y.; Moore, B. S.; Shen, B. Predictive Model for Epoxide Hydrolase-Generated Stereochemistry in the Biosynthesis of Nine-Membered Enediyne Antitumor Antibiotics. *Biochemistry* **2013**, *52* (31), 5217–5224. https://doi.org/10.1021/bi400572a.

(207) Stapleton, A.; Beetham, J. K.; Pinot, F.; Garbarino, J. E.; Rockhold, D. R.; Friedman, M.; Hammock, B. D.; Belknap, W. R. Cloning and Expression of Soluble Epoxide Hydrolase from Potato. *The Plant Journal* **1994**, *6* (2), 251–258. https://doi.org/10.1046/j.1365-313X.1994.6020251.x.

(208) Mowbray, S. L.; Elfström, L. T.; Ahlgren, K. M.; Andersson, C. E.; Widerstein, M. X-Ray Structure of Potato Epoxide Hydrolase Sheds Light on Substrate Specificity in Plant Enzymes. *Protein Science* **2006**, *3* (15), 1628–1637. https://doi.org/10.1110/ps.051792106.

(209) Guo, A.; Durner, J.; Klessig, D. F. Characterization of a Tobacco Epoxide Hydrolase Gene Induced during the Resistance Response to TMV. *Plant Journal* **1998**, *15* (5), 647–656. https://doi.org/10.1046/j.1365-313X.1998.00241.x.

(210) Li, F. L.; Kong, X. D.; Chen, Q.; Zheng, Y. C.; Xu, Q.; Chen, F. F.; Fan, L. Q.; Lin, G. Q.; Zhou, J.; Yu, H. L.; Xu, J. H. Regioselectivity Engineering of Epoxide Hydrolase: Near-Perfect Enantioconvergence through a Single Site Mutation. *ACS Catalysis* **2018**, *8* (9), 8314–8317. https://doi.org/10.1021/acscatal.8b02622.

(211) Xu, W.; Xu, J. H.; Pan, J.; Gu, Q.; Wu, X. Y. Enantioconvergent Hydrolysis of Styrene Epoxides by Newly Discovered Epoxide Hydrolases in Mung Bean. *Organic Letters* **2006**, *8* (8), 1737–1740. https://doi.org/10.1021/ol060407u.

(212) Zhu, Q. Q.; He, W. H.; Kong, X. D.; Fan, L. Q.; Zhao, J.; Li, S. X.; Xu, J. H. Heterologous Overexpression of Vigna Radiata Epoxide Hydrolase in Escherichia Coli and Its Catalytic Performance in Enantioconvergent Hydrolysis of P-Nitrostyrene Oxide into (R)-p-Nitrophenyl Glycol. *Applied Microbiology and Biotechnology* **2014**, *98* (1), 207–218. https://doi.org/10.1007/s00253-013-4845-6.

(213) Gehret, J. J.; Gu, L.; Geders, T. W.; Brown, W. C.; Gerwick, L.; Gerwick, W. H.; Sherman, D. H.; Smith, J. L. Structure and Activity of DmmA, a Marine Haloalkane Dehalogenase. *Protein Science* **2012**, *21* (2), 239–248. https://doi.org/10.1002/pro.2009.

(214) Foster, M. D. The Colorimetric Determination of Fluorine in Water With Ferric Thiocyanate. *J Am Chem Soc* **1932**, *54* (11), 4464–4465. https://doi.org/10.1021/ja01350a511.

(215) Dagley, S.; Rodgers, A. Estimation of Glycollic Acid. *BBA - Biochimica et Biophysica Acta* **1953**, *12* (1–2), 591. https://doi.org/10.1016/0006-3002(53)90196-6.

(216) Wixtrom, R. N.; Hammock, B. D. Continuous Spectrophotometric Assays for Cytosolic Epoxide Hydrolase. *Analytical Biochemistry* **1988**, *174* (1), 291–299. https://doi.org/10.1016/0003-2697(88)90548-9.

(217) Borhan, B.; Mebrahtu, T.; Nazarian, S.; Kurth, M. J.; Hammock, B. D. Improved Radiolabeled Substrates for Soluble Epoxide Hydrolase. *Analytical Biochemistry*. 1995, pp 188–200. https://doi.org/10.1006/abio.1995.1520.

(218) Jones, P. D.; Wolf, N. M.; Morisseau, C.; Whetstone, P.; Hock, B.; Hammock, B. D. Fluorescent Substrates for Soluble Epoxide Hydrolase and Application to Inhibition Studies. *Analytical Biochemistry* **2005**, *343* (1), 66–75. https://doi.org/10.1016/j.ab.2005.03.041.

(219) Hoang, D. T.; Chernomor, O.; von Haeseler, A.; Minh, B. Q.; Vinh, L. S. UFBoot2: Improving the Ultrafast Bootstrap Approximation. *Molecular Biology and Evolution* **2018**, *35* (2), 518–522. https://doi.org/10.1093/molbev/msx281.

(220) Berman, H. M.; Battistuz, T.; Bhat, T. N.; Bluhm, W. F.; Bourne, P. E.; Burkhardt, K.; Feng, Z.; Gilliland, G. L.; Iype, L.; Jain, S.; Fagan, P.; Marvin, J.; Padilla, D.; Ravichandran, V.; Schneider, B.; Thanki, N.; Weissig, H.; Westbrook, J. D.; Zardecki, C. The Protein Data Bank. *Acta Crystallographica Section D: Biological Crystallography* **2002**, *58* (6 I), 899–907. https://doi.org/10.1107/S0907444902003451.

(221) Anandakrishnan, R.; Aguilar, B.; Onufriev, A. V. H++ 3.0: Automating PK Prediction and the Preparation of Biomolecular Structures for Atomistic Molecular Modeling and Simulations. *Nucleic Acids Research* **2012**, *40* (W1), 537–541. https://doi.org/10.1093/nar/gks375.

(222) Hanwell, M. D.; Curtis, D. E.; Lonie, D. C.; Vandermeersch, T.; Zurek, E.; Hutchison, G. R. Avogadro: An Advanced Semantic Chemical Editor, Visualization, and Analysis Platform. *Journal of Cheminformatics* **2012**, *4* (17). https://doi.org/https://doi.org/10.1186/1758-2946-4-17.

(223) Halgren, T. A. Merck Molecular Force Field. I. Basis, Form, Scope, Parameterization, and Performance of MMFF94. *J Comput Chem* **1996**, *17* (5–6), 490–519.

(224) Vanquelef, E.; Simon, S.; Marquant, G.; Garcia, E.; Klimerak, G.; Delepine, J. C.; Cieplak, P.; Dupradeau, F.-Y. R.E.D. Server: A Web Service for Deriving RESP and ESP Charges and Building Force Field Libraries for New Molecules and Molecular Fragments. *Nucleic Acids Research* **2011**, *39* (suppl_2), W511–W517. https://doi.org/10.1093/nar/gkr288.

(225) Trott, O.; Olson, A. J. AutoDock Vina: Improving the Speed and Accuracy of Docking with a New Scoring Function, Efficient Optimization, and Multithreading. *Journal of Computational Chemistry* **2010**, *31* (2), 455–461. https://doi.org/https://doi.org/10.1002/jcc.21334.

(226) Sanner, M. F. Python: A Programming Language for Software Integration and Development. *J Mol Graph Model* **1999**, *17* (1), 57–61.

(227) Sanner, M. F.; Olson, A. J.; Spehner, J. C. Reduced Surface: An Efficient Way to Compute Molecular Surfaces. *Biopolymers* **1996**, *38* (3), 305–320. https://doi.org/10.1002/(SICI)1097-0282(199603)38:3%3C305::AID-BIP4%3E3.0.CO;2-Y.

(228) The PyMOL Molecular Graphics System. Schrödinger, LLC.

(229) Gasteiger, E.; Hoogland, C.; Gattiker, A.; Duvaud, S.; Wilkins, M. R.; Appel, R. D.; Bairoch, A. The Proteomics Protocols Handbook. *The Proteomics Protocols Handbook* **2005**, 571–608. https://doi.org/10.1385/1592598900.

(230) Fernández-Fueyo, E.; Younes, S. H. H.; Van Rootselaar, S.; Aben, R. W. M.; Renirie, R.; Wever, R.; Holtmann, D.; Rutjes, F. P. J. T.; Hollmann, F. A Biocatalytic Aza-Achmatowicz Reaction. *ACS Catalysis* **2016**, *6* (9), 5904–5907. https://doi.org/10.1021/acscatal.6b01636.

(231) Hasan, Z.; Renirie, R.; Kerkman, R.; Ruijssenaars, H. J.; Hartog, A. F.; Wever, R. Laboratory-Evolved Vanadium Chloroperoxidase Exhibits 100-Fold Higher Halogenating Activity at Alkaline PH. **2006**, *281* (14), 9738–9744. https://doi.org/10.1074/jbc.M512166200.

(232) Winn, M. D.; Ballard, C. C.; Cowtan, K. D.; Dodson, E. J.; Emsley, P.; Evans, P. R.; Keegan, R. M.; Krissinel, E. B.; Leslie, A. G. W.; McCoy, A.; McNicholas, S. J.; Murshudov, G. N.; Pannu, N. S.; Potterton, E. A.; Powell, H. R.; Read, R. J.; Vagin, A.; Wilson, K. S. Overview of the CCP4 Suite and Current Developments. *Acta Crystallogr D Biol Crystallogr* **2011**, *67* (Pt 4), 235–242. https://doi.org/10.1107/S0907444910045749.

(233) McCoy, A. J.; Grosse-Kunstleve, R. W.; Adams, P. D.; Winn, M. D.; Storoni, L. C.; Read, R. J. Phaser Crystallographic Software. *J Appl Crystallogr* **2007**, *40* (Pt 4), 658–674. https://doi.org/10.1107/S0021889807021206.

(234) Kovalevskiy, O.; Nicholls, R. A.; Long, F.; Carlon, A.; Murshudov, G. N. Overview of Refinement Procedures within REFMAC5: Utilizing Data from Different Sources. *Acta Crystallogr D Struct Biol* **2018**, *74* (Pt 3), 215–227. https://doi.org/10.1107/S2059798318000979.

Appendix

Contents

A1 Additional results

A1.1 Capturing intermediate with mass spectrometry

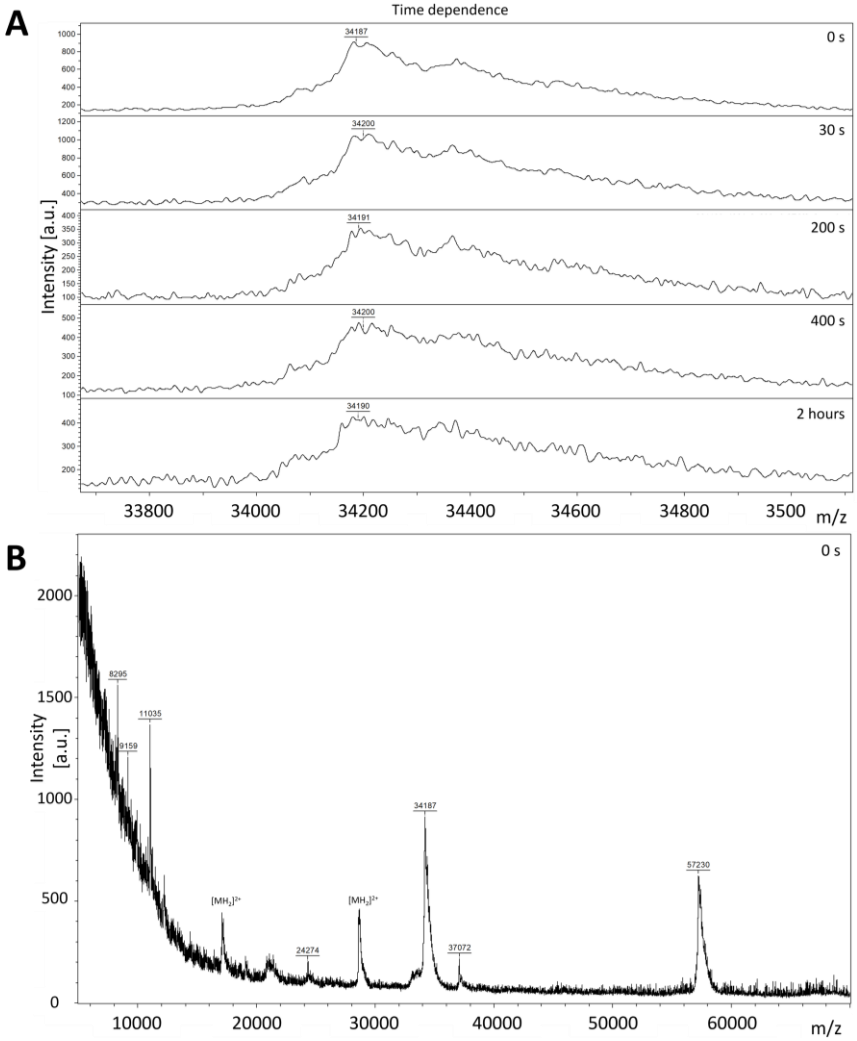

Figure S1. Mass spectrometry data with CorEH H264F. A) MS spectra at several different time points. The MS data did not allow monitoring of the formation of the alkyl-enzyme intermediate. B) Mass spectrum of the sample at 0 s. The sample contains a mixture of multiple proteins.

A1.2 SDS-PAGE

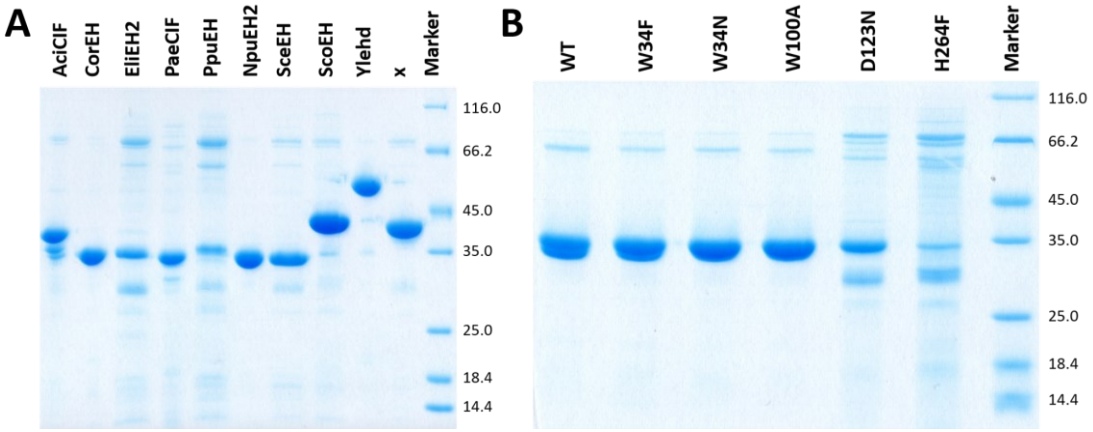

Figure S2. SDS-PAGE of selected epoxide hydrolases and CorEH variants. Samples of His6-tagged enzymes purified by immobilised metal-affinity chromatography as described in Appendix A2.5. Target proteins are expected between 30 and 40 kDa. Molecular weights are listed in Table S6 in Appendix A2.6. A) The epoxide hydrolases selected for screening including Ylehd. B) Wild-type CorEH and variants.

A1.3 Molecular docking results

For some substrates bind with favourable energies, but no potentially reactive conformation is observed resulting in a NO under Docking while binding mode and binding energies are shown (Table S1).

Table S1. Summary of molecular docking results and comparison with experimental data.

Enzyme	Substrate	Substrate Activity	Experimental activity	Docking	Binding mode	Binding energy [kcal·mol^{-1}]
CorEH (PDB ID: 7AC0)	1,2-dibromoethane	HLD	YES	YES	7	-2.5
	1-bromobutane	HLD	YES	YES	10	-3.0
	1-iodopropane	HLD	YES	NO	10	-2.6
	1-iodobutane	HLD	YES	NO	10	-3.1
	epibromohydrin	EH/HLD*	YES (EH)	YES	8 / 3	-2.8 / -2.9
	1,2-epoxybutane	EH	YES	YES	3	-3.1
	1,2-epoxyhexane	EH	YES	YES	1	-4.0
	chlorophenyloxirane	EH	YES	YES	10	-4.2
DhlA (PDB ID: 1B6G)	1,2-dibromoethane	HLD	YES	YES	1	-2.4
	1-bromobutane	HLD	YES	YES	1	-3.1
	1-iodopropane	HLD	YES	YES	2	-2.0
	1-iodobutane	HLD	YES	YES	2	-1.8
	epibromohydrin	EH/HLD*	YES (HLD)	YES	3 / 2	-2.1 / -2.4
	1,2-epoxybutane	EH	NO	NO	2	-3.2
	1,2-epoxyhexane	EH	NO	NO	6	-0.2
	chlorophenyloxirane	EH	NO	NO	1	1.4
PaeCIF (PDB ID: 3KD2)	1,2-dibromoethane	HLD	NO	NO	-	-
	1-bromobutane	HLD	NO	NO	-	-
	1-iodopropane	HLD	NO	NO	-	-
	1-iodobutane	HLD	NO	NO	-	-
	epibromohydrin	EH/HLD*	YES (EH)	YES	- / 3	- / -3.1
	1,2-epoxybutane	EH	YES	YES	3	-3.1
	1,2-epoxyhexane	EH	YES	YES	10	-3.6
	chlorophenyloxirane	EH	YES	YES	7	-3.8

*The substrate epibromohydrin contains both an epoxide-ring and a halogen atom and is a substrate for both epoxide hydrolases and dehalogenases. However, the product of epoxide hydrolysis, 3-bromo-1,2-propanediol, is very unstable and it is impossible to distinguish between dehalogenase activity and epoxide hydrolysis using assays for the detection of halide release like the HOX assay.

A1.4 Homology models

Table S2. Summary of SWISS-MODEL[160] homology modelling.

Enzyme	Template PDB ID	Template	Template Organism	%ID	Sequence similarity
ScoEH	6GXL	Fluoroacetate dehalogenase	*Rhodopseudomonas palustris*	29.7	0.35
SceEH	6XY9	DbeA - Haloalkane dehalogenase	*Bradyrhizobium elkanii*	24.2	0.32
NpuEH2	3A2L	DbjA - Haloalkane dehalogenase	*Bradyrhizobium japonicum*	20.5	0.31
PpuEH	3A2N	DbjA - Haloalkane dehalogenase	*Bradyrhizobium japonicum*	19.3	0.29
EliEH2	4KAF	Haloalkane dehalogenase	*Rhodococcus sp.*	19.0	0.29
Anc159	3R3U	Fluoroacetate dehalogenase	*Rhodopseudomonas palustris*	81.2	0.56
Anc153	4B9A	Putative epoxide hydrolase	*Pseudomonas aeruginosa*	54.5	0.46
Anc152	4B9A	Putative epoxide hydrolase	*Pseudomonas aeruginosa*	54.2	0.46
Anc149	5TNS	PaeCIF - Epoxide hydrolase	*Pseudomonas aeruginosa*	47.2	0.43
Anc117	1BN6	DhaA - Haloalkane dehalogenase	*Rhodococcus rhodochrous*	53.9	0.47
Anc116	2V9Z	Haloalkane dehalogenase	*Rhodococcus rhodochrous*	52.0	0.45
Brno86	3SK0	DhaA - Haloalkane dehalogenase	*Rhodococcus rhodochrous*	50.9	0.44
Brno119	5MXD	VraEH1 - Epoxide hydrolase	*Vigna radiata*	46.3	0.43
Brno157	4B9A	Putative epoxide hydrolase	*Pseudomonas aeruginosa*	47.7	0.43

A1.5 Characterised dataset

Table S3. Characterised dataset details on the active site.

Name	H-G-X-P motif / HS2(c28-c31)				G-X-Sm-X-S/T motif (c58-c62)					CN (c96)	HS_1/CB_1 (c97)	CB_2 (c100)	CRA_1 (c121)	RO_1 /HP_1	HP_2	HS_3	RO_2/HP_3 (c132)	CRA_2 (c159)	B (c188)
aCif	H89	G90	F91	G92	G118	L119	G120	Q121	S122	D158	L159	T162	D182	H206	F207		Y267	G299	H329
AniEH	H115	G116	W117	P118	G151	Y152	T153	F154	S155	D192	I193	F196	L215	Y251	A252		Y314	D348	H374
AthEH	H	G	F	P	G	Y	G	D	S	D	W	I	S	-	-		Y	D	H
AtsEH	H	G	F	P	G	Y	G	D	S	D	W	L	S	-	-		Y	D	H
BfuEH	H	G	W	P	G	Y	G	F	S	D	W	V	N	-	-		Y	E	H
BmeEH	H28	G29	F30	P31	G57	Y58	N59	L60	S61	D97	W98	G101	N121	Y144	A145		Y203	D239	H267
BnaEH																			
BsuEH	H	G	F	P	G	Y	N	L	S	D	W	A	N	-	-		Y	D	H
CelEH1	H	G	Y	P	G	Y	N	L	S	D	W		N				Y	D	H
CelEH2	H	G	F	P	G	Y	N	T	T	D	W		N				Y	D	H
ChinaEH	H	G	F	P	G	Y	R	G	S	D102	W103	A105	N127	Y150	I151		Y209	D249	H280
CorEH	H32	G33	W34	P35	G61	L62	G63	D64	S65	D99	W	S	D123	H149	G150		Y209	G	H264
CsiEH	H	G	F	P	G	Y	G	D	T	D	W	L	S	-	-		Y	D	H
DraEH	H	G	F	P	G	Y	N	I	S	D	W	V	N				M	D	H
EchA	H36	G37	W38	P39	G65	F66	G67	D68	S69	D107	F108	I111	D131	Y150	S153		Y215	D246	H275
ElaEH																			
EliEH2	H	G	Y	P	G	F	G	L	S	D	Y		N				H	D	H
EliEH3	H	G	F	P	G	Y	G	E	T	D	W	I	N				Y	D	H
GmaxEH	H	G	F	P	G	Y	G	D	T	D	W	I	S	-	-		Y	D	H
HsaEH1	H	G	W	P	G	Y	G	F	S	D	W	L	M	-	-		Y	E	H
HsaEH2	H	G	F	P	G	Y	G	E	S	D	W		N				Y	D	H
HsaEH3	H	G	F	P	G	Y	G	P	S	D	W		S				Y	D	H
MmuEH	H263	G264	F265	P266	G293	Y294	G295	D296	S297	D333	W334	V337	N357	Y381	Q382		Y465	D495	H523
MtheEH	H33	G34	F35	P36	G63	Y64	G65	G66	S67	D103	W104	L107	S127	Y152	S153		Y238	D268	H297
MtuEH	H	G	F	P	G	Y	G	R	S	D	W	P	S	V162	W163		Y	D	H
MtuEH_ephF	H	G	F	P	G	A	G	W	S	D	W		N				Y	D	H
NPuEH1	H	G	F	P	G	Y	N	D	S	D	W		N				Y	D	H
NpuEH2	H	G	F	P	G	Y	F	N	S	D	Y		N				Y	D	H
PaeClF	H61	G62	F63	G64	G90	L91	G92	Q93	S94	D129	I130	W133	E153	H177	F178		Y239	H269	H297
PaePEH	H37	G38	Y39	P40	G66	Y67	G68	E69	S70	D107	R108	R111	T131	H152*	W153		Y214	E245*	H274
PigEH											W								
PpuEH	H	G	F	P	G	F	G	D	S	D	Y		N				Y	D	H
RgluEH																			
RnoEH	H	G	F	P	G	Y	G	D	S	D	W	V	N	-	-		Y	D	H
RpaEH	H	G	W	P	G	F	G	R	S	D	W	P	S				Y	D	H
ScaEH1	H97	G98	W99	P100	G136	F137	G138	F139	S155	D175	L176	W179	F199	Y235	M236		Y304	D336	H363
ScaEH2	H	G	W	P	G	F	G	L	S	D	I	F	L	G234	P235		H	A	H
SceEH	H	G	F	P	G	F	G	F	T	D	Y	P	N	-	-		Y	D	H
ScoEH	H	G	V	P	G	L	G	D	S	D	W	V	E	(G156)	(F157)		Y	F	H
SgloEH	H	G	W	P	G	Y	G	F	S	D	W	V	M	-	-		Y	D	H
SibeEH	H	G	F	P	G	Y	N	E	T	D	W	I	N	Y148	V149		Y	D	H
StuEH1	H31	G32	F33	P34	G61	Y62	G63	D64	T65	D105	W106	L109	S129	Y154	I155		Y235	D265	H300
StuEH2																			
TabaccoEH	H	G	F	P	G	Y	G	L	S	D	F	R	G	-	-		Y	D	H
TfuEH	H	G	W	P	G	F	T	F	S	D	L	A	G	(L243)	(G244)		G	D	H
VraEH1																			
VraEH2	H31	G32	F33	P34	G61	Y62	G63	D64	T65	D101	W102	I105	S125	Y150	I152		Y232	D262	H297
BceHacD	H	G	H	P	G	Y	G	A	S	D	R	R	D	H150	W151		Y	G	H
BurkHacD	H32	G33	F34	P35	G61	Y62	G63	G64	S65	D104	R105	R108	D128	H149*	W150		Y212	G243	H271
DarHacD	H	G	Y	P	G	Y	G	D	S	D	R	R	D	H152	W153		Y	G	H
DelftHacD1	H	G	F	P	G	Y	G	D	S	D	R	R	D	H150	W151		Y	G	H
NostocHacD	H32	G33	Y34	P35	G61	Y62	G63	D64	S65	D104	R105	R108	D128	H150*	W151		Y211	G242	H270
PolaHacD	H	G	F	P	G	Y	G	D	S	D	R	R	D	H162	W163		Y	G	H
RpaHacD	H38	G39	F40	P41	G67	Y68	G69	W70	S71	D110	R111	R114	D134	H155*	W156		Y219	G252	H280
DatA	H41	G42	N43	P44	G70	Y71	G72	Q73	S74	D108	Y109	A112	E132	R150	R151		P208	G246	H274
DbeA	H	G	N	P	G	Y	G	Q	S	D	W		E				P	G	H
DbjA	H	G	N	P	G	F	G	Q	S	D	W		E				P	G	H
DccA	H53	G54	E55	P56	G83	F84	G85	R86	S87	D123	W124	L127	N147	-	-	W163	P212	D249	H278
DgpA	H	G	Q	P	G	F	G	K	S	D	W		N				P	D	H
DhaA	H50	G51	N52	P53	G79	M80	G81	K82	S83	D117	W118	A121	E141	F160	Q161		P217	G255	H283
DhcA	H	G	N	P	G	F	F	L	S	D	W		N				P	D	H
DhlA	H54	G55	E56	P57	G84	F85	G86	K87	S88	D124	W125	F128	N148	-	-	W175	P223	D260	H289
DhmA	H	G	E	P	G	F	G	R	S	D	W		N			(W173)	P	D	H
DhmeA	H	G	N	P	G	F	G	L	S	D	W		N				R	D	H
DmbA	H	G	N	P	G	M	G	A	S	D	W		E				P	G	H
DmbB	H	G	E	P	G	F	G	R	S	D	W		N			(W164)	P	D	H
DmlA	H	G	N	P	G	Y	G	Q	S	D	W		E				P	G	H
DmmA	H	G	N38	P	G	M	G	D	S	D104	W105	V108	E128				P209	G247	H275
DmrA																W164			
DmsA	H	G	N	P	G	M	G	A	S	D	W		E				P	G	H
DmsaA	H	G	E	P	G	F	G	K	S	D	W		N			(W168)	P	D	H
DmxA	H	G	Q	P	G	Y	G	M	S	D	W		E				P	G	H
DpaA	H	G	E	P	G	F	G	R	S	D	W		N			(W165)	P	D	H
DpaB	H	G	E	P	G	F	G	R	S	D	W		N			(W164)	P	D	H
DpcA	H	G	E	P	G	F	G	R	S	D	W		N			(W164)	P	D	H
DppA	H	G	E	P	G	F	G	R	S	D	W		N			W163	P	D	H
DpsA	H	G	N	P	G	M	G	R	S	D	W		E				P	G	H
DsbA	H	G	N	P	G	M	G	D	S	D	W		E				P	G	H
DsxA	H	G	E	P	G	F	G	K	S	D	W		N			W164	P	D	H
DtaA	H	G	N	P	G	F	G	D	S	D	W		E				P	G	H
HanR																			
Jann2620	H	G	N	P	G	M	G	A	S	D	W		E				P	G	H
LinB	H36	G37	N38	P39	G65	M66	G67	D68	S69	D108	W109	A112	E132	F151	-		P208	G246	H272
Sav4779	H	G	N	P	G	M	G	E	S	D	W		E				P	G	H

Table S4. Characterised dataset details and references.

Name	Identifier	Crystal Structure	Activity	Organism	Reference
aCif	A0A014BSV4	4MEA	EH (Styrene oxide)	*Acinetobacter sp*	165
AniEH	Q9UR30	1QO7	EH	*Aspergillus niger*	63, 174, 187
AthEH	Q9M9W5		EH (Large acid oxide)	*Arabidopsis thaliana*	188
AtsEH	A0A178VUJ2		EH (Trans-stilbene oxide) [Wixtrom[216]]	*Arabidopsis thaliana*	189
BfuEH	Q141B3		EH (Multiple substrates) [Adrenaline assay[163,164]]	*Burkholderia fungorum*	63
BmeEH	4INZA	4INZ	EH (Multiple substrates, HPLC, whole-cell)	Bacillus megaterium	190, 191
BnaEH	Q8L5G6		EH	*Brassica napus*	192
BsuEH	O31581		EH (Multiple substrates) [Adrenaline assay[163,164]]	*Bacillus subtilis*	63
CelEH1	G5EBI4		EH [Borhan[217], Jones[218]]	*Caenorhabditis elegans*	193
CelEH2	G5EDL5		EH [Borhan[217], Jones[218]]	*Caenorhabditis elegans*	193
ChinaEH	A0A1U9WZ58	5NFQ	EH	Unknown	194
CorEH	O52866	7AC0	EH (Multiple substrates) [Adrenaline assay[163,164]]	*Corynebacterium sp*	63, 153, 154
CsiEH	A0A067H5C3		EH (Stilbene oxide)	*Citrus sinensis*	195
DraEH	Q9RRE3		EH (Multiple substrates) [Adrenaline assay[163,164]]	*Deinococcus radiodurans*	63
EchA	O31243	1EHY	EH	*Agrobacterium radiobacter*	86, 104, 106
ElaEH	Q84ZZ3		EH	*Euphorbia lagascae*	196
EliEH2	Q2N9R2		EH (Styrene oxide)	*Erythrobacter litoralis*	155
EliEH3	Q2N9T8		EH (Styrene oxide)	*Erythrobacter litoralis*	155
GmaxEH	Q39856		EH (Styrene oxide)	*Glycine max*	197
HsaEH1	P07099		EH	*Homo sapiens*	
HsaEH2	P34913	1S8O	EH	*Homo sapiens*	198, 199
HsaEH3	Q9H6B9		EH	*Homo sapiens*	
MmuEH	1CQZA	1CQZ	EH	*Mus musculus*	200
MtheEH	G7CF24	5CW2	Activity not tested (Structure known, unpublished)	*Mycobacterium thermoresistibile ATCC 19527*	
MtuEH	A0A0H3LAC4	2E3J	EH	*Mycobacterium tuberculosis*	201
MtuEH_ephF	A0A0E8V1N1		EH (Multiple substrates) [Adrenaline assay[163,164]]	*Mycobacterium tuberculosis*	63
NPuEH1	NpuEH1		EH (Multiple substrates) [Adrenaline assay[163,164]]	*Nostoc punctiforme*	63
NpuEH2	NpuEH2		EH (Multiple substrates) [Adrenaline assay[163,164]]	*Nostoc punctiforme*	63
PaeCIF	A0A071KVQ1	3KD2	EH	*Pseudomonas aeruginosa UCBPP-PA14*	85, 89, 100, 110
PaePEH	A0A1F0IDJ9	4B9A	Putative EH (Unpublished)	*Pseudomonas aeruginosa PAO1*	
PigEH	Q6Q2C2		EH	*Sus scrofa*	202
PpuEH	KMU96261.1		EH (Multiple substrates) [Adrenaline assay[163,164]]	*Pseudomonas putida*	63
RgluEH	Q8J2N5		EH	*Rhodotorula glutinis*	203
RnoEH	P80299		EH (Trans-stilbene oxide)	*Rattus norvegicus*	204
RpaEH	Q6N645		EH (Multiple substrates) [Adrenaline assay[163,164]]	*Rhodopseudomonas palustris*	63
ScaEH1	5F4ZA	5F4Z	-	*Streptomyces carzinostaticus*	205
ScaEH2	4I19A	4I19	-	*Streptomyces carzinostaticus*	205
SceEH	Sceeh		EH (stilbene-oxide {low}, phenanthrene 9-10-oxide)	*Saccharomyces cerevisiae*	156
ScoEH	Q9K3Q1		EH (Multiple substrates) [Adrenaline assay[163,164]]	*Streptomyces coelicolor*	63
SgloEH	Q8GMH6		EH (Styrene oxide)	*Streptomyces globisporus*	206, 207
SibeEH	A0A1U9WZ52	5NG7	EH	Unknown	194
StuEH1	Q41415	2CJP	EH (Trans-stilbene oxide) [Wixtrom[216]]	*Solanum tuberosum*	207, 208
StuEH2	Q41413		-	*Solanum tuberosum*	
TabaccoEH	Q9ZP87		EH (Stilbene oxide)	*Nicotiana tabaccum*	209
TfuEH	Q47QJ2		EH (Multiple substrates) [Adrenaline assay[163,164]]	*Thermobifida fusca*	63
VraEH1	E5L4L1	5XMD	EH (Multiple substrates) [Adrenaline assay[163,164]]	*Vigna radiata*	210-212
VraEH2	A0A0R5NGA4	5XM6	EH (Multiple substrates)	*Vigna radiata*	210-212
BceHacD	A0A0H2XT25		HacD	*Burkholderia cenocepacia*	180
BurkHacD	Q1JU72	1Y37	HacD [Foster[214]/Dagley[215]/Iwasaki[107]]	*Burkholderia sp*	111, 181, 182
DarHacD	Q479B8		HacD	*Dechloromonas aromatica*	180
DelftHacD1	Q01398		HacD [Iwasaki[107]]	*Delftia acidovorans (Moraxella sp)*	183-185
NostocHacD	3QYJA	3QYJ	HacD	*Nostoc sp*	180
PolaHacD	Q123C8		HacD	*Polaromonas sp. JS666*	180
RpaHacD	Q6NAM1	3R3U	HacD	*Rhodopseudomonas palustris*	149, 186
DatA	Q8U671	3WI7	HalD	*Agrobacterium fabrum*	80
DbeA	E2RV62	4K2A	HalD	*Bradyrhizobium elkanii*	80
DbjA	P59337	3A2M	HalD	*Bradyrhizobium diazoefficiens*	80
DccA	B8H3S9	5ESR	HalD	*Caulobacter crescentus*	82
DgpA	B8KHS4		HalD	*gamma proteobacterium*	80
DhaA	P0A3G2	1BN6	HalD	*Rhodococcus rhodochrous*	80
DhcA	Q2SAV4		HalD	*Hahella chejuensis*	80
DhlA	2HADA	2HAD	HalD	*Xanthobacter autotrophicus*	80
DhmA	A0A0E2WEQ4		HalD	*Mycobacterium avium complex*	80
DhmeA	I3R766		HalD	*Haloferax mediterranei*	80
DmbA	A5U5S9	2QVB	HalD	*Mycobacterium tuberculosis*	80
DmbB	P9WMS2		HalD	*Mycobacterium tuberculosis*	80
DmlA	Q98C03		HalD	*Rhizobium loti*	80
DmmA	Q6DND9	3U1T	HalD	*Lyngbya majuscula*	80, 213
DmrA	G4I2J6	4MJ3	HalD	*Mycobacterium rhodesiae JS60*	78
DmsA	Q938B4		HalD	*Mycobacterium smegmatis*	80
DmsaA	M7CRB9		HalD	*Marinobacter santoriniensis*	80
DmxA	A3JB27	5MXP	HalD	*Marinobacter sp*	80
DpaA	K6XNL5		HalD	*Paraglaciecola agarilytica*	80
DpaB	K6XZ18		HalD	*Paraglaciecola agarilytica*	80
DpcA	Q1QBB9		HalD	*Psychrobacter cryohalentis*	80
DppA	A6G7B1	2XT0	HalD	*Plesiocystis pacifica*	80
DpsA	XP_794172.2		HalD	*Strongylocentrotus purpuratus*	80
DsbA	D7C5E0		HalD	*Streptomyces bingchenggensis*	80
DsxA	WP_017667204.1		HalD	*Sandarakinorhabdus sp*	80
DtaA	G9P2E2		HalD	*Trichoderma atroviridis (Hypocrea atroviridis)*	80
HanR	A0A023I2Y1	4BRZ	HalD [Colorimetric assay Holloway[114]]	*Rhodobacteraceae bacterium*	81
Jann2620	Q28P25		HalD	*Jannaschia sp*	80
LinB	P51698	1MJ5	HalD	*Sphingomonas paucimobilis*	80
Sav4779	Q82E37		HalD	*Streptomyces avermitilis*	80

A2 Experimental procedures

A2.1 Materials

1,2-dibromoethane and 1-hexanediol were purchased from Fluka (Buchs, Switzerland). 1,2-epoxydecane was obtained from abcr GmbH (Karlsruhe, Germany). 1,2-octanediol and 1-bromohexane was acquired from Alfa Aesar (Kandel, Germany). All other chemicals and solvents were bought from Sigma-Aldrich (St. louis, MO, US). Synthetic genes were codon-optimized for expression in *Escherichia coli* and subcloned into pET-28a(+) by BioCat GmbH (Heidelberg, Germany). All plasmids encoded N-terminal His_6-tags.

A2.2 Phylogenetics

Sequences of characterized epoxide hydrolases and dehalogenases were collected from literature and aligned using MAFFT[14]. The multiple sequence alignment was fed to IQ-TREE[21] (version 1.6.2 for LINUX) to infer a phylogenetic tree by maximum likelihood, using ultrafast bootstrap with 1000 replicates (UFBoot)[219]. The built-in ModelFinder[151] was used to find LG+F+R6 as the best model for the characterised dataset.

A2.3 Molecular docking studies

The X-ray structure of CorEH was determined in this study (PDB ID: 7AC0). The X-ray structures of DhlA and PaeCIF were downloaded from the Protein Data Bank[220] with PDB IDs: 1B66 (DhlA) and 3KD2 (PaeCIF). The protein structures were prepared for docking calculations by removal of hydrogen atoms, ions and waters and adding any missing heavy atoms and hydrogen atoms in the residue side chains. Orientations of asparagine, glutamine and histidine side chains were optimized using the H++ server at pH 7.5[221]. The tree-dimensional ligand structures of eight substrates were prepared in Avogadro[222] and the geometry was optimized by the MMFF94 force-field[223]. Partial atomic charges were derived by the R.E.D. server[224]. Input geometry was optimized by the Gaussian 2009 D.01 program of the R.E.D. server and a multi-orientation RESP fit with RESP-A1A charge model was performed.

The AutoDock Vina[225] algorithm was used for molecular docking. AutoDock atom types and Gasteiger charges were added to the protein and ligand structures by MGLTools[226,227]. The docking grid was selected to be a 30x30x30 Å cube centred at the OD1 atom of the nucleophilic aspartate of all three protein structures, covering the active site and the access tunnel. -exhaustiveness=100 was used to sample the conformational space thoroughly and the number of output conformations of the docked ligand was explicitly set to 10. The binding modes were visually compared using PyMOL[228]. Modes with the best binding free energy in a pre-reactive conformation for dehalogenation or epoxide hydrolysis were selected and compared with experimental results (Appendix A1.3 Table S1).

A2.4 Mutagenesis

CorEH variants were made using the Q5® Site-Directed Mutagenesis kit from New England Biolabs (Ipswich, MA, US). Primers were designed using NEBaseChanger (https://nebasechanger.neb.com/) and synthesized by ThermoFisher (Germany). The amplified PCR products were treated with the KLD Enzyme mix (a mixture of a kinase, a ligase and DpnI) and incubated at room temperature for 30 min. Chemically competent *E. coli* TOP10 cells were transformed with the amplified PCR product and plated on LB agar containing 50 µg/mL kanamycin. Plasmid DNA was isolated (innuPREP Plasmid Mini Kit 2.0, Analytic Jena, Jena, Germany) from individual colonies and sent for Sanger sequencing (Eurofins Genomics Germany GmbH, Ebersberg, Germany).

Table S5. Forward (F) and reverse (R) primers for mutagenesis of CorEH. Primer lengths, GC contents, melting temperatures (Tm), and annealing temperatures (Ta) are shown.

Variant	Primer	Oligo	Length	%GC	Tm	Ta
W34F	F	GCTGCATGGCtttCCGCAGAGCT	23	61	69°C	66°C
	R	AGAACCAGCGGATAACCAC	19	53	65°C	
W34N	F	GCTGCATGGCaacCCGCAGAGCT	23	65	65°C	64°C
	R	AGAACCAGCGGATAACCA	18	50	63°C	
W100A	F	TGGCCATGATgcgGGTGGTAGCG	23	65	65°C	62°C
	R	ATAACACCAACTTTATCATAGCC	23	35	61°C	
D123N	F	GTTTATTCTGaatATGATTCCGGGTC	26	38	60°C	61°C
	R	AGACGTTCCACCAGATCAC	19	53	64°C	
H264F	F	AAATTGCGGTtttTTTGTGCCGGAAGAAAAACCG	34	41	68°C	69°C
	R	TCCACGGCACCGCCTTCA	18	67	73°C	

A2.5 Expression and purification of His_6-tagged enzyme sequences

Chemically competent *E. coli* BL21(DE3) cells were transformed with the appropriate expression vectors and plated on LB agar containing 50 µg/mL kanamycin. Typically, pre-cultures (5 mL of LB containing 50 µg/mL kanamycin) were inoculated with single colonies and incubated for 7-8 h (37 °C, 180 rpm). ZYM-5052 autoinduction medium[161] (50 mL containing 100 µg/mL kanamycin) was inoculated with 1% (v/v) of pre-culture. The autoinduction medium did not include the optional trace metal solution. The cultures were incubated for 1 h at 37 °C, after which the temperature was lowered to 20 °C and the culture was incubated for another 40 h. The cells were harvested by centrifuging (4,5000 x g, 4 °C, 40 min) and resuspended in 5 mL buffer A (50 mM NaH_2PO_4, 500 mM NaCl, and 10 mM imidazole, pH 7.5). The cells were lysed through ultrasonication on ice (1 cycle of 5 min sonication at 50% intensity, 50% pulsed cycle) using a SONOPULS HD 2070 (BANDELIN electronic GmbH & Co. KG, Berlin, Germany). Lysates were clarified by centrifugation (10,000 x g, 60 min) and filtered through a 0.45 µm filter (Filtropur S, Sarstedt AG & co. KG). The His_6-tagged proteins were purified by immobilized metal-affinity chromatography using 1 mL of Roti®garose-His/Co Beads or Roti®garose-His/Ni Beads (Carl Roth GmbH + Co. KG, Karlsruhe, Germany). The Co/Ni-NTA resin was washed with deionized water and equilibrated with buffer A.

The lysates were applied by gravity and the column was washed with 10 column volumes of buffer A. The protein was eluted with approximately 3 mL of buffer B (50 mM NaH_2PO_4, 500 mM NaCl, and 500 mM imidazole, pH 7.5). Protein concentrations were determined by measuring absorbance at 280 nm using a NanoDrop™ device (Thermo Fisher, Germany) device. Theoretical extinction coefficients and molecular weights were calculated from the protein sequences using ExPASy ProtParam[229] (Table S6). The eluted protein fractions were dialysed at 4 °C into buffer C (50 mM NaH_2PO_4, and 20 mM $NaSO_4$, pH 7.5) using ZelluTrans dialysis membranes (6,000-8,000 MWCO; Carl Roth). For each dialysis, 100x volume of buffer C was used and the buffer was exchanged twice after a minimum incubation time of 4 h. The dialysed enzymes were stored at 4 °C.

A2.6 SDS-PAGE analysis

The purities of the protein samples were analysed by SDS-PAGE. Samples of the purified proteins were denatured by heating (95 °C, 10 min) in SDS-sample buffer (65 mM Tris, 4% (w/v) glycerol, 2% (w/v) SDS, 0.01% (w/v) bromophenol blue, 5% (v/v) β-mercapto ethanol) with final protein concentrations of approximately 0.8 mg/mL. The proteins were separated on 12.5% acrylamide gels at a constant voltage of 200 V for approximately 40 min. The gels were stained using Coomassie Brilliant Blue G-250.

Table S6. Extinction coefficients and molecular weights.

Enzyme	Extinction coefficient (M^{-1} cm^{-1})	Molecular weight (kDa)
CorEH WT	62005	34.304
CorEH W34F	56505	34.265
CorEH W34N	56505	34.232
CorEH W100A	56505	34.189
CorEH D123N	62005	34.303
CorEH H264F	62005	34.314
***Ci*VCPO**	93405	70.145
***Ci*VCPO variant**	93280	70.105
PpuEH	64650	36.643
EliEH2	61420	34.497
NpuEH2	67270	35.613
ScoEH	32890	34.289
SceEH	45965	34.919
AciCIF	50310	40.770
PaeCIF	46995	36.714
Ylehd	90425	46.058
Anc159	74955	35.336
Anc153	55390	34.227
Anc152	70400	34.284
Anc149	68090	34.700
Anc117	72670	36.760
Anc116	66265	35.858
Brno86	50880	35.821
Brno119	59025	35.777
Brno157	70025	35.435

A2.7 Adrenaline assay

The epoxide hydrolase activity of CorEH was determined using the adrenaline assay performed as described by Fluxa *et al*[164]. Epoxide hydrolysis produces 1,2-diols, which can be oxidized by periodate. Back-titration of the oxidant with adrenaline to produce the red adrenochrome allows for quantification of the diols (Figure S3). The reactions were performed with 0.1 mg/mL enzyme and 10 mM substrate in 50 mM NaH_2PO_4 at pH 8.0 containing 1.25 mM $NaIO_4$ (total volume 100 µL). The reactions were incubated at 37 °C for at least 30 min. A sample of the reactions (42.5 µL) was added to 7.5 µL 10 mM L-adrenaline in a 384-well plate and the absorbance was measured at 490 nm. The absorbance at 490 nm is an indirect measure for determining the formation of diols. A lower absorbance compared to the negative control indicates activity. 10 mM substrate stocks were prepared in DMSO. 1,2-decanediol was used as a standard (1 to 10 mM).

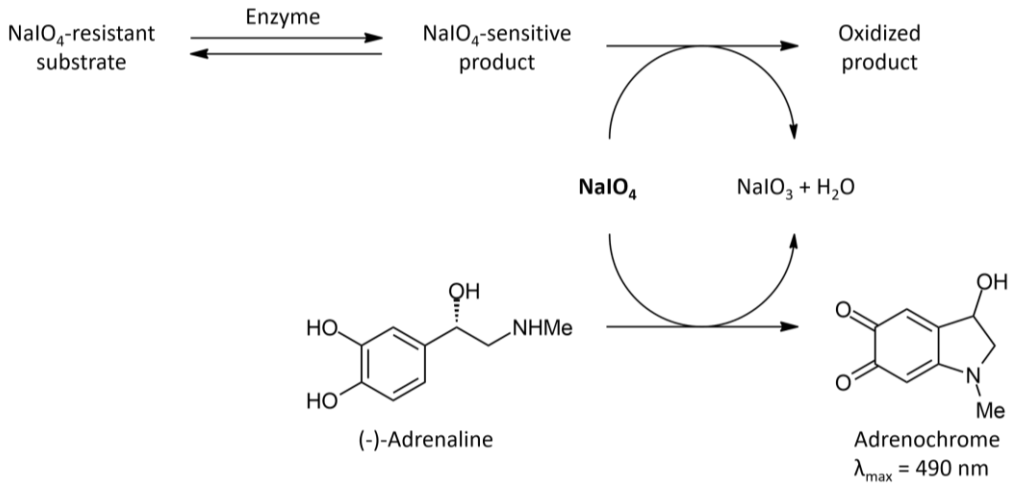

Figure S3. Principle of the adrenaline assay for enzymes. A $NaIO_4$-resistant substrate is converted into a $NaIO_4$-sensitive product by an enzyme, the $NaIO_4$-sensitive product is then oxidized, consuming the $NaIO_4$. Next, adrenaline is added which is oxidized by the remainder of the $NaIO_4$ to form adrenochrome (red, detectable at 490 nm).

A2.8 Halide assays

Reactions for the determination of dehalogenase activity (total volume 50 µL) were performed with 0.7 mg/mL enzyme and 20 mM substrate in 50 mM NaH_2PO_4 (pH 8.0). Reactions were incubated at 37 °C for varying incubation times. Halide oxidation (HOX) assay reactions (total volume 40 µL) contained 2 mM H_2O_2, 25 µM aminophenyl fluorescein, 1 mM orthovanadate, 2.5 U/mL *Curvularia inaequalis* vanadium-dependent chloroperoxidase *(Ci*VCPO)[230] and 2 µL undiluted reaction sample[115]. Reactions were incubated in black 384-well plates for 40 min at room temperature before measuring fluorescence at 525 nm (excitation at 488 nm). Standard curves ranging from 0.1 to 2 µM NaBr were also measured for each assay. Iodide assay reactions (total volume 50 µL) contained 1.4 U/mL *Ci*VCPO variant[231] in ready-to-use 3,3',5,5'-tetramethylbenzidine (TMB) Liquid Substrate System from Sigma and 2 µL undiluted reaction sample. Reactions were incubated in transparent 384-well plates at room temperature for 1 h, while the absorbance at 570 nm was measured every minute. Iodide standards ranging from 0.04 to 0.4 µM KI were also measured for each assay.

A2.9 Gas chromatography

Reactions for analysis on GC-MS (total volume 500 µL) were performed with 0.7 mg/mL enzyme and 20 mM 1-bromobutane in 50 mM NaH_2PO_4 at pH 8 at 37 °C for 20-22 h. Reactions were stopped by the addition of phosphoric acid (160 mM) and extracted using 150 µL *tert*-butyl methyl ether for GC-MS analysis. Standard curves for the reaction product 1-butanol were prepared using the same extraction method. Samples were analysed using a GCMS-QP2010 SE device (Shimadzu, Duisburg, Germany) with a ZB-5MSi column (30m x 0.25 mM, thickness 0.25 µm). Injection temperature was set at 220 °C and flow rate at 1.08 mL/min. Initial temperature of 33 °C was held for 8 min, increased at 25 °C/min until 180 °C. Temperature of the mass spectrometer ion source was 200 °C and the interface temperature was 220 °C.

A2.10 Crystallisation of wild-type CorEH

Crystallisation and data collection

For crystallisation experiments, CorEH was further purified by gel filtration on a HiLoad 26/600 Superdex200 column (GE Healthcare, Freiburg, Germany) with 50 mM phosphate buffer (pH 7.5). Protein concentrations were determined as described under expression and purification. CorEH was concentrated to 17 mg/mL using a Vivaspin™ concentrator with 10 kDa cut-off (Sartorius, Germany). Crystals were obtained at 20 °C from hanging drops with 2 µL protein solution + 2 µL reservoir (10 % PEG8000, 0.2 M $Mg(OAc)_2$) over 0.5 mL reservoir. After two weeks, crystals were briefly soaked in cryo solution (10 % PEG8000, 12% PEG400, 0.2 M $Mg(OAc)_2$) and transferred to liquid nitrogen. Data were collected at BESSY, beamline 14.2. Data collection statistics are given in Table S7.

Table S7. Statistics of the X-ray diffraction data collection.

Detector	Pilatus 3S 2M
Radiation source	BESSY, beamline 14.2
Wavelength	0.9184 Å
Resolution range (last shell)	50 – 2.18 Å (2.31 – 2.18 Å)
Space group	$P2_12_12$
a-axis / *b*-axis / *c*-axis	140.02 Å 156.57 Å 112.58 Å
Number of independent reflections (last shell)	129462 (20548)
Completeness (last shell)	99.7% (98.9%)
Redundancy (last shell)	6.7 (6.4)
I/σ(I) (last shell)	9.1 (1.3)
R_{sym} (last shell)	0.203 (1.410)
Wilson B-factor	37.6 $Å^2$
Matthews coefficient (V_M)	2.31 ^{3}/Da

Structure solution and refinement

Crystallographic computing used programs of CCP4[232]. The structure was solved by molecular replacement with Phaser (Version 2.8.3[233]) using the coordinates of PDB[220] entry 3QYJ as template. MR was repeated with 4, 6, 7, and 8 monomers / asymmetric unit as the quality of the model increased. Refinement was performed with Refmac5 (Version 5.8.0267[234]). Neither twinning nor non-crystallographic symmetry were applied. B-factors were refined isotropically with 8 TLS groups. The entry channel to the active site (ca. 8 Å between substrate electrophile position and channel entrance) contains density not well described by localized water molecules, but no ligands or buffer components were identified. The oligomerisation state of CorEH in solution is most likely a tetramer (Figure S9). Refinement statistics are given in Table S8.

Table S8. Statistics of structure refinement.

Refinement	
R_{cryst} / R_{free} (test data set with 5 % of all data)	0.175 / 0.226
Number of non-hydrogen atoms of CorEH / water	18139 / 1121
Average isotropic B-factors	
Protein main chain / side chain	20.1 / 21.0 Å^2
Water	34.7 Å^2
R.m.s. deviations from ideal geometry	
Bond lengths	0.011 Å
Bond angles	1.715°
Torsion angles	7.269°
Molprobity score/percentile	1.5 /98th
Protein data bank entry	7AC0

A2.11 Oligomeric state of CorEH

To determine the oligomeric state of CorEH in solution, purified CorEH protein was analysed by analytical size-exclusion chromatography using a Superose 6 10/300 GL column (GE healthcare) (Figure S4). To this end, 100 µl of purified CorEH protein was injected at a concentration of 2 g/L and the absorption at 280 nm (A_{280}) was recorded. The run was performed in buffer composed of 20 mM Na_2SO_4, 50 mM K_2HPO_4/KH_2PO_4 pH7.5. The molecular weight calibration of the column was performed using the following proteins: Thyroglobulin (660 kDa), g-Globulin (150 kDa), Ovalbumin (43 kDa), RNase A (14 kDa) and *p*-aminobenzoic acid (140 Da).

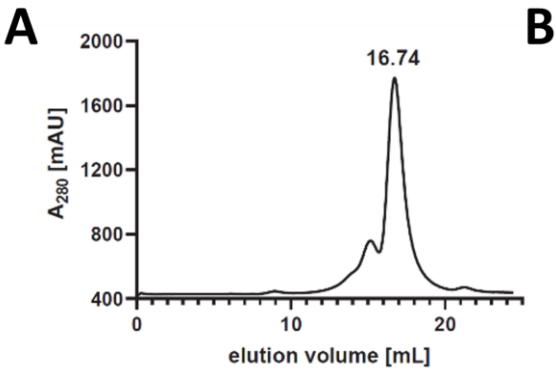

B

protein	expected MW [Da]	calculated MW [Da]	oligomeric state
CorEH	34173.6	199710.0	5.8

Figure S4. Analytical size-exclusion chromatography of CorEH. (A) Analytical size-exclusion chromatography run of 200 µg of CorEH on a Superose 6 10/300 GL column. To follow the elution of CorEH, the UV absorbance was followed at 280 nm(A_{280}) in mAU (AU: absorbance units) as a function of the elution volume. (B) CorEH forms an apparent hexamer in buffer containing 20 mM Na_2SO_4, 50 mM K_2HPO_4/KH_2PO_4 pH7.5. Shown is the expected molecular weight (MW) of a CorEH monomer and the calculated MW using the calibration curve.

A3 Sequences

A3.1 *Ci*VCPO

Amino acid sequence of *Ci*VCPO[230]

The secretion sequence encoded by the pBAD vector is shown in grey. The sequence differs from PDB 1IDQ at two positions, highlighted in grey (D164A and P544R).

*MKKLLFAIPLVVPFYSHSTMASH*MGSVTPIPLPKIDEPEEYNTNYILFWNHVGLELNRVTHTVGGPLTGPPLSARALGMLHLAIHDAYFSICPPT
DFTTFLSPDTENAAYRLPSPNGANDARQAVAGAALKMLSSLYMKPVEQPNPNPGANISDNAYAQLGLVLDRSVLEAPGGVDRESASFMFGE
AVADVFFALLNDPRGASQEGYHPTPGRYKFDDEPTHPVVLIPVDPNNPNGPKMPFRQYHAPFYGKTTKRFATQSEHFLADPPGLRSNADETA
EYDDAVRVAIAMGGAQALNSTKRSPWQTAQGLYWAYDGSNLIGTPPRFYNQIVRRIAVTYKKEEDLANSEVNNADFARLFALVDVACTDAGI
FSWKEKWEFEFWRPLSGVRDDGRPDHGDPFWLTLGAPATNTNDIPFKPPFPAYPSGHATFGGAVFQMVRRYYNGRVGTWKDDEPDNIAID
MMISEELNGVNRDLRQPYDPTAPIEDQPGIVRTRIVRHFDSAWELMFENAISRIFLGVHWRFDAAAARDILIPTTTKDVYAVDNNGATVFQNV
EDIRYTTRGTRED**R**EGLFPIGGVPLGIEIADEIFNNGLKPTPPEIQPMPQETPVQKPVGQQPVKGMWEEEQAPVVKEAP

Amino acid sequence of *Ci*VCPO variant[231]

Mutations from the wild type are highlighted in grey.

MGSSHHHHHHSSGLVPRGSHMGSVTPIPLPKIDEPEEYNTNYILFWNHVGLELNRVTHTVGGPLTGPPLSARALGMLHLAIHDAYFSICPPTD
FTTFLSPDTENAAYRLPSPNGANDARQAVAGAALKMLSSLYMKPVEQPNPNPGANISDNAYAQLGLVLDRSVLEAPGGVDRESASFMFGE**D**
VADVFFALLNDPRGASQEGYHPTPGRYKFDDEPTHPVVLIPVDPNNPNGPKMPFRQYHAPFYGKTTKRFATQSEHF**V**ADPPGLRSNADETAE
YDDAVRVAIAMGGAQALNSTKRSPWQTAQGLYWAYDGSNLIGTPPRFYNQIVRRIAVTYKKEEDLANSEVNNADFARLFALVDVAC**A**DAGIF
SWKEKWEFEFWRPLSGVRDDGRPDHGDPFWLTLGAPATNTNDIPFK**D**PFPAYPSGHATFGGAVFQMVRRYYNGRVGTWKDDEPDNIAID
MMISEELNGVNRDLRQPYDPTAPIEDQPGIVRTRIVRHFDSAWELMFENAISRIFLGVHWRFDAAAARDILIPTTTKDVYAVDNNGATVFQNV
EDIRYTTRGTRED**P**EGLFPIGGVPLGIEIADEIFNNGLKPTPPEIQPMPQETPVQKPVGQQPVKGMWEEEQAPVVKEAP

A3.2 Selected epoxide hydrolases

The N-terminal His6-tag encoded by the pET28a(+)-vector is shown in grey. PaeCIF has a C-terminal His6-tag.

Sequence of PpuEH from *Pseudomonas putida* (Accession: KMU96261.1)

MGSSHHHHHHSSGLVPRGSHMPMAEIPLCVWRTRAQSFMFRGQSIRYWTAGQGEPLLLLHGFPTASWDWHYLWGPLSQRFRVIACDML
GFGDSDKPVDHTYSLMEQADLQQALLVHLQVAQPVHLLAHDYGGSVAQELLARHHEQRADIASCVFLNSGLFPESCRMLLIQKLLLSRFGWLV
GRSFGRDDLVRNVMQVYGPCTHPSESALDDFWSLIAANRGTRILHKLVGYMPERRLHRERWVGAMQRKGVPLRLINGVVDPLSGAHMLERY
RQLVPEPDTVQLLGIGHYPHTEAPVQVLRHYLAFREQPLSFYPPKVAWS

Sequence of EliEH2 from *Erythrobacter litoralis* (Accession: Q2N9R2)

MGSSHHHHHHSSGLVPRGSHMAGPSLGEWKAKAQHFAYDGLQIAFWTGGKPDARPLLLVHGYPTASWDWHRVWETLGSKYHLVAPDMI
GFGLSDKPRSGYSIHRQADMHVALLDHLGIGAFDALVHDYGVSVGQELLARRAERSAAQGLGQTVFLNGGIFPDQHRPRPIQKLGTSPLGFLV
GLLTNREKFGRSFSEVFGPDTQPGAQELDEFWDLVSHNGGNRIMHKLLHYIADRKEHAERWFDALRIAQGDIGLINGALDPVSGRHAYEAWR
ERLPDARHHLIPTVGHYPQVEDPQTVSRVTLDWLAR

Sequence of SceEH from *Saccharomyces cerevisiae* (Accession: NP_014462.1)

MGSSHHHHHHSSGLVPRGSHMSNIIARFHKIQVQDGVKVWYREAGAAGNPTILLLHGFPTSSNMFRNLIPLLAGQFHIIAPDLPGFGFTETPE
NYKFSFDSLCESIGYLLDTLSIEKFAMYIFDYGSPVGFRLALKFPSRITGIVTQNGNAYEEGLDDRFWGPLKEYWKSYQSDPVFVKSLIPYLEDPAN
VICQYHDGVPAIESVDPAAYTLDIALIQRTGQTDIQLRLFFDYQNNIKLYPAFQKFLRDSKIPVLVAWGANDTIFSVAGAEAYRKDVDNLKVVYY
DTGHFALETHVVAIAEEIISMFAEN

Sequence of NpuEH2 from *Nostoc punctiforme* (Accession: WP_012408640.1)

MGSSHHHHHHSSGLVPRGSHMTTYRTVSIDGLDIFYREAGSRNNPTILLLHGFPTSSHMFRNLIPALADKFHLVAPDYPGYGNSSMPTVNEFD
YTFDNLAEIVEKFIAAIALKKYSLYVMDYGAPIGYRIAAKYPERVQSLIVQNGNAYEEGLREFWEPIKAYWQERSPENAEKLKYLVTLEATKWQYT
NGVRNLEAISPDTWTMDQHFLDRPGNDEIQLALLYSYGTNPLLYPQWQEYFRNYQPPTLIVWGKNDYIFPADGAYPYQRDLKDVEFHLLDTG
HFALEEDGDAIANYIDQFLTSRLQSIPV

Sequence of ScoEH from *Streptomyces coelicolor* (Accession: Q9K3Q1)

MGSSHHHHHHSSGLVPRGSHMFDHDGTPVRTGRAAVNGTSLHYRAAGSGPAVVLLHGVPKTSYHWRHLVPKLTPHYTVVAPDLRGLGDSA
RPADGYDSATMSDDIAELMNHLGHESYAVVGEDWGAVIGYQLAARHRDRVTALVFAEALFPGFGFEDHTALTAENVAGGMHLWHLGFYFQ
PDIPEMLIAGHERELITYMIKFERSRPDSATPEAIDEYVRCYSMPGGIRAMLAVYRAMLVDAEQNRRAARKKLDIPVLALGGSAFIGDRNESQM
RLMAHDVTGHVFDAGHDLAEEVPDEMADVLLPFLATHQ

Sequence of AciCIF from *Acinetobacter sp.* (Accession: A0A014BSV4)

MGSSHHHHHHSSGLVPRGSHMKKFFKVMTLSAAMGMFGLNQANAEYDPNLKSIDTPPAVSQQMFNKVKSNGLGQYAYAKGLSSKFIESEG
VKLHYVEGGSKGTPIVFIHGFGSTWKMWEPVMLSYMKDHKVIAIDLPGLGQSGPILNDDYSAENTSKILIGAIKKIAGKGPIYYVSHDLGNTASY
PLVANNQGYIKKAVFMDSPIPDRAMFEYPGYTADGPGLGWHFGYFSFGDIAEKQIANDPNLFFSYFIKTYAGKKEIFTPELLAELIEPYSTRDKLK
AAFGYYRSHADSIRQNEALLANGKKLTIPSMALTGQKGVNDVLVKEMRARFVADPAQYTAIILPDTGHWMVEENAEGVEKSLSNFLFK

Sequence of Ylehd from *Yarrowia lipolytica* (Accession: XP_504164)

MGSSHHHHHHSSGLVPRGSHMASMAHLTKEYYEPFHHDVILGGKRWHYLDIPPEGKDNGRVLVLVHGFPDFWYGWRHQIPVFRKRGHRII
LPTLMGFPGSEVPEPPAMEEFEENEDGINIYTELGQEDDCRELHFYGFKFFADCMAELLKKLNIKSATFLGHDWGAHYVPKVWAYHPEIVDAIS
SACWYYQVPEPEWVPLTDFSDKWPTTKYQLQFGGDAVNNIGPGMIPFFLRRSYTVGANFDGEPDPEAPMHMTEEEFAVYEEHFSKEKRSLA
GPFTYYRSRKLNWEQDKENFLDKGATKKDLTVNVPYLYIGSTNDIALIPEMSMHLDEYVEKGKLTREHVPTSHWALFEAPDQINKIYVDWLDKL
DKTSKLSGGSGGSGGSRDHMVLHEYVNAAGIT

Sequence of CorEH from *Corynebacterium sp.* C12 (Accession: O52866)

MGSSHHHHHHSSGLVPRGSHMSTEITHHQAMINGYRMHYVTAGSGYPLVLLHGWPQSWYEWRNVIPALAEQFTVIAPDLRGLGDSEKPM
TGFDKRTMATDVRELVSHLGYDKVGVIGHDWGGSVAFYFAYDNRDLVERLFILDMIPGLIKAGDSFPIPVALMINHIFFHGGNPDWATALISKD
VNLYLRRFLTTLDYNYSPNVFSEEDIAEYVRVNSLPGSIRSGCQWYATGLREDTENLAKATDKLTIPVIAWGGSHFLGDIRPAWQEVAENVEGG
AVENCGHFVPEEKPQFVIDTALKFFAPLR

Sequence of PaeCIF from *Pseudomonas Aeruginosa* (Accession: A0A071KVQ1)

MILDRLCRGLLAGIALTFSLGGFAAEEFPVPNGFESAYREVDGVKLHYVKGGQGPLVMLVHGFGQTWYEWHQLMPELAKRFTVIAPDLPGLG
QSEPPKTGYSGEQVAVYLHKLARQFSPDRPFDLVAHDIGIWNTYPMVVKNQADIARLVYMEAPIPDARIYRFPAFTAQGESLVWHFSFFAADD
RLAETLIAGKERFFLEHFIKSHASNTEVFSERLLDLYARSYAKPHSLNASFEYYRALNESVRQNAELAKTRLQMPTMTLAGGGHGGMGTFQLEQ
MKAYAEDVEGHVLPGCGHWLPEECAAPMNRLVIDFLSRGRLEHHHHH

A3.3 CorEH variants

Mutations from the wild type are highlighted in grey.

Amino acid sequence of CorEH W34F

MGSSHHHHHHSSGLVPRGSHMSTEITHHQAMINGYRMHYVTAGSGYPLVLLHG**F**PQSWYEWRNVIPALAEQFTVIAPDLRGLGDSEKPMT
GFDKRTMATDVRELVSHLGYDKVGVIGHDWGGSVAFYFAYDNRDLVERLFILDMIPGLIKAGDSFPIPVALMINHIFFHGGNPDWATALISKD
VNLYLRRFLTTLDYNYSPNVFSEEDIAEYVRVNSLPGSIRSGCQWYATGLREDTENLAKATDKLTIPVIAWGGSHFLGDIRPAWQEVAENVEGG
AVENCGHFVPEEKPQFVIDTALKFFAPLR

Amino acid sequence of CorEH W34N

MGSSHHHHHHSSGLVPRGSHMSTEITHHQAMINGYRMHYVTAGSGYPLVLLHG**N**PQSWYEWRNVIPALAEQFTVIAPDLRGLGDSEKPM
TGFDKRTMATDVRELVSHLGYDKVGVIGHDWGGSVAFYFAYDNRDLVERLFILDMIPGLIKAGDSFPIPVALMINHIFFHGGNPDWATALISKD
VNLYLRRFLTTLDYNYSPNVFSEEDIAEYVRVNSLPGSIRSGCQWYATGLREDTENLAKATDKLTIPVIAWGGSHFLGDIRPAWQEVAENVEGG
AVENCGHFVPEEKPQFVIDTALKFFAPLR

Amino acid sequence of CorEH W100A

MGSSHHHHHHSSGLVPRGSHMSTEITHHQAMINGYRMHYVTAGSGYPLVLLHGWPQSWYEWRNVIPALAEQFTVIAPDLRGLGDSEKPM
TGFDKRTMATDVRELVSHLGYDKVGVIGHD**A**GGSVAFYFAYDNRDLVERLFILDMIPGLIKAGDSFPIPVALMINHIFFHGGNPDWATALISKD
VNLYLRRFLTTLDYNYSPNVFSEEDIAEYVRVNSLPGSIRSGCQWYATGLREDTENLAKATDKLTIPVIAWGGSHFLGDIRPAWQEVAENVEGG
AVENCGHFVPEEKPQFVIDTALKFFAPLR

Amino acid sequence of CorEH D123N

MGSSHHHHHHSSGLVPRGSHMSTEITHHQAMINGYRMHYVTAGSGYPLVLLHGWPQSWYEWRNVIPALAEQFTVIAPDLRGLGDSEKPM
TGFDKRTMATDVRELVSHLGYDKVGVIGHDWGGSVAFYFAYDNRDLVERLFIL**N**MIPGLIKAGDSFPIPVALMINHIFFHGGNPDWATALISK
DVNLYLRRFLTTLDYNYSPNVFSEEDIAEYVRVNSLPGSIRSGCQWYATGLREDTENLAKATDKLTIPVIAWGGSHFLGDIRPAWQEVAENVEG
GAVENCGHFVPEEKPQFVIDTALKFFAPLR

Amino acid sequence of CorEH H264F

MGSSHHHHHHSSGLVPRGSHMSTEITHHQAMINGYRMHYVTAGSGYPLVLLHGWPQSWYEWRNVIPALAEQFTVIAPDLRGLGDSEKPM
TGFDKRTMATDVRELVSHLGYDKVGVIGHDWGGSVAFYFAYDNRDLVERLFILDMIPGLIKAGDSFPIPVALMINHIFFHGGNPDWATALISKD
VNLYLRRFLTTLDYNYSPNVFSEEDIAEYVRVNSLPGSIRSGCQWYATGLREDTENLAKATDKLTIPVIAWGGSHFLGDIRPAWQEVAENVEGG
AVENCG**F**FVPEEKPQFVIDTALKFFAPLR

DNA sequence of wild-type CorEH

CATATGAGCACCGAAATTACCCATCATCAGGCAATGATTAATGGTTATCGCATGCATTATGTTACCGCCGGTAGTGGTTATCCGCTGGTTCTGCTGCATGGC
TGGCCGCAGAGCTGGTATGAATGGCGTAATGTTATTCCGGCCCTGGCCGAACAGTTTACCGTGATTGCCCCGGATCTGCGTGGCCTGGGTGACAGTGAAA
AACCGATGACCGGCTTTGATAAACGCACCATGGCCACCGATGTTCGTGAACTGGTTAGTCATCTGGGCTATGATAAAGTTGGTGTTATTGGCCATGATTGG
GGTGGTAGCGTGGCATTTTATTTTGCCTATGATAATCGTGATCTGGTGGAACGTCTGTTTATTCTGGATATGATTCCGGGTCTGATTAAGGCCGGCGATAGC
TTTCCGATTCCGGTTGCCCTGATGATTAATCATATTTTCTTTCATGGCGGCAATCCGGATTGGGCAACCGCCCTGATTAGCAAAGATGTGAATCTGTATCTGC
GTCGTTTTCTGACCACCCTGGATTATAATTATAGTCCGAATGTGTTTAGCGAAGAAGATATTGCCGAATATGTTCGTGTGAATAGTCTGCCGGGTAGCATTC
GTAGCGGTTGTCAGTGGTATGCCACCGGCCTGCGCGAAGATACCGAAAATCTGGCCAAAGCCACCGATAAACTGACCATTCCGGTTATTGCCTGGGGTGG
CAGCCATTTTCTGGGTGACATTCGCCCGGCATGGCAGGAAGTGGCAGAAAATGTTGAAGGCGGTGCCGTGGAAAATTGCGGTCATTTTGTGCCGGAAGAA
AAACCGCAGTTTGTGATTGATACCGCACTGAAATTTTTCGCCCCGCTGCGTTAAGCGGCCGC

A3.4 Reconstructed ancestral sequences

Amino acid sequence of Anc159

MGSSHHHHHHSSGLVPRGSHMPDDPDFPGFGYEWINTSAGRIFVRVKGDGPPLLLLHGYPQTHVMWHRIAPKLAERYKVIVADLPGYGWS
DMPEPYTKRAMAKQQIETMEQLGfEHFALVGHDRGARVSYRLALDHPGRLSKFVVLDILPTYWQAMNKAYALKIYHWFFLAQPYPLPENLIG
GDPDHYVKYKLRRWTQGRDVYHPQAVEHYRRAFRDPMRRHVMCEDYRAGVYVDFEHDKIDRERKIPCPMQVLWQERGYHPLDIWKKWA
SQVQGAPIESGHMLPEEAPDQTAEHLVRFFSS

Amino acid sequence of Anc153

MGSSHHHHHHSSGLVPRGSHMSFPGFESRTVDTSDARIHCRVGGNGPPLLLLHGYPQTHVMWHRVAPRLANHFTVVCADLRGYGDSSKPA
NYSKRAMAQDQVEVMSQLGYERFHVCGHDRGARVAHRLALDHPGRVQKLCVLDIVPTYVWQTTNRAFATAYYHWFFLIQPAPLPENMIGA
DHPDYYLKACLGRWGKGLSAFDPQALEEYRRCFSNPAAIHAMCEDYRAAAGTIDLEHDKADMGRKISCPMLVLWGEKGIVGRMFDPLAVW
RKWASDVSGASLPCGHFLPEEAPDETAQALLEFLAH

Amino acid sequence of Anc152

MGSSHHHHHHSSGLVPRGSHMSTFPGFEHRTVNVNGARIHCVVGGSGPPLLLLHGYPQTHVMWHRVAPRLAEHFTVVCPDLRGYGDSDK
PATNYSKRAMAQDQVEVMSHLGYERFHVVGHDWGARVAYRLALDHQDRVQKLCVLDIVPTLVWETAFALMIYHWFFLAQPPPWPENLIG
ADHPDFYLKRCLSKWGHNpNAFDPQALEEYRRCFSNPAAIHASCEDYRAAAIDLEHDKADMGRKVSCPMLVLWGEWGVVGRLYDPLPVWR
EWASDVEGASIPCGHFLPEEAPDEVVEALLKFFAP

Amino acid sequence of Anc149

MGSSHHHHHHSSGLVPRGSHMSDFPGFESNGRHVEVNGTRLHYVTGGSGPPVVLLHGFPQTWYQWHHVVPKLAEHYTVVAPDLRGLGDS
EKPATGYSKRTMAQDIVELMNHLGHERFAVVGHDWGATVAYQLAANHQDRVTKLVFMDAVPPNWETYDYPGFTAAGGMHIWHFFFYFQ
PPDLPETLIAGDPRYYLKYFIKTWGSNPDVFTPEALDEYVRCYSMPGSIRAMCEYYRAMAIDLEQGKKLSCPVMVLWGSKGVVGRLYDPLEVM
REHATDVEGHVLPGCGHWLPEECPDEMAEVLLEFLAR

Amino acid sequence of Anc117

MGSSHHHHHHSSGLVPRGSHMTDWHYVEVGGSRMHYVDEGPRNDGENDPILLLHGNPTSSYLYRNMIPHLAGKYRCIAPDLIGFGQSDKP
TDWIDYTFEDHCRYLEAFIDALGLENITLVCQDWGSPIGFRWAMKHPDRVKGIVVMNTMMWEPMPGWDDQPWEPFQAFRSPGVNGQK
MVQEPENMFVEHIMPGMGVIRPLSEEEMDAYRAPFPNPGESRKACLRQFFFPRQVPIEPDDPADVVALIEAHREWLWLRQSDIPTLLIWGEK
DAIFPPEEVMDHFRQTLKNCEVVHIDGGHFIQEDQGDEIARPIVEWFTR

Amino acid sequence of Anc116

MGSSHHHHHHSSGLVPRGSHMTDWYPFAPHYIEVGGLRMHYWDAGPDGDPILLLHGYPTSSYMWRNMIPTLAGKYRCIAPDLIGFGQSDK
PTDTDYTFENHCEYLEAFIDQLGLENITLVCHDYGGPIGFRLAARHPDRVKGIVIMNTMLWEPDPARDDQPWEPFQAFRKMCQEPDNMFVE
HLMKGMGVVPCKPLSEEEMDAYRALFPNPGESNKVCLRLFFFYRQVPIKPEDPADVVALIEHSREWLQSDIPTLLIWGEKDPIFGPEEVMERW
RQTLPNCETVHIDGAGHFVQEDDPDEIARAIIEWFTR

Amino acid sequence of Brno86

MGSSHHHHHHSSGLVPRGSHMDVLRTDPAEFPFKHHYVEVNGVRIHYVEAGPRGDPILLLHGNPTSSYLWRNLIPPLAGKYRVIAPDLIGFGE
SDKPPDDYDYTFEDMAESLEAFIDALGLEKVTLVCHDWGGAIGFHLALRHPDRVKGLVIMNAIVPTPPGWEAYPREMYQFFQSPGGERMISS
DNAFVKRLLPGGLPDPLSEEELDAYRDAFPNPESRTPALTFYRALLRSGEDPADVPELREAWAEWLRKVDVPTLLIWGEKDPVLSPEALEEYRRY
LPNLETVTIADAGHFVQEEKPEEIAQAIADFLRRLRP

Amino acid sequence of Brno119

MGSSHHHHHHSSGLVPRGSHMSTDPAMEGFKHRHVEVNGVRIHYVEAGPGPPVLLLHGNPQSWYEWRHVIPPLAEHYRVIAPDLRGYGDS
DKPESVESYTLDEMADDLAALLDSLGVGEKVTLVGHDWGGVVAYHLALRHPDRVKKLVIMNAVVPSLPRGPRTHPTQCRAYWFFFQQPGVA
ERLISSNNPKKFLKNLLTGWGRPDAFTEEELDAYVNCFSKPGARTAMLNFYRAMLRNELTEAWLEAHRKIDVPVLLIWGEGDPVISPELLEEWR
KKYVPNNLTVKTIPDCGHFVQEEKPEEVAQAILEFLKKARP

Amino acid sequence of Brno157

MGSSHHHHHHSSGLVPRGSHMSTDPLMTGFEHRHVEVNGVRIHYVEGGPGPPVLLLHGNPQTWYEWRHVIPKLAEHYTVIAPDLRGYGDS
DKPASHTGYSKRTMADDLVELMNHLGYGEKFAVVGHDWGAVVAYHLALKHPDRVTKLVIMEAIIPSFAMWEHTGPTAFHWFFFAQPDVPE
RLIAANDPEYFLKHLLTGWHAGRPDAFTPEALDEYVRCFSKPGAIHAMCEDYRAMLRNEHNEAWLEAGRKIDVPVLVLWGERGIGPEDPLEA
WRKWADNVTAGAVPDCGHFLPEEKPDEVAEALLEFLARHRPA

Eigenständigkeitserklärung

Hiermit erkläre ich, dass diese Arbeit bisher von mir weder an der Mathematisch-Naturwissenschaftlichen Fakultät der Universität Greifswald noch einer anderen wissenschaftlichen Einrichtung zum Zwecke der Promotion eingereicht wurde.

Ferner erkläre ich, dass ich diese Arbeit selbstständig verfasst und keine anderen als die darin angegebenen Hilfsmittel und Hilfen benutzt und keine Textabschnitte eines Dritten ohne Kennzeichnung übernommen habe.

Unterschrift des Promovenden

List of publications

- ***'Promiscuous Dehalogenase Activity of the Epoxide Hydrolase CorEH from Corynebacterium sp. C12'***
  E.D. Schuiten, C.P.S. Badenhorst, G.J. Palm, L. Berndt, M. Lammers, J. Mican, D. Bednar, J. Damborský, U.T. Bornscheuer,
  ACS Catalysis 2021, *11* (10), 6113-6120
  https://doi.org/10.1021/acscatal.1c00851

- ***'An Ultrasensitive Fluorescence Assay for the Detection of Halides and Enzymatic Dehalogenation'***
  A.S. Aslan-Üzel, A. Beier, D. Kovář, C. Cziegler, S.K. Padhi, **E.D. Schuiten**, M. Dörr, D. Böttcher, F. Hollmann, F. Rudroff, M.D. Mihovilovic, T. Buryška, J. Damborský, Z. Prokop, C.P.S. Badenhorst, U.T. Bornscheuer,
  ChemCatChem 2020, *12* (7), 2032-2039
  https://doi.org/10.1002/cctc.201901891

- ***'Enzymatic Photometric Assays for the Selective Detection of Halides'***
  Q. Tang, A.S. Aslan-Üzel, **E.D. Schuiten**, C.P.S. Badenhorst, I.V. Pavlidis, U.T. Bornscheuer,
  Multienzymatic Assemblies: Methods and Protocols 2022, 361-375
  https://doi.org/10.1007/978-1-0716-2269-8_22

- **'Discovery of Novel Bacterial Chalcone Isomerases by a Sequence-Structure-Function-Evolution Strategy for Enzymatic Synthesis of (S)-Flavanones'**
  H. Meinert, D. Yi, B. Zirpel, **E.D. Schuiten**, T. Geißler, E. Gross, S.I. Brückner, B. Hartmann, C. Röttger, J.P. Ley, U. Bornscheuer,
  Angew. Chem. Int. Ed. 2021, *60* (31), 16874-16879
  https://doi.org/10.1002/anie.202107182

- ***'Biocatalytic Production of Amino Carbohydrates through Oxidoreductase and Transaminase Cascades'***
  V. Aumala, F. Mollerup, E. Jurak, F. Blume, J. Karppi, A. E. Koistinen, **E.D. Schuiten**, M. Voß, U. Bornscheuer, J. Deska, E. R. Master,
  ChemSusChem 2019, *12* (4), 848-857
  https://doi.org/10.1002/cssc.201802580

- ***'Enzyme Cascade Reactions for the Biosynthesis of Long Chain Aliphatic Amines from Renewable Fatty Acids'***
  D.-S. Lee, J.-W. Song, M. Voß, **E.D. Schuiten**, R. K. Akula, Y.-U. Kwon, U. Bornscheuer, J.-B. Park,
  Adv. Synth. Catal. 2019, *361* (6), 1359-1367
  https://doi.org/10.1002/adsc.201801501

- ***'Whole-Cell Photoenzymatic Cascades to Synthesize Long-Chain Aliphatic Amines and Esters from Renewable Fatty-Acids'***
  H.-J. Cha, S.-Y. Hwang, D.-S. Lee, A.R. Kumar, Y.-U. Kwon, M. Voß, **E.D. Schuiten**, U.T. Bornscheuer, F. Hollmann, D.-K. Oh, J.-B. Park,
  Angew. Chem. Int. Ed. 2020, *59* (18)
  https://doi.org/10.1002/anie.201915108